BEHAVIOR AND DESIGN OF SHEATHED COLD-FORMED STEEL STUD WALLS UNDER COMPRESSION

by

Luiz Carlos Marcos Vieira Junior

A dissertation submitted to Johns Hopkins University in conformity with the requirements for the degree of Doctor of Philosophy

Baltimore, Maryland
July 2011

Abstract

Cold-formed steel may be used to frame the walls, floors, and roofs of modern buildings. The individual cold-formed steel members (studs) have sheathing attached to provide appropriate architectural enclosures. This sheathing also serves to brace the cold-formed steel studs under load. This thesis is dedicated to the study of sheathed cold-formed steel walls under axial loads.

Current design methods are highly developed regarding the design of isolated cold-formed steel members such as columns and beams, but cold-formed steel wall studs that rely on sheathing for bracing are not fully addressed. A series of tests on single columns with sheathing, and full-scale walls with sheathing are completed herein and compared with previous design methods adopted by the American Iron and Steel Institute (AISI) Specification. The comparison shows that previous design methods lead to overly conservative strength prediction. This is particularly true for the case of dissimilar sheathing, e.g. oriented strand board on one face and gypsum board on the other face of the stud.

The sheathing supplies beneficial restraint to the wall studs and the stiffness of this sheathing-based restraint is characterized experimentally and analytically herein. The lateral bracing stiffness and resistance supplied by the fastener-sheathing combination that braces the stud is explored, taking into account typical design variables as well as the influence of humidity and construction flaws. For the first time, the lateral bracing stiffness is correctly divided into a local fastener and global diaphragm stiffness. While local stiffness considers the damage around the fastener connection, the diaphragm stiffness considers the shear stiffness of the whole sheathing.

Particular emphasis on the single-column and full-wall tests is placed on the behavior and the observed limit states given the different sheathing configurations. Demands on the fasteners that connect the sheathing to the studs are also explored analytically and numerically with finite element models of sheathed single columns and sheathed wall studs. A unique application of the Direct Strength Method of design is explored where the sheathing-based restraint is used explicitly in determination of the elastic buckling loads of the wall studs, and then these elastic buckling loads are utilized to determine the strength. An analytical solution for determining the buckling loads is provided, although it is involved and numerical methods are preferred. Good agreement is demonstrated for the new approach both in terms of strength and limit states prediction. The new approach is considered to be a suitable and reliable design method for adoption in the AISI Specification.

Advisor: Dr. Benjamin William Schafer
Readers: Dr. Judith Mitrani-Reiser
Dr. Narutoshi Nakata

This research was funded by the American Iron and Steel Institute and the Steel Stud Manufacturers Association

Para a minha família
(To my family),

"I don't know what I may seem to the world; but as to myself I seem to have been only like a boy playing on the seashore, and diverting myself in now and then finding a smoother pebble or a prettier shell than ordinary, whilst the great ocean of truth lay all undiscovered before me"

Sir Isaac Newton

Acknowledgements

There is probably a philosopher who once said something along these lines: “It seems forever while you are living a challenge, but it seems so short when you look back on it.” While I still have the vivid memories of the “forever” I would like to acknowledge all the people who have helped me:

My family has never let me down. In fact, the inconveniences of life made me rediscover them. Mom and Dad, thanks for everything; nobody could ever do better than you two did. Grandma and Grandpa, thanks for understanding my absence, and for calling me every Sunday afternoon to tell me jokes, to talk about the chickens, and to listen to my plans to take over the world. Cousins, thanks for together making our family indestructible, young, and happy; let’s keep it up forever. Aunts and Uncles, thanks for managing to keep the family together.

Stefanie, thanks for your unconditional love. Your excitement for life is contagious, and you showed me that my time in Baltimore is part of my life and that I should enjoy it. You helped me find myself again. I hope to one day be as good to you as you are to me. Thanks also to your parents and brother for caring for us, especially your dad for setting such a great example.

Hopkins Harriers, thanks for welcoming me into the group and making me one of you. Every day I was certain that after our run I would feel energized and ready to go the extra mile in my research. Also, thanks for being my friends; we had so much fun together. I especially thank Tom for his friendship and for showing me that I could do what I once judged impossible.

Marc Calaf, my first two years in Baltimore were shared with you. Thanks for your companionship and for listening to all my lamentations; your calmness brought me a lot of peace.

Roger Maioli, the man, the legend. It was a gift living with you for two years. Thanks for cheering me up and entertaining me with the craziest stories that a man can ever dream of. I am your fan.

Patrick Boner, thanks for your great friendship and for putting all the effort into creating the Meeting of the Minds (MoMs), which later merged with the DaDs group. Thanks also to our seasonal members: Guillermo, Slickie, and William.

My friends and colleagues at JHU, especially Ali (all of them), Cris, Hannah, Jiazhen, Mina, Kara, Yared, Vahid, Zhanjie, thank you for your kindness and for putting up with my dirty running clothes in the office. Nick, we had a lot of fun in the lab; thanks for being so helpful.

My dearest friends from USP, Filipe, Gustavo, Marlos, and Klaus, I will always be in debt to you. The distance somehow made our friendship stronger.

Professor Buchaim and Malite, thanks for guiding me in my career, and for becoming my friends. Talking to or emailing you is such a great pleasure.

Professor Schafer, thanks for the opportunity to be part of your research group. I didn't know that I could do so much. Your excitement for research is amazing. Please never lose it; you are a source of energy to all of your students. And thanks, Ben, for your friendship. Our runs/talks/emails will remain forever in my memory.

I always tell people that I want to have stories to tell my grandkids as my grandpa always has so many to share with me. So just a little message to my future grandkids:

Dear Grandkids,

I am probably old by now and my memory is failing me, but the people I have just mentioned are part of one of the biggest challenges that I ever faced in my life, and all of them are heroes for me.

Be kind to them,

Grandpa.

TABLE OF CONTENTS

CHAPTER 1 - INTRODUCTION

Building systems framed from cold-formed steel members are increasingly common in the built environment, motivating the need to efficiently account for the interaction of different components in such systems. Cold-formed steel studs, which generally form the walls of such buildings, can be braced by bridging, as depicted in Figure 1.1 (a). However, the studs are also commonly attached to wallboards (sheathing): oriented strand board (OSB), plywood, and gypsum board are common (Figure 1.1(b)), and these boards may potentially provide the necessary bracing instead of bridging or blocking. For largely economical reasons a common practice in research is to test a sheathed single stud (Figure 1.1(c)) instead of a full-scale wall. Most researchers idealize the problem down to a bar element to represent the stud, and translational-spring elements to represent the restriction provided by the sheathing (Figure 1.1(d)). Or, in a more involved manner as explored here, where the stiffness contribution that the stud-fastener-sheathing system supplies to the stud is represented as divided into three parts: rotational (k_ϕ), translational in the plane of the board (k_x), and translational out of the plane of the board (k_y) (Figure 1.1(d)).

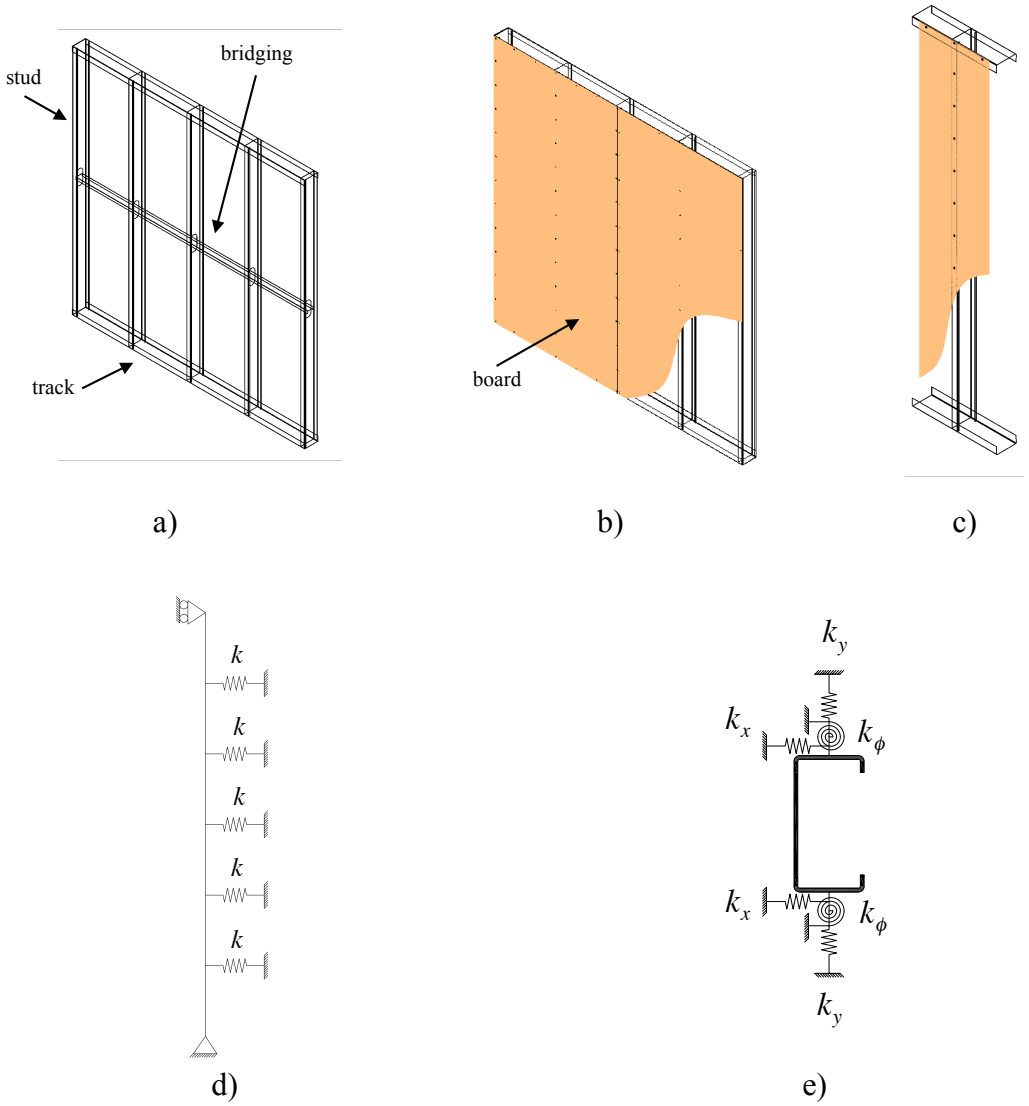

Figure 1.1 – Cold-formed steel walls and bracing of the studs. a) All-steel design with studs braced by bridging, b) Sheathed wall design with stud braced only by sheathing, c) Isolated single column with sheathing, d) Schematic model of stud bracing by sheathing, e) Detailed model of bracing springs applied to the cross-section.

1.1. HISTORICAL BACKGROUND

In 1947 George Winter, with his students and colleagues, was the first to formalize the increase of stud capacity due to its connection to sheathing in cold-formed steel studs [1.1]. In 1962 the AISI Specification [1.2] incorporated the design method of [1.1] which Winter expanded in [1.3]. The design method is based on a minimum stud-to-sheathing

stiffness, determined by test (local stiffness test), and incorporated into a simple flexural buckling model of the stud, as depicted in Figure 1.1(d). The approach is known as Winter's method, or the local method.

Basically the method insures that connection stiffness and spacing is enough to achieve the limit state covered by the method (i.e., insures strong-axis buckling by bracing weak-axis buckling). The method is limited since it covers only studs with sheathing connected to both sides and with the same material on both sides. The method requirements, even though rational, include arbitrary checks, such as considering the buckling length equal to twice the fastener spacing (known as the "2a" assumption) and it only applies to flexural buckling (not flexural-torsional a common buckling mode in lipped channel cold-formed steel studs).

In 1976 an alternative to Winter's method was developed by Simaan and Peköz [1.4] that considered the contribution provided by the sheathing shear stiffness or diaphragm stiffness to the flexural, torsional, or flexural-torsional buckling modes. Simaan and Peköz also investigated the spring stiffness but they used the diaphragm test [1.4], Figure 1.2(a), instead of the translational tests used by Winter [1.3], Figure 1.2(b). As reported in [1.5], both tests results can be compared and the differences are found to be relatively small regarding spring stiffness. This is explained by the fact that the major contributor to the diaphragm stiffness in many typical configurations is local deformations at the fasteners, well captured in Winter's simple local test. Simaan and Peköz's design method was ultimately adopted by the AISI Specification in 1980, but it was abandoned in 2004 and replaced by a simplified version of Winter's earlier method [1.1].

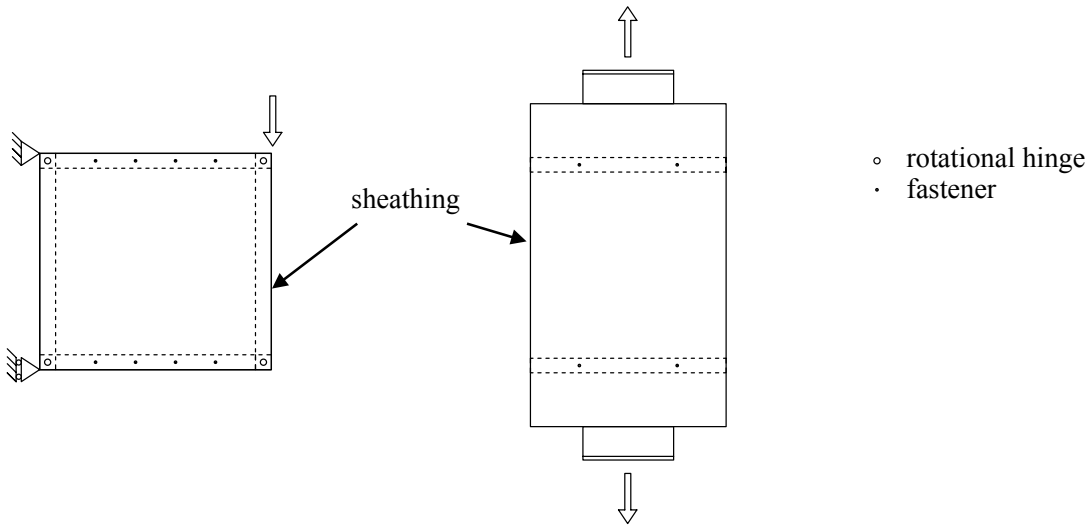

a) Diaphragm stiffness test. b) Translational/Local stiffness test.

Figure 1.2 – Tests proposed for finding lateral stiffness in the x direction (k_x).

Currently the design of cold-formed steel wall studs in compression follow AISI-S211-07 [1.6] the "Wall Stud Design" standard, which defines two methodologies for the design: "all-steel design" and "sheathing braced design". All-steel design ignores the sheathing contribution (relying on bridging and blocking alone) and thus is not the focus of this discussion. The general requirements for sheathing braced design are provided in B1(b) of [1.6]:

> *"Wall stud assemblies using a sheathing braced design shall be designed assuming that identical sheathing is attached to both sides of the wall stud and connected to the bottom and top horizontal members of the wall to provide lateral and torsional support to the wall stud in the plane of the wall. Wall studs with sheathing attached to both sides that is not identical shall be designed based on the assumption that the weaker of the two sheathings is attached to both sides."*

The requirement of designing the stud based on the weaker sheathing imposes a barrier to a more efficient design method. It is common to have studs with OSB or plywood connected to one flange and the other flange is either (i) not connected or (ii) it is connected to gypsum sheathing. Case (i) would result in designing the studs as if nothing was attached and case (ii) would be designed as if gypsum sheathing was connected to both sides. The origin of the "weaker of the two sheathings" concern is that such configurations may exacerbate torsion problems related to flexural-torsional buckling of the stud.

With the weaker sheathing rule in mind, it is worth previewing one of the findings in this research: in a full wall test, which had studs connected one side to OSB and the other side bare (OSB-Bare), even though the peak load was higher than a completely bare wall, which would be the assumption in current design, the test showed that there is no post-peak reserve, resulting in an abrupt failure after peak load. The absence of post-peak reserve is common in global modes, but particularly pronounced in these failures, so engineers must be informed of this.

Existing research is highlighted throughout the thesis, but it is worth mentioning that a few researchers have been providing key contributions to the field such as Telue [1.7] that researched the behavior of steel wall frames using plasterboard, Okasha [1.8] and Fiorino [1.9] concentrated on the fastener stiffness, Laboube [1.10] worked on what stud-to-track gap is acceptable, and Miller [1.11, 12] investigated the behavior of cold-formed wall stud-assemblies and the idea of using different buckling length to take in account the semi-restricted boundary conditions of the stud.

1.2. METHODOLOGY USED IN THIS RESEARCH

The goal of this project is to propose a new design method and to understand the behavior of sheathed cold-formed steel wall studs under compression. The dissertation first presents a literature review of the research in the field, briefly covered in this introduction, but further explored in Chapter 2. Each design method is discussed with respect to strengths and weakness, and key assumptions are explained and evaluated.

The literature review highlighted that little had been done to find out the translational stiffness in the plane of the board/sheathing (k_x). Therefore the next phase of the project was to explore k_x, this study can be found in Chapter 3 together with comments about the rotational stiffness (k_ϕ) and translational stiffness out of the plane of the board/sheathing (k_y).

In parallel to the studies commented above a Multi Degree of Freedom (MDOF) testing rig was being designed and built. The machine fondly called Big Blue Baby (BBB) is capable of applying 890 kN (200 kips) of compression load and it can test a full wall 2.44 x 2.44m (8 by 8 feet). Other than compression, it is also able to apply bending and shear to the wall. The structural, hydraulic and electronic design as well as the computer program to control and collect data were developed by the author, Dr. Rachel Sangree, Prof. Ben Schafer and Sr. Instrument Designer Nick Logvinovsky.

After the MDOF was finally built, full-scale walls and single studs were tested. It was decided to begin testing single studs in order to explore the impact of unbraced length and to learn more about the testing methods and apparatus. An example of finding is related to how the load should be applied to the stud to isolate composite action, which is not guaranteed in cold-formed steel buildings. It was found that if we apply the load on

the sheathing and stud at the same time we would get a peak load around 20% higher than if we apply the load only to the stud. The considerable increase of the peak load showed the need to build an apparatus that allows the load to be applied only to the stud and so isolate composite action. On the other hand, the variation of unbraced lengths was fundamental to understanding behavior of cold-formed steel studs where the dominant/expected limit state is length dependent: changing from local, to distortional, and finally to global buckling modes interacting with local buckling as unbraced length increases. More details about the single column testing can be found in Chapter 4.

After several conclusions were drawn from the single stud tests, we tested full-scale wall-stud assemblies, which is critical for fully exploring the system effects that exist in the wall. Thirteen walls in total were successfully tested. The main variable was the different combinations of sheathings. More details can be found in Chapter 5.

The test results of columns and full-scale walls were compared to the design methods proposed in past standards [1.6, 13]. Even though the design method developed by Winter and used nowadays presented higher nominal loads than the method proposed by Simaan and Peköz both showed to be conservative when compared to the tests.

The comparison between the design methods and tests showed in this dissertation showed the necessity of a new design method, as the available design methods showed to be conceptually limited, and overly conservative. Two design methods were developed: (i) use analytical approaches to find the buckling load and then the main specification to find the nominal load, or (ii) use CUFSM [1.14] to find the elastic buckling load and Direct Strength Method (DSM) to find the nominal load.

Proposed method (i) provides a hand-solution to engineers and it employs the effective width method found in the main spec of [1.15]. Timoshenko [1.16] presents a solution for studs connected to springs (Figure 1.1(d)). The solution was generalized and simplified and found an analytical approach to find the global buckling values. Local and distortional buckling, as will be shown, are slightly affected and so it remained almost the same solution as it was given before in the specification [1.15]. The equations to find the nominal load also remained the same.

Proposed method (ii) is based on the Direct Strength Method (DSM) as presented in Appendix 1 of AISI-S100-07 [1.15]. DSM relates the critical elastic buckling values: local, distortional and global buckling ($P_{cr\ell}$, P_{crd}, P_{cre}) of a column to the ultimate strength (nominal load (P_n)). The same method can be applied to beams using the proper variables ($M_{cr\ell}$, M_{crd}, M_{cre}) to find the ultimate strength (M_n). We used the program CUFSM developed by Schafer and Ádàny [1.14] to obtain the critical buckling values. CUFSM uses the finite strip method to find the eigenvalue of a cross-section at a given half-wave length, Figure 1.3.

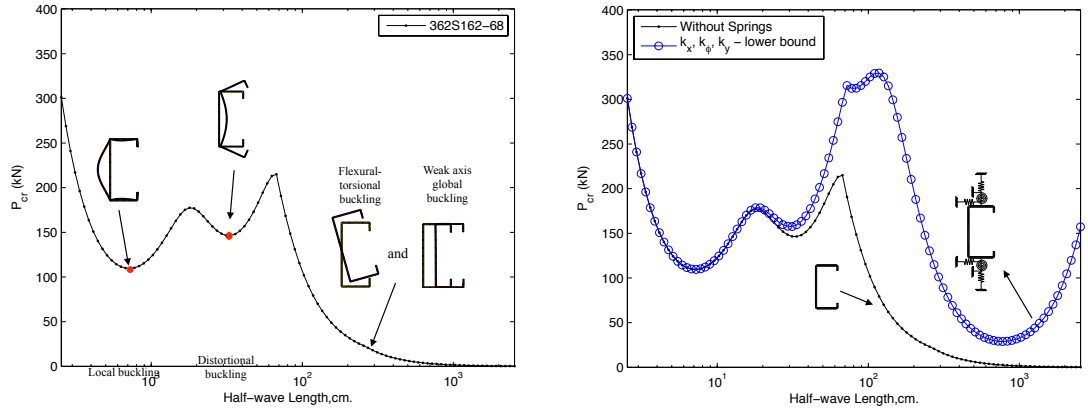

a) Buckling curve and modes for unrestrained cross-section.

b) Comparison between restrained and unrestrained buckling curves.

Figure 1.3 – Buckling curves for pin-pin 362S162-68 SSMA [1.17] cross-section using CUFSM.

The buckling curve of a lipped channel section 362S162-68 [1.17] is presented in Figure 1.3(a), as we can see it is clear that the minimum/critical eigenvalue load ($P_{cr\ell}$, P_{crd}, P_{cre}) and the correspondent buckling mode can be readily found if CUFSM is used. It is also interesting to note the effect of adding the appropriate springs (accounting for sheathing) to the cross-section, Figure 1.3(b); there is little influence in local and distortional buckling, but global buckling – including flexural-torsional and weak axis buckling – is significantly changed.

Chapter 6 and 7 present the design method proposed in this work. While Chapter 6 focus on the elastic stability solution of studs sheathed including numerical and analytical solution, Chapter 7 explains how the elastic values found can be used with DSM or the main specification to find the nominal load. Also explained in Chapter 6 and 7 the demands on the connections, and how they should be designed.

REFERENCES CHAPTER 1

1.1. Giles G. Green, G.W., T. R. Cuykendall, *Light Gage Steel Columns in Wall-braced Panels.* Cornell University Engiineering Experiment Station, 1947. **35**: p. 1-50.

1.2. AISI, *Light Gage Cold-Formed Steel Design Manual.* American Iron and Steel Institute, 1962.

1.3. Winter, G., *Lateral Bracing of Beams and Columns.* Journal of the Structural Division, 1960.

1.4. Simaan, A. and T.B. Pekoz, *Diaphragm Braced Members and Design of Wall Studs.* ASCE J Struct Div, 1976. **102**(1): p. 77-92.

1.5. Iourio, O. and B.W. Schafer, *Compilation of k values*, in *A supplemental report for AISI-COFS Project on Sheathing Braced Design of Wall Studs*2008, The Johns Hopkins University: Baltimore.

1.6. AISI-S211, *North American Specification for the Design of Cold-Formed Steel Structural Members.* American Iron and Steel Institute, 2007.

1.7. Telue, Y. and M. Mahendran, *Behaviour of cold-formed steel wall frames lined with plasterboard.* Journal of Constructional Steel Research, 2001. **57**(4): p. 435-452.

1.8. Okasha, A.F., *Performance of Steel Frame/Wood Sheathing Screw Connections Subjected to Monotonic and Cyclic Loading*, 2004, McGill University.

1.9. Fiorino, L., G. Della Corte, and R. Landolfo, *Experimental tests on typical screw connections for cold-formed steel housing.* Engineering Structures, 2007. **29**(8): p. 1761-1773.

1.10. Laboube, R.A. and P.F. Findlay, *Wall stud-to-track gap: Experimental investigation.* Journal of Architectural Engineering, 2007. **13**(2): p. 105-110.

1.11. Miller, T.H. and T. Pekoz, *Behavior of Gypsum-Sheathed Cold-Formed Steel Wall Studs.* Journal of Structural Engineering, 1994. **120**(5): p. 1644-1650.

1.12. Miller, T.H. and T. Pekoz, *Behavior of cold-formed wall stud-assemblies.* Journal of structural engineering New York, N.Y., 1993. **119**(2): p. 641-651.

1.13. AISI, *Light Gage Cold-Formed Steel Design Manual.* American Iron and Steel Institute, 1980.

1.14. Schafer, B.W. and S. Adany. *Buckling analysis of cold-formed steel members using CUFSM: Conventional and constrained finite strip methods*. in *Eighteenth International Specialty Conference on Cold-Formed Steel Structures: Recent Research and Developments in Cold-Formed Steel Design and Construction*. 2006. Orlando, FL.

1.15. AISI-S100, *North American Specification for the Design of Cold-Formed Steel Structural Members.* American Iron and Steel Institute, 2007.

1.16. Timoshenko, S.P., Gere, James M., *Theory of Elastic Stability*1961, New York: McGraw-Hill.

1.17. SSMA, *Product Technical Information, ICBO ER-4943P*, S.S.M. Association, Editor 2001.

CHAPTER 2 - PAST AND EXISTING DESIGN METHODS FOR SHEATHED COLD-FORMED STUD WALLS

This chapter discusses the three design methods that were proposed by AISI. The first method used to design sheathed stud walls was proposed in 1962 [2.1], the design method was revisited and a new proposal was published in 1980 [2.2], which remained on the specification until 2004 when a newer method was adopted [2.3].

The discussions include the development of an understanding of the equations used in the design methods, which aim largely to establish the assumptions and simplifications used. Special attention is given to the "2a" rule that has been used since 1962 in all design methods, even though – as it will be shown – it is an arbitrary assumption that doesn't reflect reality.

2.1. AISI 1962-1980 AND 2004-PRESENT(2011)

The 1962 AISI Specification [2.1] was based on two papers: one was published in 1947 by Cornell University that included three authors: Green, Winter and Cuykendall [2.4], and the other paper revisits the problem, published in 1960 by Winter [2.5] who had been a co-author on the previous paper. Winter highlighted at the very beginning of his paper:

> *"[A] simple elementary method is developed that permits the lower limits of strength and rigidity of lateral support to be computed in order to provide "full bracing" to columns and beams.*

"Full bracing" is defined as equivalent in effectiveness to immovable lateral support" [2.5]

Winter [2.5] found that a small strength and stiffness were necessary to guarantee "full bracing" to the stud, therefore the connection should be checked just to make sure that the sheathing is able to restrain it. Additionally to strength and stiffness the AISI-1962 [2.1] specification also requires that maximum space between fasteners is checked (For more information on the design methods see [2.6]).

Even though the AISI-1962 [2.1] specification and the AISI-2007 [2.3] are based on the same research, they have some differences. The AISI-2007 [2.3] is more of an "analysis" method in that it attempts to provide the capacity regardless of how the member fails, while the AISI-1962 [2.1] is a more "prescriptive" method where the limit state has been pre-selected and the provisions are intended to insure that stiffness (k) and fastener spacing (a) are selected such that this limit state does occur.

The 1962 specification [2.1] insures that global buckling load in the weak axis (P_{cry}) over a buckling length equal to two times the fastener spacing ($2a$) is greater or equal to the strong axis buckling load over the column length (L). P_{cry} over L and supported by lateral springs at the fastener location is also required to be greater or equal to the squash load ($P_y=Af_y$). If both requirements for P_{cry} are guaranteed the global buckling load (P_{cr}) is given by the buckling load in the strong axis (P_{crx}) over L. It is important to note that AISI-1962 [2.1] did not check for flexural-torsional buckling.

While AISI-1962 [2.1] insures that the buckling load is governed by P_{crx}, the buckling load in AISI-2007 [2.3] is given by lowest buckling load between weak-axis

buckling (P_{cry}) and flexural-torsional buckling (P_{crFT}). However, P_{cry} must be checked over a buckling length of 2a and P_{crFT} must be checked over a buckling length *2a* for torsion and *L* for strong-axis buckling, in both checks – P_{cry} and P_{crFT} – the springs that represents the fasteners are disregarded (*k=0*).

The fastener demand on the fastener-sheathing assembly shall also be checked. While AISI-1962 [2.1] adopted the equations proposed by Winter [2.5], the AISI-2007 [2.3] simplified the problem and adopted the well know 2% rule, where the bracing force is given by 2% of the axial load. In fact, Schafer [2.6] shows that the use of AISI-1962 [2.1] equations to check fastener demand will lead values similar than the 2% rule. Table 2.1 summarizes the comparison between AISI-1962 [2.1] and AISI-2007 [2.3].

Table 2.1 – Summary of comparison between AISI-1962 [2.1] and AISI-2007 [2.3].

AISI-1962 [2.1]	AISI-2007 [2.3].
$P_{cr}=P_{crx}((KL)_x=L)$ subject to $P_{cry}(k=0, (KL)_y=2a) \geq P_{crx}((KL)_x=L)$ $P_{cry}(k@a, (KL)_y=L) \geq Af_y$ and ~2%P for fasteners	$P_{cr}=\min(P_{cry}, P_{crFT})$ where $P_{cry}(k=0, (KL)_y=2a)$ $P_{crTF}(k=0, (KL)_x=L, (KL)_t=2a)$ and 2%P for fasteners

2.2. AISI 1980-2004

From 1980 to 2004 AISI adopted the design method for sheathed walls developed by Simaan and Peköz [2.7]. In [2.7] the buckling load is found by solving an energy problem. The total potential energy of the sheathed wall (Π), Eq. (2.1), consists in three components: (i) the strain energy of the stud (U_{stud}), which incorporates the contribution of bending, warping and twist, (ii) the potential energy of the concentric axial load

(W_{load}), and (iii) the energy of the diaphragm ($U_{diaphragm}$), which a priori includes the contribution of diaphragm strain energy due to shear distortion ($U_{diaphragm-shear}$), and strain energy of diaphragm due to rotational distortion ($U_{diaphragm-rotation}$).

$$\Pi = U_{stud} + U_{diaphragm} + W_{load} \tag{2.1}$$

The buckling load is given in [2.7] by using the Rayleigh-Ritz method to solve Eq. (2.1). An important observation is that there is no mention about the stiffness k_y and k_ϕ showed in Figure 1.1(e) of Chapter 1. In the solution $U_{diaphragm-shear}$ is the strain energy contribution given by a rotational spring on the plane of the sheathing. In fact, the rotational restriction provided by the connection sheathing-fastener-stud is little if any, but the rotational spring in discussion is actually the product of the binary created by two fasteners with lateral stiffness k_x.

AISI [2.8] in 1980 adopted a couple of simplifications, an example is that they ignored the diaphragm rotational stiffness since it provided very little resistance. An important advance of the design method is that it provides a way to verify not only flexural buckling but also flexural-torsional buckling, which hadn't been considered before. In the method flexural buckling still considered the buckling length in the minor axis equal to "2a", more discussions about this assumption are provided in the following sections. The design method [2.8] also proposed a way of checking the shear strain resistance of the sheathing, and it allows the engineer to design studs with sheathing on

one flange only, or with different sheathing, even though it is not explicit in [2.8] how to proceed with the design.

Nonetheless the design method given in [2.8] is considered, as agreed by other authors [2.6, 9], too complex for ordinary design method. Trestain [2.9] even highlighted that "Provided there is adequate steel bridging, the approach in Section D4 (a) [the method discussed here] can produce a lower capacity than an all steel approach". Due to its complexity and inefficiency the method was abandoned in 2004.

2.3. THE "2a" FASTENER SPACING RULE

As detailed in the previous sections, since the first specification in 1962, the "2a" rule has been used. There is no explanation for this rule other than one fastener may be defective or missed and so design should account for a stud in this condition.

The study of this section aims to show the inefficiency of this arbitrary rule. The study consists of analyzing a column under flexural buckling, in which the sheathing is modeled as translational spring elements. The springs are considered as random variables, all other variables are deterministic, see Figure 2.1. In the study expected statistics for the fastener stiffness are first established, and then used to find the flexural buckling load (P_{cr}) of the column. A Monte Carlo simulation is performed to determine the variation in P_{cr} due to the variation of the spring stiffness and the probability of failure of a fastener. The P_{cr} values are used to find the resistance of each configuration.

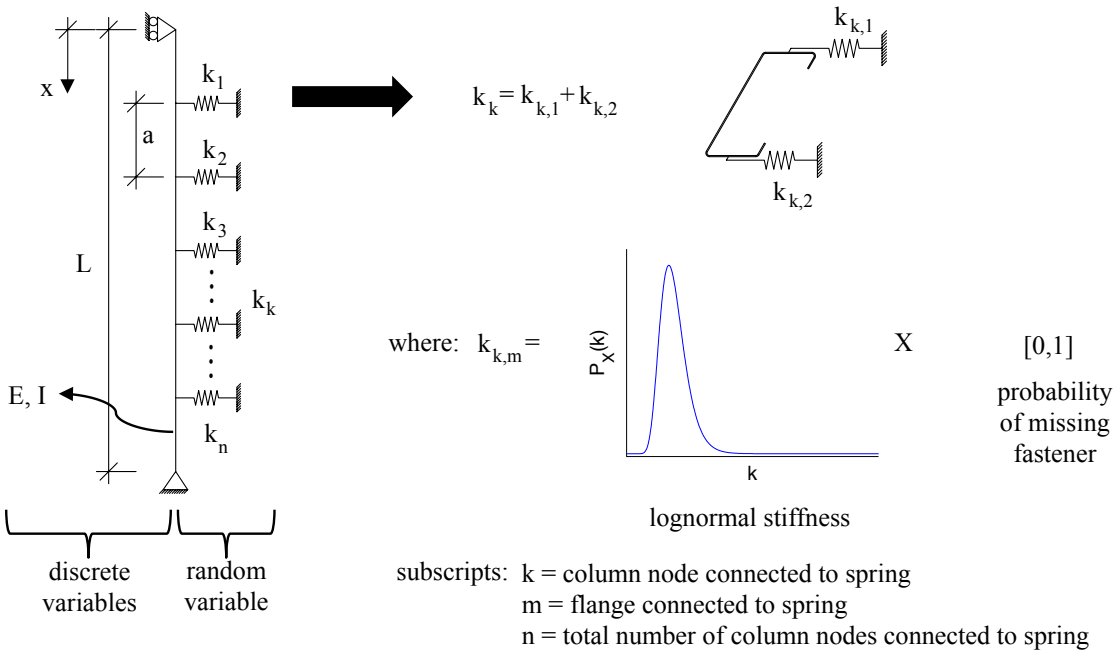

Figure 2.1 – Problem definition.

2.3.1. STATISTICAL STUDY OF THE IN-PLANE TRANSLATIONAL SPRING STIFFNESS (k_x)

In Chapter 3, lateral stiffness tests are performed in which fastener spacing, distance to the edge of the board, sheathing humidity level and possibility of overdriving a fastener were varied. This section is based on the tests reported in Chapter 3 that used OSB boards (a total of 21 tests). In the tests, two-lipped channels are pulled apart (tension) or pushed together (compression), but they are connected by the flanges to two pieces of sheathing through eight fasteners, which provide a resistance to the movement. The resistance can be determined as stiffness since the displacement is also recorded. Chapter 3 includes complete results and discussions about the lateral stiffness test (see Figure 3.3 for reference).

To perform the Monte Carlo simulation varying the spring stiffness, it was necessary to find the best probability distribution for the available test results. Two distributions were considered: normal and lognormal. Figure 2.2 shows both distributions compared to the test results in a Cumulative Distribution Function (CDF) plot. The goodness of fit was compared using the Kolmogorov-Smirnov test, while the normal curve gives a statistically significant difference (p-value) of 0.76, the lognormal curve gives a p-value of 0.98. The lognormal distribution was considered appropriate to be used in the reliability study.

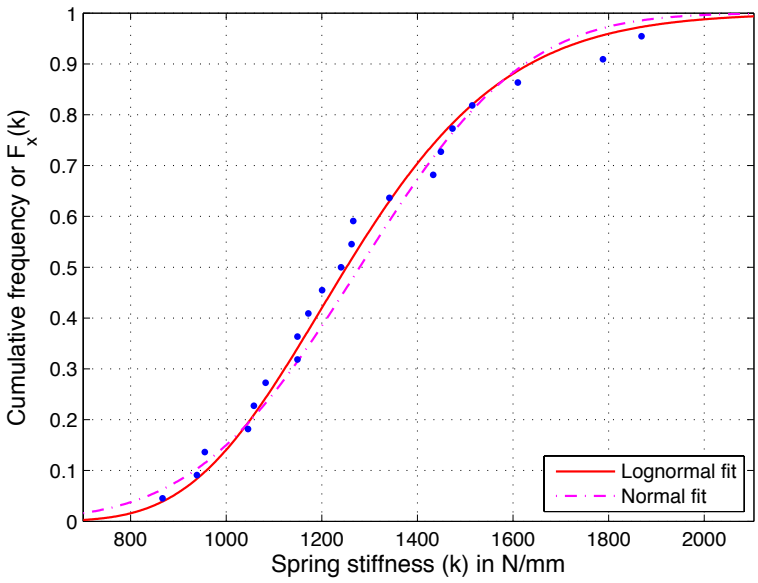

Figure 2.2 – Curve fitting study for spring stiffness (k). Mean of k is 1,278.5 N/mm (7.2974 kip/in) and variance is 72,511 $(N/mm)^2$ $(2.3623\ (kip/in)^2)$.

2.3.2. RAYLEIGH-RITZ APPROACH TO FIND THE GLOBAL BUCKLING LOAD (P_{cre}) OF COLUMNS SUPPORTED BY DISCRETE SPRINGS (k_x)

Chen and Lui [2.10] provide a clear explanation of the Rayleigh-Ritz method used – in this case – to find the buckling load or eigen-value of a column supported laterally by discrete springs. They summarize that by using the Rayleigh-Ritz method and assuming a displacement function that satisfies the geometric boundary condition: "[A] structural system with an infinite degree of freedom is now reduced to a system of finite degrees of freedom. As a result of this simplification, the total potential energy function reduces from a functional to a function, and, so, instead of using the calculus of variations (which operates on functionals), we can now use ordinary calculus (which operates on functions) to obtain solutions directly from the total potential energy function." Given that we assumed a displacement equation, Eq. (2.2):

$$\bar{v} = \sum_{i=1}^{n} a_i \phi_i = \sum_{i=1}^{n} a_i \sin(\frac{i\pi x}{L}) \tag{2.2}$$

The strain energy, the potential energy due to the axial force P and the potential energy due to the discrete springs can be expressed respectively by Eq. (2.3), (2.4) and (2.5), the bar above the strain and potential energy represents that the energy equations are using an approximate deflection curve. The total potential energy is equal to the sum of Eq. (2.3), (2.4) and (2.5).

$$\bar{U} = \frac{1}{2}\int_0^L EI(\frac{d^2\bar{v}}{dx^2})^2 dx \tag{2.3}$$

$$\bar{V}_P = \frac{-P}{2}\int_0^L \left(\frac{d\bar{v}}{dx}\right)^2 dx \tag{2.4}$$

$$\overline{V_S} = \sum_{k=1}^{n} \frac{1}{2} k_k \left(\bar{v}\right)^2 \tag{2.5}$$

By the principle of stationary total potential energy, the total potential energy differentiated for a_i is equal to zero, Eq. (2.6), and so the global-buckling load can be found by solving this eigen-value problem.

$$\frac{\partial(\overline{U} + \overline{V_P} + \overline{V_S})}{\partial a_i} = 0 \tag{2.6}$$

The components of the total potential energy (Eq. (2.3), (2.4) and (2.5)) differentiated for a_i can be represented in a matrix format (Eq. (2.7), (2.8) and (2.9)).

$$\frac{\partial \overline{U}}{\partial a_i} = \frac{EI\pi^4}{2L^3} \begin{bmatrix} 1^4 & 0 & 0 & 0 & 0 \\ & \ddots & 0 & 0 & 0 \\ & & i^4 & 0 & 0 \\ & & & \ddots & 0 \\ sym & & & & n^4 \end{bmatrix} \begin{bmatrix} a_1 \\ \vdots \\ a_i \\ \vdots \\ a_n \end{bmatrix} \tag{2.7}$$

$$\frac{\partial \overline{V_P}}{\partial a_i} = \frac{-P\pi^2}{2L} \begin{bmatrix} 1^4 & 0 & 0 & 0 & 0 \\ & \ddots & 0 & 0 & 0 \\ & & i^4 & 0 & 0 \\ & & & \ddots & 0 \\ sym & & & & n^4 \end{bmatrix} \begin{bmatrix} a_1 \\ \vdots \\ a_i \\ \vdots \\ a_n \end{bmatrix} \tag{2.8}$$

$$\frac{\partial \overline{V_S}}{\partial a_i} = \sum_{k=1}^{n} k_k B \begin{bmatrix} a_1 \\ \vdots \\ a_i \\ \vdots \\ a_n \end{bmatrix} \tag{2.9}$$

where B is:

$$B = \begin{bmatrix} \sin\left(\frac{1\pi x_k}{L}\right)\sin\left(\frac{1\pi x_k}{L}\right) & \cdots & \sin\left(\frac{1\pi x_k}{L}\right)\sin\left(\frac{j\pi x_k}{L}\right) & \cdots & \sin\left(\frac{1\pi x_k}{L}\right)\sin\left(\frac{n\pi x_k}{L}\right) \\ & \ddots & \vdots & \vdots & \vdots \\ & & \sin\left(\frac{i\pi x_k}{L}\right)\sin\left(\frac{j\pi x_k}{L}\right) & \cdots & \sin\left(\frac{i\pi x_k}{L}\right)\sin\left(\frac{n\pi x_k}{L}\right) \\ & & & \ddots & \vdots \\ sym & & & & \sin\left(\frac{n\pi x_k}{L}\right)\sin\left(\frac{n\pi x_k}{L}\right) \end{bmatrix} \quad (2.10)$$

The eigen-value problem cannot be simplified since the buckled shape developed by the minimum elastic buckling load may require many sine waves, Figure 2.3, depending on the spring stiffness. If the spring stiffnesses are very small, the column buckles in just one half-wave length, on the other extreme, if the springs are very rigid the column is forced to buckle in several waves, which coincides to the number of springs plus one. For the spring stiffnesses reported in Chapter 3, the half-wave lengths are close to two times the fastener spacing "2a", which might be a justification for the "2a" rule, but such stiffnesses may not always be provided to the column.

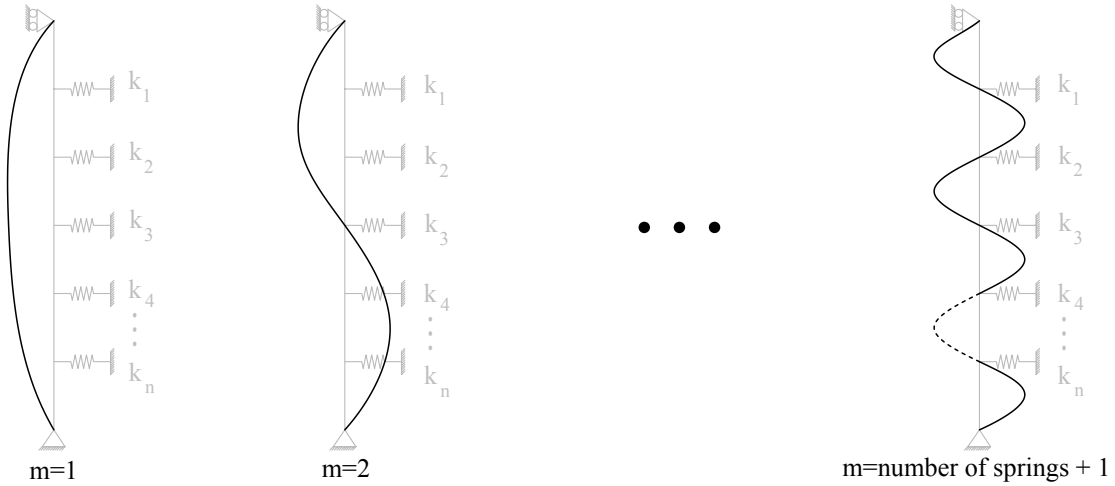

Figure 2.3 – Buckled shape for different wavelengths ("m" is the number of half waves).

For validation a finite element (FE) model was generated in ABAQUS [2.11], the model consisted of a column L=2.54m (100in) long, cross-section area A=211mm^2 (0.327in^2), moment of inertia I=47,158mm^4 (0.1133in^4), Young's modulus E=203GPa (29500ksi), yield stress f_y=227MPa (33ksi) and fastener spacing a=20.3cm (8in), starting at 5.1cm (2in) from the stud end by a springs of stiffness k_k=2.3kN/mm (k_k=13kip/in = 2 springs of 6.5kip/in). Comparing P_{cr} of the analytical solution to the FE model a difference of only 1.3% is found, thus suggest that the analytical solution is a good approximation.

2.3.3. MONTE CARLO SIMULATION OF RESTRICTED COLUMNS

Since both flanges of a stud are connected to the sheathing, there are two ways of understanding the defective fastener: case (i) both fasteners are defective and we would have to consider no fasteners over a length "2a"; and case (ii) a single fastener is defective but the other flange still connected, which is the more likely defect. Both cases are simulated here.

The details for the models (L, E, I, and a) are the same as provided in the previous section, but the spring stiffness is generated using the lognormal PDF curve defined in section 2.3.1, also to each fastener location (case (i)) or fastener by itself (case (ii)) there is a probability of failure (P_f) associated to it, P_f is varied from 0, 1, 2, 5, 8, and 10%. For each probability of failure 1000 models were analyzed, Figure 2.4.

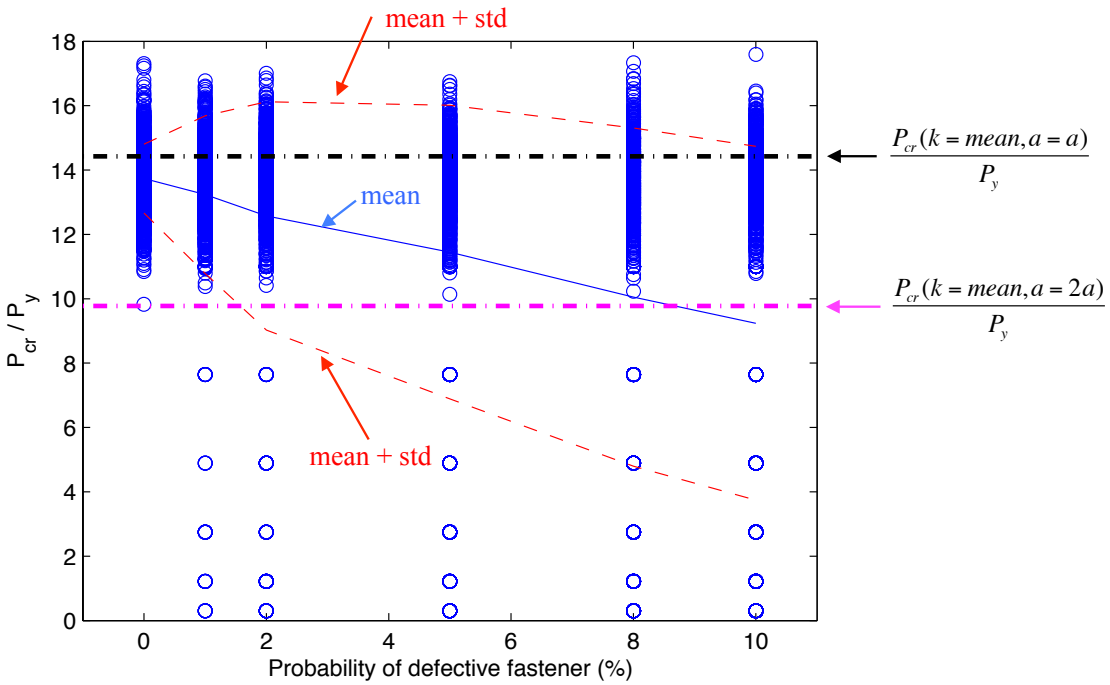

a) Case (i) – perfectly correlated fastener failure

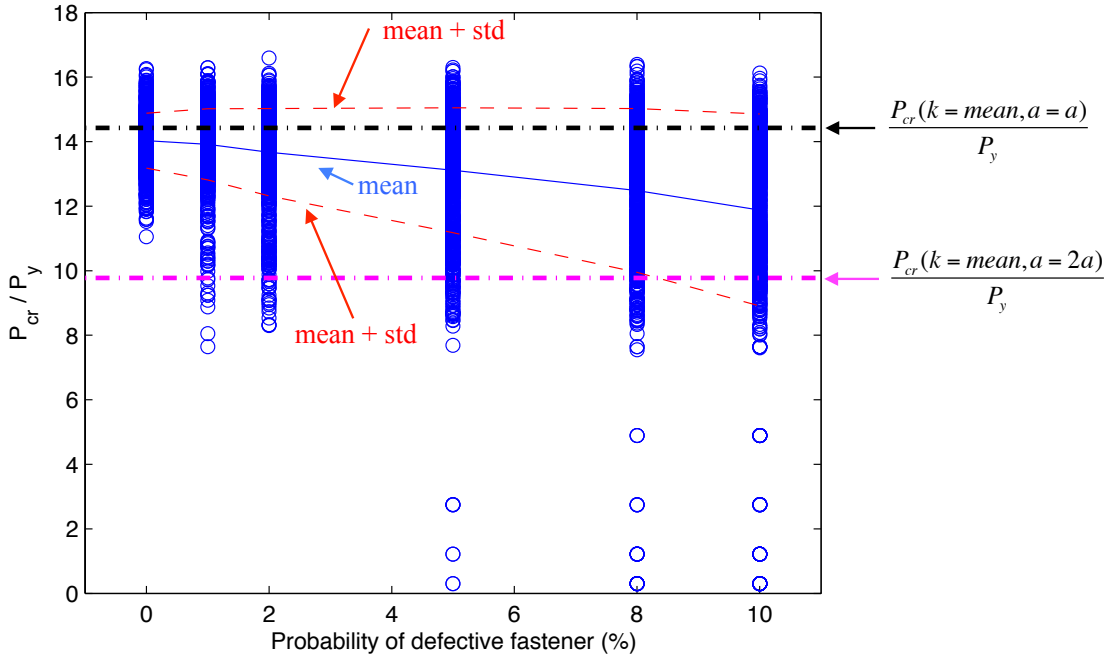

b) Case (ii) – independent fastener failure

Figure 2.4 – Global buckling Monte Carlo simulation of columns with discrete connections

As depicted in Figure 2.4, case (ii) shows less variability and higher mean values for the buckling load. In the same graph the buckling load of models that consider the fastener spacing of "a" or "2a" (8in (20.3cm) or 16in (40.6cm)), k_k equal to the mean value found in the tests and no fastener failure (P_f=0%) is also plotted. The mean value for all the simulations without fastener failure (P_f=0%) is very close to the value of P_{cr}(k=mean, a=a) as expected. The line defined by P_{cr}(k=mean, a=a) also shows how much the mean buckling load varies depending on the probability of fastener failure. The second horizontal line (P_{cr}(k=mean, a=2a)) clearly shows how conservative it is to consider a buckling length equal to "2a", the mean buckling load only gets closer to the horizontal line (P_{cr}(k=mean, a=2a)) in case (i) with P_f=10%.

2.3.4. RESISTANCE FACTOR

To explore the impact of "2a" rule on design, we consider the means by which variability is intended to be added to the design methods. According to the Load and Resistance Factor Design (LRFD) method the nominal resistance of a member (R_n) shall be multiplied by a resistance factor (ϕ). Assume the nominal load (P_n) is given by P_n=P_{cr} we may then explore what resistance factor (ϕ) would be appropriately used to establish a target reliability index of 2.5.

AISI-2007 [2.12] presents in chapter F an equation to find the resistance factor (ϕ), Eq. (2.11).

$$\phi = C_\phi \left(M_m F_m P_m \right) e^{-\beta_o \sqrt{V_M^2 + V_F^2 + C_P V_P^2 + V_Q^2}} \tag{2.11}$$

In Eq. (2.11) the values for the variables were selected according to the instructions in [2.12], meaning that: C_ϕ (calibration coefficient) is equal to 1.52, M_m (mean value of material factor) is equal to 1.10, F_m (mean value of fabrication factor) is equal to 1.00, Pm (mean value of professional factor) is equal to 1.00, β_o (target reliability index) is equal to 2.5, V_M (coefficient of variation of material) is equal to 0.1, C_P (correction factor) is given by the result of $C_P=(1+1/n)*((n-1)/(n-3))$, "n" being the number of simulations (n=1000), which results in our case to $C_P=1.003$,V_P (coefficient of variation of test results) is given by calculating the coefficient of variation for each probability of failure, and finally V_Q (coefficient of variation of load effect) is equal to 0.21. With all these values the resistance factor (ϕ) can be found using Eq. (2.11).

As provided in Table 2.2 the resistance factor (ϕ) decrease – as expected – with the increase of the probability of defective fastener failure (P_f) in both cases, but it decreases a lot faster in case (i) than in case (ii). Given ϕ=0.85 in column design today and given uncorrelated fastener failure (case(ii)), this study shows that about 5% of fasteners may be defective and it would still be reasonable to ignore the loss in capacity due to defective fasteners.

Table 2.2 – Resistance factor (ϕ) for different probability of defective fastener perfectly correlated (case (i)) vs. uncorrelated (case (ii)) defective fasteners.

	Problem conception	Probability of defective fastener (P_f)					
		0%	1%	2%	5%	8%	10%
Resistance factor (ϕ)	Case (i)	0.89	0.79	0.66	0.52	0.40	0.34
	Case (ii)	0.91	0.89	0.88	0.83	0.76	0.70

Therefore, the use of ϕ to take in account the probability of a defective fastener instead of an unrealistic and conservative rule would be a considerable advance in the

design of wall-studs. But, at the same time, a less complex design method has to be developed that takes in account the additional energy provided by the springs to the studs. This research project has as one of its main goals to develop a realistic and less complex design method.

REFERENCES CHAPTER 2

2.1. AISI, *Light Gage Cold-Formed Steel Design Manual.* American Iron and Steel Institute, 1962.

2.2. AISI, *Light Gage Cold-Formed Steel Design Manual.* American Iron and Steel Institute, 1980.

2.3. AISI-S211, *North American Specification for the Design of Cold-Formed Steel Structural Members.* American Iron and Steel Institute, 2007.

2.4. Giles G. Green, G.W., T. R. Cuykendall, *Light Gage Steel Columns in Wall-braced Panels.* Cornell University Engiineering Experiment Station, 1947. **35**: p. 1-50.

2.5. Winter, G., *Lateral Bracing of Beams and Columns.* Journal of the Structural Division, 1960.

2.6. Schafer, B.W., O. Iourio, and L.C.M. Vieira Jr, *Notes on AISI Design Methods for Sheathing Braced Design of Wall Studs in Compression*, in *A supplemental report for AISI-COFS Project on Sheathing Braced Design of Wall Studs*2008, The Johns Hopkins University: Baltimore.

2.7. Simaan, A. and T.B. Pekoz, *Diaphragm Braced Members and Design of Wall Studs.* ASCE J Struct Div, 1976. **102**(1): p. 77-92.

2.8. AISI-S100, *North American Specification for the Design of Cold-Formed Steel Structural Members.* American Iron and Steel Institute, 2001.

2.9. Trestain, T., *AISI Cold-Formed Steel Framing Design Guide CF02-1*, 2002, American Iron and Steel Institute: Washigton D.C.

2.10. Chen, W.-F., *Structural Stability: Theory and Implementation*, ed. E.M. Lui1987, New York: Elsevier.

2.11. ABAQUS, *ABAQUS/Standard Version 6.7-1*, D. Systemes, Editor 2007.

2.12. AISI-S100, *North American Specification for the Design of Cold-Formed Steel Structural Members.* American Iron and Steel Institute, 2007.

CHAPTER 3 - FASTENER STIFFNESS

The objective of this chapter is to provide the stiffness and strength characteristics for walls comprised of cold-formed steel studs stabilized by sheathing. A short summary of rotational stiffness (k_ϕ) and out-of-plane stiffness (k_y) is presented. But the main focus of this chapter is on the primary source of stability resistance for the studs, which is the translational (lateral) stiffness (k_x). This chapter separates the source of this translational stiffness into two parts: local and diaphragm. To analyze the local stiffness an experimental study consisting of small-scale stud-fastener-sheathing assemblies is conducted. In these tests, sheathing type, stud spacing, fastener spacing, edge distance, environmental conditions, and construction flaws are all varied. The results provide a characterization of the local stiffness and strength that is supplied as the fasteners bear and rotate in a stud-sheathing assembly. A simplified and conservative analytical model, supported by more detailed finite element modeling is also developed, and is appropriate for finding the local stiffness when testing is unavailable. Diaphragm stiffness develops as the sheathing itself undergoes shear, which translates into a lateral resistance at the stud-to-fastener locations. A simple analytical model for the translational stiffness supplied by the sheathing diaphragm action is also proposed and validated. The importance of including both local and diaphragm stiffness is illustrated with a test on a full-scale cold-formed steel stud wall. For the first time, a comprehensive bracing model for sheathing-braced stud walls that integrates the two forms of lateral resistance: local and diaphragm is provided.

3.1. INTRODUCTION

The stud-to-fastener connection undergoes different mechanisms as the stud deforms laterally (e.g. due to the amplification of weak-axis bending from a flexural buckling mode) and forces develop between the stud and sheathing, including: tilting, Figure 3.1(b); tilting and bending, Figure 3.1(c); and tilting, bending, and initiation of pull-through of the sheathing, Figure 3.1(d).

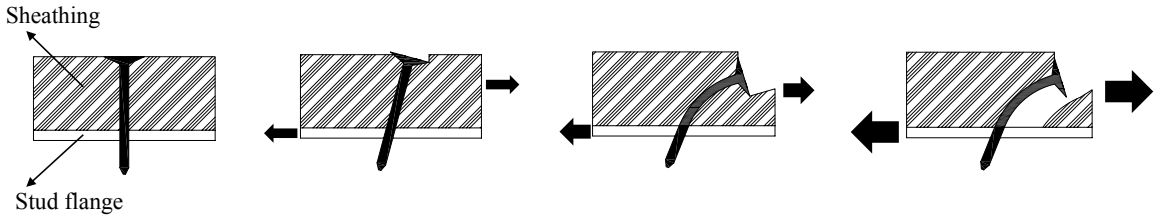

Figure 3.1 – Basic behavior of fastener in stud-to-sheathing connection under increasing lateral deformation of the stud flange. a) Fastener attaching sheathing to steel, b) Tilting of fastener under small lateral deformation, c) Tilting and bending of fastener under increased lateral deformation d) Tilting, bending, and bearing of the fastener under large lateral deformation

The stiffness contribution that the stud-fastener-sheathing system supplies to the stud, as said before, may be divided into three parts: rotational, translational in the plane of the board, and translational out of the plane of the board. The rotational stiffness (k_ϕ) is engaged when the stud flange rotates against the sheathing, causing an axial force in the fastener and a compression force at the stud flange edge in contact with the sheathing (creating a moment couple resisting further rotation) as detailed in [3.1] and summarized in Section 3.2. The out-of-plane lateral resistance, k_y, that develops from the sheathing bending is discussed in [3.2] and summarized in Section 3.3.

The translational stiffness (k_x) is engaged when the stud flange tries to translate (shear) relative to the sheathing. The stud flange translation may derive from weak-axis flexural buckling of the stud (where both of the flanges move in the same direction), or from torsional buckling of the stud (where the flanges translate, but in opposite directions). Thus, k_x is the primary source of resistance for the weakest two global buckling modes of the stud: weak-axis flexure and flexural-torsional buckling. The translational resistance derives from two parts: local tilting and bearing resistance at the fastener location (depicted in Figure 3.1) and termed $k_{x\ell}$ in this work, and direct diaphragm resistance of the sheathing as a whole, k_{xd}.

3.2. ROTATIONAL STIFFNESS (k_ϕ)

As the flange attempts to rotate (due to buckling or other deformations) local tilting of the fastener combined with bending of the sheathing and contact between the flange and sheathing restricts this movement in a manner that may be idealized by a rotational resistance, k_ϕ. Rotational tests were performed on the configurations tested herein (362S162-68 studs connected every 12 in. Oriented strand board (OSB) (11.1 mm, (7/16 in.), rated 24/16, exposure 1) - number 8 screws (Simpson #8 x 49.2 mm (1 15/16 in.)) and gypsum board (GYP) (12.7 mm, (½ in.) Sheetrock Regular) - number 6 screws (Simpson #6 x 41.3 mm (1 5/8 in.)) to check the methodology developed by Schafer et al. [3.3], Table 3.1.

Table 3.1 – Rotational stiffness tests – Stiffness reported in units lbf-in./in./rad

Test	k_ϕ	$k_{\phi w}$	$k_{\phi c}$	k_ϕ - 10%Mmax
BBB-GYP-12-6-6-01	68	283	90	77
BBB-GYP-12-6-6-03	78	-	-	67
BBB-GYP-12-6-6-04	79	255	115	79
BBB-GYP-12-6-6-05	58	193	82	52
average	70.8	243.7	95.7	68.9
COV	0.14	0.19	0.18	0.18

Test	k_ϕ	$k_{\phi w}$	$k_{\phi c}$	k_ϕ - 10%Mmax
BBB-OSB-12-8-6-02	81	288	113	103
BBB-OSB-12-8-6-06	64	201	95	85
BBB-OSB-12-8-6-07	67	212	98	86
BBB-OSB-12-8-6-08	69	243	97	91
average	70.3	236.0	100.8	91.4
COV	0.11	0.17	0.08	0.09

The semi-empirical method developed in Schafer et al. [3.3] may be summarized in three equations shown below. Eq. (3.1) provides the stiffness due to the connection itself, as a function of the stud thickness t (in in.) and steel modulus, E (in psi). Eq. (3.2) gives the rigidity provided by the sheathing $(EI)_w$ for different materials and grain orientations (as commonly tabled by APA [3.4]), and different tributary width, d_f. Finally Eq. (3.3) combines both stiffnesses as two rotational springs in series.

$$k_{\phi c} = 0.00035Et^2 + 75 \tag{3.1}$$

$$k_{\phi w}=(EI)_w/d_f \tag{3.2}$$

$$k_\phi=1/(1/k_{\phi c} + 1/k_{\phi w}) \tag{3.3}$$

The test values may be compared to the values predicted by the Eq.'s (3.1) to (3.3). For the connection stiffness, Eq. (3.1) predicts a $k_{\phi c}$ of 529 N-mm/mm/rad (119 lbf-in/in/rad), while the mean measured values are 427 N-mm/mm/rad (96 lbf-in/in/rad) in the gypsum and 449 N-mm/mm/rad (101 lbf-in/in/rad) in the OSB, as reported in Table 3.1. Noting that the standard deviation on the original data used to calibrate Eq. (3.1) in [3.3] was 107 N-mm/mm/rad (24 lbf-in/in/rad) the measured connection stiffness is 1 standard deviation below the average values, reasonable if not perfect agreement.

For the sheathing stiffness $k_{\phi w}$ is determined by Eq. (3.2) and the appropriate industry standard $(EI)_w$ values. For gypsum, $k_{\phi w}$ is expected to be between 556 and 1481 N-mm/mm/rad (125 and 333 lbf-in/in/rad) (from min and max values reported by [3.5]) compared with an average measured $k_{\phi w}$ of 1080 N-mm/mm/rad (243 lbf-in/in/rad). The limited rotational capacity of gypsum sheathed specimens is again noted. For OSB Eq. (3.2) predicts $k_{\phi w}$ of 494 N-mm/mm/rad (111 lbf-in/in/rad) for stress perpendicular to strength axis (as-tested here) and 2406 N-mm/mm/rad (541 lbf-in/in/rad) for stress parallel to the strength axis, which may be compared with an average measured $k_{\phi w}$ of 1050 N-mm/mm/rad (236 lbf-in/in/rad). The APA [3.4] values are again shown to provide a conservative estimate.

3.3. OUT-OF-PLANE LATERAL STIFFNESS (k_y)

Traditionally, when considering sheathing as bracing, the out-of-plane stiffness of the sheathing is ignored. In-plane the sheathing restrains weak-axis bending and torsion of the stud, while out-of-plane the sheathing increases major-axis bending stiffness. As flexural-torsional buckling is a common mode in wall studs, this out-of-plane restraint may be influential. The out of plane stiffness that develops from the sheathing under major-axis bending, Figure 3.2, is the ratio of the force in each fastener to the respective deflection at the fastener. The force at each fastener can be found by the difference in the shear force over the tributary length, thus Eq. (3.4) gives the out-of-plane stiffness (this is the solution for a beam that deforms in a single-half-sine wave).

$$k_y = \frac{2E_w I\pi^3}{L^3}\sin\left(\frac{\pi d_f}{2L}\right) \approx \frac{E_w I\pi^4 d_f}{L^4} \tag{3.4}$$

If the sheathing is fully composite with the stud, then the inertia of the board *I*, takes its upperbound value: $I=w_{tf}t_{board}^3/12+bt_{board}(y_{GC}+t_{board}/2)^2$). Or, if no composite action develops then I is simply $w_{tf}t_{board}^3/12$ resulting in a lower bound value. Industry tabled values for EI as utilized for $k_{\psi w}$ determination may provide this lower bound approximation.

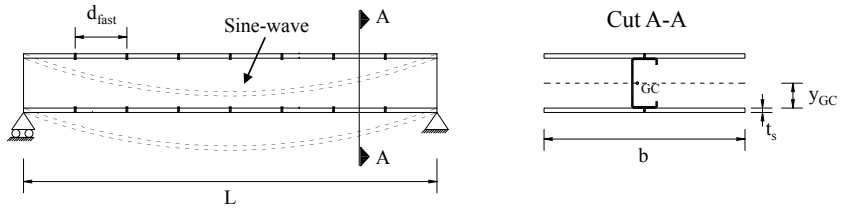

a) Stud under a sine-wave curve on the major axis b) Cross-section

Figure 3.2 – Analytical model for k_y

3.4. LOCAL MODEL FOR TRANSLATIONAL STIFFNESS ($k_{x\ell}$) AND STRENGTH

3.4.1. Test setup

Winter's method for determining the translational stiffness of a stud-sheathing assembly employs a simple symmetrical shear test, as illustrated in Figure 3.3. Two sections of studs are connected by identical sheathing on both sides and then pulled laterally (perpendicular to the long direction of the studs), such that shear must develop in each of the fasteners to resolve the applied tension. In the testing reported here, to minimize bending of the studs under the applied force, the stud webs are "sandwiched"

between a 7.94 mm (5/16 in.) thick steel plate and two angles 6.35 mm (¼ in. thick), bolted together at 10 locations along the length of the stud (see Figure 3.3(c) section A-A). The plate is attached to two hot-rolled 38.1 by 38.1 by 6.35 mm (1½ by 1½ by ¼ in.) angles that are then bolted to a larger structural WT section (WT 11 x 9) that connects to the actuators in the universal test frame: a 445kN (100 kips) MTS actuator with 152.4 mm (6 in.) stroke is utilized to apply the loads.

The studs used in the test are 362S162-68's [3.6] throughout. This is the same stud utilized in the tests conducted in chapter 4 and 5. The stud spacing, *w*, fastener spacing, *s*, and edge distance, *e*, (see Figure 3.3(c)) are varied in the testing. Two types of sheathing are employed: OSB (11.1 mm (7/16 in.), rated 24/16, exposure 1) and gypsum (12.7 mm (½ in.) Sheetrock). Number 6 fasteners (Simpson #6 x 1 5/8'' (41.3 mm)) were used to connect to the gypsum boards and number 8 fasteners (Simpson #8 x 1 15/16'' (49.2 mm)) to connect to the OSB boards.

Environmental conditions are varied in the conducted testing. Three conditions are considered: humid (saturated), dry, and normal. Humid (saturated) conditions are established by keeping the sheathing inside a tank filled with water for seven days. Dry conditions are established by keeping the sheathing in an oven for seven days at a temperature of 103°C. Normal conditions are established by keeping the sheathing in an environmental chamber for seven days at a temperature of 20°C and 65% humidity.

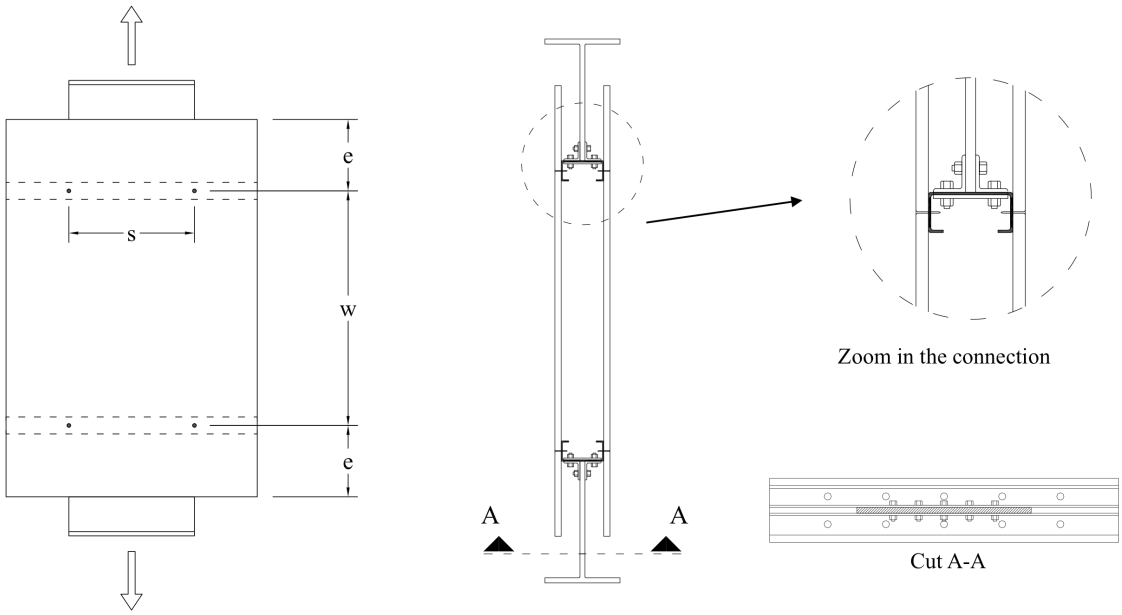

a) b) c)

Figure 3.3 – Test setup of lateral stiffness test for measurement of local translational stiffness of stud-fastener-sheathing assembly. a) front view, b) side view, c) details.

3.4.2. Strength and stiffness per screw

The per screw strength is determined simply as the tested strength T divided by 4, as illustrated in the free body diagrams of Figure 3.4.

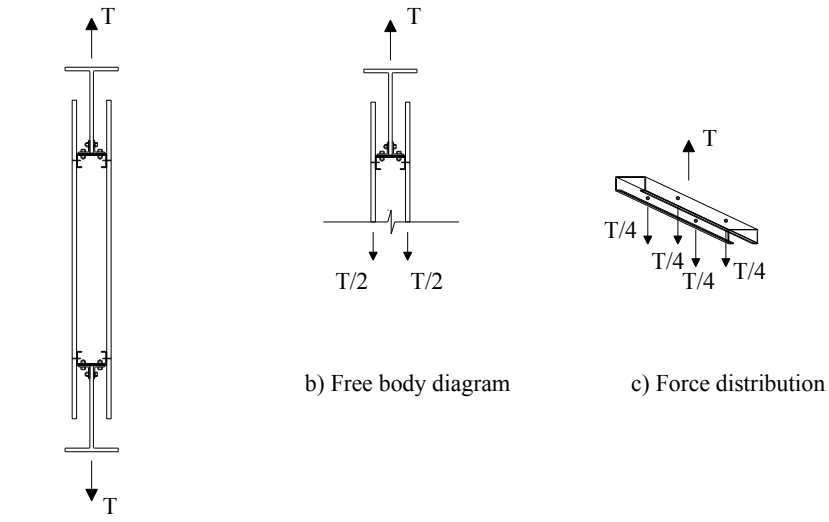

Figure 3.4 – Load per screw

The per screw stiffness requires a more sophisticated treatment, but results in a simple answer. For each test the global load-displacement response: T vs. Δ is recorded. (The test frame keeps the upper beam in a fixed position and allows the actuator to pull down from the bottom, Figure 3.5(b)). The global stiffness is then simply the slope of the T-Δ results.

Determination of the initial global stiffness may be completed in a variety of ways. The secant stiffness up to 40% of T max has been used in the past (e.g. by Winter in [3.7]) while the secant stiffness up to 80% of T max is common in earthquake engineering, see Iuorio et al. [3.8] for further discussion. An alternative approach has been selected here, rather than focus on force levels the tangent stiffness in a specific displacement regime was selected. Here the initial stiffness was defined as the tangent

stiffness[1] for displacement levels less than L/384 (where L is set to 8 ft, the length of the columns considered in the larger testing). The accuracy of this notion may be assessed graphically via the results in the Appendix A, which provides the selected initial stiffness along with the T-Δ response for every specimen.

However, the stiffness determined is the stiffness of the system and not the per screw (or per fastener) stiffness. The stiffness of each connection can be found knowing that the displacement, Δ, is equal to the sum of the displacement at the top connection, Δ_{top}, and the displacement at the bottom connection, Δ_{bot}, and the displacement of the sheathing, $\Delta_{sheathing}$, Eq. (3.5) and Figure 3.5(b):

$$\Delta=\Delta_{top}+\Delta_{sheathing}+\Delta_{bot} \tag{3.5}$$

Assuming the sheeting displacement is dominated by deformations near the connections and thus can be combined with the fastener displacement ($\Delta_{sheathing}=0$) Eq. (3.5) can then be rewritten as:

$$(T/k)=(F_{top}/k_{top})+(F_{bot}/k_{bot}) \tag{3.6}$$

Where T is the load, k is the global stiffness, and the force at the top, F_{top}, and the force at the bottom, F_{bot}, is equal to the force T, while the stiffness at the top, k_{top}, and

[1] the tangent stiffness was defined by segmenting the results below L/384 into groups of at least 10 points and using the greatest tangent stiffness in that regime. This definition avoids artificially low stiffness results due to initial accommodation of the specimen, or due to pre-mature degradation as the L/384 limit is approached. See Appendix A for comparison to each sample.

stiffness at the bottom, k_{bot}, are the same and equal to the stiffness of four screws, k_{4screw}. Then:

$$(1/k)=(1/k_{4screw})+ (1/k_{4screw}) \tag{3.7}$$

Assuming that each connection deforms equally and therefore has the same stiffness, k_{4screw} is equal to four times the stiffness of each screw, k_{screw}. Substituting this equality in Eq. (3.7), yields:

$$k=2*k_{screw} \tag{3.8}$$

This results in the assumption of the spring model of Figure 3.5(c). Where the springs in each stud are in parallel followed by the same systems in series due to be connected to two studs. Hence, the total load has to be divided by four to represent the load in each screw and the system stiffness has to be divided by two to represent the stiffness of each screw.

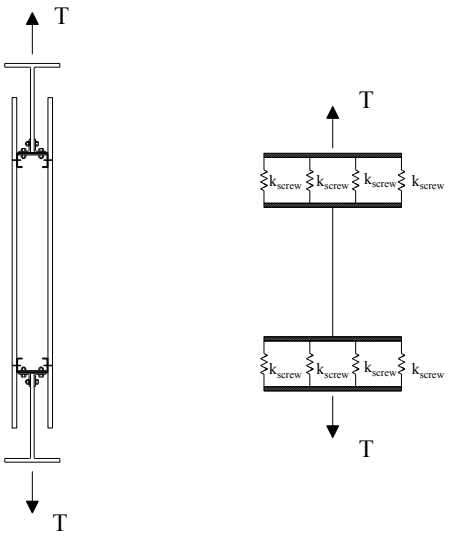

a) Force applied T b) Spring model

Figure 3.5 – Stiffness per screw

3.4.3. Use of Q tests to determine k instead

Simaan and Peköz [3.9] developed their research based on the shear diaphragm test as discussed in Chapter 1 (see Figure 1.2 for reference). Nonetheless, the lateral stud restraint (k) provided by the fastener-sheathing combination may be derived from the shear diaphragm tests. Two methods are considered here for determining k from shear diaphragm tests: spring and foundation spring, as illustrated in Figure 3.6.

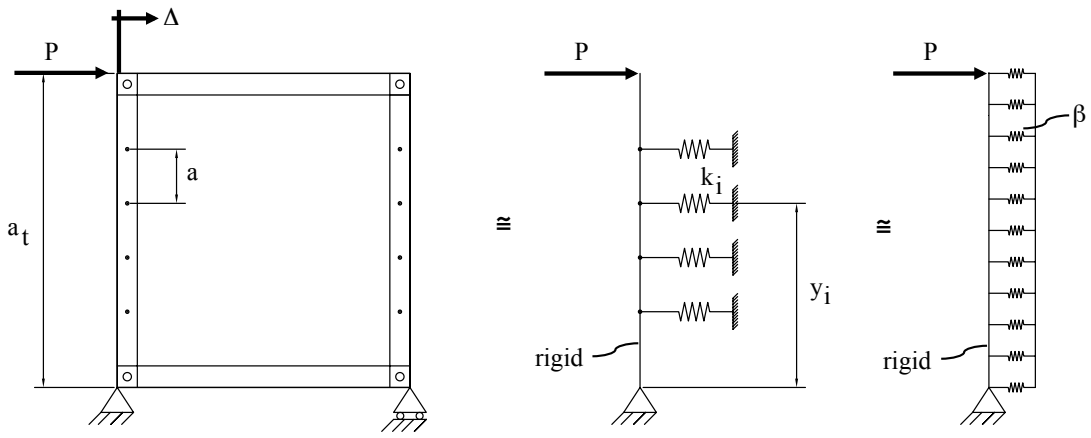

Figure 3.6 – Lateral spring models for diaphragm test.

In both cases moment equilibrium between the diaphragm test and the spring model are achieved. For the discrete spring model the moment equilibrium takes the form:

$$Pa_t = \sum_{i=1}^{2n} k_i \Delta_i y_i \tag{3.9}$$

where P is the applied load on the diaphragm, a_t is the distance to the applied load, k_i is the stiffness of each of the 2n fasteners (2 because there are 2 studs with fasteners providing support), Δ_i is the deflection at each fastener, and y_i is the height to a given fastener. Assuming all fasteners have the same stiffness k and noting that $\Delta/a_t=\Delta_i/y_i$:

$$Pa_t = \frac{2k\Delta}{a_t} \sum_{i=1}^{n} y_i^2 \tag{3.10}$$

which may be readily solved for k, resulting in:

$$k = \frac{Pa_t^2}{2\Delta \sum y_i^2} \quad \text{(discrete spring model)} \tag{3.11}$$

Alternatively, for a lateral foundation of stiffness β, moment equilibrium implies:

$$Pa_t = \frac{1}{2} a_t \beta \Delta \cdot \frac{2}{3} a_t \tag{3.12}$$

and for fasteners on 2 studs spaced distance, a, apart k=βa/2, thus:

$$k = \frac{3Pa}{2\Delta a_t} \qquad \text{(foundation spring model)} \tag{3.13}$$

Schafer [3.10] compares the k values available in the literature to these approximations and shows the developed k of section 3.4.2.

3.4.4. Results and Discussion

Complete load-displacement response was recorded for all testing, but is summarized well by three simple metrics: maximum load (P_{max}), displacement at maximum load (δ at P_{max}), and translational stiffness ($k_{x\ell}$). The maximum load provides the strength of the connection; the displacement at the maximum load gives a sense of the capacity of the connection to deform (and dissipate energy if needed), while the translational stiffness gives the relationship between load and displacement in the initial response (load less than 10% maximum load) typically appropriate for stability bracing. A condensed summary of the test results is provided in Table 3.2, see Appendix A for full results. Appendix B presents the results for a study done in parallel to this research that compared American and Canadian Plywood.

Stylized (but to scale) load-displacement curves in Figure 3.7 provide a graphical depiction of the average results and dramatically show the difference between the two sheathing types. OSB sheathed test specimens outperform gypsum sheathed specimens by a wide margin. For nominally identical studs, fasteners, and spacing, the lateral stiffness of an OSB sheathed specimen is 3 times greater than gypsum board, the shear

capacity in OSB is nearly 7 times greater than gypsum board as the failure mode switches from fastener shear (in the OSB) to tear out (in the gypsum), and the displacement at peak load is 2 times greater in OSB than in gypsum. As indicated in Figure 3.7 the impact of humidity and over-driving the fasteners is the same for both sheathing types. Humidity decreases stiffness and strength. Over-driving the fasteners increases stiffness, but decreases strength and deformation capacity.

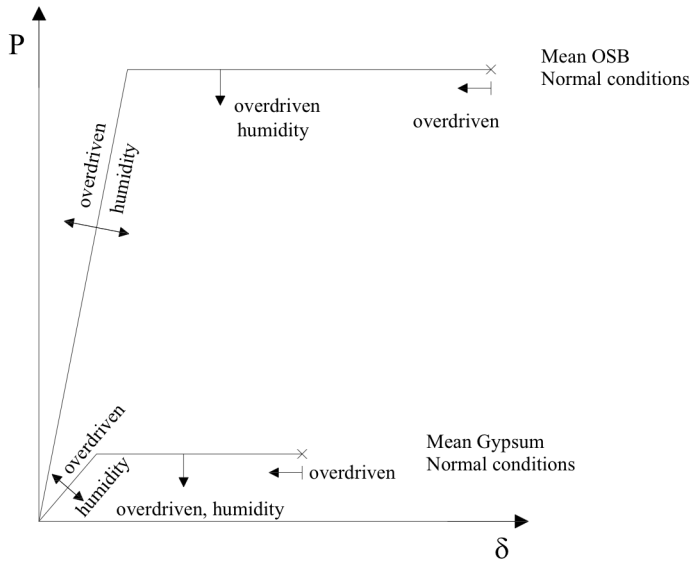

Figure 3.7 – Schematic of load (P) deformation (δ) response in lateral stiffness test for OSB and gypsum sheathing (drawn to scale)

Table 3.2 – Condensed summary of test results.

Sheathing	Test Condition	$k_{x\ell}$ mean (N/mm)	n	CoV	P_{max} mean (N)	CoV	δ @ P_{max} mean (mm)	CoV
OSB	Normal Conditions[1]	1241	6	0.07	2572	0.03	15.7	0.02
	Overdriven[2]	1640	3	0.10	1821	0.05	8.7	0.27
	Humid (saturated)[3]	1108	2	0.10	1171	0.04	13.0	0.21
Gypsum	Normal Conditions[1]	426	3	0.02	382	0.03	8.7	0.13
	Overdriven[2]	612	3	0.14	299	0.02	3.7	0.57
	Humid (saturated)[3]	41	1	-	92	-	10.5	-

(1) Dimensions for normal condition: w = 609.6 mm (24 in.); s = 101.6, 304.8 or 508 mm (4, 12, or 20 in.); and e = 152.4 mm (6 in.)
(2) Dimensions for overdriven condition: same w, s, and e as normal conditions, but the fastener is overdriven by 3.175 mm (1/8 in.).
(3) Dimensoins for humid (saturated) condition: w = 203.2 mm (8 in.); e = 50.8 mm (2 in.); and s = 228.6 and 304.8mm (9 and 12 in.) for OSB and 152.4 mm (6 in.) for gypsum.

The lateral support supplied by a fastener-sheathing assembly with dry OSB has greater initial stiffness and ultimate strength than one with humid (saturated) OSB. The cases with humid (saturated) OSB show an average percent reduction of 22% in stiffness and 47% in strength. Under normal conditions the gypsum board has a significant initial stiffness and is able to carry 382 N/fastener (85 lb/fastener). In the humid or dry condition the gypsum board suffers significant stiffness loss and is only able to sustain about ¼ the fastener capacity. Given the low deformation capacity in addition to the low strength, in the dry or humid condition the gypsum board essentially ceases to behave as a structural material. The substantial variation of gypsum board to environmental conditions means its structural properties must be treated with great care in design.

For the studied fastener spacing: *s* varied from 101.6 to 508 mm (4 to 20 in.), neither the initial stiffness nor the strength varied significantly as a function of fastener spacing. This strongly suggests that the developed deformations and failure mechanisms are local to the fastener.

During installation in the field it is possible that the fastener will be overdriven. Aware of this possibility, a series of tests were conducted with fasteners intentionally overdriven. Overdriving the fasteners increases the initial stiffness (32% on average for OSB and 43% for gypsum), but at a cost, the strength decreases (30% on average for OSB and 22% for gypsum) and deformation capacity also decreases (45% on average for OSB and 55% for gypsum).

From the standpoint of providing bracing for a wall, the increased stiffness from overdriving the fastener is likely beneficial enough (higher stiffness actually lowers the needed bracing forces) to outweigh the decreased capacity, and thus one is likely to find

that over-driving has little impact on stud strength. However, for a shear wall or other situation where the strength of the fasteners limits the system capacity, the increased stiffness only drives more load to the fastener, and the precipitous loss in capacity means it fails earlier. The impact of overdriving the fastener thus depends significantly on the function and controlling limit state.

Although local stiffness in this chapter was determined experimentally via Winter's method [3.11] as depicted in Figure 3.3, alternative methods exist. In particular, a method that develops a more isolated measure of $k_{x\ell}$ [3.12] has been used relatively extensively to characterize this same local stiffness (see, e.g. [10]). The testing rig in [10] consists of a short stud segment fully restrained against translation and rotation. A small strip of sheathing is fastened to the flange of the stud with a single fastener. The specimen is carefully aligned to avoid any extra moment in the system, and the out-of-plane movement of the sheathing is restricted by teflon sliders connected to the sheathing.

The author's selected Winter's method for their study for two reasons. First, the testing rig employed in Winter's method was judged easier to construct, and more forgiving in its details. Second, while isolation of $k_{x\ell}$ is desirable, in practice stud flanges in a wall stud system are free to bend such that the fasteners are able to bear and tilt in the sheathing without the extra stiffness provided by the flange being fully restrained.

3.5. ANALYTICAL MODEL FOR LOCAL TRANSLATIONAL STIFFNESS ($k_{x\ell}$)

For design, a simple analytical model for predicting the available stiffness from the fastener-sheathing system to the stud, as a brace, would complement the experimental procedure. Modeling of the response of such systems has been studied particularly in the context of timber sheathed systems fastened by nails, and under cyclic loading in direct shear [3.13-16]. These models attempt to capture the basic deformation phenomena of Figure 3.1 as well as loading and unloading; however, the specifics are for nails and timber, not self-drilling screws and cold-formed steel. Due to the large number of variables involved (material, geometric, friction, damage, etc.) existing models require extensive calibration with testing, and while playing a vital role in nonlinear static and dynamic analysis of timber sheathed walls (see e.g., [3.14] and [3.16] in particular), they do not provide simple direct analytical expressions appropriate for bracing design in cold-formed steel systems.

The flexibility under lateral deformation between the stud flange and sheathing largely derives from bending of the stud flange itself, and bending of the fastener. Bending of the stud flange occurs due to the fact that the line of action of the fastener resistance resides in the thick sheathing, far from the thin steel sheet of the stud flange, thus creating an eccentricity that applies a moment that locally bends the stud flange. Bending of the fastener occurs due to the fact that the self-drilling fastener is anchored in the thin steel flange, again with a line of action in the thicker sheathing material. Fastener bending is resisted by bearing deformation against the sheathing. Here we propose a simple baseline

model that ignores the sheathing bearing deformation resistance and focuses only on the direct flange and fastener bending.

The simple baseline model, for use in design when information is limited, or testing unavailable is depicted in Figure 3.8. The "frame" consists of the flange modeled as a column of height 3*d* and cross-sectional area 3*d* × *t*; where, d is the fastener diameter, t the flange thickness, and 3*d* is the approximate local area engaged by the fastener. To the column (stud flange) is connected a beam that simulates the fastener. The beam (fastener) has a circular cross-section with diameter d, and a length equal to the board thickness, t_{board}. The loading is applied at the fastener head and reacted in the stud flange.

The location and distribution of the force on the fastener is a function of the bearing stiffness of the sheathing material, and the extent of loading (penetration). A triangular distributed load along the length of the fastener (beam) was considered, and results in a displacement 35% smaller than having the concentrated load at the fastener head. However, given that the real distribution is unknown, and in the spirit of keeping the model simple and conservative, a concentrated load at the fastener head was assumed.

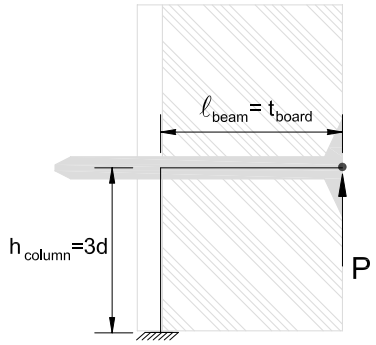

Figure 3.8 – Frame model for fastener-flange bending contribution

Using the preceding assumptions the deflection at the tip of the idealized model is:

$$\delta = \frac{P\left(t_{board}\right)^2}{E}\left(\frac{3d}{I_{column}} + \frac{t_{board}}{3I_{beam}}\right) \tag{3.14}$$

where:

P=applied load at the connection

t_{board}=board thickness

d=fastener diameter

I_{column}=Moment of inertia of column

I_{beam}=Moment of inertia of beam.

which after substituting in the appropriate dimensions and solving for the stiffness results in:

$$k_{x\ell} = \frac{P}{\delta} = \frac{3Ed^4t^3\pi}{4t_{board}^2\left(9d^4\pi + 16t_{board}t^3\right)} \tag{3.15}$$

where:

t=flange thickness.

For the tests reported in Table 3.2, E = 203 GPa (29500 ksi), d = 3.35 mm (0.132 in.), t = 1.67 mm (0.0656 in.), and t_{board}= 11.11 mm (7/16 in.). The resulting $k_{x\ell}$ = 516 N/mm (2.95 kip/in.) using Eq. (3.15). The $k_{x\ell}$ of Eq. (3.15) may be compared with the mean tested response under normal environmental conditions of 426 N/mm (2.43 kip/in.) for gypsum sheathed specimens and 1,241 N/mm (7.08 kip/in.) for OSB sheathed specimens.

Eq. (3.15) provides a reasonable lower bound estimate, ignoring the benefit of stiffer sheathing in bearing, and is recommended if tests results are not available. The key assumptions regarding this simple model, particularly the flange engagement area of 3*d* x 3*d*, were developed through additional modeling which are described in the following sections.

3.5.1. Three-dimensional Shell Finite Element Model of Connection

To examine the extent to which the fastener engages local deformations in the stud flange a three-dimensional shell finite element model of the stud-fastener assembly was developed. Consistent with the testing conducted herein (following [3.17], as shown in Figure 3.3(a)) the model only includes the stud flange (Figure 3.9) as the stud web is restrained between steel plates. Using ABAQUS [3.18], the 41.28 mm (1.625 in.) wide flange and 12.7mm (0.5in) lip are modeled using shell (S4R) elements. The #8 fastener, with a diameter of 3.35mm (0.132 in.) is modeled using a beam element (B310S) with a length of 11.11 mm (7/16 in.), which is the same as the OSB board thickness (t_{board}), Figure 3.9. Loading is applied at the fastener head.

The deformed shape and von Mises stress under a load = 2670N (600lb) are provided in Figure 3.9(b) and (c). The stresses in the flange are localized to a region with a radius approximately equal to 3*d*. The exact size of the localized region is a function of the relative stiffness between the fastener and the stud, but 3*d* provides a rational and simple approximation for typical dimensions employed in cold-formed steel framing.

Since the out-of-plane dimension is explicitly modeled in the three-dimensional models the transverse bending resistance provided by the lip may be readily included.

Direct analysis with and without the lip shows that the lip increases the stiffness by 11%. This beneficial additional resistance is ignored in Eq. (3.15).

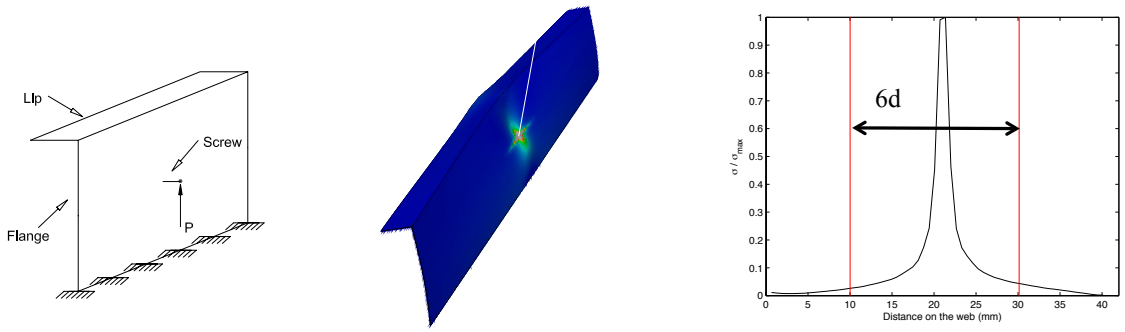

a) b) c)

Figure 3.9 – Shell element model of lip and flange, the fastener is modeled using a beam element. a) Flange+Lip+Fastener, b) Deformed shape and Von Mises stress, c) Normalized Von Mises stress on the line where the fastener is connected

3.5.2. Two-dimensional Plane Strain Model of Connection

The two previous models of the stud-fastener-sheathing connection (Figure 3.8, Figure 3.9) do not explicitly account for the sheathing. Here a plane strain model is developed that allows for an examination of the bearing between the fastener and sheathing. The developed plane strain model consists of ¼ of the local shear test as shown in Figure 3.10(a) and (b). Symmetry boundary conditions are enforced on the sheathing end and the stud is assumed fixed at the flange/web junction. Bearing between the fastener and sheathing is modeled by constraining the vertical displacements together on the compression face between the fastener and sheathing, but leaving horizontal displacement unconstrained (free to slide) as shown in Figure 3.10(b). Loading is applied at the fastener head.

Out-of-plane dimensions for the model are equal to 3d for the stud flange and sheathing, and d for the fastener, where d = 3.35 mm (0.132 in.). The OSB sheathing is modeled as linear elastic with E_{xx}, E_{yy} and E_{zz} = 6426 MPa (932 ksi), G_{xy}, G_{xz} and G_{yz} = 1310 MPa (190 ksi) and ν_{xy}, ν_{xz} and ν_{yz} = 0.3, values selected from [3.4, 19], while gypsum sheathing is modeled with E_{xx}, E_{yy} and E_{zz} = 993 MPa (144 ksi), G_{xy}, G_{xz} and G_{yz}= 552 MPa (80 ksi) and ν_{xy}, ν_{xz} and ν_{yz} = 0.3, values selected from [3.5, 19].

Stiffness of the model, without sheathing, is within 1% of the three-dimensional shell model of the previous section. With the sheathing (and bearing) modeled the $k_{x\ell}$ values are 31% stiffer with OSB, and 62% stiffer with gypsum board, than tested values. While the model incorporates the beneficial stiffness provided from direct bearing, it does not incorporate the detrimental loss in stiffness due to local tearing, as shown in Figure 3.10(d). The gypsum sheathing provides little resistance to tearing, and thus the gypsum model without tearing significantly overestimates stiffness.

Despite limitations, the value of this model with sheathing included, particularly compared to Eq. (3.15), may be demonstrated by varying the sheathing dimensions. The simple model of Eq. (3.15), ignoring bearing, indicates that as the thickness of any sheathing (t_{board}) increases, the stiffness decreases. However, with bearing included, as in the present plane strain model, a more nuanced response is predicted: for OSB thicker sheathing leads to increased stiffness, but for gypsum board, thicker board leads to decreased stiffness. Thus, if the sheathing is too flexible, bending of the fastener and flange prevails over the additional resistance provided by the sheathing. However, if the sheathing is stiff enough, the additional moment due to the use of thicker sheathing, is compensated by bearing in the sheathing.

Ultimately, modeling the stud-fastener-sheathing stiffness provides a small conundrum: if a precise analytical answer is needed an even more robust, though relatively unpractical model, has to be explored, whereas if the uncertainties are accepted for the sake of simplicity, then the model should likely disregard the stiffness provided by bearing. Thus it is proposed that determination of $k_{x\ell}$ be conducted by testing per [3.11] which include bearing and fully capture the intended deformations, or in the absence of testing the simplified expression of Eq. (3.15) which assume ideal, simplified, and largely conservative behavior.

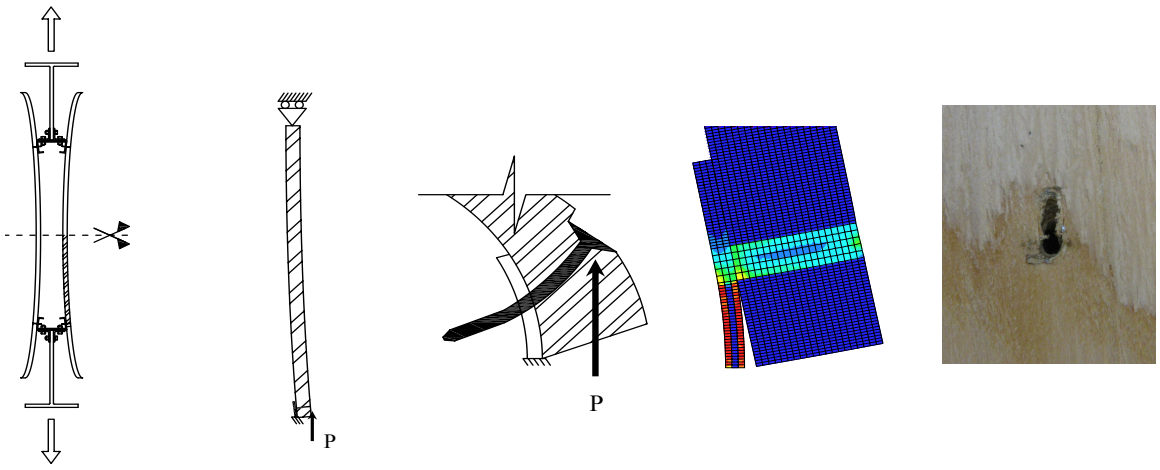

Figure 3.10 – Two dimensional plain-strain model of connection plus sheathing. a) translational test with amplified displacements, hatched area corresponds to the FE model, b) schematic of FE model, c) schematic of stud flange, sheathing, fastener deformations, d) FE deformed shape and von Mises stress contour under lateral force. e) tearing of the sheathing (not included in FE model).

3.6. DIAPHRAGM MODEL FOR TRANSLATIONAL STIFFNESS

Consider a wall where the studs are buckling in global weak-axis flexural buckling, as illustrated in Figure 3.11. If the sheathing deforms in a manner compatible with flexural buckling it undergoes predominately a shear demand. That is, the sheathing must behave like a shear diaphragm. (As described in the introduction with respect to the fastener-sheathing assembly, flexural-torsional buckling also places a similar shear demand on the sheathing, though opposite on the two faces.) Simaan and Peköz [3.9] postulated that this shear deformation of the panel is the key component of bracing resistance that the sheathing supplied to the studs. This observation was used in an energy solution for the stability of cold-formed steel studs that added the energy from the shear diaphragm to the classical solution (driven by the shear modulus of the sheathing material) and was utilized from 1980-2004 in the AISI Specification.

The Simaan and Peköz analytical model ignored (simplified) the fact that the shear diaphragm must be resolved through the fasteners and only included flexibility from the diaphragm (the sheathing) itself. However, they partially resolved this issue by employing a test method for determining the diaphragm stiffness. The test method, depicted in Figure 3.11, requires forcing a large panel into simple shear and measuring the panel distortion. Since the panel must be connected to a testing rig the local fastener deformations are thus included in determination of the panel shear stiffness. Recent comparisons show for sheathing typical of cold-formed steel framing that these tests are primarily controlled by local fastener stiffness, as the local stiffness resulting in these tests is similar to that from Winter's tests [3.11], Figure 3.3. The goal here is to isolate the shear diaphragm stiffness from the local stiffness so that they may be considered

independently, and to determine the stiffness the shear diaphragm (independent of the local fastener stiffness) supplied to the stud at each fastener location.

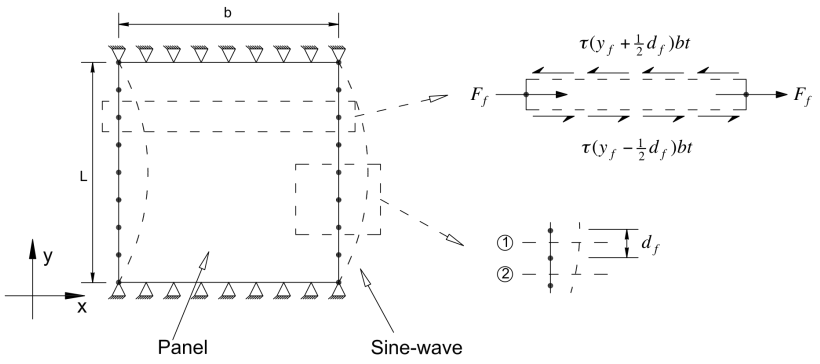

Figure 3.11 – Plate model

3.6.1. Analytical model for diaphragm stiffness

Consider again the sheathed wall under a sine curve (due to flexural buckling or flexural-torsional buckling). The lateral deformation, u, is:

$$u = \sin(\pi y/L) \tag{3.16}$$

The stiffness at a fastener location is the force at the fastener, developed from an integration of the shear stress over the tributary area of the fastener, divided by the deformation, u, at the fastener location. The sheathing will be in pure shear as the studs undergo flexural buckling if the sheathing has a low shear modulus or if the sheathing panel is wide and short, both of which are commonly the case. As a result the stresses are controlled by shear deflections consistent with diaphragm action. Thus, the shear stress at any point is simply

$$\tau = G\theta \tag{3.17}$$

From the free body diagram of Figure 3.11, the force in the fasteners, F_f, at height y_f, with fasteners spaced d_f apart for sheathing of width, b, thickness, t_{board}, bracing n studs, is

$$nF_f = \tau(y_f + d_f/2)bt_{board} - \tau(y_f - d_f/2)bt_{board} \tag{3.18}$$

where the expressions inside the parentheses indicate the height at which τ is determined. The stiffness at the fastener location is simply

$$k_{xd} = F_f / u_f \tag{3.19}$$

where u_f is the deformation u at height y_f (the fastener location). Noting $\theta = du/dy$, then Eq. (3.16) may be differentiated and substituted into Eq. (3.17), then τ of Eq. (3.18) may be evaluated at the appropriate locations, and substituted into Eq. (3.19), leading after simplification to:

$$k_{xd} = \frac{2\pi Gbt_{board}}{Ln}\sin\left(\frac{\pi d_f}{2L}\right) \approx \frac{\pi^2 Gbtd_f}{L^2 n} \tag{3.20}$$

3.6.2. Finite element comparison of diaphragm stiffness

Physical testing of the diaphragm stiffness does not typically provide a meaningful comparison to k_{xd}, because isolation of k_{xd} from the local fastener stiffness ($k_{x\ell}$) is difficult to impossible in conventionally detailed sheathed walls. To provide examination of the derived expressions a finite element model of a panel undergoing a half sine-wave deformation (i.e., Figure 3.11) is completed in ABAQUS [3.18]. The model consists of a plate, 2.44 × 2.44 m (96 × 96 in.), modeled using linear four-node shell elements (S4R) elements. The boundary conditions are consistent with Figure 3.11 and include a sine curve applied every 25 mm (1 in.) in the y direction on both edges (right and left).

Assuming 11.1 mm (7/16 in.) OSB, the panel material is modeled as orthotropic with a Young's modulus of 6,426 MPa (932 ksi) [3.20]. The shear modulus, G, is systematically varied; however, note, the usual value of G is around 1,310 MPa (190 ksi) [3.20] and for an isotropic homogenous material with ν=0.3, G would be 2,385MPa (346 ksi). The developed diaphragm fastener stiffness in the FE model (k_{xdFE}) is compared to k_{xd} in Figure 3.12. At G = 1,310MPa (190 ksi), k_{xdFE} is very close to k_{xd} ; thus direct use of k_{xd} is reasonable for practical situations. At G = 2,385MPa (346 ksi), $k_{xdFE} \sim k_{xd}$; thus k_{xd} is sufficiently accurate up to the isotropic limit.

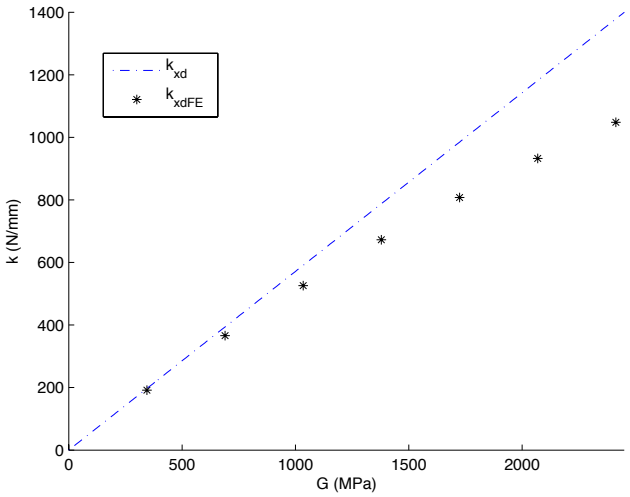

Figure 3.12 – Diaphragm stiffness compared with FE, for plate 2.44x2.44m (96x96in.), *E*=6,426MPa (932ksi)

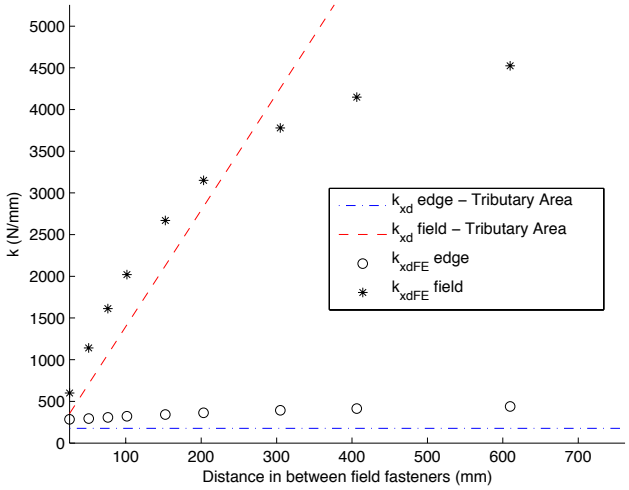

Figure 3.13 – Limitation of tributary area for k_d, for plate 2.44x2.44m (96x96in.), *E*=6,426MPa (932ksi), *G*=1,310Mpa (190ksi), 3studs

3.6.3. Multiple studs with fasteners differently spaced

Generalization of Eq. (3.20) is needed when fastener spacing is nonuniform; in particular, the boundary studs are commonly at a tighter fastener spacing than the studs in the field of the board. It is proposed that the tributary area for each fastener be employed, therefore b/n of Eq. (3.20) is replaced by w_{tf}, the fastener tributary width, and d_f is the fastener spacing, Figure 3.14, and may vary:

$$k_{xd} = \frac{2\pi G t_{board} w_{tf}}{L} \sin\left(\frac{\pi d_f}{2L}\right) \approx \frac{\pi^2 G t_{board} d_f w_{tf}}{L^2} \tag{3.21}$$

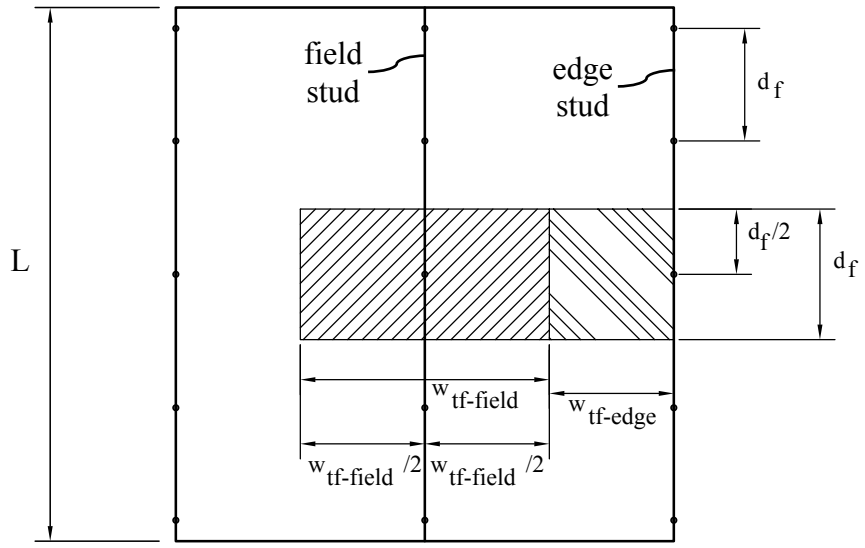

Figure 3.14 – Tributary fasteners areas defined for the "edge" and "field" fastener.

The model of the previous section is exercised to explore the validity of Eq. (3.21). The edge fastener spacing is 25.4 mm (1 in.), and the field fastener spacing is varied from 25.4 mm to 609.6 mm (1 in. to 24 in.), results are provided in Figure 3.13. The fastener

stiffness is consistent with the tributary area, up to tributary areas in the field that are 32 × greater than the edge tributary area. As the distance between fasteners in the field is increased over this limit the edge fasteners act as if there were no fasteners in the field and the stiffness goes back to the case of only being connected at the edges. The observed limitation is not a practical problem since the relation between tributary areas is typically no greater than 4 × (e.g., 152.4mm (6 in.) on the edge, 304.8mm (12 in.) in the field). Thus, Eq. (3.21) is recommended for use in design.

3.7. FULL SCALE TEST

As is reported in Chapter 5 of dissertation, the author tested 2.44 by 2.44m (8 by 8 ft) cold-formed steel stud walls comprised of five 362S162-68 (345Mpa (50ksi)) studs spaced 610mm (24 in.) o.c. and 362T125-68 (345Mpa (50ksi)) track in compression. Without bridging, blocking, or sheathing the walls fail in global flexural buckling at an average load of 249 kN (56 kips). When sheathed with OSB on both sides the walls fail in local buckling at an average load of 489 kN (110 kips). The enormous difference between the two strengths shows the positive benefit of the sheathing, both in terms of increasing the strength and limiting global buckling failure modes.

Winter's model (where bracing stiffness k of Figure 2c is derived based on translational tests, Figure 3, alone) assumes that the critical bracing stiffness and strength that sheathing supplies to the stud is derived only at the fastener location in direct shear. In essence, arguing that only local deformations must be understood to design the column. The hypothesis is put to the test, instead of sheathing with full boards, OSB strips (2 in. wide) were connected to the studs, see Figure 3.15(a). The use of strips

negates the shear diaphragm resistance (i.e., k_{xd}). The wall failed in flexural buckling at 311 kN (70 kips). Supplying only the local fastener stiffness provided a small increase in axial capacity, but no change in limit state. Thus, providing evidence that sheathing bracing derives from *both* the local and diaphragm resistance. They are, in fact, in series with one another.

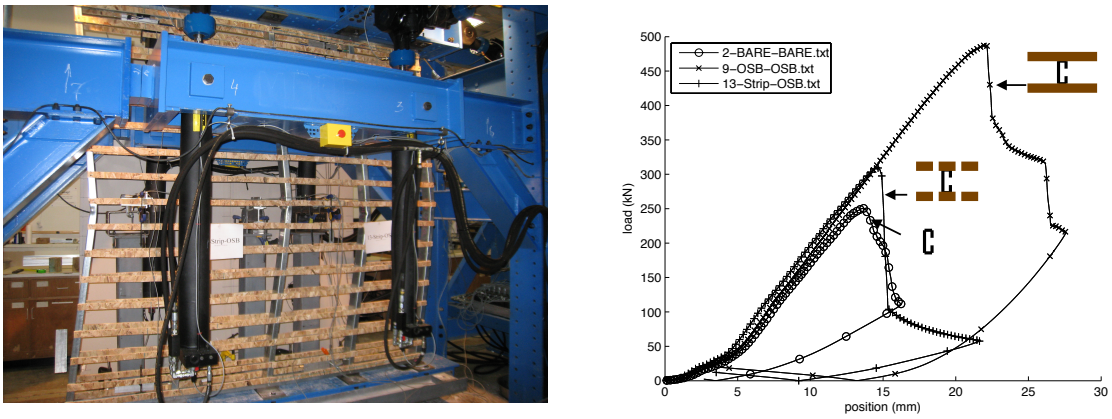

a) b)

Figure 3.15 – Effectiveness of strips compared to Bare-Bare and OSB-OSB: a) full wall test, strips instead of full boards, b) comparison between loading curves

3.8. COMBINED LOCAL AND DIAPHRAGM MODEL

Sheathing provides bracing to studs. Characterization of this bracing has proven historically difficult, in part because the two competing models for the explanation of the bracing: local and diaphragm, draw such different conclusions on the behavior. For example, diaphragm stiffness is influenced strongly by the stud spacing and the fastener spacing; while the local stiffness is not. Full-scale testing has provided, what to date was considered contradictory evidence, sometimes indicating these variables are important sometimes not. However, if one realizes that the local stiffness is in series with the

diaphragm stiffness then the explanation becomes clear. If local stiffness is low enough (and just as importantly diaphragm stiffness high enough) one will only see the local stiffness in the response and stud and fastener spacing will be largely irrelevant. Conversely, if local stiffness is high enough, say for example from a welded specimen with a steel sheet (and diaphragm stiffness low enough) then only the diaphragm stiffness will be important and stud spacing will be enormously important. Mathematically this may be handled by realizing k_x of Figure 1(d) may be approximated as

$$k_x=(1/k_{x\ell}+1/k_{xd})^{-1} \tag{3.22}$$

where $k_{x\ell}$ is determined experimentally (Figure 3) or analytically (Eq. (3.15)), and k_{xd} utilizes Eq. (3.21).

REFERENCES CHAPTER 3

3.1. Schafer, B.W., et al., *Rotational Restraint and Distortional Buckling in Cold-formed Steel Framing Systems.* Revista Sul-Americana de Engenharia Estrutural 2010.

3.2. Vieira Jr, L.C.M. and B.W. Schafer. *Behavior and Design of Axially Compressed Sheathed Wall Studs*. in *20th International Specialty Conference on Recent Research and Developments in Cold-Formed Steel Design and Construction*. 2010.

3.3. B. W. Schafer, L.C.M.V.J., R. H. Sangree, Y. Guan, *Rotational Restraint and Distortional Buckling in Cold-Formed Steel Framing Systems.* Revista Sul-Americana de Engenharia Estrutural, 2010.

3.4. APA-D510C, *Panel Design Specification*, A.-T.e.W. Association, Editor 2008: Tacoma, Washington, USA.

3.5. GA-235-10, *Gypsum Board Typical Mechanical and Physical Properties*, 2010, Gypsum Association: Hyattsville, MD, USA.

3.6. SSMA, *Product Technical Information, ICBO ER-4943P*, S.S.M. Association, Editor 2001.

3.7. Winter, G., *Lateral Bracing of Beams and Columns.* Journal of the Structural Division, 1960.

3.8. Iourio, O. and B.W. Schafer, *Compilation of k values*, in *A supplemental report for AISI-COFS Project on Sheathing Braced Design of Wall Studs*2008, The Johns Hopkins University: Baltimore.

3.9. Simaan, A. and T.B. Pekoz, *Diaphragm Braced Members and Design of Wall Studs.* ASCE J Struct Div, 1976. **102**(1): p. 77-92.

3.10. Schafer, B.W., O. Iourio, and L.C.M. Vieira Jr, *Notes on AISI Design Methods for Sheathing Braced Design of Wall Studs in Compression*, in *A supplemental report for AISI-COFS Project on Sheathing Braced Design of Wall Studs*2008, The Johns Hopkins University: Baltimore.

3.11. Giles G. Green, G.W., T. R. Cuykendall, *Light Gage Steel Columns in Wall-braced Panels.* Cornell University Engiineering Experiment Station, 1947. **35**: p. 1-50.

3.12. ASTM, *Standard Test Method for Mechanical Fasteners in Wood*, in *ASTM D1761*1995, American Society for Testing and Materials: West Conshohocken, PA.

3.13. Chui, Y.H., C. Ni, and L. Jiang, *Finite-element model for nailed wood joints under reversed cyclic load.* Journal of Structural Engineering, 1998. **124**(1): p. 96-102.

3.14. Folz, B. and A. Filiatrault, *Cyclic analysis of wood shear walls.* Journal of Structural Engineering, 2001. **127**(4): p. 433-441.

3.15. Pang, W.C., et al., *Evolutionary parameter hysteretic model for wood shear walls.* Journal of Structural Engineering, 2007. **133**(8): p. 1118-1129.

3.16. Van De Lindt, J.W., et al., *Three-dimensional seismic response of a full-scale light-frame wood building: Numerical study.* Journal of Structural Engineering. **136**(1): p. 56-65.

3.17. AISI, *Light Gage Cold-Formed Steel Design Manual.* American Iron and Steel Institute, 1962.

3.18. ABAQUS, *ABAQUS/Standard Version 6.7-1*, D. Systemes, Editor 2007.

3.19. NDS, *National Design Specification (NDS) for Wood Construction, ANSI/AF&PA NDS*, A.F.a.P. Association, Editor 2005: Washington, DC.

3.20. APA, *Panel Design Specification.* APA – The Engineered Wood Association, 1997.

CHAPTER 4 - SINGLE COLUMN

The stability and strength of cold-formed steel C-section columns (studs) with sheathing attached to the flanges is the subject of this chapter. Stud configurations both with and without sheathing, either oriented strand board or gypsum board, are tested to failure in compression. A total of twenty-six tests covering short, intermediate and long specimens, varied sheathing configurations, and varied end boundary conditions are completed. Dimensions and geometric imperfections of the specimens are measured in detail. The measured geometric imperfections are reduced to scalar magnitudes consistent with local, distortional, and global buckling modes. During the testing, mid-height cross-section deformations are recorded using five position transducers. The deformations indicate the impact of the different combinations of sheathing, and of the end boundary conditions, on the strength and stability of the studs. Composite action between the stud and sheathing, and isolating direct loading of the sheathing, are shown to be significant in determining the strength and controlling limit state of the stud. Tested strengths are compared with existing North American (American Iron and Steel Institute) Specification methods and potential improvements explored.

4.1. STUD COMPRESSION TESTS

4.1.1. Test Apparatus and Loading Details

The tests reported herein are completed using (a) a universal two-post MTS machine capable of compressive load up to 448.5 kN (100 kips) for the 0.61, 1.22 and 1.83 m (2, 4, and 6 ft) specimens and (b) for the longest 2.44 m (8 ft) specimens a custom

built multi-degree-of-freedom (MDOF) testing rig capable of 897 kN (200 kips) compressive load that is being utilized for testing of full walls, chapter 5.

For the 0.6, 1.2 and 1.8 m (2, 4 and 6 ft.) long tests conducted in the MTS machine compressive load is applied through the bottom, and vertical displacement is measured through the built-in position transducer (PT). During testing it was determined that a small isolation plate should be provided between the loading platen and the track, as labeled in Figure 4.1(a) and shown in Figure 4.1(a) and (b).

For the MDOF machine, compressive loading is applied through four actuators at the top and the vertical displacement is measured as the average of the vertical displacements measured through built-in PTs in these actuators.

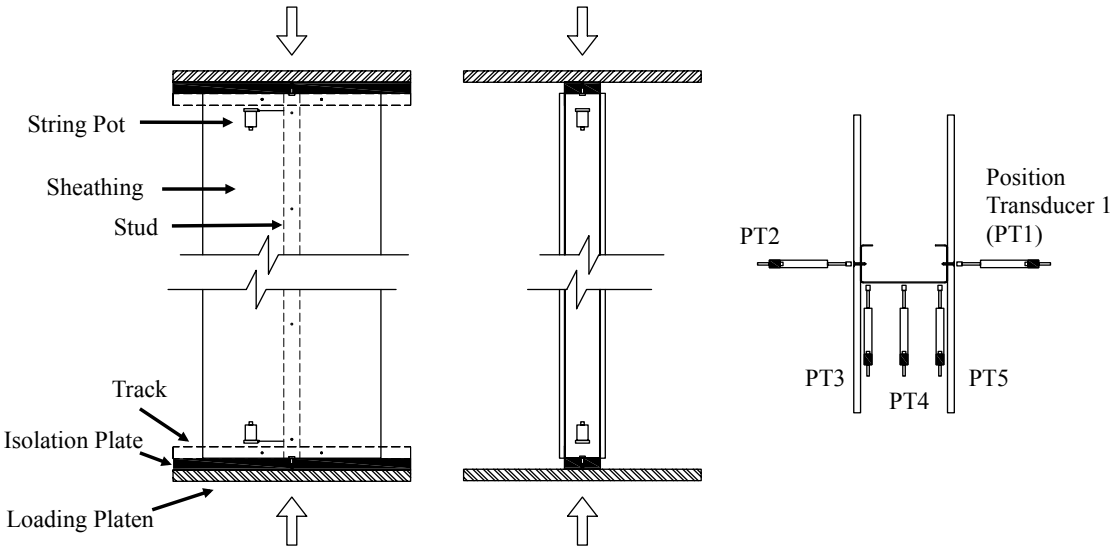

Figure 4.1 – MTS and MDOF test schematic
a) Side view of the specimen components and isolation plate, b) Front view of specimen with emphasis on string pots (SP) and isolation plate, c) PTs placed at mid height of the stud.

Five PTs and two string pots (SP) are set up at the midpoint and ends of the members respectively, as shown in Figure 4.1(c), to capture local and global buckling for the different test configurations.

4.1.2. Cross-sections

Average cross-section (out-to-out) dimensions of the tested 362S162-68 (SSMA/ASTM nomenclature) studs (Figure 4.2) and 362T125-68 tracks are given in Table 4.1 and provided for each stud specimen in Appendix E. To account for the variation in cross-section, three measurements are taken at the ends and center of the studs for each of the dimensions reported. In the case of the tracks, only one measurement is taken at the center for each of the dimensions. Thicknesses of the web and flange includes galvanizing are reported as t^* in Table 4.1, see the coupon results in Section 4.1.4 for base metal thickness.

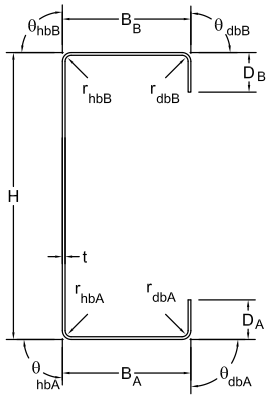

Figure 4.2 – Cross-section dimension notations

Table 4.1 – Out-to-out cross-section measurements

Specimen	statistic	H (mm)	B_B (mm)	B_A (mm)	D_B (mm)	D_A (mm)	t* (mm)	r_{hbB} (mm)	r_{dbB} (mm)	r_{hbA} (mm)	r_{dbA} (mm)	θ_{hbB} (deg)	θ_{dbB} (deg)	θ_{hbA} (deg)	θ_{dbA} (deg)
Stud[1]	mean	93.577	42.084	41.984	12.982	12.936	1.86	4.366	4.366	4.366	4.366	89.17	89.01	89.10	88.91
	CoV	0.0082	0.0094	0.0074	0.0142	0.0144	0.0325	-	-	-	-	0.0069	0.0091	0.0096	0.0106
Track[2]	mean	98.294	30.719	30.784	-	-	2.124	3.969	-	3.969	-	87.45	-	87.16	-
	CoV	0.0002	0.0013	0.0012	-	-	5E-04	-	-	-	-	0.0088	-	0.0076	-

(1) 24 studs 362S162-68 (SSMA/ASTM nomenclature[3]) were measured, each stud was measured at three positions along the length (both ends and the middle), which means a total of 72 measurements for each variable on this table.
(2) 42 tracks 362T125-68 (SSMA/ASTM nomenclature[3]) were measured, each track was measured only at the middle, which means a total of 42 measurements for each variable of this table.
(3) SSMA nomenclature consists of: the first three numbers are the member depth in 1/100in. (ex.: 362➔362*1/100=3.62in.), the following letter designates the cross-section type (ex.: S, stands for Stud), the next three numbers are the flange width in 1/100in. (ex.: 162➔162*1/100≈1.625in.), and the last two numbers are the minimum base metal thickness in mils (ex.: 68➔68*1/1000=0.068in.).

4.1.3. Imperfections

Imperfections are measured via a rig synchronized with a PT, Figure 4.3(a), and are automatically recorded. Figure 4.3(b) shows the locations in the cross-section where imperfection measurements are performed. As shown in Figure 4.4, for one specimen, "local" imperfection measurements (point D) are made at 12.7 mm (½ in.) spacing along a 0.3 m (1 ft) span at the center and either ends, resulting in 75 local imperfection measurements for each specimen. A total of 25 "distortional" imperfection measurements (points A and F) are made at 25.4 mm (1 in.) spacing along a 0.6 m (2 ft) span at the center, and 8 "global" imperfections (points B, C and E) are recorded every 0.3 m (1 ft) along the length of the member. Measurements at locations A – F of Figure 4.3(b) are denoted as δ_A, δ_B, δ_C, δ_D, δ_E and δ_F. Hence the following parameters are derived for assessing imperfection magnitudes.

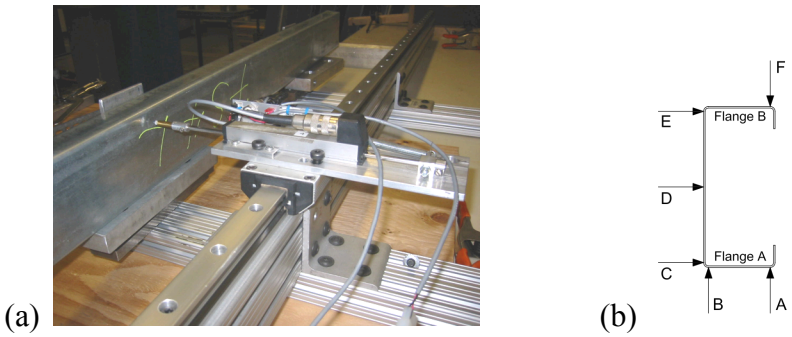

Figure 4.3 – Imperfection measurement set-up a) Imperfection measurement rig b) Cross-section imperfection measurement locations

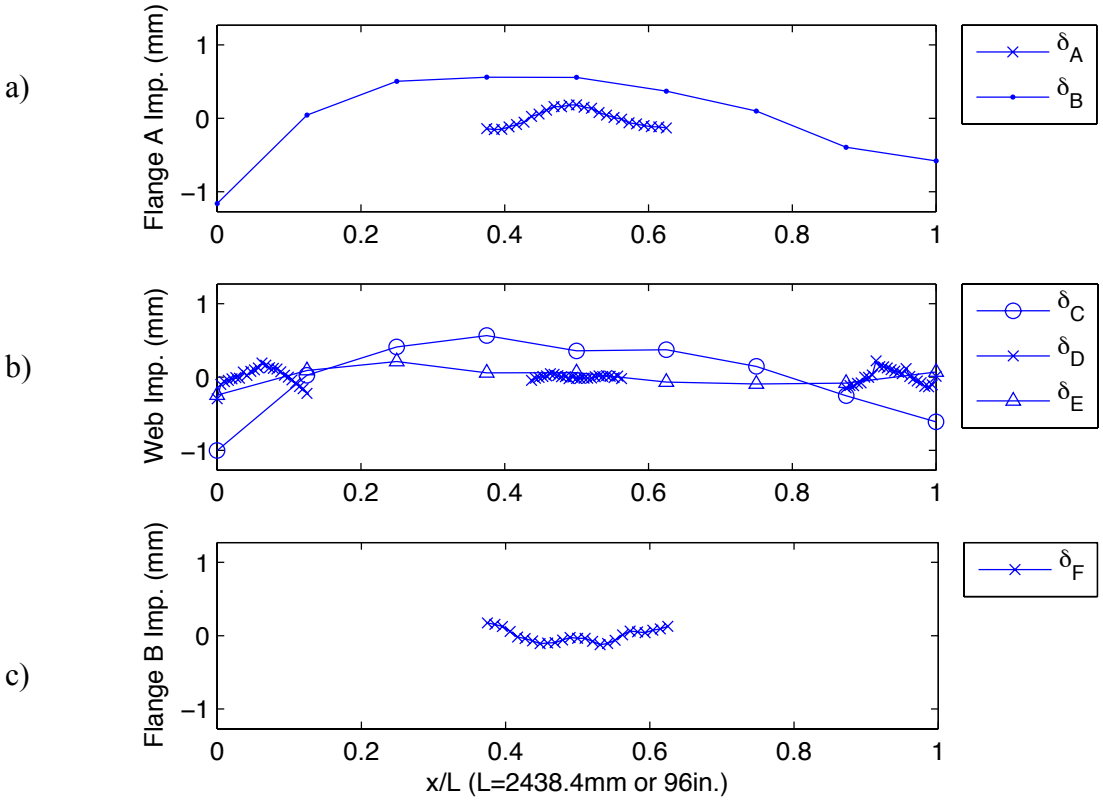

Figure 4.4 – Imperfection measurements of stud 65S8L. a) Imperfection measured on Flange A, b) Imperfection measured on the Web, c) Imperfection measured on Flange B.

For global imperfections, bow (*b*), camber (*c*) and twist (θ) are approximated by:

$$d_b = \max(\text{mean}([\delta_C\ \delta_E])) - \min(\text{mean}([\delta_C\ \delta_E])) \quad (4.1)$$

$d_c = \max(\delta_B) - \min(\delta_B)$ (4.2)

$d_\phi = \max((\delta_C - \delta_E)/h) - \min((\delta_C - \delta_E)/h)$ (4.3)

where h = web height between C and E, h=91.95mm (3.62 in.)

The "local" imperfection magnitude, d_1 is approximated by:

$d_1 = \max([\max(\delta_{D,i}) - \min(\delta_{D,i})])$ (4.4)

where $\delta_{D_{i,max}} = max(\delta_{D_i}) - min(\delta_{D_i})\ for\ i = 1,2,3$. The subscript i indicates the different positions that δ_D was measured (both ends and the middle of the stud)

The "distortional" imperfection magnitude, d_2 is approximated by:

$d_2 = \max([\delta_{A,max}\ \delta_{F,max})])$ (4.5)

where $\delta_{A,max} = \max(\delta_A) - \min(\delta_A)$ and $\delta_{F,max} = \max(\delta_F) - \min(\delta_F)$

Based on the imperfection records, Table 4.2 provides the normalized global imperfections: bow, camber and twist; and the local imperfections Type 1 (local – d_1/t) and Type 2 (distortional – d_2/t). To compare the results to the literature, Table 4.2 also summarizes the global imperfection measurements from Schafer and Zeinoddini [4.1] and Type 1 and Type 2 imperfection measurements from Schafer and Peköz [4.2]. Appendix E presents the imperfection values for each specimen.

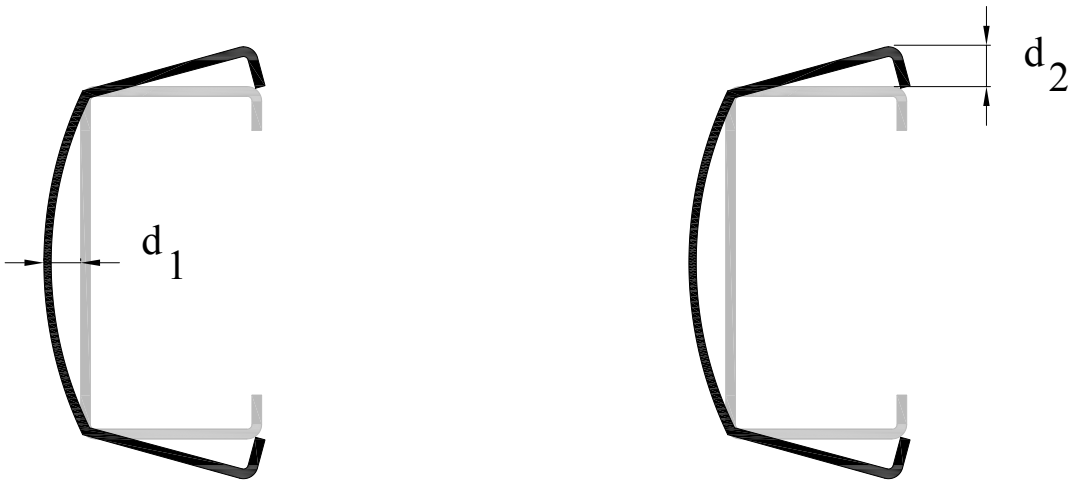

Figure 4.5 – Definition of local geometric imperfection.

Comparison of the global imperfections with [4.1] (which includes 210 samples of different size studs) indicates that the global imperfections measured in this study, of nominally identical studs, has a smaller magnitude for camber and twist, bow is nearly the same, and the variation (CoV) measured is generally smaller than [4.1]. Comparison of the Type 1 and Type 2 imperfections measured in this study, with those in [4.2], indicate lower mean and variation in Type 1 imperfections, and significantly lower mean values in the Type 2 imperfections.

Table 4.2 – Average global, local and distortional imperfections

L (m)	number of specimens	d_Φ (deg)	d_b (L/bow)	d_c (L/camber)	d_1/t	d_2/t
0.61	6	0.375	1287.8	1106.7	0.332	0.767
1.22	6	0.526	2270.5	922.6	0.295	0.236
1.83	7	0.581	3429.4	2080.4	0.264	0.176
2.44	5	0.704	2839.1	1596.2	0.335	0.240
	Total Average	0.547	2456.7	1426.5	0.306	0.354
	CoV	0.323	0.439	0.589	0.282	0.846
Schafer and Zeinoddini, Ref. [4.1]	Total Average	0.91	2242	3477	-	-
	CoV	0.648	1.362	1.623	-	-
Schafer and Peköz, Ref. [4.2]	Total Average	-	-	-	0.5	1.29
	CoV	-	-	-	1.320	0.829

4.1.4. Coupon Tests

For material testing, coupon samples are machined to ASTM standards [4.3] from the web of the stud and track specimens. To measure the base metal dimensions, the specimens are immersed in a 15% hydrochloric acid bath for 10 minutes*, which removes the zinc coating. The 0.2% offset and the autographic method are both used to define the yield stress. The 0.2% offset method is chosen as the most appropriate method to find the yield stress for the steel used in the studs because there is no yielding plateau, whereas the steel used in the track shows yielding plateau making the autographic method more appropriate. Summary of the yield stress, ultimate stress, and ultimate strain values is given in Table 4.3, see Appendix C for full results.

* The reaction (bubbling) ends after about 7 minutes, but to be consistent all the specimens were kept for 10 minutes.

Table 4.3 – Coupon test results

Specimen	number of specimens	statistic	f_y 0.2% offset (MPa)	f_y autographic method (MPa)	f_u (MPa)	ε_u	$t_{base\ metal}$ (mm)
Stud[1]	8	mean	382.9	390.2	543.9	0.19	1.666
		COV	0.011	0.009	0.009	0.163	0.003
Track[2]	2	mean	487.5	476.4	537.9	0.24	1.976
		COV	N/A[3]	0.012	0.007	0.001	0.005

(1) samples taken from the web of 362S162-68 (SSMA/ASTM nomenclature) – 345MPa (50ksi)
(2) samples taken from the web of 362T125-68 (SSMA/ASTM nomenclature) – 345MPa (50ksi)
(3) the CoV is not applicable in this case because the measured values (to available accuracy) were identical.

4.1.5. Sheathing Types and Test Configurations

Oriented strand board (OSB) (11.1 mm, (7/16 in.), rated 24/16, exposure 1) and gypsum board (GYP) (12.7 mm, (½ in.) Sheetrock Regular) are the two types of sheathing used in the tested conducted herein. When no sheathing is placed on one flange this is designated as BARE. The mechanical properties of the OSB boards are given as: Young's modulus of 6426 MPa (932 ksi) by [4.4] and shear modulus of 1310 MPa (190 ksi) by [4.5]. While the gypsum boards mechanical properties are given as: Young's modulus of 993 MPa (144 ksi) by [4.6] and shear modulus of 552 MPa (80 ksi) by [4.5]. The gypsum panels comply with ASTM C36 and additional information regarding fire rating is available in [4.7].

The testing facility is modestly climate controlled, the humidity level at storage and during testing was approximately (no higher than) the average ambient relative humidity level during that time: 62%. Gypsum properties may vary considerably depending on humidity, this issue is addressed in chapter 3, where the change in the local fastener-gypsum translational stiffness was determined in climate-controlled specimens and

shown to depend on the steady-state humidity in the gypsum boards, particularly at the extremes (near 0% or 100%) of relative humidity.

The sheathing-stud-track connection details, number 6 screws (Simpson #6 x 41.3 mm (1 5/8 in.)) are used for the gypsum boards and number 8 screws (Simpson #8 x 49.2 mm (1 15/16 in.)) for the OSB boards. The spacing between screws for the sheathing-stud connection is maintained at 305 mm (12 in.).

The specimens were named using the following nomenclature: number of test, sheathing on side 1, sheathing on side 2, shorthand designator used in pictures, length of stud, presence of track, presence of sheathing, and presence of isolation plate. For example: 2-Bare-Bare-1S6L-6-T-S-P was the second test, side 1 and side 2 didn't have sheathing (bare), the sign on any photos indicates the test as 1S6L, it has total length of 6 feet (1.83 m), it was attached to the track, it had sheathing, and the isolation plate was used.

4.2. OVERALL TEST RESULTS

Summary of the peak loads and failure mechanisms for the tests are given in Table 4.4. For the BARE-BARE configuration, the 2.44 m (8 ft) studs undergo a flexural buckling failure mechanism, the 1.83 m (6 ft) and 1.22 m (4 ft) studs show combinations of local and global failures depending on the presence of tracks, and the 0.61 m (2 ft) studs failed either in local or distortional buckling. For the OSB-BARE configuration, the 2.44 m (8 ft) and 1.83 m (6 ft) studs fail in flexural-torsional buckling with the rest of studs fail in local buckling near the member ends. For the configurations: OSB-OSB,

OSB-GYP and GYP-GYP all the studs, at all lengths, are observed to fail in local buckling near one or both of the member ends.

Table 4.4 – Peak load and failure mechanisms

Sheathing	Isolation Plate	Track	Length (m)	Peak Load (kN)	Failure Mode	Nomenclature
BARE-BARE	No	No	0.61	82.87	D[1]	4-BARE-BARE-1S2L-2
			1.22	86.08	D	3-BARE-BARE-1S4L-4
			1.83	59.62	F[2]	2-BARE-BARE-1S6L-6
		Yes	0.61	87.95	D	5-BARE-BARE-2S2LT-2-T
			1.22	84.63	FT[3]	6-BARE-BARE-2S4LT-4-T
			1.83	60.46	FT	7-BARE-BARE-2S6LT-6-T
	Yes		2.44	57.11	F	22-BARE-BARE-61S8LTP-8-T-P
OSB-BARE	Yes	Yes	0.61	95.41	L[4]	18-OSB-BARE-4S2LTSP-2-T-S-P
			1.22	97.82	L	14-OSB-BARE-3S4LTSP-4-T-S-P
			1.83	80.13	FT	12-OSB-BARE-6S6LTSP-6-T-S-P
			2.44	69.57	FT	23-OSB-BARE-62S8LTSP-8-T-S-P
Gyp-Gyp	No	Yes	1.83	105.44	L	11-GYP-GYP-8S6LTSP-6-T-S
	Yes		0.61	96.71	L	19-GYP-GYP-3S2LTSP-2-T-S-P
			1.22	99.61	L	15-GYP-GYP-4S4LTSP-4-T-S-P
			1.83	88.70	L	10-GYP-GYP-5S6LTSP-6-T-S-P
			2.44	95.05	L	25-GYP-GYP-64S8LTSP-8-T-S-P
OSB-Gyp	Yes	Yes	0.61	97.82	L	20-OSB-GYP-5S2LTSP-2-T-S-P
			1.22	96.17	L	16-GYP-OSB-5S4LTSP-4-T-S-P
			1.83	91.11	L	13-OSB-GYP-7S6LTSP-6-T-S-P
			2.44	99.86	L	24-OSB-GYP-63S8LTSP-8-T-S-P
OSB-OSB	No	Yes	1.83	119.28	L	8-OSB-OSB-3S6LTS-6-T-S
	Yes		0.61	101.59	L	21-OSB-OSB-6S2LTSP-2-T-S-P
			1.22	98.99	L	17-OSB-OSB-6S4LTSP-4-T-S-P
			1.83	99.53	L	9-OSB-OSB-4S6LTSP-6-T-S-P
			2.44	102.70	L	26-OSB-OSB-65S8LTSP-8-T-S-P

(1) D – Distortional buckling
(2) F – Minor axis flexural buckling
(3) FT – Flexural-torsional buckling
(4) L – Local buckling

As can be observed from Table 4.4, sheathing increases the capacities of the studs. The OSB-OSB sheathing configuration provides the maximum observed strength and the BARE-BARE configuration the minimum observed strength. The load-displacement response of the 2.44 m (8 ft) tests series (across sheathing types) is provided in Figure 4.6. Although axial stiffness is not greatly influenced by the presence of the sheathing, capacity and limit state are influenced by the sheathing.

In addition to the sheathing, the short segment of track at the stud ends has some influence on the behavior, as provided in Table 4.4. The addition of the track increases the peak loads of the 0.61 m (2 ft) BARE-BARE stud by 6%, but provides no significant increase for the 1.22 and 1.83 m (4 and 6 ft) studs. For the shorter stud where the failure is in distortional buckling the small end restraint provided by the track appears beneficial, while for longer specimens failing in global buckling modes, the track alone, in this isolated single testing does not have a significant impact.

Another important observation that may be concluded from the results of Table 4.4 is the effect of adding an isolation plate between the track and loading platen, so that the sheathing may not engage in direct bearing. The peak load is significantly reduced (by 20%) when the sheathing is not allowed to directly bear. Despite the fact that the sheathing is much less axially stiff than the studs direct bearing must be removed in the testing to yield a conservative result for comparison with design, where direct bearing often does not occur. This detail has not been common practice in previous testing.

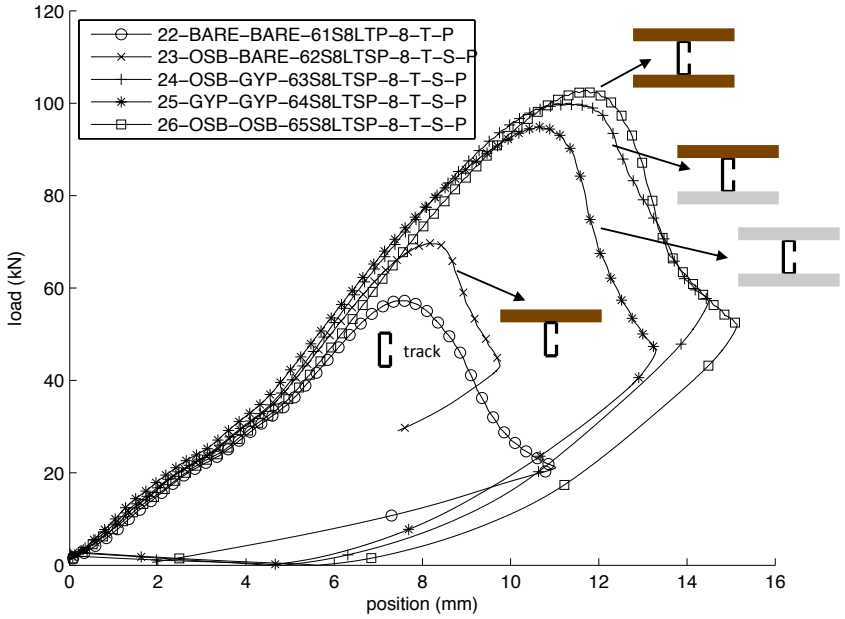

Figure 4.6 – Comparison between different sheathing combinations on the studs 2.44m (8 feet) long.

Overall, the peak load and failure mode of GYP-GYP, OSB-GYP and OSB-OSB sheathed specimens are found to be comparable. They all fail in local buckling, and the difference between the strongest configuration (OSB-OSB) and the weakest (GYP-GYP) does not vary by more than 12%. More detailed results are provided in the next section.

4.3. DISCUSSION OF OBSERVED LIMIT STATES AS A FUNCTION OF SHEATHING TYPE

Detailed experimental observations, organized by sheathing type, are provided in this section. The discussion addresses the influence of the length of the stud, end boundary conditions, and sheathing type on the observed strength and stability behavior.

For the unsheathed specimens (BARE-BARE) the importance of end conditions, and the change in buckling modes from distortional at short length to global flexural and

local-global interaction at the long length is the focus of the discussion. The BARE-BARE studs are the weakest tested and thus provide a lower bound. Specimens sheathed with OSB on only on side (OSB-BARE) radically depart in behavior from the BARE-BARE specimens: distortional buckling is replaced by local buckling at short lengths, while at long lengths flexural-torsional buckling occurs. Due to the unrestricted global buckling modes, BARE-BARE and OSB-BARE tests present excessive lateral displacements when compared to the tests with sheathing on both sides.

Specimens sheathed on both sides: GYP-GYP, OSB-GYP, OSB-OSB are discussed separately due to differences observed in the results, particularly at the fastener locations; nonetheless, they may all be grouped together given they have the same stud failure mode and similar peak load. The attachment of boards on both sides (even gypsum) mitigates global buckling, so that local and sometimes distortional buckling takes place. Differentiation between the observed failure modes, and which initiates failure, is only possible by the analysis of the observed displacements, primarily from the mid-height PT configuration depicted in Figure 4.1(c).

4.3.1. Behavior of unsheathed specimens (BARE-BARE)

4.3.1.1. Influence of track on the member end

To understand the influence of a track connected to the end of a stud, two different tests were conducted: (i) a stud loaded directly through bearing at the member ends and (ii) a stud with an attached track loaded through bearing at its ends. In both cases bearing is against a level stiff loading platen (as opposed to field conditions) so the

primary expected benefit of the track is not in improving the bearing condition, but in providing some partial rotational and warping rigidity at the member ends.

A test of an unsheathed specimen (4-BARE-BARE-1S2L-2) was carried out for a 0.61 m (2 ft) long stud with ends directly bearing against the load platens of the MTS machine (no track). At the top end, there was a noticeable gap between the load platen and stud end at the web. It is observed that the initial contact with the load platen is on the lip side only. The loading rate on the MTS machine is 0.335 mm/sec (0.013 in./sec). After loading for 45.76 kN (10.29 kips) the gap is still present though closing and it is observed that the lips open out at the top end. Global deformation can also be observed from the beginning of the test as the load bearing on the lips directly lead to eccentric loading as seen from the movement of web PT3, PT4 and PT5 (Figure 4.1(b)). At 61.02 kN (13.72 kips) the gap closes with distortional buckling starting to form at the top end and continuing through the length of the member. Distortional buckling at the mid length of the member is captured by PT1 and PT2. As the top end's gap closed failure is seen to be concentrated at the bottom end where there is a large imperfection. This resulted in the bottom end's local failure close to 80.39 kN (18.07 kips). At the peak load (82.87 kN (18.63 kips)) visible distortional and web plate (local) failures are observed at the bottom end as shown in Figure 4.7(c).

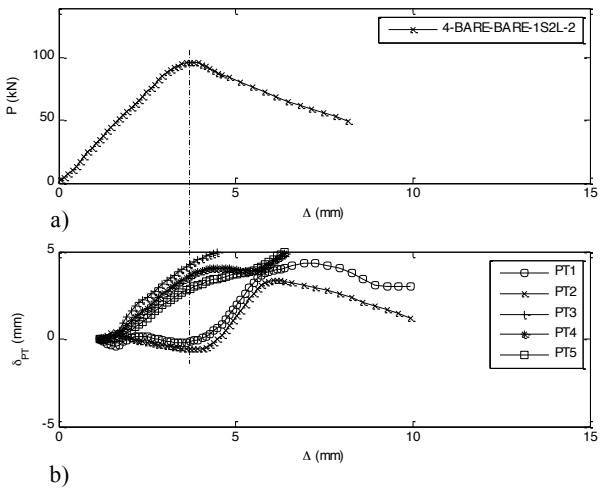

c)

Figure 4.7 – Distortional buckling failure over 0.61m (2 feet) specimen without sheathing directly bearing against load platens. a) Load-displacement, b) PT displacement, and c) buckling failures for test 4-BARE-BARE-1S2L-2

An unsheathed specimen (5-BARE-BARE-1S2LT-2-T) was tested for a 0.61 m (2 ft) stud with 610 mm (2 feet) track segments connected at the top and bottom ends. Small Gaps between track and load platen and between track and stud are observed at both ends, with the top end showing a larger gap (approximately 1.5 mm). Distortional buckling is observed as the load reaches 80.04 kN (18 kips) with the channel lips distorting inward as indicated by PT 1 and 2 in Figure 4.1(b) and those at the ends distorting outward. Local buckling waves at the ends are observed at 87.67 kN (19.71 kips), near the peak load. The bottom end of the stud is found to have more local deformation than the top, correlating with higher imperfections observed at this end [4.8]. After the peak load, weak axis global buckling is observed.

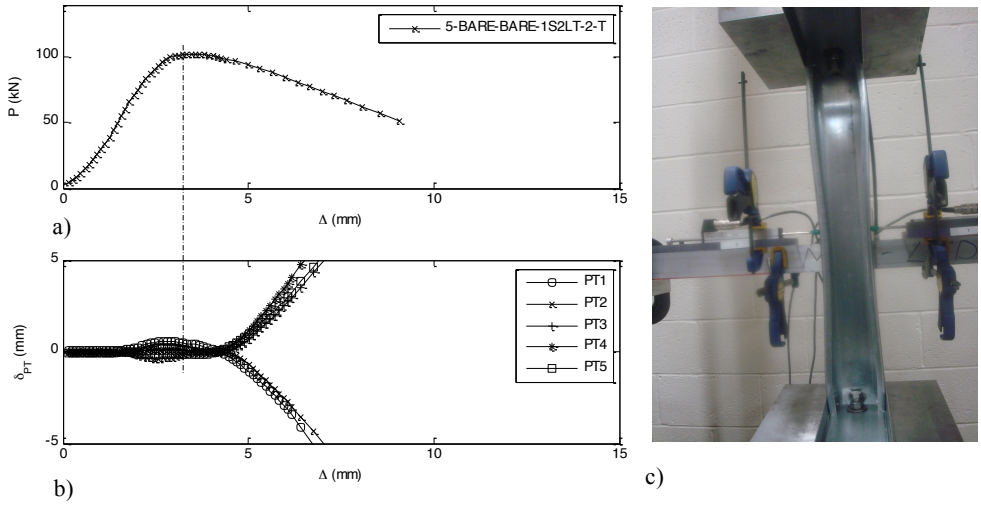

Figure 4.8 – Distortional buckling failure over 0.61m (2 feet) specimen without sheathing, the stud is connected to the track, which is loaded directly through the loading platens. a) Load-displacement, b) PT displacement, and c) buckling failure for test 5-BARE-BARE-1S2LT-2-T

4.3.1.2. Longer unsheathed studs (BARE-BARE)

A stud with length 2.44 m (8 ft) connected to the track (22-BARE-BARE-61S8LTP-8-T-P) is axially loaded using the MDOF machine. Weak axis flexure is observed as the load reaches 53.4 kN (12 kips), which can be observed in the three PTs on the web (PT3, PT4 and PT5), as shown in Figure 4.9(b). The peak load is found to be 57.1 kN (12.84 kips). Flexural-torsional buckling is also observed along with local buckling (primarily in the stud web) due to bending in the post-peak range, as shown in Figure 4.9(c).

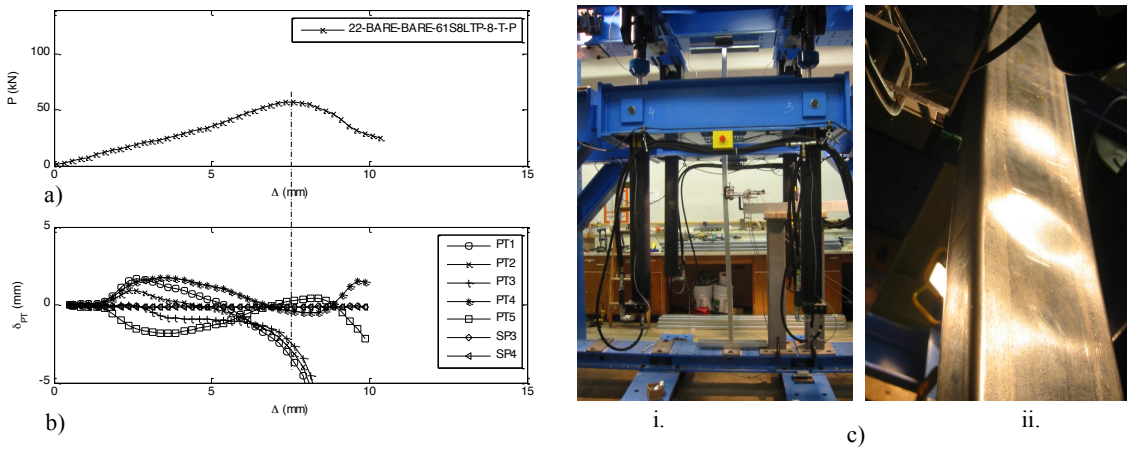

Figure 4.9 – Flexural buckling with local buckling interaction of 2.44m (8 feet) specimen without sheathing. a) Load-displacement, b) PT displacement, and c) Buckling modes (i) Side view of flexural buckling failure, (ii) Local buckling on compression side of flexural buckling wave.

4.3.2. Behavior of specimens sheathed with OSB on one side only (OSB-BARE)

The sheathing configuration in the OSB-BARE tests are such that OSB is provided on only one side of the stud. Tracks are attached to the top and bottom of the stud, with small isolation plates transferring load directly to the tracks, i.e. no direct loading of the sheathing is allowed. Typical results for a 2.44 m (8 ft) stud (i.e., 23-OSB-BARE-62S8LTSP-8-T-S-P specimen) include failure in flexural-torsional buckling, and displacements in PT 4 and 5 as provided in Figure 4.10(b). A peak load of 69.6 kN (15.65 kips) is observed. The same failure mode is found in the 1.83 m (6 ft) long studs, while the shorter studs 0.61 m (2 ft) and 1.22 m (4 ft) fail in local buckling. For shorter studs (unbraced lengths) the buckling mode is the same as found in the studs without sheathing, but for longer unbraced lengths the attachment of a sheathing on one side of the stud is

able to restrain weak-axis flexural buckling of the stud, and instead the stud fails at a higher and different, flexural-torsional buckling, mode.

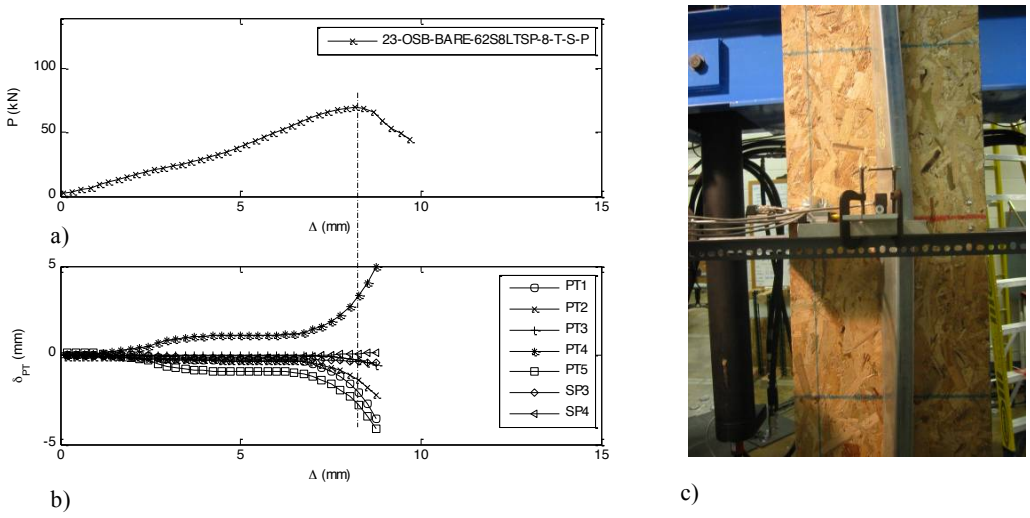

Figure 4.10 – Flexural-torsional buckling of 2.44m (8 feet) specimen with OSB on one side only. a) Load-displacement, b) PT displacement, and c) buckling failure for test 23-OSB-BARE-62S8LTSP-8-T-S

4.3.3. Behavior of specimens sheathed with gypsum on both sides (GYP-GYP)

Typical tests with gypsum sheathing on both sides of the stud fail in local buckling at the member ends, with bearing and pull-through failures at the fastener-gypsum connections in the post-peak range. However, distortional buckling is also observed, consider the 0.61 m (2ft) test with gypsum sheathing on both sides (19-GYP-GYP-3S2LTSP-2-T-S-P). In the test, the gypsum sheathing is not in direct contact with the load platen, due to the isolation plate, Figure 4.1 (a,b) With loading close to 85.79 kN (19.3 kips) distortional buckling was observed at the ends, followed by local buckling of the web at the ends at 95.30 kN (21.43 kips)(Figure 4.11(c)). Peak load for this specimen

was 96.71 kN (21.74 kips) and was followed by screws pulling-through from the side of gypsum, as indicated in Figure 4.11(d).

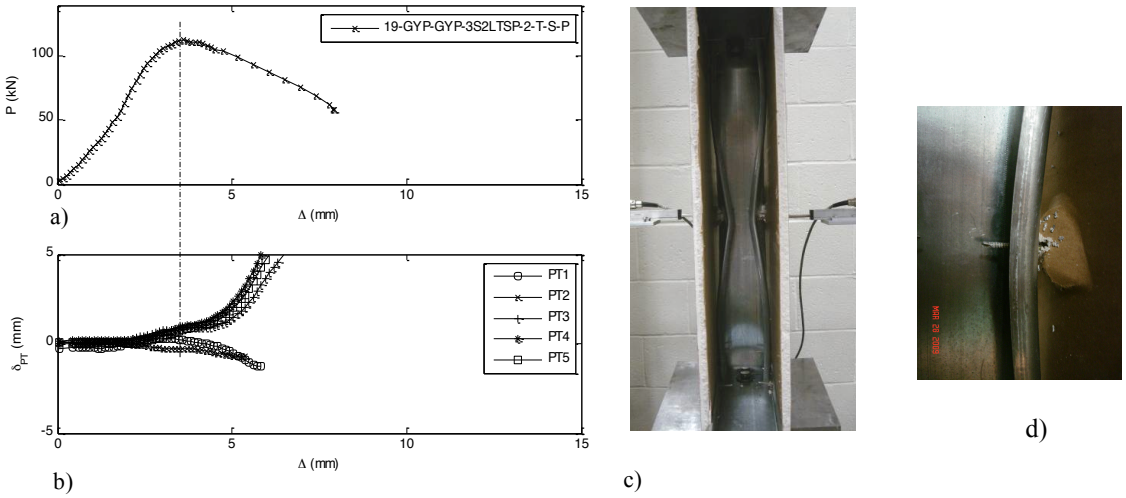

Figure 4.11 – Local buckling with distortional buckling interaction of 0.61m (2 feet) specimen with gypsum sheathing on both sides. a) Load-displacement, b) PT displacement, c) buckling failure for test 19-GYP-GYP-3S2LTSP-2-T-S-P, d) zoomed view of screw pulling-through from the side of gypsum sheathing.

4.3.4. Behavior of specimens sheathed with OSB on one side and gypsum on the other (OSB-GYP)

The typical failure mode in the OSB-GYP sheathed studs is local buckling at the member ends, but distortional buckling is also observed, such as in the 0.61 m (2 ft) stud test (20-OSB-GYP-5S2LTSP-2-T-S-P) and the 2.44 m (8 ft) stud test (24-OSB-GYP-63S8LTSP-8-T-S-P). In the 0.61 m (2 ft) OSB-GYP test at 85.79 kN (19.29 kips), local buckling waves are observed at the ends, but at the peak load (Figure 4.12(a)), distortional buckling along with local buckling at the ends is observed (Figure 4.12(c)). In the 2.44 m (8 ft) stud tests string pots (SP) are added at the ends to record the local deformation, Figure 4.13(b). Local buckling followed by distortional buckling at the top end of the 2.44 m (8 ft) OSB-GYP stud test leads to significant damage in the gypsum In

all the OSB-GYP tests more damage occurs at the fastener locations on the GYP side, with screws pulling-out, as opposed to the OSB side, which remains largely intact with some minor bearing damage.

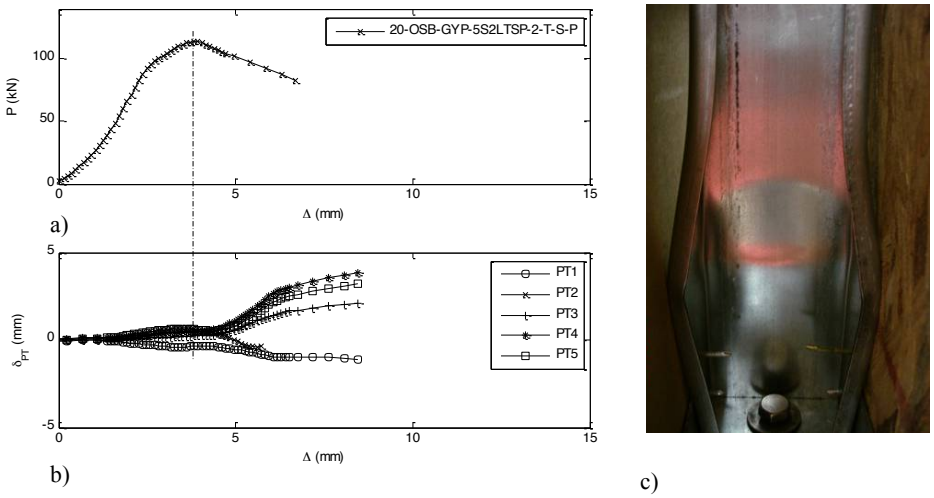

Figure 4.12 – Local buckling at the end of 0.61m (2 feet) specimen with OSB sheathing on one side and gypsum on the other. a) Load-displacement, b) PT displacement, and c) buckling failures for test 20-OSB-GYP-5S2LTSP-2-T-S-P

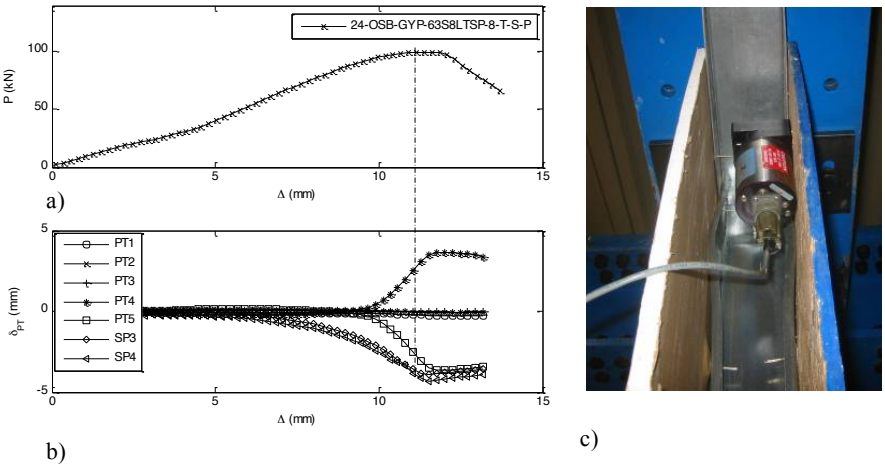

Figure 4.13 – Local buckling at the end of 2.44m (8 feet) specimen with OSB sheathing on one side and gypsum on the other. a) Load-displacement, b) PT displacement, and c) buckling failures for test 24-OSB-GYP-63S8LTSP-8-T-S-P

4.3.5. Behavior of specimens sheathed with OSB on both sides (OSB-OSB)

The specimens with OSB sheathing on both sides fail in local buckling. Consider for example a 2.44 m (8ft) stud test (26-OSB-OSB-65S8LTSP-S-T-S-P). As the load reaches the peak at 93.4 kN, (21 kips) the string pot (SP) on the top is first observed to record the movement, as shown in Figure 4.14(b). As the peak load approaches (Figure 4.14(a)), the bottom string pot (SP) is also observed to pick up the corresponding local buckling at that end, Figure 4.14(c).

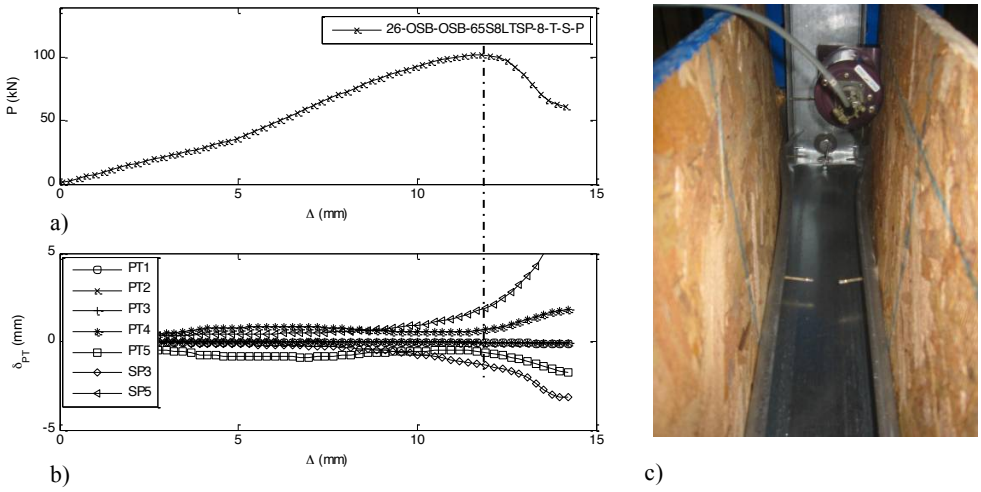

Figure 4.14 – Local buckling at the end of 2.44m (8 feet) specimen with OSB sheathing on both sides. a) Load-displacement, b) PT displacement, and c) buckling failures for test 26-OSB-OSB-65S8LTSP-S-T-S-P

4.4. COMPARISON WITH DESIGN METHOD PREDICTIONS

4.4.1. Boundary Conditions

In the testing conducted herein the end boundary conditions were observed to be highly influential. From a design standpoint, the effective length factor (K) which is also

a function of end conditions, has one of the most significant impacts on predicted strength, but is generally poorly understood for stud-to-track connections [4.9, 10]. An ABAQUS [4.11] model was developed to explore this issue further, Figure 4.15. The finite element model of the track and stud consists of linear 9 nodes shell elements (S9R5). The fasteners and contact between stud and track were simulated using linear multi-point constraints. The stud-to-track fasteners were idealized by coupling all degrees of freedom except the rotation around the axis of the fastener at the stud-to-track fastener locations. The contact between track and the stud end was simulated by coupling the translational displacements in the longitudinal direction of the stud, but leaving the stud still free to slide in the plane of the track's web, i.e. a full contact (no friction) condition.

The model was compressed from the top and the resulting eigenbuckling modes explored. As shown in Figure 4.15, the studs can buckle in flexural buckling about the minor axis, flexural-torsional buckling, and local buckling at the ends. The buckling loads calculated in the model for pure flexural buckling and flexural-torsional buckling had a maximum of 3% difference when compared to the theoretical values ([4.12]) considering fixed-fixed boundary conditions ($K_x=K_y=K_t=0.5$). Also, it is significant that the first local buckling mode was at the member ends, consistent with the tests.

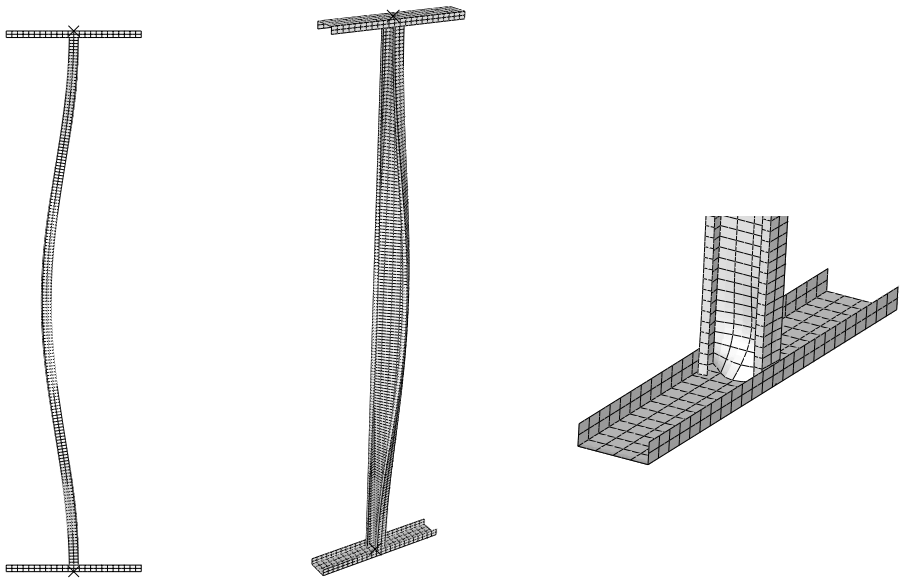

Figure 4.15 – Buckling modes for studs connected to track. a) Flexural Buckling in the minor axis, b) Flexural-torsional buckling, c) Local buckling at the end.

The modeling evidence that the global end conditions can be approximated as fix-fix ($K_x=K_y=K_t=0.5$) is also supported by the experimental observations. Figure 4.16 compares the BARE-BARE test results against the AISI Specification [4.13]. As can readily be observed the choice of end condition is far more important than local buckling design method (Eff. Width or DSM) and fixed-fixed end conditions with $K_x=K_y=K_t=0.5$ provide the best agreement with testing.

The use of $K_x=K_y=K_t=0.5$ in design/practice requires additional discussion, and may not be warranted in many important cases. First, in the testing the stud-to-track gap was eliminated to the maximum extent possible through pre-compression of the assembly in a jig. The impact of stud-to-track gap on performance is discussed further in [4.9]. More importantly, the tested members bear against stiff, level end surfaces. This allows for an excellent bearing condition, that under sufficient axial load, results in warping end restraint (similar to the model above). For uneven bearing surfaces this restraint may not

be present. Testing under field, or simulated field conditions would be useful for potentially extending the observed beneficial end conditions to practice.

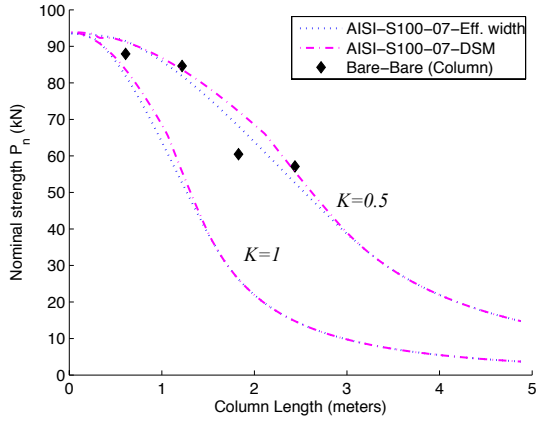

Figure 4.16 – Bare tests and code predictions.

4.4.2. Diaphragm stiffness developed by the board

For sheathing to provide buckling restraint to a stud, forces must develop at the stud-to-sheathing fastener (local) locations, and the sheathing itself must be capable of resisting deformation as a shear diaphragm. All of the specimens with sheathing on both sides (OSB-OSB, OSB-GYP, GYP-GYP) received sufficient restraint from the sheathing to restrict global and distortional buckling and develop local buckling limit states. As detailed analytically and experimentally in chapter 3 the local (fastener) and diaphragm (sheathing) resistances are in series with one another. Thus, both resistances must be present to restrain the global and distortional buckling modes.

Given that the test setup (Figure 4.1) consists of only a single vertical row of fasteners from the stud to the sheathing, and no restraint along the vertical sheathing edges, it was somewhat surprising that the sheathing was able to successfully act as a shear diaphragm and resist the forces at the fasteners. Testing conducted in Chapter 3

demonstrates that board continuity (no horizontal breaks) is the main factor necessary to guarantee the existence of the diaphragm stiffness. If horizontal breaks exist the shear resistance of the diaphragm cannot be engaged to resist the differential in local forces at the stud-to-fastener connection and thus no resistance is provided to the stud at the fastener locations. These results indicate that sheathing diaphragm resistance is available even in narrow aspect ratio walls.

For design, caution must be exercised when extending the assumption that any sheathing provides adequate resistance to resist global and distortional buckling modes. First, the bracing demands on the sheathing are dependent on the stud and the fastener-sheathing system stiffness; second the bracing capacity of the sheathing is dependent on local details of the fastener, and strength of the sheathing. Chapter 3 provides insights on determining the available stiffness from the fastener-sheathing system and properly incorporating the influence of fastener spacing, stud spacing, etc. in the stiffness determination. For OSB and plywood sheathing general guidance exists, but the use of diaphragm resistance derived from gypsum board remains a complicated issue. Under controlled conditions, such as the testing reported herein, the reasonably large shear stiffness of gypsum board is typically sufficient to develop adequate bracing forces. In reality one must be careful to consider humidity, low-cycle damage, and gypsum boards inability to accommodate even small deformations without damage.

4.4.3. Comparison between design methods

The test results are compared to the available North American design specifications in Figure 4.17. Included in the comparison are: (a) AISI-S100-07-Eff. Width which ignores any sheathing restraint as provided in the main body of the 2007 AISI Specification, (b) AISI-S100-01-restricted-Gyp-Gyp ([4.14]) based on the method developed by Simaan and Peköz [4.15] and utilized in the 2001 AISI Specification (c) AISI-S210-07 ([4.16]) assuming that the sheathing is able to restrain the stud at an unbraced length equal to twice the fastener spacing, this design curve is based loosely on Green et al. [4.17], also known as Winter's method, as provided in the Wall Stud Standard of the 2007 AISI Specification. All of the design curves assume $K_x=K_y=K_t=1$ as the codes suggest, Figure 4.17.

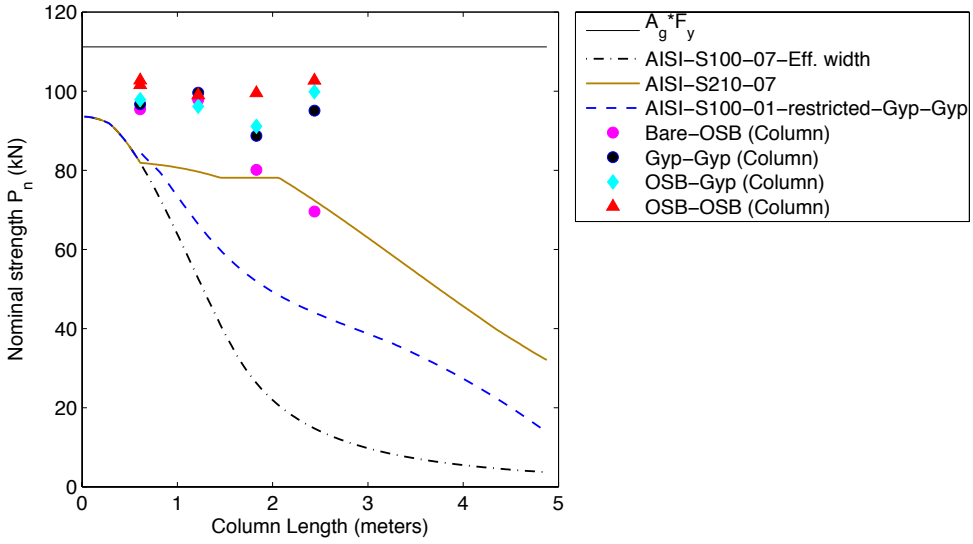

Figure 4.17 – Design curves, focus on Winter and Pekoz's method

As implemented in Figure 4.17, AISI-S100-07 ignores the beneficial end condition and the benefit of sheathing restraint. This is too conservative to be practical and shows the enormous benefits to be gained from properly including the end and sheathing restraint. As Figure 4.16 shows, for known end conditions the configuration without sheathing can be reliably predicted, but the additional benefit of the sheathing would still be ignored. Design methods for including sheathing bracing are important for economical structures.

As implemented in Figure 4.17, AISI-S100-01 also known as the Simaan and Peköz method receives some of the benefit from the additional sheathing restraint, but is far below the tested capacity. Additional limitations of this approach were discussed in Chapter 2 and also in [4.18], and while observed to be conservative in nature, the approach is not currently recommended for design (AISI dropped this method from its Specification in 2004).

As implemented in Figure 4.17, AISI-S210-07, a modern interpretation of Winter's method, provides predicted capacities closest to the testing. The model assumes that the effective stud length (KL) is equal to twice the fastener spacing. As shown in [4.18] and also discussed in Chapter 2, this is accurate in isolated cases, but not is a general rule. In fact, it entirely depends on the relative stiffness between the stud and the fastener-sheathing system that braces the stud.

REFERENCES CHAPTER 4

4.1. Schafer, B.W. and V.M. Zeinoddini. *Impact of global flexural imperfections on the cold-formed steel column curve*. in *19th International Specialty Conference on Recent Research and Developments in Cold-Formed Steel Design and Construction*. 2008.

4.2. Schafer, B.W. and T. Peköz, *Computational modeling of cold-formed steel: Characterizing geometric imperfections and residual stresses*. Journal of Constructional Steel Research, 1998. **47**(3): p. 193-210.

4.3. ASTM, *E 8M-04, Standard Test Methods for Tension Testing of Metallic Materials (Metric)*. 2004, ASTM International: West Conshohocken, PA.

4.4. APA-D510C, *Panel Design Specification*, A.-T.e.W. Association, Editor 2008: Tacoma, Washington, USA.

4.5. NDS, *National Design Specification (NDS) for Wood Construction, ANSI/AF&PA NDS*, A.F.a.P. Association, Editor 2005: Washington, DC.

4.6. GA-235-10, *Gypsum Board Typical Mechanical and Physical Properties*, 2010, Gypsum Association: Hyattsville, MD, USA.

4.7. USG, *Panels and Acessories, Gypsum Products*, in *SA927 09250/USH*, U.S.G. Company, Editor 2002: Chicago, IL, USA.

4.8. Shifferaw, Y., L.C.M. Vieira Jr, and B.W. Schafer, *Compression Testing of Single Column Studs with Sheathing Configurations*, in *A supplemental report for AISI-COFS Project on Sheathing Braced Design of Wall Studs*2009, The Johns Hopkins University: Baltimore.

4.9. Laboube, R.A. and P.F. Findlay, *Wall stud-to-track gap: Experimental investigation.* Journal of Architectural Engineering, 2007. **13**(2): p. 105-110.

4.10. Miller, T.H. and T. Pekoz, *Behavior of cold-formed wall stud-assemblies.* Journal of structural engineering New York, N.Y., 1993. **119**(2): p. 641-651.

4.11. ABAQUS, *ABAQUS/Standard Version 6.7-1*, D. Systemes, Editor 2007.

4.12. Sarawit, A., *CUTWP Thin-Walled Section Properties*, www.ce.jhu.edu/bschafer/cutwp, Editor 2006, November 2010.

4.13. AISI-S100, *North American Specification for the Design of Cold-Formed Steel Structural Members.* American Iron and Steel Institute, 2007.

4.14. AISI-S100, *North American Specification for the Design of Cold-Formed Steel Structural Members.* American Iron and Steel Institute, 2001.

4.15. Simaan, A. and T.B. Pekoz, *Diaphragm Braced Members and Design of Wall Studs.* ASCE J Struct Div, 1976. **102**(1): p. 77-92.

4.16. AISI-S210, *North American Specification for the Design of Cold-Formed Steel Structural Members.* American Iron and Steel Institute, 2007.

4.17. Giles G. Green, G.W., T. R. Cuykendall, *Light Gage Steel Columns in Wall-braced Panels.* Cornell University Engiineering Experiment Station, 1947. **35**: p. 1-50.

4.18. Schafer, B.W., O. Iourio, and L.C.M. Vieira Jr, *Notes on AISI Design Methods for Sheathing Braced Design of Wall Studs in Compression*, in *A supplemental report for AISI-COFS Project on Sheathing Braced Design of Wall Studs*2008, The Johns Hopkins University: Baltimore.

CHAPTER 5 - FULL-SCALE TEST OF CFS WALL

A series of twelve full-scale walls, cold-formed steel studs with different sheathing configurations, were tested under axial compression. This chapter concentrates on the impact of different types of sheathing being attached to the side of the wall, specifically BARE (no sheathing), oriented strand board (OSB) or Gypsum (Gyp). Wall sheathing combinations for the two sides of the wall consisting of BARE-BARE, OSB-BARE, Gyp-Gyp, OSB-Gyp and OSB-OSB were all tested. Results revealed that the attachment of boards to the side of the wall can increase the axial strength of the wall by as much as 91%, for example, when comparing the case of BARE-BARE to that of OSB-OSB. However detrimental results were also observed, specifically the OSB-BARE walls had no post-buckling reserve as they failed in a dramatic flexural-torsional mode. In walls with symmetric sheathing (OSB-OSB and Gyp-Gyp), the observed failure mode of the stud was local buckling, and exhibited deformations essentially identical for the two sheathing types. However, for the case with asymmetric sheathing (OSB-Gyp) local buckling failure modes as well as other failure modes were observed in the studs.

5.1 COLD-FORMED STEEL WALL STUDS

5.1.1 Design

The studs, boards and screws are essentially the same as those used in the column tests (Chapter 4), but they are again provided here: The studs used in the test are 362S162-68's (345MPa (50 ksi)) (SSMA/ASTM nomenclature) throughout, the same used in the columns tests (Chapter 4). Two types of sheathing are employed: OSB (11.1 mm, (7/16 in.), rated 24/16, exposure 1) and Gypsum (12.7 mm, (½ in.) Sheetrock

Regular). Number 6 screws (Simpson #6 x 41.3 mm (1 5/8 in.)) were used to connect to the Gypsum boards and number 8 screws (Simpson #8 x 49.2 mm (1 15/16 in.)) to connect to the OSB boards. The boards are connected to the studs every 152mm (6 in.) at the edge studs and every 305 mm (12 in.) inches in the field studs. The wall design is summarized in Figure 5.1.

The wall is connected to the upper load beam and lower fixed beam of the MDOF machine through 12.7mm (½ in.) bolts through the track at every stud location. In addition 12.7mm (½ in.) plates are used below each stud to insure the wall board (sheathing) are never allowed to engage in direct bearing. This detail was shown in Chapter 4 to have a significant impact on axial bearing capacity and is an important consideration when comparing to experimental results of others.

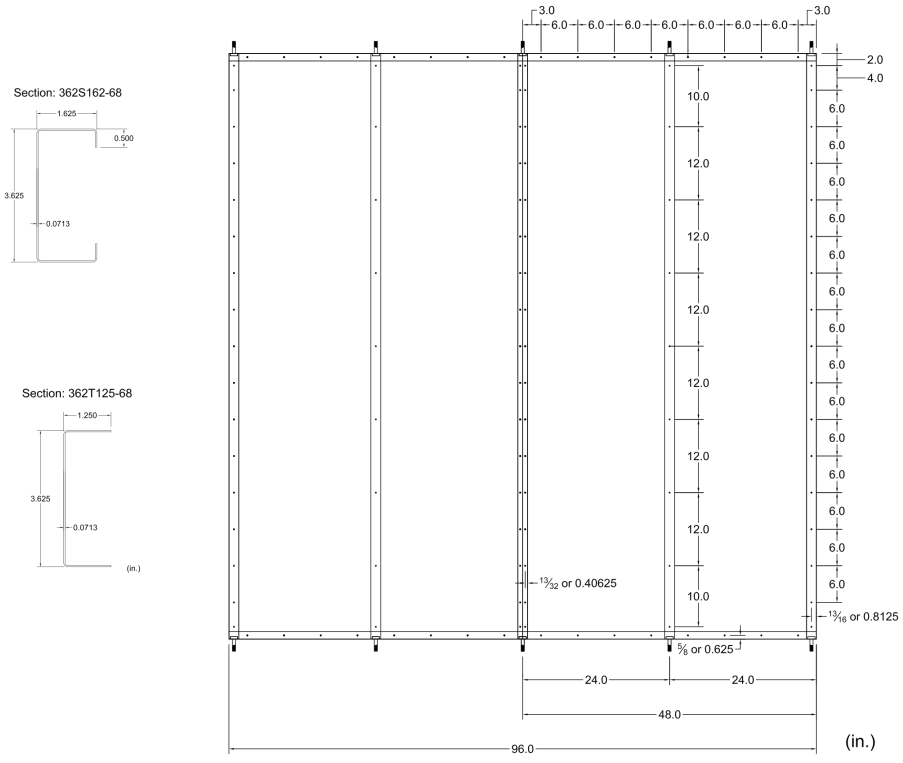

Figure 5.1 – Wall detail with typical fastener schedule

5.1.2 Instrumentation

Position transducers and string pots were utilized to record supplemental displacements. The exact position transducer setup and location depended on the test and the previous data collected. Therefore, a record indicating where the position transducers (PT) were located was created for each test, see Appendix F. Five string pots and eleven position transducers were installed in each test.

Four string pots were positioned on the top of the upper load beam and one was placed over the horizontal shear actuator. The string pot data is useful to confirm the actuator displacements and to determine deformations of the testing rig that connects the actuator to the beam. To have a "fixed" reference point the string pots were connected to the ceiling of the lab (which supports a mezzanine area which sees little if any use and may be regarded as static), see Figure 5.2(a).

The PTs were grouped in different formations. Single PTs that measure the out-of-plane displacement of the wall, Figure 5.2(b), or the displacement of the web (local buckling of the web), Figure 5.2(c). There are also groups of three PTs that are able to capture eventual twisting, local and global buckling; one of the PTs is placed in the middle and the other two (edge) are placed right after the outside corner web and flange, Figure 5.2(d). Also, groups of two PTs are similarly placed, but are only capable of capturing twisting and global buckling, Figure 5.2(e). In some tests a webcam was placed close to the single PT that reads the displacement at the end of the stud, Figure 5.2(c).

a) String Pot, checking actuator displacement

b) PT checking displacement out of the wall plane

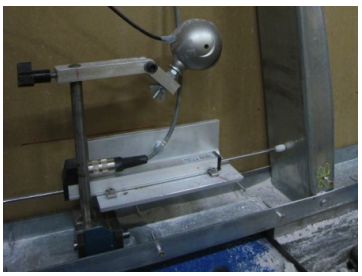

c) PT checking local buckling at the end of stud and webcam

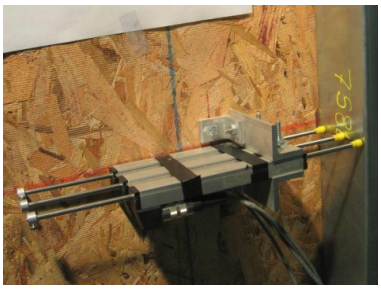

d) PT checking flexural, torsional and local buckling

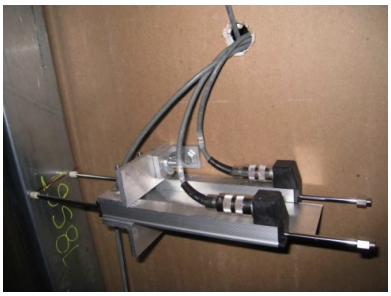

e) PT checking flexural and torsional buckling

Figure 5.2 – Typical instrumentation installed on walls

5.2 RESULTS AND DISCUSSION

A condensed summary of the test results is provided in Table 5.1. As expected the ascending order of values for peak load is BARE-BARE, OSB-BARE, Gyp-Gyp, OSB-Gyp and OSB-OSB. The walls with Gypsum on both sides support more load than the walls with OSB board on only one side, increasing the peak load 10%. The attachment of boards on both sides, independently of which kind (a point discussed further in the next section), is experimentally observed to provide post-buckling reserve. If the wall has one side OSB and the other Gypsum, there is a boost in the peak load of 9% compared to the Gyp-Gyp walls, and if both sides are covered with OSB there is a boost of an additional 3% compared to the OSB-Gyp wall. This means that for the walls with sheathing on both

sides strength varies 12% from the weakest (Gyp-Gyp) to the strongest (OSB-OSB), additionally relatively stable post-buckling and post-peak response is observed and the wall gradually loses its capacity to support the load under deformation controlled load application, unlike the OSB-BARE wall, which abruptly fails. It should be noted that in all cases there is a significant change in the peak load compared to the BARE-BARE wall.

Table 5.1 – Condensed summary of test results, ascending order of load.

Sheathing	Nomenclature	Peak Load (kN)	Limit State	Mean (kN)	CoV
BARE-BARE	2-BARE-BARE	250.56	FT[1] and F[2]	250.56 (250.56/5=50.11)	-
OSB-BARE	12-OSB-BARE	362.82	FT	389.96 (389.96/5=77.99)	0.06
	1-OSB-BARE	396.81	FT		
	6-OSB-BARE	410.24	FT		
Gyp-Gyp	7-GYP-GYP	418.42	L[3]	428.74 (428.74/5=85.75)	0.02
	11-GYP-GYP	429.94	L		
	4-GYP-GYP	437.86	L		
OSB-Gyp	10-OSB-GYP	458.37	L	466.67 (466.67/5=93.33)	0.02
	3-OSB-GYP	470.20	L		
	8-OSB-GYP	471.44	L		
OSB-OSB	5-OSB-OSB	471.67	L	479.47 (479.47/5=95.89)	0.02
	9-OSB-OSB	487.28	L		

(1) FT – Flexural-torsional buckling
(2) F – Minor axis flexural buckling
(3) L – Local buckling

5.3 TEST DISCUSSIONS

The following sub-items bring a discussion of each test configuration.

5.3.1 Behavior of unsheathed specimens (BARE-BARE)

For the BARE-BARE configuration only one test was done (labeled 2-BARE-BARE). Figure 5.3 shows the test set up and one of the studs undergoing unrestrained

flexural-torsional buckling, Figure 5.3(c). Figure 5.4 shows the position transducers (PTs), their location, and a plot of the measured displacement. All the PT data is relative from a fixed point, in this case the ground. The horizontal axis in the graph is relative to the vertical displacement of the actuators and the vertical axis is the displacement measured by the PTs.

At around 200kN (45 kips) position transducer number 7, which was placed at stud number 2 (S2, Figure 5.4), was the first stud to initiate buckling (see inset of Figure 5.4) in flexural-torsional buckling. This was followed by stud 4, which also buckled in flexural-torsional buckling (see Figure 5.4 for stud locations in the wall). The peak load was reached at 250kN (56 kips), and although the other studs were already showing some deformation according to the PT data, only after the peak were the other studs (S1, S3, S5) visually buckling. Stud number 3 and 5 buckled in a pure flexural mode and all the others buckled in a flexural-torsional mode. The test demonstrated that studs in a full wall at 2.44m (8ft) may fail in competing global buckling modes depending on the imperfections and redistribution of load within the walls.

As related in Chapter 4 the (BARE-BARE) single column test resisted 71kN (16 kips), which if extrapolated to the wall should theoretically be able to carry 290kN (65kips) (5 studs · 71kN); however, the wall carried only 250kN (56 kips). It is postulated that this lower result is because the wall fails when the weakest of 5 wall studs fails. As without the sheathing in place effective redistribution is nearly impossible.

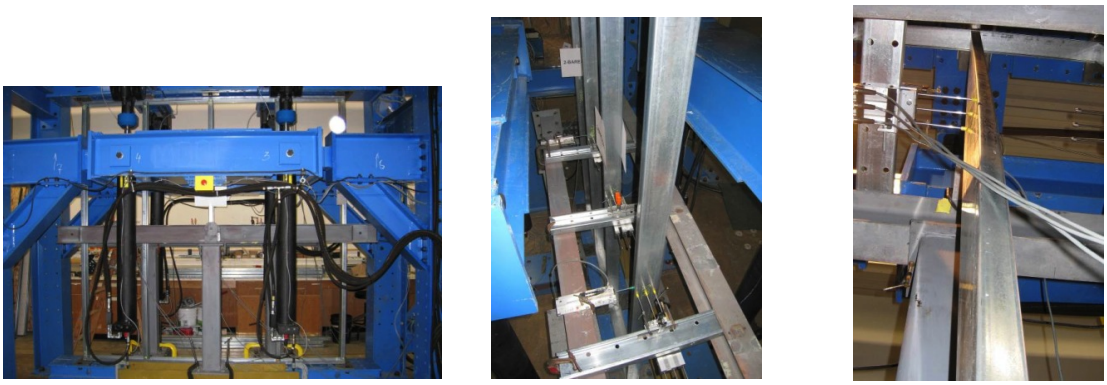

a) Side view

b) Position Transducers

c) Flexural torsional buckling

Figure 5.3 – Response of specimen 2-BARE-BARE

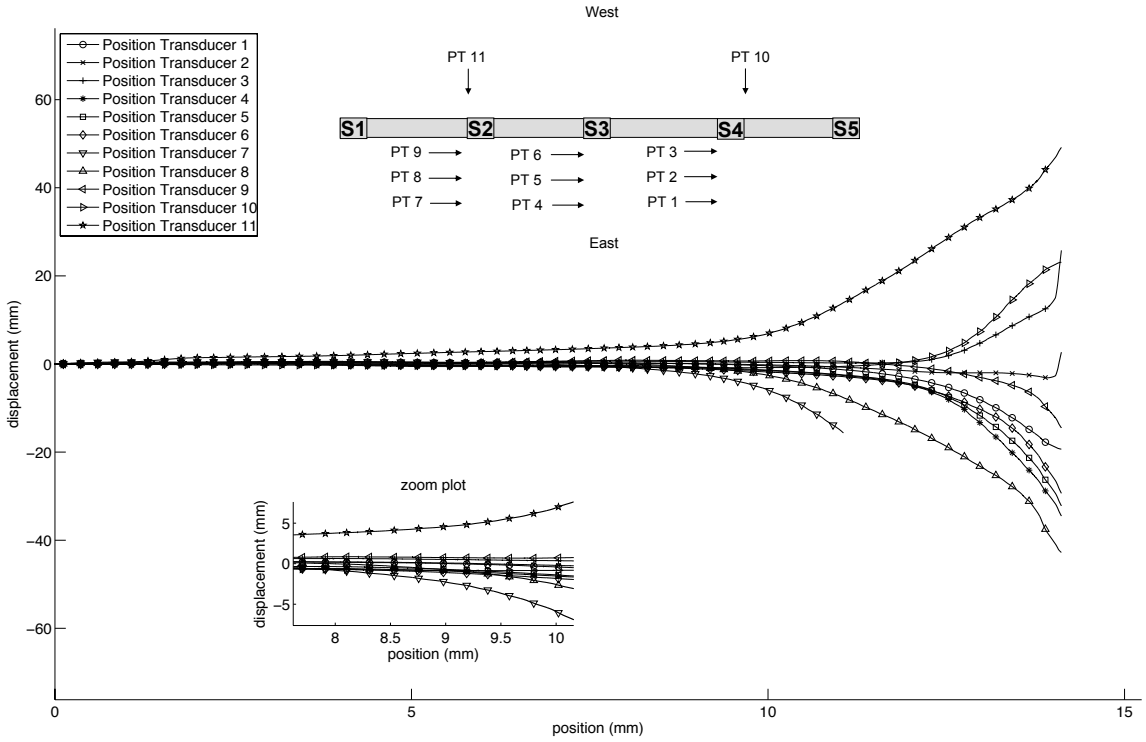

Figure 5.4 – Measured displacements for wall 2-BARE-BARE

Another important observation is the behavior at the connection between the track and stud, Figure 5.5, which is also discussed in section 4.4.1. The track and studs are

connected through two screws, one in each flange. Those two points are fixed and they stay connected throughout the whole test. The stud is free to lift off the track but it does not have enough strength to penetrate the track. The restriction, even though unique to the test, can be considered a kind of partial fixity against twist at the stud ends. That is the member ends are not theoretical simple supports, even when sheathing is not in place.

a) Contact web and track

b) Contact flange and track

Figure 5.5 – Stud to track contact during testing

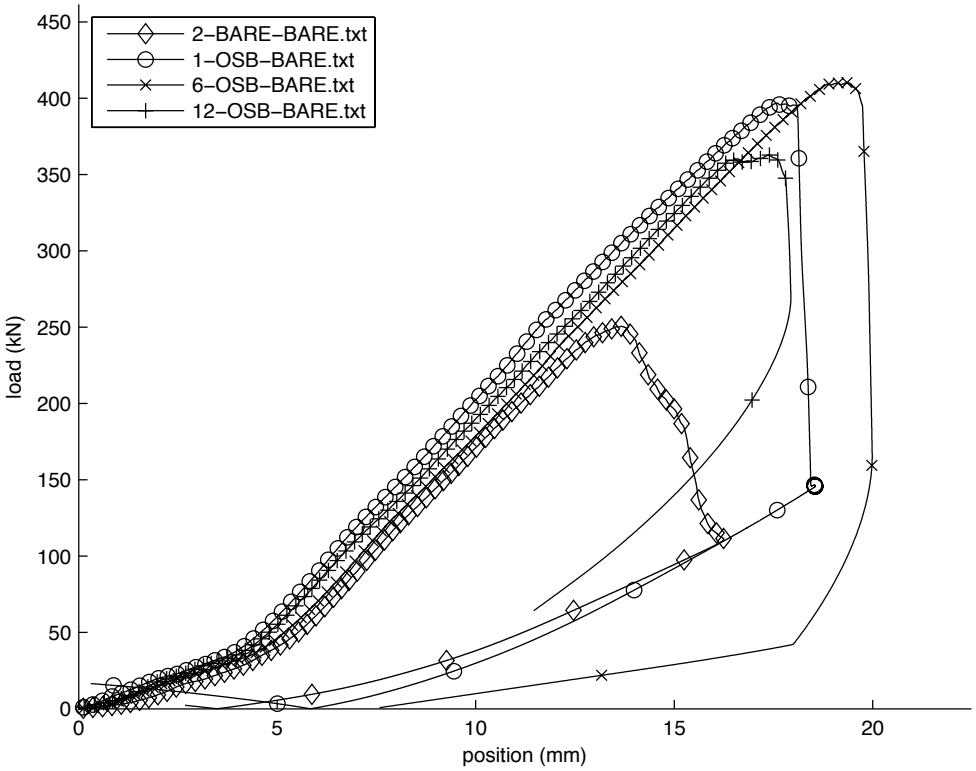

Figure 5.6 – P-Δ for BARE-BARE and OSB-OSB walls

The BARE-BARE wall test also serves as a lower bound, and may be compared with the OSB-OSB upperbound as in Figure 5.6. The dramatic difference in the load carrying capacity, from the addition of the sheathing, is illustrated by Figure 5.6.

5.3.2 Behavior of specimens sheathed with OSB on one side only (OSB-BARE)

Figure 5.7 provides an overview of the 1-OSB-BARE wall test, including setup and observed failure: restrained flexural-torsional buckling. PT7 is the first instrument to indicate the resulting instability, see inset of Figure 5.8(a). PT7 is the farthest PT from the board (at stud number 7) and its large response indicates the presence of twist.

Specifically, the difference between PT 7 and 9 gives the rotation of the stud, and the difference between the imaginary line connecting PT 7 and 9, compared to PT 8, gives the local buckling wave formed.

All of the PTs (Figure 5.4) followed the same trend (except number 10 which was measuring the out of plane displacement and as it was predicted PT10 displaced from the beginning of the test). At approximately 191 kN (43 kips) PT 7 showed an abrupt change in direction and indicated failure of the wall, at stud 7, in twist. The wall failed in flexural-torsional buckling with no post-buckling (or post-peak) reserve.

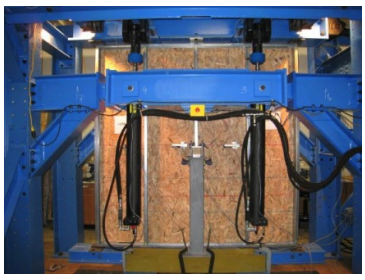

a) Side view

b) Position transducers measuring displacement

c) Wall after test

Figure 5.7 – Response of Specimen 1-OSB-BARE

Variation in the load response of the OSB-BARE tests was relatively high (see Table 5.1). Consider test 6-OSB-BARE, which had the highest peak load of the OSB-BARE tests, at 410 kN (92 kips); interestingly, what occurred during the test was that one of the studs started to twist towards the flange side instead of towards the lip side (the usual side that buckles). After the other studs all buckled towards the lip side the stud had to reverse its initial twist before finally twisting to the lip side and failing along with the

rest of the wall. Thus, providing a physical demonstration of the imperfection sensitivity of this failure mode.

The most important feature of the OSB-BARE wall tests was the pronounced lack of post-buckling reserve. The failures were dramatic, in sharp contrast even to the single column tests (Chapter 4) with the same sheathing configuration. The load-displacement response of Figure 5.9 does not do justice to the violent nature of the observed collapse, even in displacement controlled loading. Given the nature of this collapse the common practice of using strap on the BARE side may not be sufficient to restrict this mode (i.e., blocking or sheathing may be necessary).

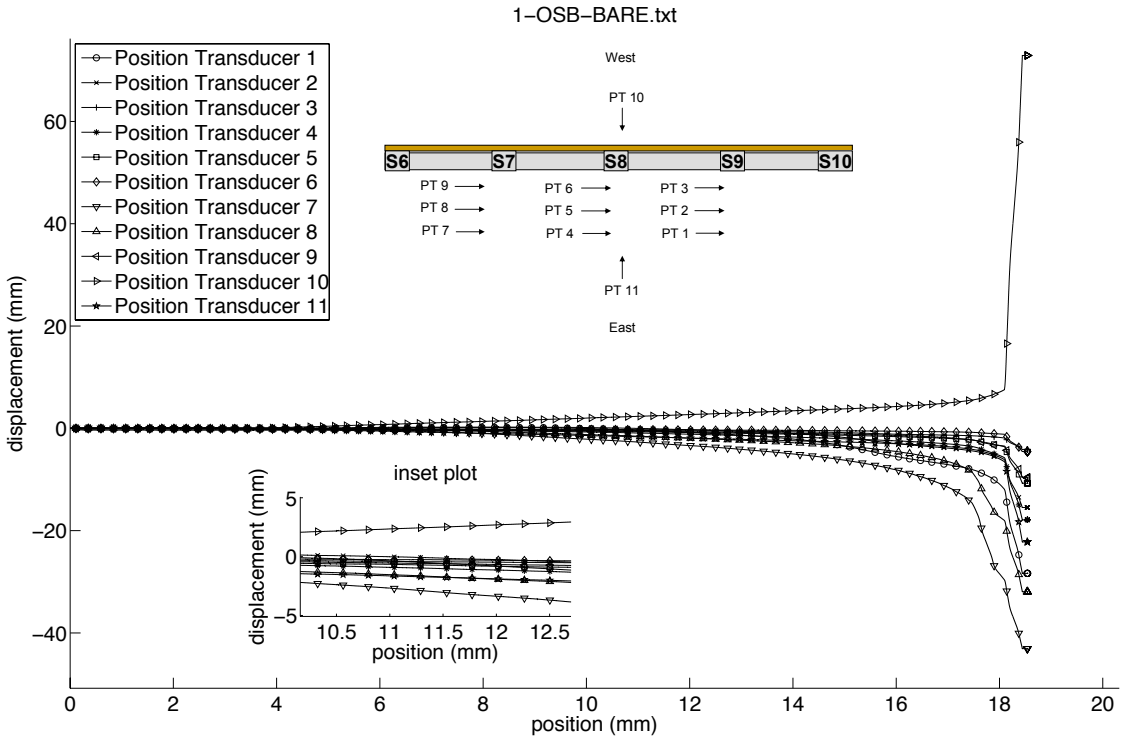

Figure 5.8 – Measured displacements for wall 1-OSB-BARE

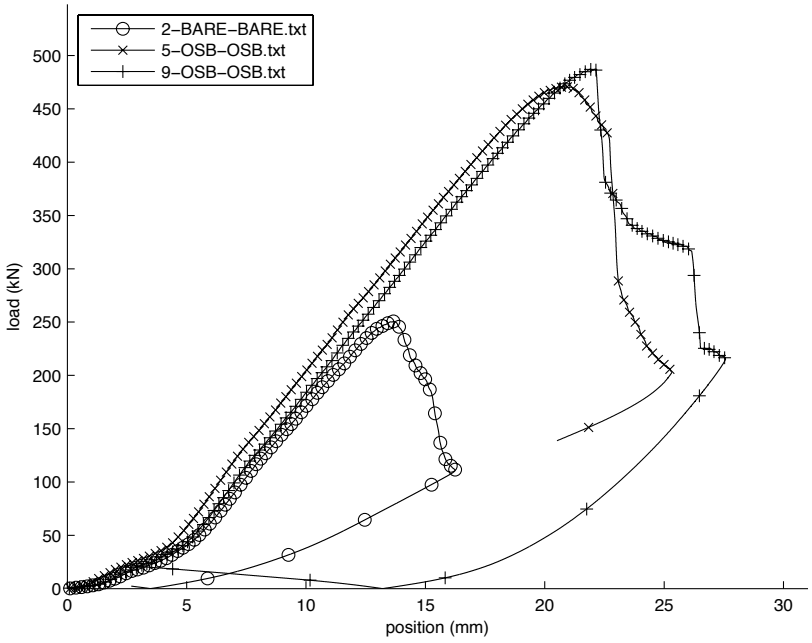

Figure 5.9 – P-Δ for OSB-BARE walls

5.3.3 Behavior of specimens sheathed with gypsum on both sides (GYP-GYP)

The walls with gypsum sheathed on both sides failed in local buckling, as Figure 5.10 shows for the 4-Gyp-Gyp test. The peak load was 436 kN (98 kips), and Figure 5.10(b) and (c) shows the wall after being opened, where it is more clear how the local buckling develops and what yielding mechanisms occur as the stud inevitably collapses. Another interesting feature of Figure 5.10(a) is the damage in the Gypsum board. At some point as the local buckling deformations increase the gypsum board loses its ability to restrain the fastener and the "brace" at this discrete location is lost.

A more detailed analysis of the 4-Gyp-Gyp test is provided in Figure 5.11, where the inset shows that stud number 18 was the one that initiated failure, due to local buckling at the bottom. However, it is interesting to note that PT 3, at the top of stud 17,

was also showing signs of local buckling at the same level of deformation. Although both locations had similar deformations stud number 18 had greater initial imperfections than stud 17 and this was what probably triggered the local failure (see Appendix E). But, in fact, stud 19 had the biggest initial local imperfection and the difference was not enough to buckle stud 19 before the others.

a) Local buckling at the end

b) Wall opened after the test

c) Local buckling followed by distortional buckling

Figure 5.10 – Response of specimen 4-Gyp-Gyp

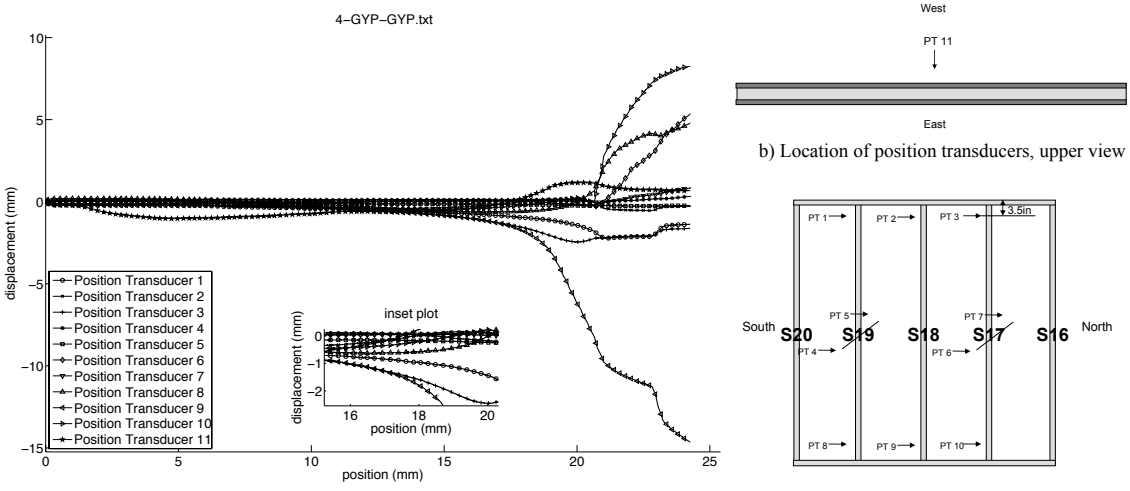

a) Position transducers plot

b) Location of position transducers, upper view

c) Location of position transducers, side view

Figure 5.11 – Measured displacements for wall 4-Gyp-Gyp

Although the gypsum sheathed tests were dominated by local buckling failures, Figure 5.12 which shows pictures after the 7-Gyp-Gyp test wall was opened, indicates distortional buckling occurred as well. It should be noted that every stud failed in local buckling at the ends except for the one stud which failed in distortional buckling. The observed damage in the gypsum board provides a clue to the developed buckling mode within, with local buckling (Figure 5.12(d) and (e)) leading to "bubbling" in the paper and loss of large divots of board, and distortional buckling (Figure 5.12(c)) being connected to pull-through of the fastener. The distinction between local buckling and distortional buckling can be quite subtle and the preceding discussion relies primarily on the (half-wave) length of the observed deformations.

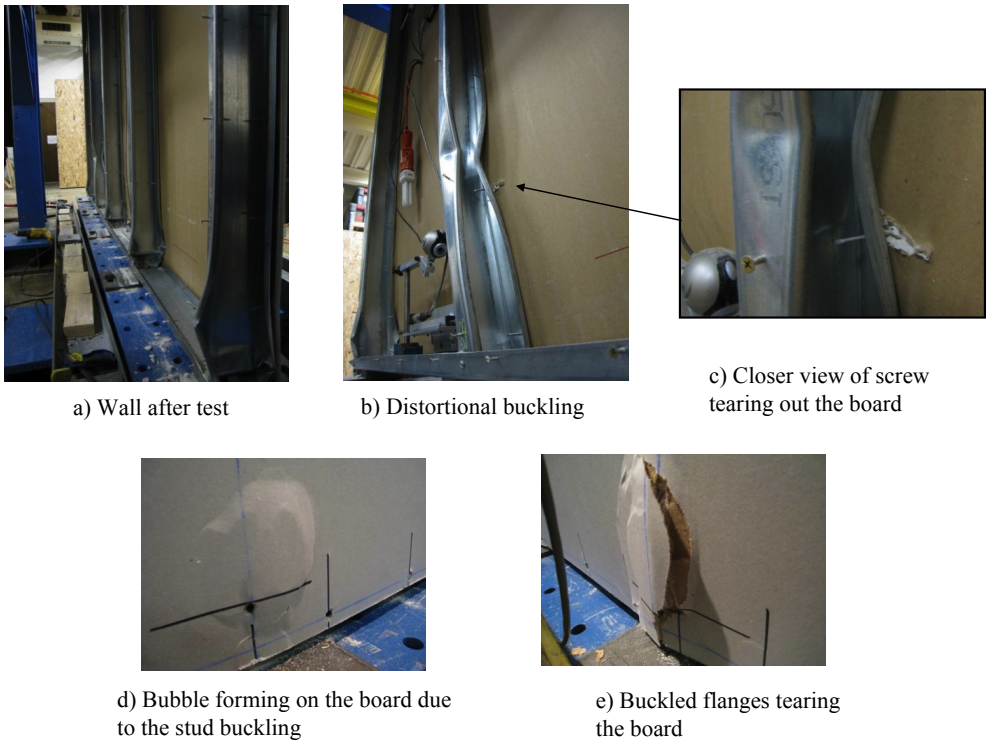

a) Wall after test

b) Distortional buckling

c) Closer view of screw tearing out the board

d) Bubble forming on the board due to the stud buckling

e) Buckled flanges tearing the board

Figure 5.12 – Response of specimens 7-Gyp-Gyp

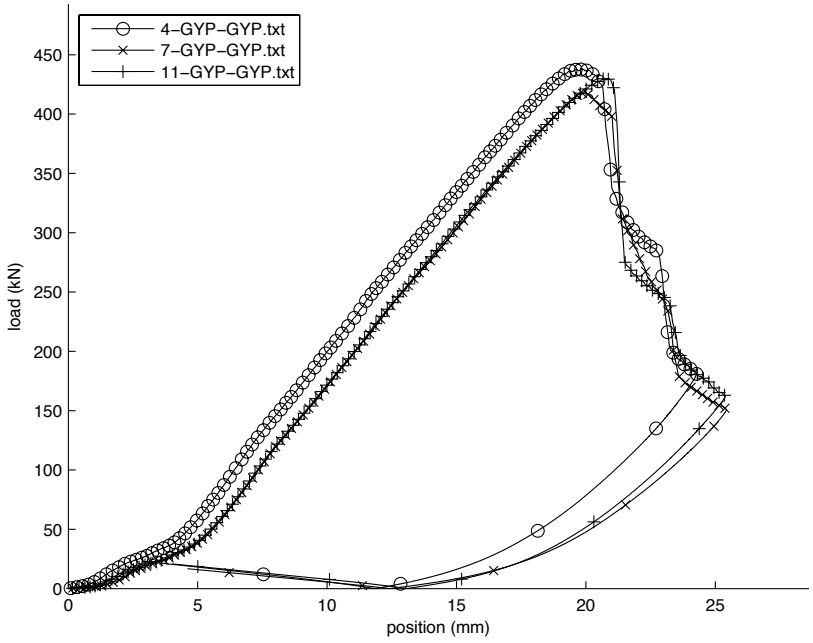

Figure 5.13 – P-Δ response of Gyp-Gyp walls

Local buckling failures were consistently observed at the member ends. It is postulated that the assembly of the walls, specifically squeezing the stud inside the track creates considerable "fabrication" initial imperfections at the ends, (as opposed to "manufacturing" imperfections) which lead to the failure at the ends.

5.3.4 Behavior of specimens sheathed with OSB on one side and gypsum on the other (OSB-GYP)

The walls sheathed with OSB on one side and Gypsum on the other present an interesting response: strength and global load-displacement of the wall is essentially the same, but observed limit states can vary, particularly in the post-buckling and post-peak regimes.

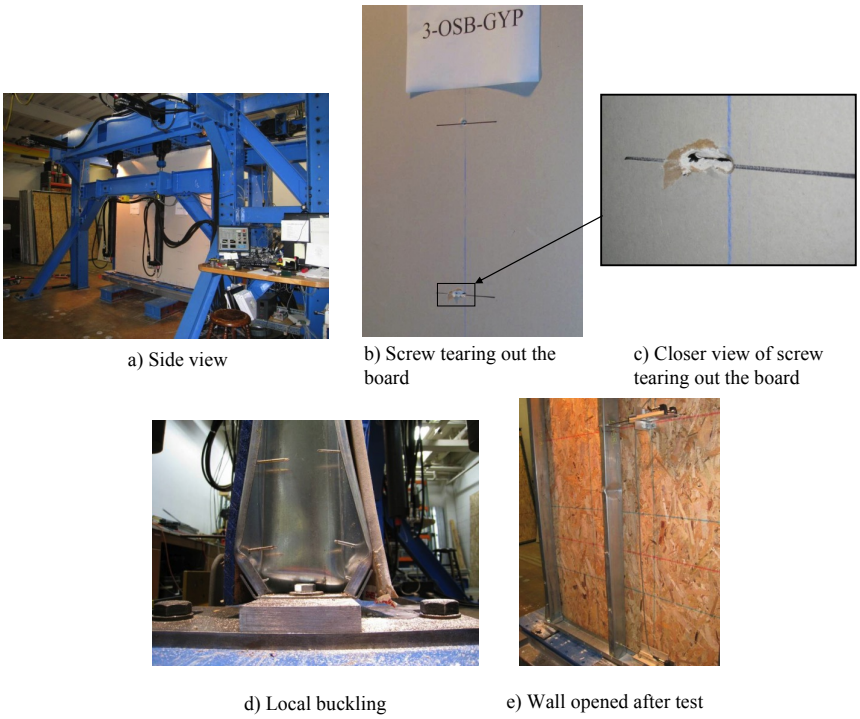

Figure 5.14 – Response of specimen 3-OSB-Gyp

For example, Figure 5.14 shows the test set up and the failure mode for test 3-OSB-Gyp which failed in local buckling at 471 kN (106 kips), but also exhibited flexural-torsional buckling in one of the field studs (stud number 14, Figure 5.15(c)) in the post-peak regime. Figure 5.14(b) and (c) show the cut in the Gypsum board formed by the fasteners and Figure 5.14(e) shows the wall after removing one side of sheathing, and the stud which failed in flexural-torsional buckling. (Note, the field studs have 305 mm (12 in). fastener spacing while chord and center studs have 102 mm (6 in.) spacing). Also failing at 106 kips was test 8-OSB-Gyp which failed in local buckling and exhibited no asymmetry in the final response.

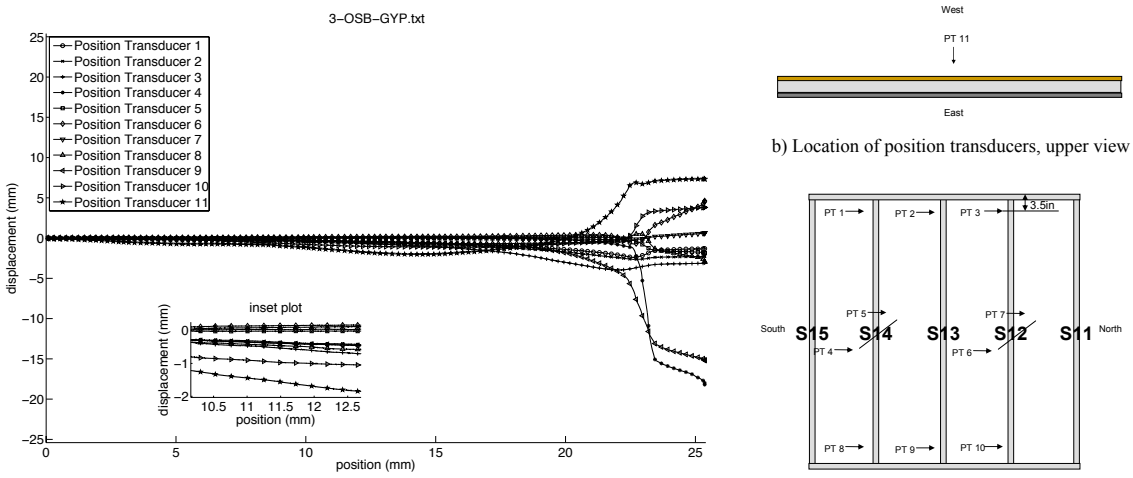

a) Position transducers plot

b) Location of position transducers, upper view

c) Location of position transducers, side view

Figure 5.15 – Measured displacements for wall 3-OSB-Gyp

The wall test 10-OSB-Gyp also had a similar peak load to the others (458 kN (103 kips) vs. 471.5 kN (106 kips)) and failed in local buckling (at the top of the wall, see Figure 5.16). However, in one stud distortional buckling was also observed, Figure 5.16(c), along with significant damage to the gypsum board, Figure 5.16(d). The OSB board and Gypsum board restrain the stud with different stiffness (and strength) which led to the observed fastener tearing in the Gypsum board since the OSB was providing a higher stiffness (and strength) at the same location. The load versus position curve for all the tests are compared in Figure 5.17.

a) Buckled flanges tearing the board

b) Local buckling at the top

c) Local buckling followed by distortional buckling

d) Gypsum was torn out in order to restrain the stud

Figure 5.16 – Response of wall 10-OSB-Gyp

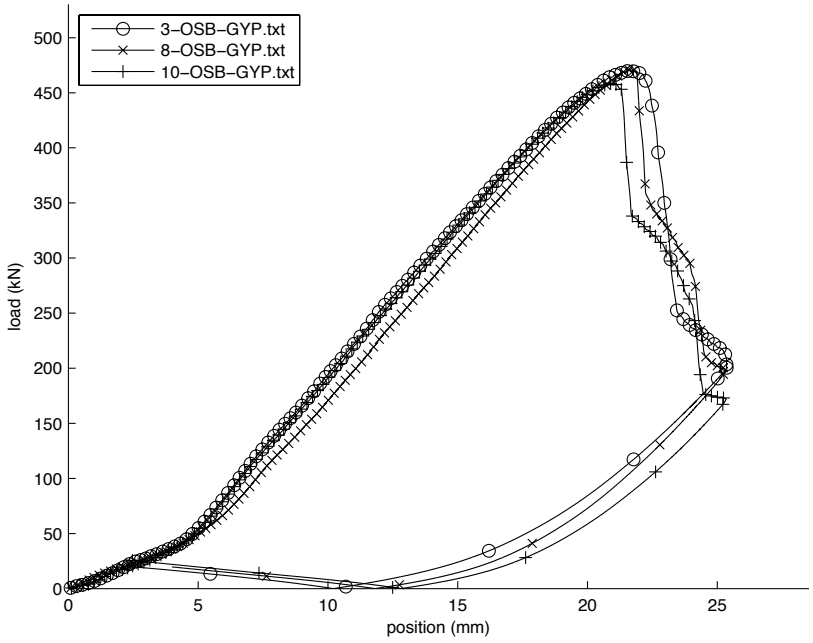

Figure 5.17 – P-Δ response for OSB-Gyp wall

5.3.5 Behavior of specimens sheathed with OSB on both sides (OSB-OSB)

The OSB-OSB tests fail in local buckling with stable post-buckling and post-peak collapse response, see Figure 5.6. For example, the peak load for the 5-OSB-OSB wall test was 471.5 kN (106 kips) and all studs failed in local buckling at the bottom. In Figure 5.18 the inset shows that PTs 10 and 9 were the first ones to capture the studs failing in local buckling, but stud 22 at the bottom (PT 10) was the one that showed larger displacements (this will be compared to measured initial imperfections in future work). Figure 5.19 shows the observed local buckling after removing the sheathing (for test 9-OSB-OSB).

The OSB-OSB tests carry 12% more load than the Gyp-Gyp tests even though the studs fail in the same limit state. This demonstrates (a) the sheathing carry axial load even though no direct bearing occurs, and (b) the stiffer OSB board can carry more than

gypsum board. Although some load sharing (composite action) occurs, in the usual models (e.g. [5.1], or [5.2]) it is presumed that the boards only provide elastic restraint and do not themselves contribute to the load carrying capacity.

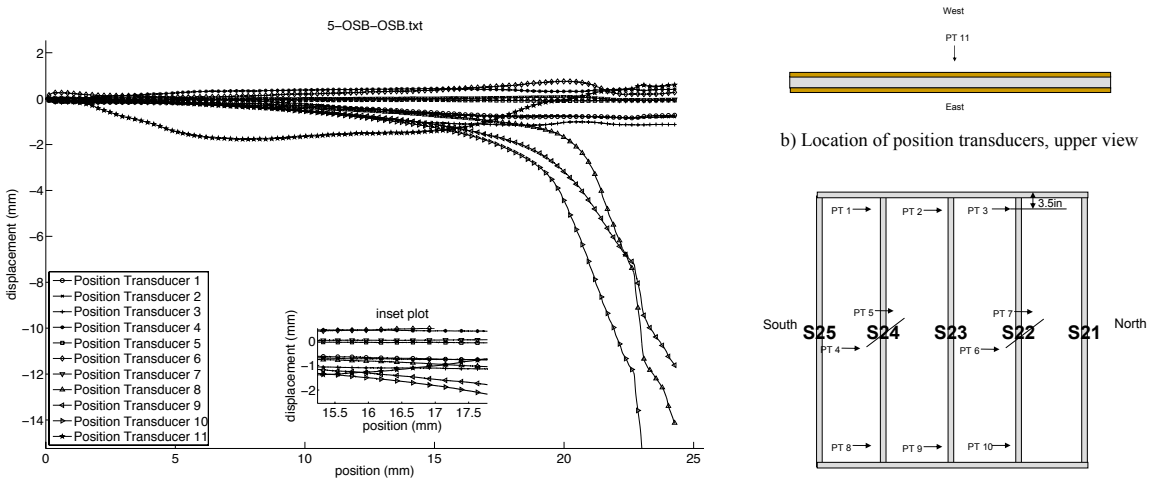

a) Position transducers plot

b) Location of position transducers, upper view

c) Location of position transducers, side view

Figure 5.18 – Measured displacements for wall 5-OSB-OSB

a) Yielding line on the web

b) Yielding lines on the flange

Figure 5.19 – Response of specimen 9-OSB-OSB

5.4 COMPARISON BETWEEN DESIGN METHODS

In Figure 5.20 we add the wall test results to the graph presented in Section 4.4.3 that compared the single column tests to the design methods available in North America.

The design methods included are: (a) AISI-S100-07-Eff. Width which ignores any sheathing restraint, (b) AISI-S100-01-restricted-Gyp-Gyp ([5.3]) based on Simaan and Peköz [5.2] (c) AISI-S210-07 ([5.4]) based on Green et al. [5.5], also known as Winter's method, as provided in the Wall Stud Standard of the 2007 AISI Specification. Since the difference between the capacity of single columns and of individual stud in a wall are small, the additional test results depicted in Figure 5.20 reinforces the conservative character of the design methods available in North America.

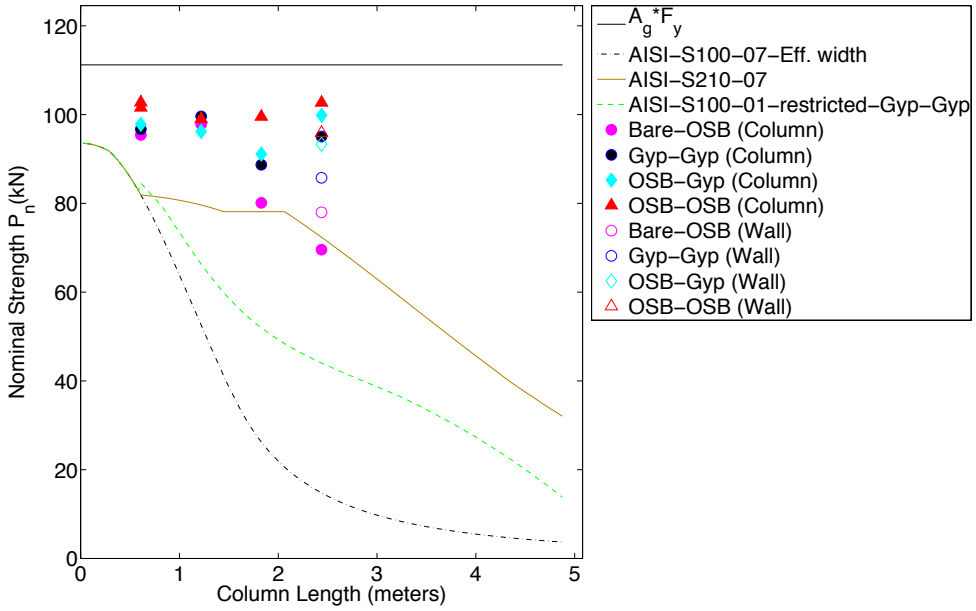

Figure 5.20 – Design curves, focus on Winter and Pekoz's method

5.5 COMPARISON BETWEEN WALL TESTS AND SINGLE COLUMN TESTS

Comparing Table 4.4 to Table 5.1 the limit states are the same for 2.44m (8 ft) single column tests and the full 2.44m x 2.44m (8 ft x 8 ft) wall, nonetheless, the peak load is usually slightly lower in the wall tests, except for the OSB-Bare tests. Postulated

reasons for the slight decrease in the full-scale wall tests, when compared with the single columns tests: (a) local buckling in the outermost studs of the wall do not always fully bear on the track since they are at the ends of the track (b) the tributary area of the board designated to each stud in the wall as engaged for sheathing resistance is modestly less than in the single column tests, (c) bracing forces in the sheathing accumulate and may have a modestly detrimental influence, (d) when the weakest of the 5 studs in the wall fail the forces must be carried by the other studs, thus observed strengths may be more of a weakest link strength as opposed to the idealized redistribution of a fully parallel system.

For the OSB-Bare case the failure is in flexural-torsional buckling and the full wall has a higher observed per stud mean strength than the single column, but the variability is significant and the failure mode in the full walls is dramatic and without any post-peak reserve.

REFERENCES CHAPTER 5

5.1. Winter, G., *Lateral Bracing of Beams and Columns.* Journal of the Structural Division, 1960.

5.2. Simaan, A. and T.B. Pekoz, *Diaphragm Braced Members and Design of Wall Studs.* ASCE J Struct Div, 1976. **102**(1): p. 77-92.

5.3. AISI-S100, *North American Specification for the Design of Cold-Formed Steel Structural Members.* American Iron and Steel Institute, 2001.

5.4. AISI-S210, *North American Specification for the Design of Cold-Formed Steel Structural Members.* American Iron and Steel Institute, 2007.

5.5. Giles G. Green, G.W., T. R. Cuykendall, *Light Gage Steel Columns in Wall-braced Panels.* Cornell University Engiineering Experiment Station, 1947. **35**: p. 1-50.

CHAPTER 6 - ANALYSIS OF SHEATHED STUDS

The specification used in the design of cold-formed steel members (AISI-S100 [6.1]) relies on elastic stability analysis to find the strength of a member. AISI-S100 [6.1] provides two ways of finding the elastic buckling loads: i) analytical (closed-form) solutions as presented in the main body of specification, and ii) rational analysis typically employing a numerical solution as emphasized in the commentary to Appendix 1 of the Specification. Both solutions – numerical and analytical – are explored and discussed in this chapter with the goal of providing new insights towards the design of sheathed studs. A full summary of the method proposed for determining the member capacity can be found in Chapter 7. We also explore, in this chapter, the fastener demands and behavior of single-columns and wall-stud assemblies. The studies involving the fastener are carried out by means of finite element models, which are compared to tests conducted in this thesis.

6.1 ELASTIC STABILITY

6.1.1 NUMERICAL SOLUTION

Elastic stability analysis may be performed using CUFSM v4.03 [6.2]. In CUFSM v4.03 [6.2] only longitudinal elements are discretized, which are called strips (as opposed to elements in the finite element method). In the transverse direction the strips utilizes a linear shape function, while in the longitudinal direction a trigonometric shape function ($Y_{[m]}$) depending on the specified boundary condition (b.c.) is employed. This research

focused on simply-supported b.c. ($Y_{[m]} = \sin(m\pi y / a)$) and clamped-clamped b.c. ($Y_{[m]} = \sin(m\pi y / a)\sin(\pi y / a)$), where m indicates the longitudinal term to be summed to form the displacement field [6.2], longitudinal functions.

CUFSM v4.03 [6.2] provides two methods to perform a buckling analysis: the conventional finite strip method (FSM) and constrained FSM (cFSM). cFSM employs the same mechanical assumptions used in generalized beam theory. FSM was largely used to understand the basic stability behavior of the studs analyzed in this research. The signature curve from conventional FSM analysis is depicted in Figure 6.1 and Figure 6.2. However, FSM uses a general methodology that does not provide any distinction between buckling modes when a minima is not clear. Due to this limitation, cFSM was used to find the buckling load and mode to be implemented in the direct strength method (DSM). It is also important to note that cFSM cannot handle rounded corners and the buckling loads are generally a few percent higher [6.2].

6.1.1.1 Unrestrained wall studs

The buckling modes of a pin-pin, unrestrained 362S162-68 SSMA cross-section [6.3], the same cross-section used in the single-columns and walls tests, are provided in the finite strip analysis signature curve results of Figure 6.1. Each buckling mode has an associated buckling half-wavelength (the length of the buckled wave). Understanding how sheathing, can or cannot change these buckling modes is critical to developing a sheathing-braced design method.

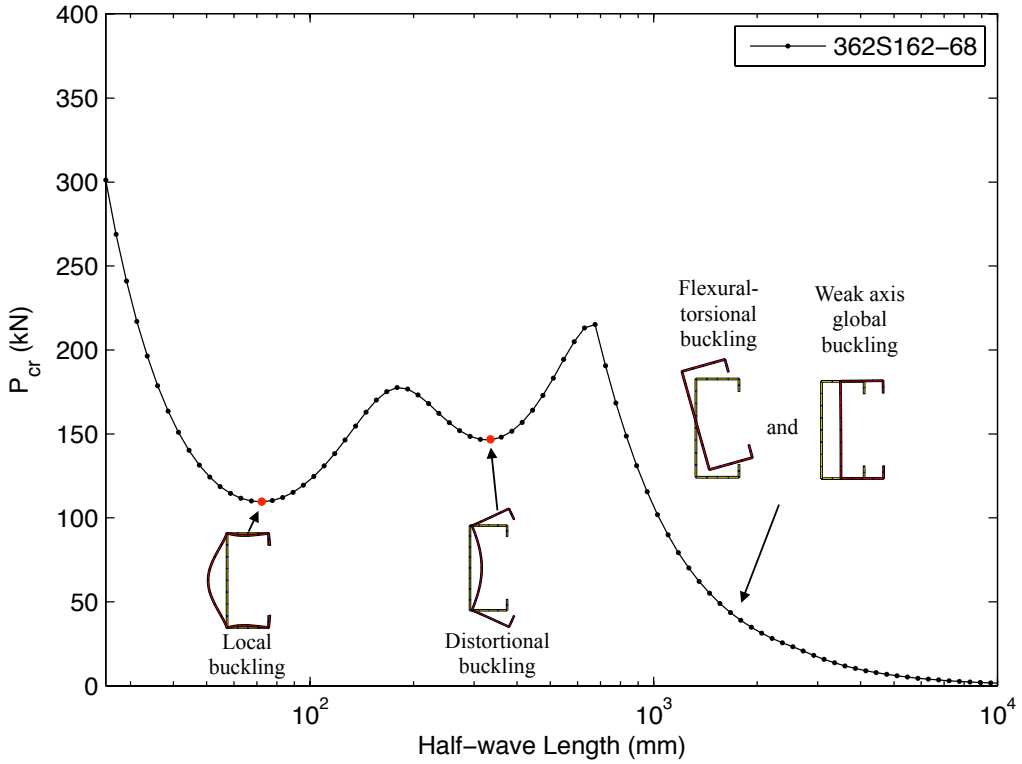

Figure 6.1 – Buckling curve and modes for pin-pin, unrestrained 362S162-68 SSMA cross-section [6.3], the out-to-out dimensions are as cataloged in [6.3] but thickness of 1.665mm (0.0655in) as reported in Appendix C.

6.1.1.2 Assumption used for the spring stiffness

Following the guidance of Chapter 3, or the step-by-step procedure depicted in Appendix G, appropriate restraints (springs) are added to the model of the cross-section to predict $P_{cr\ell}$ and the sheathing-restrained P_{crd} and P_{cre}. Table 6.1 presents the spring stiffness applied to the cross-section by means of foundation stiffness (instead of a discrete spring at the fastener locations) and the sheathing material properties considered in determining the spring stiffness.

In addition, and reflecting the findings of Chapter 4, Figure 6.2, both pin-pin and fixed-fixed end boundary conditions are considered (for all three buckling modes).

Table 6.1 – Spring stiffnesses values and material properties considered

Sheathing Material	E (MPa)	G (MPa)	k_x (N/mm/mm)	k_y-fully composite (N/mm/mm)	k_y-non-composite (N/mm/mm)	k_ϕ (kN.mm/mm/rad)
OSB	6426	1310	3.185	0.3172	0.001227	0.313
Gypsum	993	552	1.400	0.0579	0.000284	0.315

6.1.1.3 Sheathing restrained wall studs

The following results demonstrate how the elastic buckling modes of a cold-formed steel stud are influenced by the sheathing restraint, including different levels of restraint and for dissimilar restraint (different types of sheathing connected to the two flanges). For sheathing on one-side only, e.g. the OSB-Bare tests of Chapter 4 and 5, Figure 6.2(a) compares the results to the unrestrained case. Introduction of the restraint changes the global buckling mode from weak-axis flexure to flexural-torsional buckling, and the resulting flexural-torsional mode is dependent on the level of out-of-plane resistance (k_y) developed (i.e. non-composite vs. fully composite).

For sheathing on both sides, here the OSB-OSB values are used, Figure 6.2(b) compares the buckling results to the unrestrained case. Local buckling is not affected by the restraint, distortional buckling is modestly increased, while global buckling is altered significantly. If only the in-plane resistance is included, at practical lengths, weak-axis flexural buckling is replaced by flexural-torsional buckling. Introduction of the out-of-plane (k_y) resistance increases the flexural-torsional buckling load, and a strong sensitivity to the magnitude of k_y is found. The difference between using the lower bound and upper bound value for k_y is dramatic and must be carefully handled.

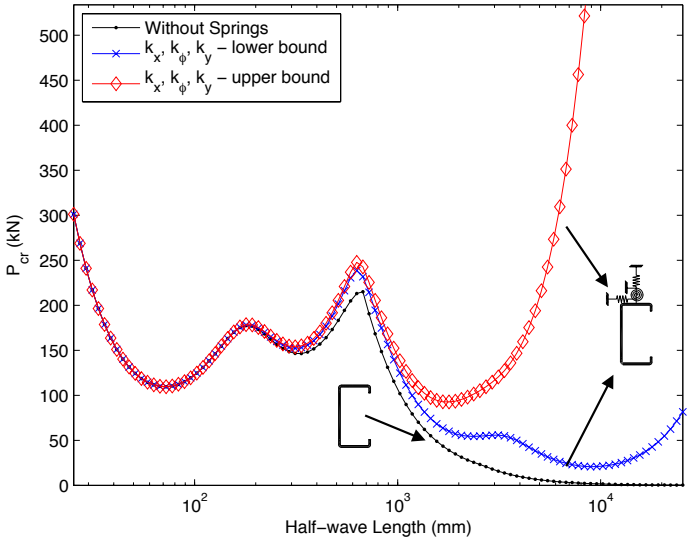

a) Springs on one flange (OSB-Bare)

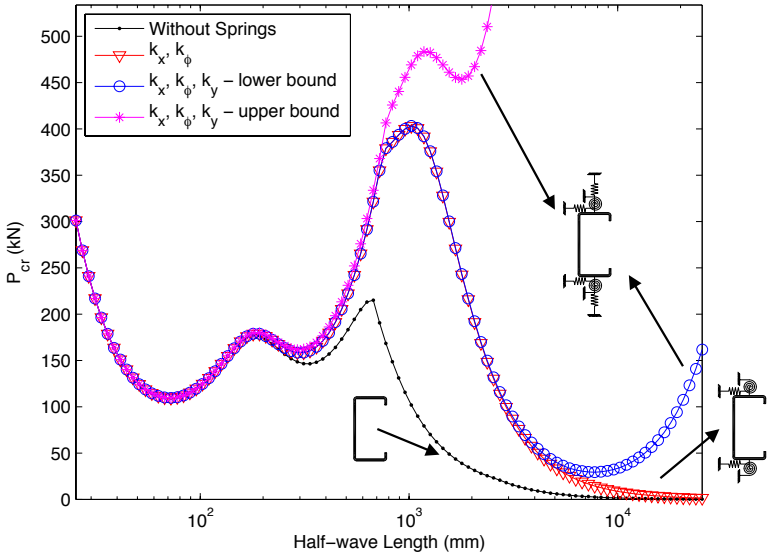

b) Springs on both flanges (OSB-OSB)

Figure 6.2 – Buckling curves for springs on one flange and both

It is interesting to note in Figure 6.2(b) that the global buckling curve may have a minima at a certain buckling length (L_{cre}), which is unusual for studs not restrained. The global minima works in the same way as local or distortional minima. Thus, if the

column buckling length (KL) is greater than L_{cre}, P_{cre} is be given by the global buckling minima. In fact, the signature curve employs only a single longitudinal term (m=1 $\rightarrow Y_{[m]} = \sin(1\pi y / a)$) [6.2], but for multiple longitudinal terms the same signature curve is just shifted to the right, meaning that the minima is repeated for other buckling lengths but the member buckles in a different number of longitudinal terms.

6.1.1.3.1 Local buckling

Sheathing does not affect local buckling. The sheathing restrains the flange, but local buckling is largely driven by the web in these sections. Even theoretically k_x and k_ϕ have no influence on local buckling, only k_y. The out-of-plane stiffness, k_y, is derived consistent with global bending resistance and not localized resistance. For local buckling predictions it is recommended to ignore the sheathing.

6.1.1.3.2 Distortional buckling

Distortional buckling is mainly influenced by k_ϕ. The AISI-S210-10 [6.4] standard provides general methods for finding k_ϕ. The rotational stiffness is the recognized means of primary resistance against distortional buckling and is derived and determined in a manner consistent with distortional buckling deformations. The in-plane stiffness, k_x, has little to no influence on distortional buckling in most cases, for very deep webs the additional restraint supplied by k_x may be influential so it may be included if desired by the engineer. However, the out-of-plane stiffness, k_y, should not be added to k_ϕ, in part because k_ϕ itself derives from a moment couple that includes k_y at the connector and bearing between the flange and sheathing. Further k_y's deformations are consistent with

beam bending, not rotation of the flange. For distortional buckling predictions it is appropriate to use k_x and k_ϕ, but ignore k_y.

6.1.1.3.3 Global buckling

Global buckling modes are (a) weak-axis flexure and (b) flexural-torsional buckling. In most cases weak-axis flexure is the lowest mode and thus k_x is critical to this resistance and should be included. For flexural-torsional buckling the torsional component is restrained primarily by the couples created from the k_x springs (but also from the k_ϕ springs), while the k_y spring restricts the major axis flexural component. For global buckling predictions at a minimum k_x should be included, but it is appropriate to include k_ϕ and k_y as well. In the absence of testing, the lowerbound k_y value is the most rational choice. For ideal boundary conditions as discussed in Chapter 4 (Section 4.4.1) it is recommended to consider fixed-fixed boundary conditions.

6.1.2 ANALYTICAL SOLUTION

Even though there is a numerical solution to the problem, an analytical solution to a braced column is desirable for the engineer. The solution for local and distortional buckling are in fact mere adaptions of methods already existent in the design code [6.4], but the derivation for global buckling expands methods in current use.

6.1.2.1 Local buckling

Since sheathing does not affect local buckling, local buckling analytical solution may rely on the use of element plate buckling coefficient, which for columns from [6.1]:

$$P_{cr\ell} = A_g f_{cr\ell} \tag{6.1}$$

where:

A_g = gross area of the member

$f_{cr\ell}$ = local buckling stress of elements, or elements combinations, per [6.1].

6.1.2.2 Distortional buckling

AISI-S210-10 [6.4] provides in Section C4.2, a method to find distortional buckling based on the rotational stiffness at the flange/web juncture. The designer may add the rotational stiffness provided by the sheathing to the stud. Thus, for columns from [6.1]:

$$P_{crd} = A_g f_{crd} \tag{6.2}$$

where:

f_{crd} = distortional buckling stress at the extreme compression fiber. Solutions and design aids for f_{crd} are available in [6.5, 6].

6.1.2.3 Global buckling

Global buckling loads may be found following the approach outlined in Timoshenko and Gere [6.7] article 5.6, which was modified here to accommodate multiple springs. The springs are considered as foundation springs, instead of discrete springs, since the assumption of foundation springs lead to a solution vastly simpler than the assumption of discrete springs (see Chapter 2 for discrete springs in flexural buckling only). Figure 6.3 depicts the nomenclature adopted for the coordinates based on the shear center (s), centroid (c) and the node that the spring is attached to (*i*).

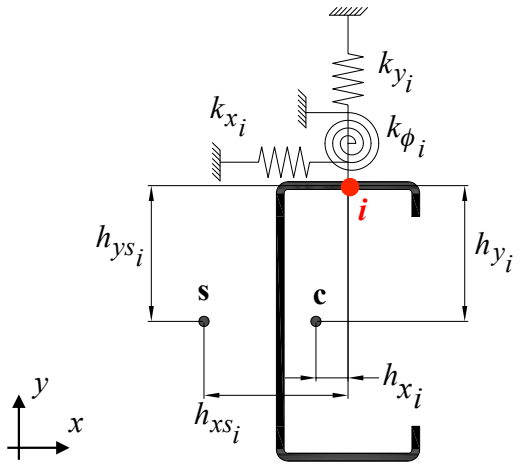

Figure 6.3 – Adopted springs coordinates nomenclature, for spring *i*

The eigenvalue problem is defined in the general form by Eq. (6.3). K_e is the elastic stiffness matrix (Eq. (6.4)), K_g is the geometric stiffness matrix (Eq. (6.5)), λ is the vector of buckling loads, and ϕ the matrix that defines the buckled shape. The elastic stiffness matrix conveniently written in terms of flexural buckling loads about x and y axes, Eq. (6.6) and (6.7) and the torsional buckling load, Eq. (6.8). Other variables must be defined such as: member length (L), Young's modulus (E), moment of inertia about principal axes x and y (I_x and I_y), polar moment of inertia about shear center (I_o), cross-sectional area (A), shear modulus of steel (G), Saint-Venant torsional constant (J), and effective length factor for flexural buckling about x, y and torsional buckling (K_x, K_y, K_t).

$$\left(K_e - \lambda K_g\right)\phi = 0 \tag{6.3}$$

$$K_e = \begin{bmatrix} P_{cry} + \frac{L^2}{\pi^2}\sum_{i=1}^{n} k_{x_i} & 0 & \frac{L^2}{\pi^2}\sum_{i=1}^{n} k_{x_i} h_{ys_i} \\ & P_{crx} + \frac{L^2}{\pi^2}\sum_{i=1}^{n} k_{y_i} & -\frac{L^2}{\pi^2}\sum_{i=1}^{n} k_{y_i} h_{xs_i} \\ sym & & \frac{I_o}{A} Pcr\phi + \frac{L^2}{\pi^2}\sum_{i=1}^{n} k_{x_i}(h_{ys_i})^2 + \frac{L^2}{\pi^2}\sum_{i=1}^{n} k_{y_i}(h_{xs_i})^2 + \frac{L^2}{\pi^2}\sum_{i=1}^{n} k_{\phi_i} \end{bmatrix} \quad (6.4)$$

$$K_g = P\begin{bmatrix} 1 & 0 & y_o \\ & 1 & -x_o \\ sym & & \frac{I_o}{A} \end{bmatrix} \quad (6.5)$$

$$P_{crx} = \frac{\pi^2 E I_x}{(K_x L)^2} \quad (6.6)$$

$$P_{cry} = \frac{\pi^2 E I_y}{\left(K_y L\right)^2} \quad (6.7)$$

$$P_{cr\phi} = \frac{A}{I_o}\left(GJ + \frac{\pi^2 E C_w}{(K_t L)^2}\right) \quad (6.8)$$

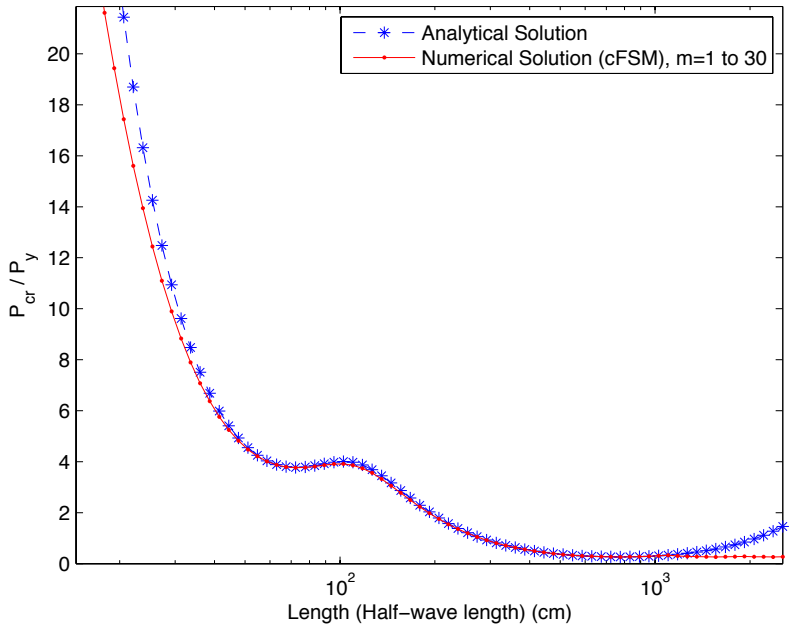

a) Analytical and numerical solution for simply-supported boundary conditions

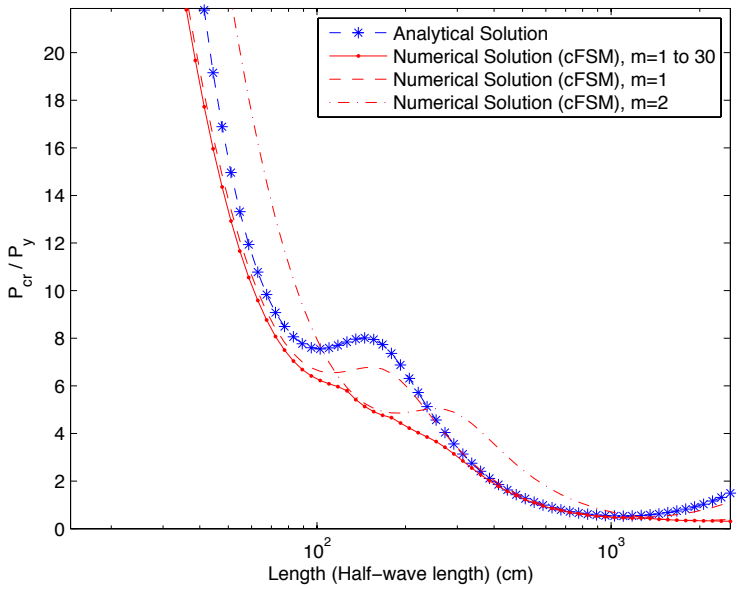

b) Analytical and numerical solution for clamped-clamped boundary conditions (K_x=K_y=K_t=0.5)

Figure 6.4 – Comparison between numerical and analytical solution for global buckling load of a 362S162-68 column.

The analytical solution to Eq. (6.3) is compared to a CUFSM v4.03 [6.2] numerical solution in Figure 6.4, and shows how the two methods diverge as expected for short lengths. This diversion happens because cFSM takes in account shear and transverse extension in the cross-section and in its geometric stiffness matrix [6.8], while the same is not considered in Eq. (6.5). For a simply-supported column the methods show good agreement for the remaining lengths, and only for very long columns do the curves start diverging again, which is predicted since the global solution presented in this section considers just a single longitudinal term (m=1 $\rightarrow Y_{[m]} = \sin(1\pi y / a)$) and for long columns more terms are needed.

The analysis of clamped-clamped boundary conditions, Figure 6.4(b), depicts an interesting fact not seeing in the simply-supported boundary conditions analysis: for intermediated lengths the proposed analytical solution may overestimate the global buckling load. Since the analytical solution considers just a single longitudinal term (m=1 $\rightarrow Y_{[m]} = \sin(1\pi y / a)$), the solution is not able to take in account the possibility of the stud buckling in two or more half-wave lengths.

The solution for the eigenvalue problem is certainly laborious and it will probably not be readily accepted as a hand solution in the main body of the design code. Timoshenko and Gere [6.7] proposed simplified solutions based on the number of symmetry axes in a cross section and they also assumed that the springs are placed along the shear center (s). Peköz and his students [6.9, 10], in addition to the assumptions adopted by [6.7], considered that the foundation spring in the y direction could be ignored and the stiffness be accounted for in the bending stiffness about y axis, and also that the rotational spring shall be replaced by two translational springs in the x direction. The combination of all

assumptions leads to a simplified solution, which unfortunately conceals the real model, Figure 6.3, and reduces the accuracy of the predicted buckling load – the latter being demonstrated in the next chapter, where the design methods and our tests are compared.

The eigen-buckling analysis presented in Eq. (6.3) results in two variables: the eigenvalue as commented above, and also the eigenvector. The eigenvector represents the shape assumed by the cross section though scale remains unknown. The eigenvector can be scaled based on the initial imperfection and the displacement can be amplified by the following relationship:

$$\beta_m = \frac{P/P_{cr,m}}{1 - P/P_{cr,m}} \tag{6.9}$$

where:

P = load being applied,

$P_{cr,m}$ = buckling load of mode (m).

The fastener demand is given by the amplified displacement at each load step (P) multiplied by the spring stiffness. The amplified displacements at the column mid height in the x and y axes (δ_x and δ_y) and the rotation (ϕ_{xy}) are given by:

$$\delta_x = \sum_{m=1}^{3}\left(\beta_m \delta_{bow} V_{1,m} + \beta_m \phi_{twist} h_{ys} V_{3,m}\right) \tag{6.10}$$

$$\delta_y = \sum_{m=1}^{3}\left(\beta_m \delta_{camber} V_{2,m} + \beta_m \phi_{twist} h_{xs} V_{3,m}\right) \tag{6.11}$$

$$\phi_{xy} = \sum_{m=1}^{3}\left(\beta_m \phi_{twist} V_{3,m}\right) \tag{6.12}$$

where:

δ_{bow} = bow initial imperfection,

δ_{camber} = camber initial imperfection,

ϕ_{twist} = initial twist imperfection (in radians) about shear center,

$V_{j,m}$ = Eigenvector for each mode (m), j=1 to 3, ϕ_m of Eq. (6.3) = $\left[V_{1,m}\ V_{2,m}\ V_{3,m}\right]^T$

The analytical solution is compared to the FE models in Section 6.3.

6.2 FASTENER DEMANDS

The commentary of AISI-S211 [6.11] states that a fastener-sheathing assembly shall be designed for a load equal to 2% of the axial load, also know as "2% rule". In order to investigate such statement a FE model was developed, which is presented bellow.

6.2.1 Single-Column FE Model

Fastener demands are explored by means of FE models of the single-column tests and the full wall-stud assemblies. The single-column model and full wall-stud models share many modeling characteristics, such as: element type, stress-strain curve for the material, boundary conditions and initial imperfections, but they are different in terms of geometry. The geometry of the models is the same as reported in Chapter 4 and 5. The models are built in ABAQUS [6.12], using S4R[1] elements to model stud, track and sheathing. The material steel is simulated using the stress-strain curves reported in Appendix C, which are transformed from engineering stress to true stress[2] for use in ABAQUS [6.12]. The material model chosen to represent the steel is non-linear, and it considers metal plasticity (von Mises yield surface) and isotropic hardening. The sheathing is modeled as an

[1] S4R elements are used rather than S4R5, because S4R elements allow the rotation on plane of the element to be restricted.

[2] Engineering strain (ε_0) is transformed to true strain (ε) by the relationship $\varepsilon=\ln(1+\varepsilon_0)$, thus by assuming a material incompressible the true stress is given by $\sigma=\sigma(1+\varepsilon_0)$.

orthotropic material with Young's modulus (E) and shear modulus (G) as discussed in Chapter 3 (OSB – E=6,426 MPa (932 ksi), G=1,310 MPa (190 ksi); Gypsum – E=993 MPa (144 ksi), G=552 MPa (80 ksi)), and ν=0.3. The modified Riks method is used to solve the nonlinear model.

The connection of stud to track is simulated in the same manner as explained in Chapter 4 (section 4.4.1), in short, the stud-to-track fasteners are idealized by coupling all the degrees of freedom except the rotation around the axis of the fastener and the stud-to-track contact is idealized by coupling all the displacements except the displacement on the plane of the track's web (stud end is free to slide). A displacement is applied to a master node that transfers this displacement to a rigid body that represents the isolation plate (see Chapter 4 Section 4.1.1 for more on this plate) on the track web.

The models have their geometry altered by an initial imperfection, which is considered as either a small initial imperfection (25^{th} percentile) or a large initial imperfection (75^{th} percentile). The magnitude of the initial imperfection is depicted in Table 6.2 and it follows [6.13] regarding local imperfections ("d1" and "d2") and [6.14] regarding global imperfections (bow, camber and twist). It was chosen to apply the initial imperfection based on published values instead of the actual measurements because the data from the measurements were being analyzed while the models were being completed.

Table 6.2 – Imperfection applied on studs

Reference	Type of imperfection	P(Δ < d)* 25th %ile	P(Δ < d)* 75th %ile
Schafer and Peköz Ref. [6.14]	Local (d_1/t)	0.14	0.66
	Distortional (d_2/t)	0.64	1.55
Schafer and Zeinoddini Ref. [6.15]	Bow	L/4755	L/1659
	Camber	L/6295	L/2887
	Twist	0.46°	1.23°

* "Probability that a randomly selected imperfection value, Δ, is less than a discrete deterministic imperfection, *d*." [6.13]

The restrictions provided to the stud can be simulated with or without the sheathing in the FE model. If the sheathing is not considered in the model, the springs are connected on one end to the node where there is a fastener on the stud and the other end to a fixed support. For models in this case the diaphragm stiffness (k_{xd}), the rotational stiffness provided by the sheathing ($k_{\phi w}$), and the out-of-plane stiffness (k_y) are considered. But if the sheathing is being included directly in the model, the same three variables are not considered since the sheathing is in place and it will automatically take in account these stiffnesses. The stiffness provided by the sheathing in the axial direction may also be considered and since there is no specific value for k_z and $k_{\phi x}$, we have used the same values of k_x and k_ϕ respectively, which in fact is a lower-bound value for these stiffnesses, Table 6.3.

Table 6.3 – Spring stiffness used in the FE models (fastener spacing considered is 305mm (12in)), Figure 6.5 depicts the spring orientation. See Appendix G for more information about how to determine the springs' stiffnesses

Sheathing Material	Spring	Sheathing in place, springs idealize just the fastener	No sheathing, springs idealize fastener and sheathing
OSB	$k_x=k_z$ (N/mm)	1241	971
	k_y (N/mm)	N/A	0.374
	$k_\phi=k_{\phi x}$ (N.mm/rad)	136660	95309
Gypsum	$k_x=k_z$ (N/mm)	426	427
	k_y (N/mm)	N/A	0.087
	$k_\phi=k_{\phi x}$ (N.mm/rad)	129745	95987

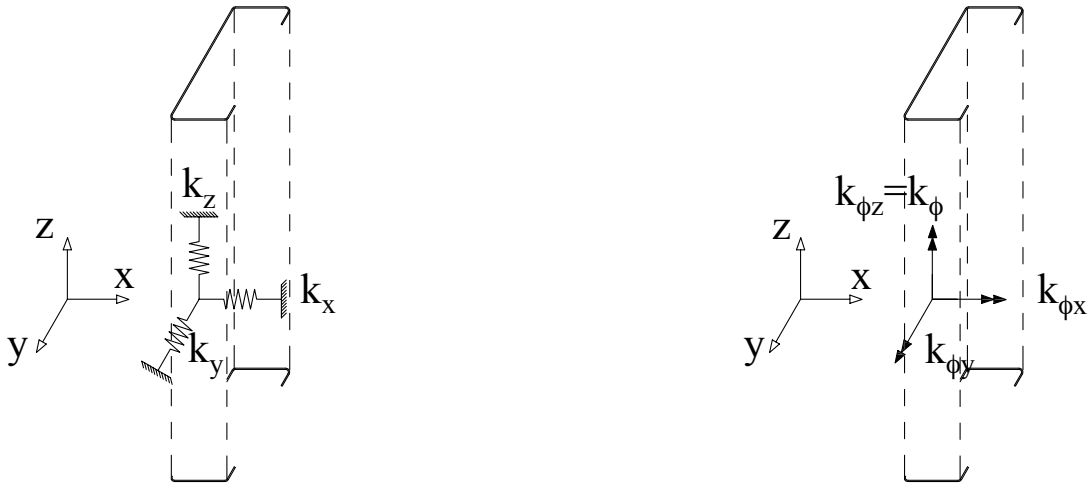

a) b)

Figure 6.5 – Springs orientation a) Translational springs, b) Rotational springs (only the reaction vector is plotted since the actual rotational spring drawing may confound the reader).

A series of FE collapse models for the sheathed simple column tests with varying degree of sophistication are summarized in Table 6.4. The first set of FE models presented compares the end boundary conditions in the models to the Bare-Bare single-column test, 2.44m (8feet) long, Table 6.4. The model that simulates stud and track when compared to a column with fixed-fixed ends did not show a great difference, and both models represent a slighter higher peak than found in the test. Our idealization of a

boundary condition that directly couples nodes instead of using contact elements leads to a slighter stiffer system, but the presence of the track is important to establish the connection between sheathing and track, which, as it will be shown further, develops an important role in distributing the load to the stud and at the same time bracing it.

The second set of models concentrates on understanding the springs that should be considered in order to simulate the tests (this all without considering the sheathing). In these models we found that if we only consider the springs k_x, k_y and k_ϕ, as used in the finite strip models, the models lead to a peak load around 16% lower than the peak load in the test, Table 6.4. However if we add k_z and $k_{\phi x}$, which are responsible for the contribution of the sheathing in the longitudinal direction of the stud, the results are in excellent agreement with the test. Suggesting modest composite action is present even though the vertical load is isolated.

The third set of models also compares the same single-column test (OSB-OSB, 2.44m (8feet)) to the tests, but this time the sheathing is also modeled; thus the spring stiffness is changed as discussed above and depicted in Table 6.3. In the first model, instead of using springs, we coupled the displacements at the stud and track to the sheathing, which created an upper bound value for the peak loads (70% higher that the test). When we actually modeled the stud and track connected to sheathing through spring elements we found a peak load only 7% lower than found in the tests, which we consider a very good prediction. Also simulated (an addendum to the third set of models) was analysis considering a linear elastic steel material: our goal with this model is to understand the fastener forces in the model if there is no plastic deformation in place. In the case of the single-column models the difference in the fastener forces are small, but the same is not

observed in the wall-stud model, because in the latter model plasticity of the stud-to-track connection plays an important role.

The last set of models simulates the sheathed wall-stud test. If the springs are considered as the elements connecting the sheathing to the wall-stud, the model reaches peak load mainly due to plastic failure at the connection of stud-to-track at a load 22% lower than the test. In fact, in our tests, failure at the stud-to-track connection was not observed; perhaps a finer mesh at the stud-to-track connection could prevent the model of reaching peak load at an early stage due to the plastic failure. Nonetheless, the most important fact is that we can already see in the model an eminent local buckling failure at the stud ends, which was the same failure type seen in the test. Also, if local buckling is the dominant failure mode, it means that the springs are able to restrain global buckling, which is our main concern. Thus, we considered this model of the sheathed wall-stud suitable for the fastener force study, its primary purpose.

Table 6.4 – FE models results

Configuration	Is the sheathing being modeled?	Characteristics	Imperfection (%ile)	Peak Load (kN)	Test peak load (kN)
Bare-Bare Single Column	No	No Track / Fixed Ends	25^{th}	71.6	57.1
		Stud + Track	25^{th} 75^{th}	69.1 58.2	
OSB-OSB Single Column		Springs (k_x,k_y,k_ϕ)	25^{th} 75^{th}	89.5 86.6	102.7
		Springs (k_x,k_y,k_z,k_ϕ,$k_{\phi x}$)	25^{th} 75^{th}	105.0 107.5	
	Yes	Instead of springs the nodes where coupled	75^{th}	174.5	
		Springs (k_x,k_z,k_ϕ,$k_{\phi x}$)	25^{th} 75^{th}	95.8 95.6	
		Springs (k_x,k_z,k_ϕ,$k_{\phi x}$), but steel material is linear elastic	75^{th}	173.9	
OSB-OSB Wall		Springs (k_x,k_z,k_ϕ,$k_{\phi x}$)	75^{th}	392.4	479.5
		Springs (k_x,k_z,k_ϕ,$k_{\phi x}$), but steel material is linear elastic	75^{th}	1934.4	

A closer look into the models leads to several conclusions regarding the fastener forces. The first model to be analyzed in depth is considered the simplest model of this series, which considers only the springs k_x, k_y and k_ϕ, and the board is not modeled, Figure 6.6. Figure 6.7 depicts the force and moments in the springs for different initial imperfection, different sides where the sheathing is connected (side 1 and 2), and different positions (ends (first spring on the stud, 50.8mm (2in) from the end) and center of stud). As discussed in the previous chapter, local and distortional buckling are slightly affected by the presence of springs, but the springs play an important role in restricting global buckling, that includes: weak axis buckling and flexural-torsional buckling.

This simple model shows that at peak load the forces on the k_x springs are at its maximum magnitude at the center of the stud, but after peak load due to local buckling, the force at the springs are transferred from the center to the ends, where local buckling

happens: Figure 6.6 (b, c). It is also shown in Figure 6.7 that for a 75th percentile magnitude of initial imperfection the fastener force is higher than a 25th percentile of initial imperfection (as expected); therefore, further studies are based on models that has its geometry altered by a 75th percentile of initial imperfection – i.e., plausible worst case scenario. Another conclusion is that the force at the k_y springs are very small, this is explained by the nature of the problem, since strong-axis buckling is not a predominant buckling mode it takes little resistance to restrict this direction. The moment in the rotational spring is also very small compared to the capacity of the connection, in the tests reported on Chapter 3 the maximum moment at the spring for OSB is on the average 47.45kN.mm (420lbf.in (351lbf.in/in*12in)) while in the models the maximum moment at the spring is of 3kN.mm (26.55 lbf.in).

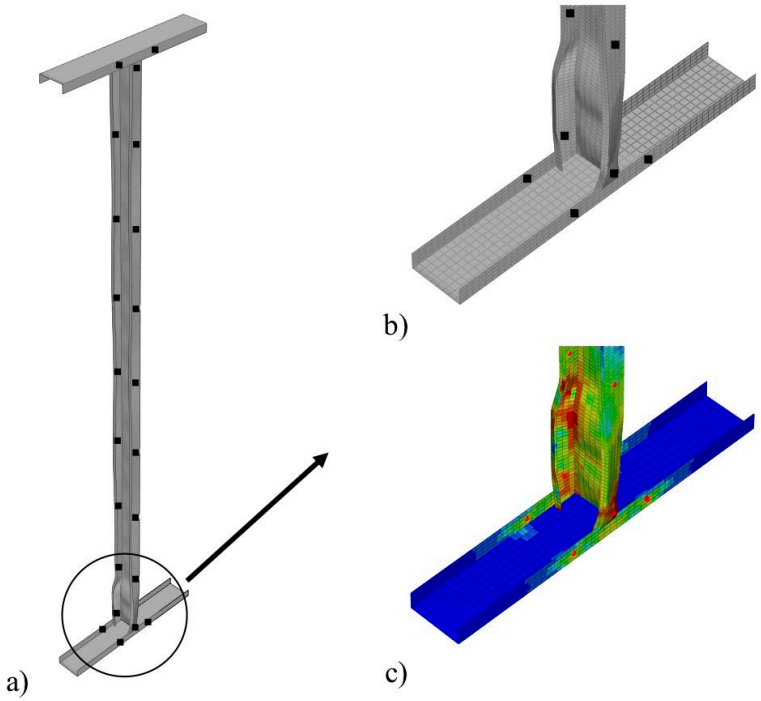

Figure 6.6 – Simple model that considers only k_x, k_y, k_ϕ, and sheathing is simulated by means of springs a) Single-column model, springs are depicted in black dots, b) Zoomed view of stud end where local buckling takes place, c) Von-Mises stresses on stud end.

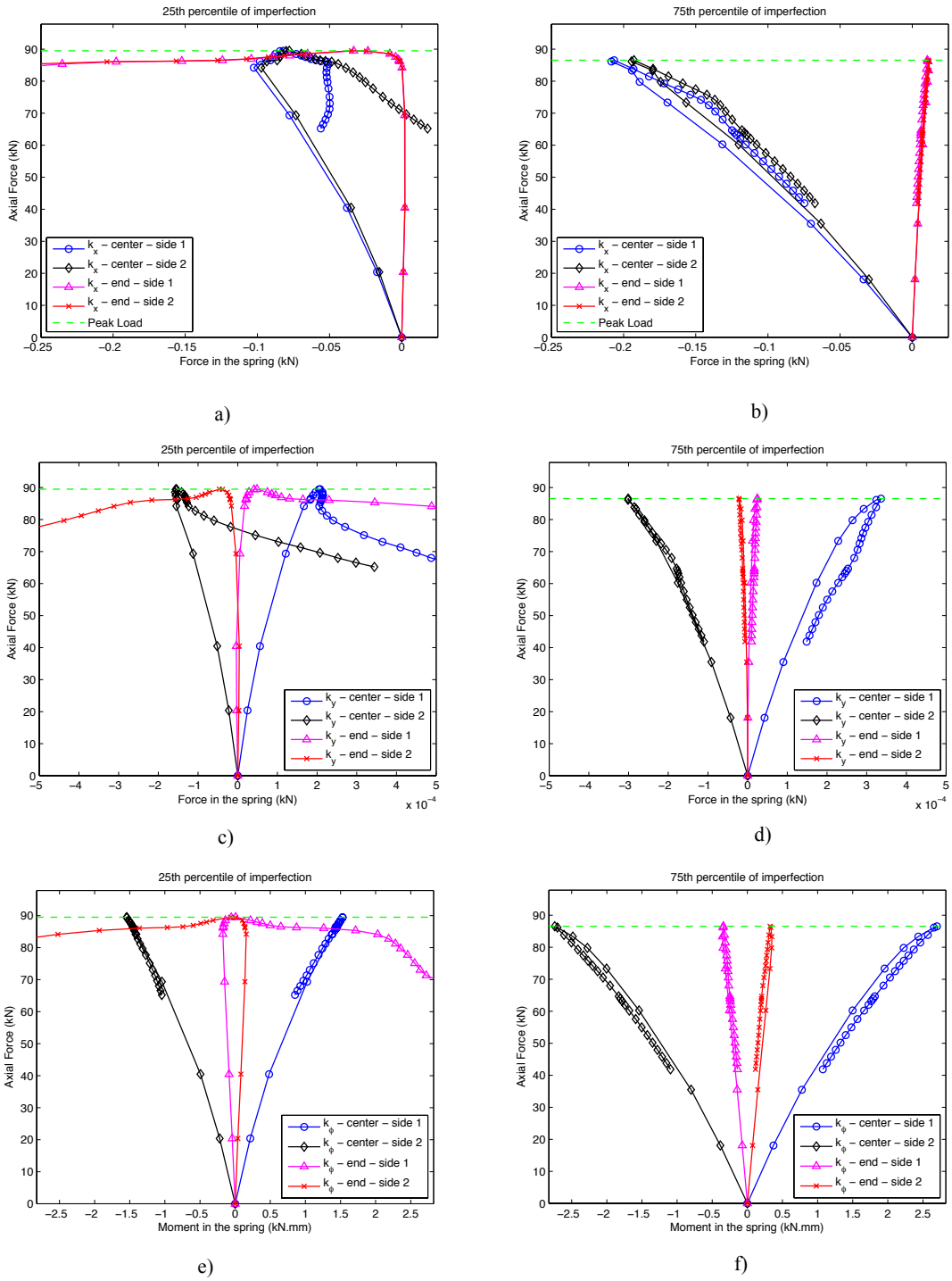

Figure 6.7 – Force and moment in the springs for models that considers only k_x, k_y, k_ϕ, and sheathing is not simulated

Another single-column model interesting to explore is the one that considers k_x, k_z, k_ϕ, $k_{\phi x}$, and the sheathing, Figure 6.8. Figure 6.9 depicts the force and moment in the springs

at peak load. The demands on side 1 and 2 are plotted in different colors, but since the single-column model presents a symmetric behavior regarding the sides, the plots of side 1 and 2 are always superimposed and little difference can be seen. In the tests reported in Chapter 3, the average peak load carried in the translation test is of 2.58kN (0.58 kips), therefore the demand in the translational springs shall not exceed the peak load reported in the tests, as it is observed in Figure 6.9 (a, b) in the value of the maximum force. The k_x spring has the greatest magnitude close to the ends where the stud buckles in local mode, Figure 6.8 (c, d). While the k_z spring has more demand at the track-to-sheathing connection and stud end, because the axial force is transferred from the loading plate to the steel members and then to the sheathing; in the middle, the applied force is counterbalanced by the reaction force and so the fasteners receive little if any load. Even though the rotational spring also has small demands, it is interesting to track their behavior. The k_ϕ spring has greatest demands in the middle of the stud. This shows that the k_ϕ spring is providing a small contribution to restrain flexural-torsional buckling. Nonetheless, the $k_{\phi x}$ springs have their greatest demands at the ends, showing that the $k_{\phi x}$ springs help restrain the stud in strong-axis buckling. The primary conclusion with this model is that the group of springs and the sheathing are able to restraint global buckling and hence the stud buckles in local buckling.

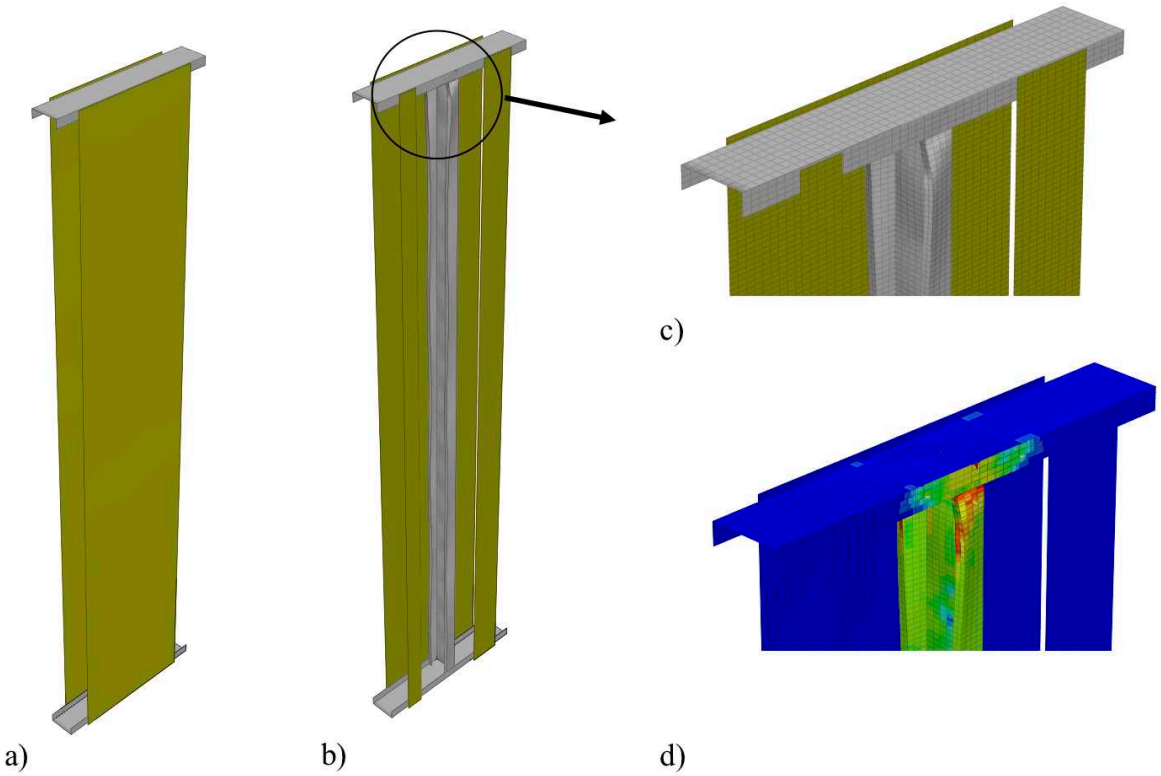

Figure 6.8 – Model that considers k_x, k_z, k_ϕ, $k_{\phi x}$, and sheathing is also simulated a) Overall view of FE model, steel members are represented in gray and OSB in brown, b) Part of the sheathing is removed to show the stud, d) Zoomed view of stud end where local buckling takes place, c) von Mises stress on stud end.

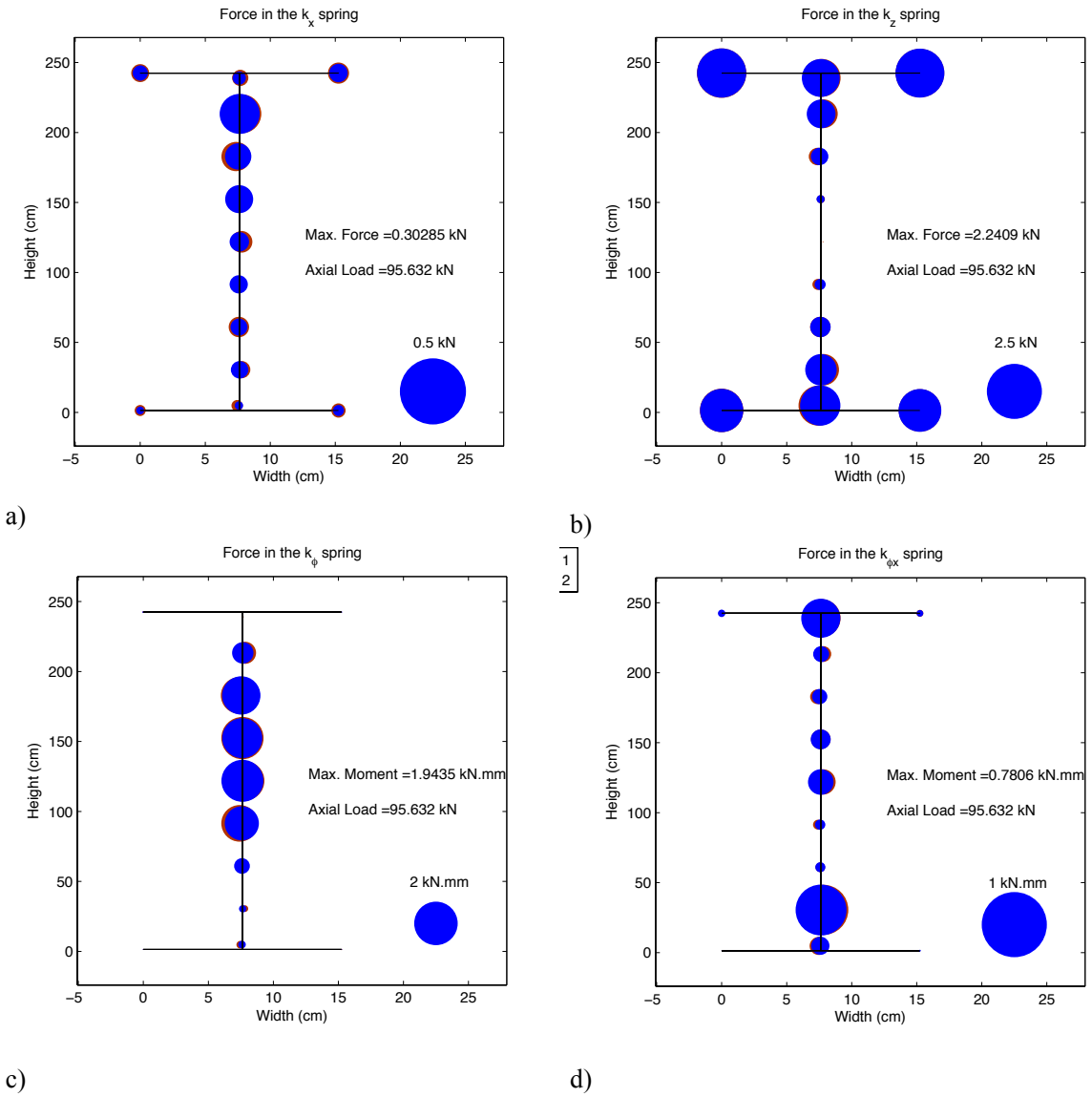

Figure 6.9 – Force and Moment in the springs at peak load for model that considers k_x, k_z, k_ϕ, $k_{\phi x}$, and sheathing is also simulated; initial imperfection of 75th percentile.

6.2.2 Full Wall Stud FE Model

6.2.2.1 Wall Stud Sheathed with OSB on Both Sides (OSB-OSB)

While the single-column models show perfect symmetry and a very predictable behavior, the full wall-stud model opens a new horizon to be explored, in fact, an asymmetric horizon replete with load redistribution. It is worth recalling that the steel

members on the edges (studs and tracks) are connected every 152mm (6in.), the field studs are connected every 254mm (12in.) and the stud in the middle that is connected to two boards is connected by two lines of fasteners (one line each board), every 152mm (6in.). The full wall FE model is depicted in Figure 6.10 (see Figure 5.1 for details).

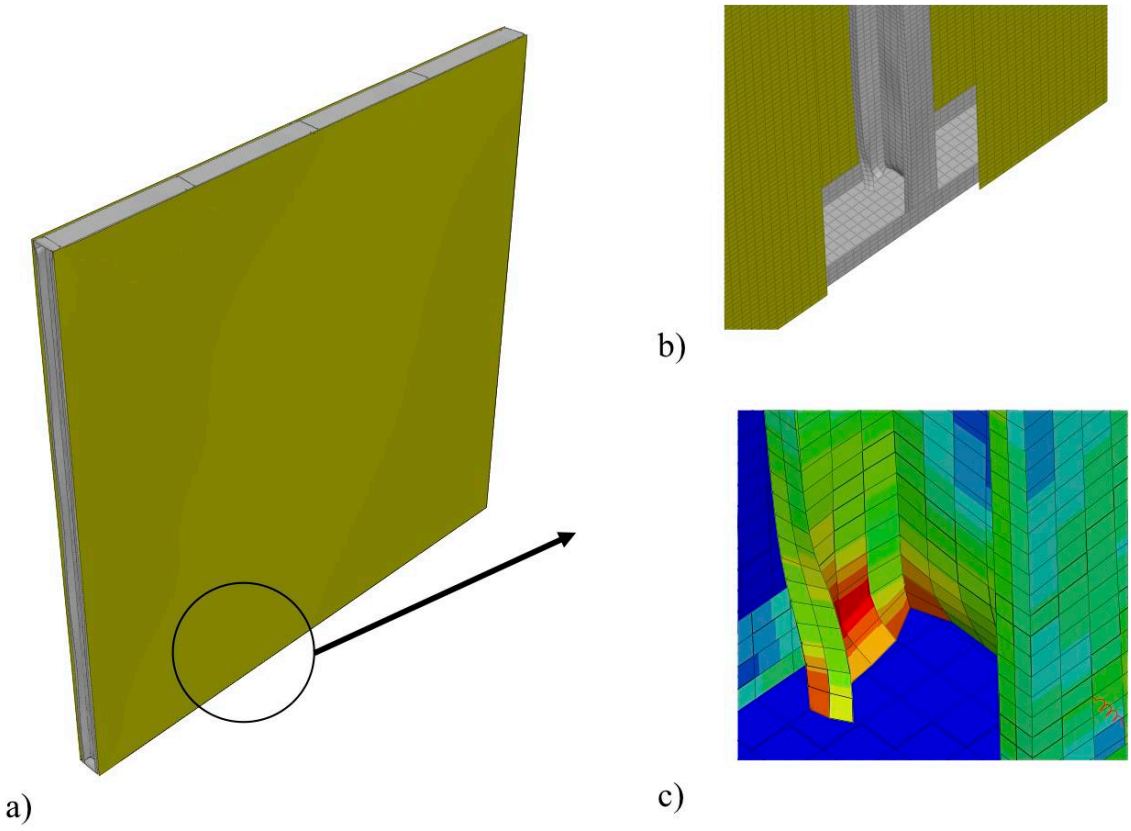

Figure 6.10 – FE Model considers k_x, k_z, k_ϕ, $k_{\phi x}$, and sheathing is also simulated (OSB-OSB) a) Overall view of FE model, steel members are represented in gray and OSB in brown, b) Zoomed view of stud end where local buckling takes place, the sheathing is partially removed to provide view of the stud, c) von Mises stress on stud end, special attention is brought to the stud-to-track connection where plastic failure takes place.

The k_x spring has highest demands at the ends where the stud is undergoing local buckling, at the peak load the corners are the places that the springs present the highest demands, Figure 6.11(a). The k_x spring is explored in more details in the following. The k_z spring reaches its full capacity (2.58kN (0.54kips)) at the bottom track, Figure 6.11(b).

This happens because the stud-to-track connection is undergoing local plastic failure, Figure 6.10 (c), and the sheathing is responsible for transferring the load to the stud. As in the single-column models, the rotational springs demonstrate small load levels compared to their resistance, but are still important for understanding the whole behavior of the system, Figure 6.11 (c, d). The higher loads in the $k_{\phi x}$ spring are at the end of the studs and track, implying that $k_{\phi x}$ helps restrain strong-axis buckling of the stud and bending of the track flanges. But k_{ϕ} loads are higher at the edge studs; due to the asymmetric contribution of the sheathing to the stud. At the edges, the flange of the stud is responsible for anchoring the sheathing that is bending out of its plane, while at the other studs the bending moment is counterbalanced by the continuation of the sheathing.

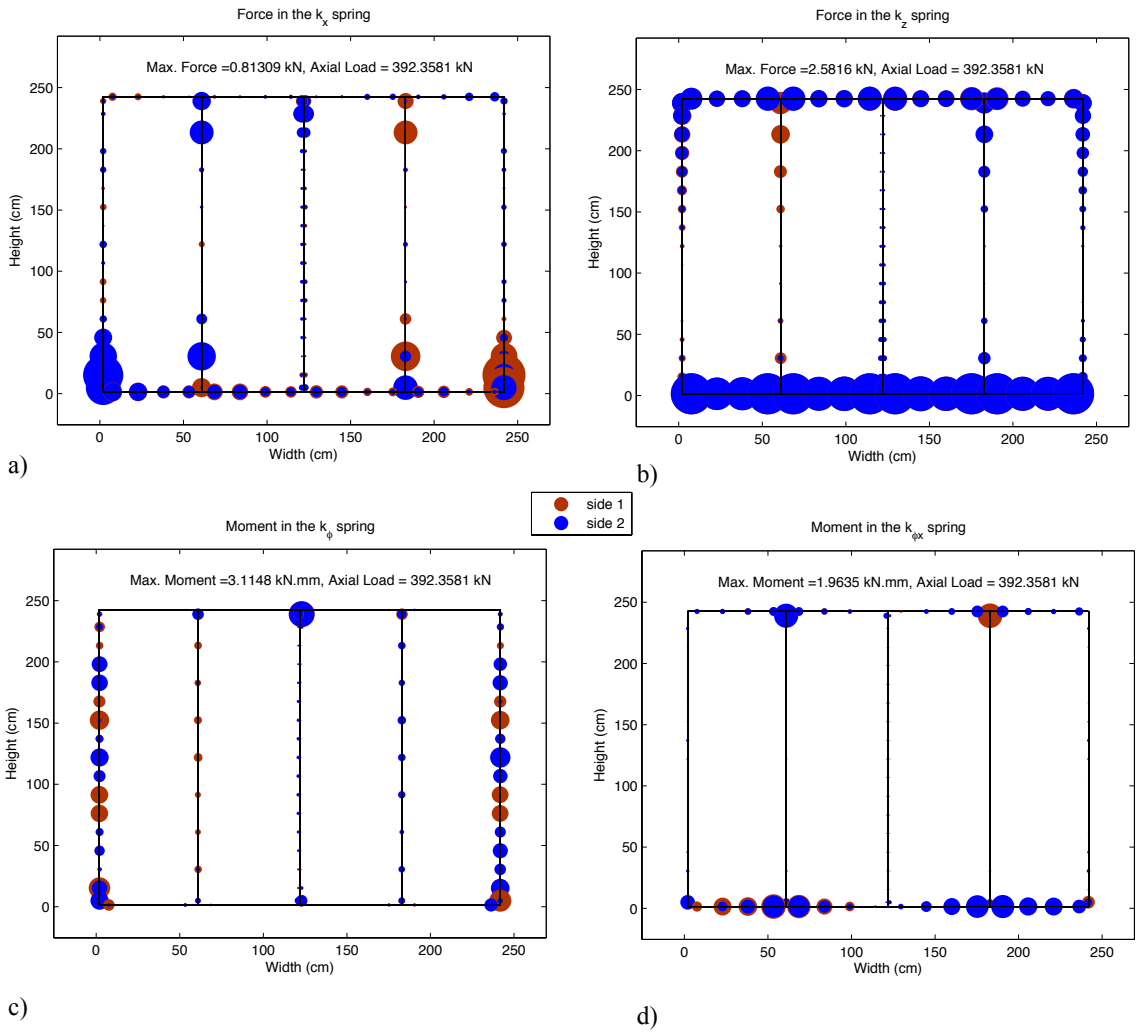

Figure 6.11 – Force and Moment in the springs at peak load for non-linear sheathed wall-stud model (k_x, k_z, k_ϕ, $k_{\phi x}$) (OSB-OSB). The biggest marker is equivalent to the maximum moment or force of each picture.

Nonetheless, a special attention has to be given to the k_x spring (Figure 6.12), which is the spring most responsible for restraining global buckling and therefore driving the stud to fail in local buckling. The first thing that is brought to attention is the asymmetric character of the force distribution. The asymmetry of the sheathing contribution to brace the stud defines the side that has greatest demands. For example, the second stud from left to right has a sheathing contribution from the right side of the stud higher than from the left side and thus the spring on side 2 receives more load than side 1, and the problem

is inverted on the fourth stud and thus the spring that receives more load is on side 1. But if both plots are superposed as in Figure 6.11 (a) the overall load plot is symmetric. Another interesting observation is the force distribution in k_x over different load steps. Until about 85% of the peak load, Figure 6.12 (a, b), the studs that has higher loads in the springs are the field studs (second and fourth studs), and this is due to the development of local buckling at the end of those studs, Figure 6.10 (b), but after 85% of peak load the force on the field studs does not increase and the connections in the corners start taking more lateral load. There is always some doubt about what is the least favorable situation: higher fastener spacing (field studs) or less sheathing contribution (edge studs). This study shows that the sheathing may be able to redistribute the loads and balance either the lower number of fasteners or the smaller effective width of the sheathing, but the redistribution depends on the extent to which local buckling is developed at the ends of the field studs.

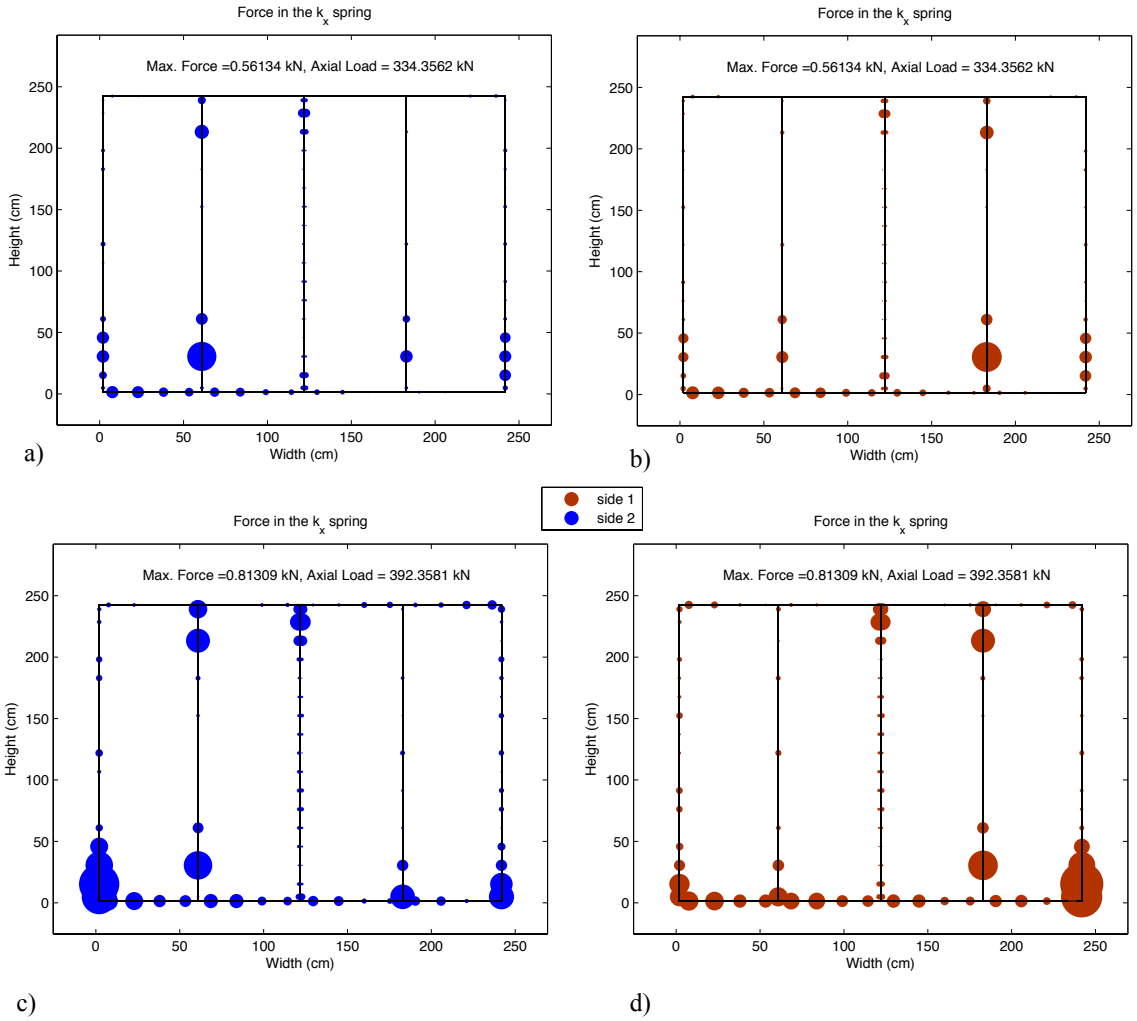

Figure 6.12 – Distribution of the forces in the k_x springs varying side that is being attached and axial load (OSB-OSB wall). The biggest marker is equivalent to the maximum moment or force of each picture.

6.2.2.2 Wall Stud sheathed with OSB on One Side Only (OSB-BARE)

Another interesting case to be explored is a wall stud sheathed with OSB on one side only (OSB-BARE), Figure 6.13. There is some concern that since the studs fail in flexural-torsional buckling the fastener demand would be bigger than walls sheathed on both sides. The models actually show that the fasteners demands in OSB-BARE walls are lower than in OSB-OSB walls, see Figure 6.14 and Figure 6.13, which correspond well to what was seen in the tests. In the OSB-BARE tests the connections were not fully

damaged after peak load, however in OSB-OSB tests the connections were fully damaged, especially close to the ends where local buckling takes place.

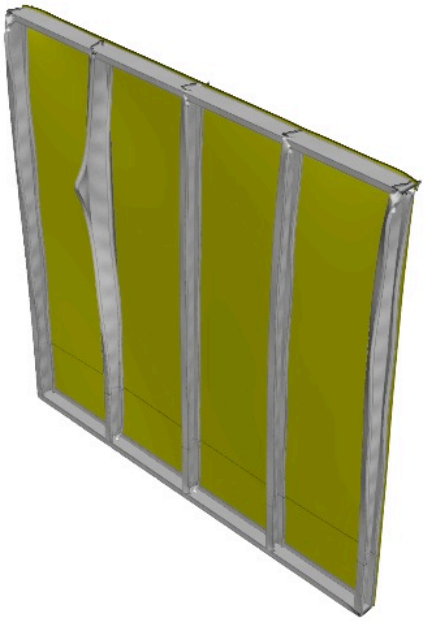

Figure 6.13 – FE Model considers k_x, k_z, k_ϕ, $k_{\phi x}$, and OSB sheathing on one side only.

The k_x springs have the greatest demands at the stud that buckles first – second stud (left to right). Unlikely the OSB-OSB model, the force doesn't redistribute to the edge studs, although the k_x springs at the edge studs still play an important role in bracing the wall, as can be observed by the amount of force in the k_x springs at the edge studs, see Figure 6.14(a). The k_z springs follow the same load distribution as in the OSB-OSB walls. The k_ϕ springs have greater demand than the OSB-OSB case, since the studs are buckling in flexural-torsional buckling and the k_ϕ spring attempts to restrain torsion of the stud. The moment magnitude at the $k_{\phi x}$ spring is slightly affected by the sheathing

asymmetry, Figure 6.14(d), but the moment resisted by the spring looses its symmetry as depicted in Figure 6.11(d).

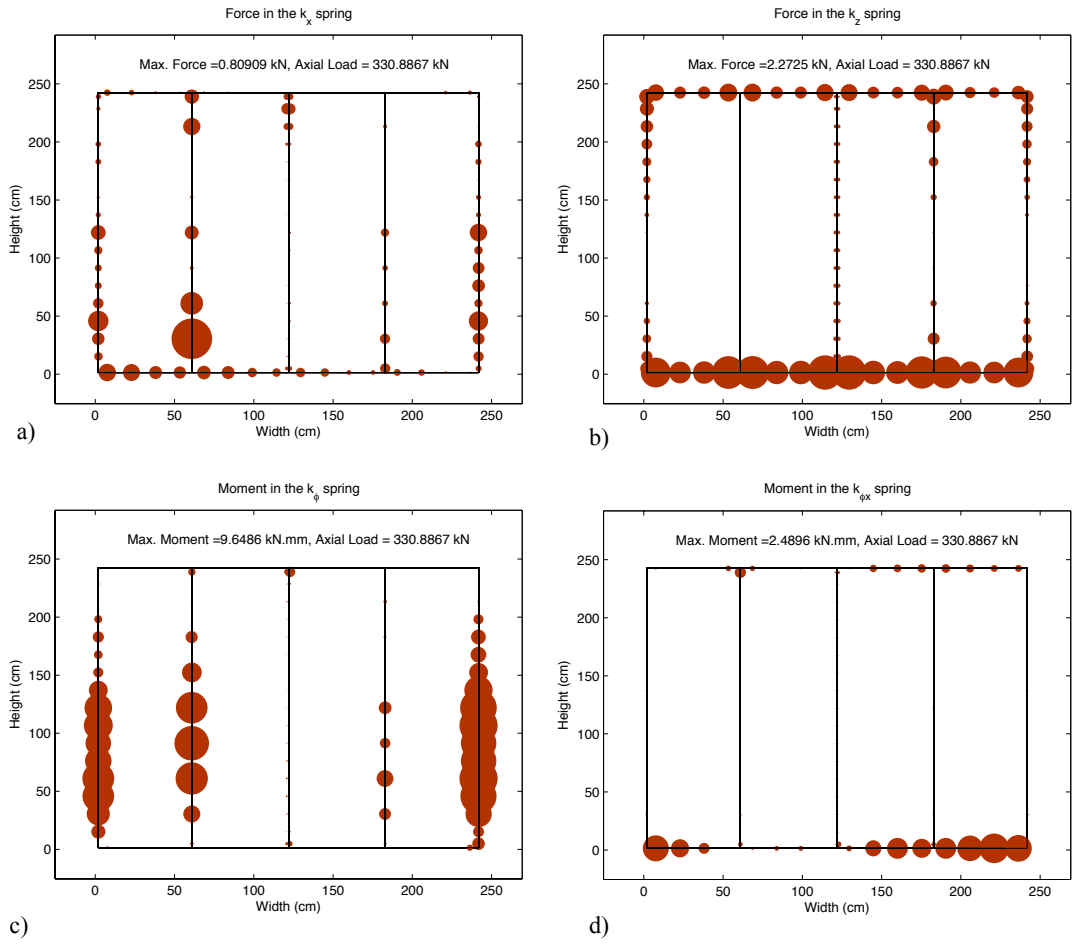

Figure 6.14 – Force and Moment in the springs at peak load for non-linear sheathed wall-stud model (k_x, k_z, k_ϕ, $k_{\phi x}$) (OSB-BARE). The biggest marker is equivalent to the maximum moment or force of each picture.

6.2.2.3 Necessary Strength of Connections

The 2% bracing rule implies that the sum of the forces resisted by the fasteners is equal to 2% of the axial load. This empirical rule has been used implicitly or explicitly since 1962 by the cold-formed steel design codes[3]. In 2008 Schafer et al. [6.15] showed

[3] For flexural buckling only AISI-S100 [6.1] in 2007 adopted a more modern strength and stiffness requirement.

that following the assumptions established by Winter [6.16] the actual necessary bracing force is in fact 1% of the axial load, therefore the design codes in essence adopted safety factor of 2. The 2% rule can be compared against the FE models. Figure 6.15 depicts the axial load versus the sum of the fastener forces on the second stud from left to right on the sheathed wall-stud model (see Figure 6.11(a) for distribution across the fasteners). The curve represents a typical magnitude of load carried by the springs, which exceeds 2% of the axial load at peak load. In fact, the comparison between the 2% rule and the FE model are important just to give an idea of fastener demand, since in the FE model the fastener force are magnified where the stud undergoes local buckling (again see Figure 6.11(a)) and the 2% rule conceptually only takes in account the strength necessary to restrain global buckling in a pinned-pinned column.

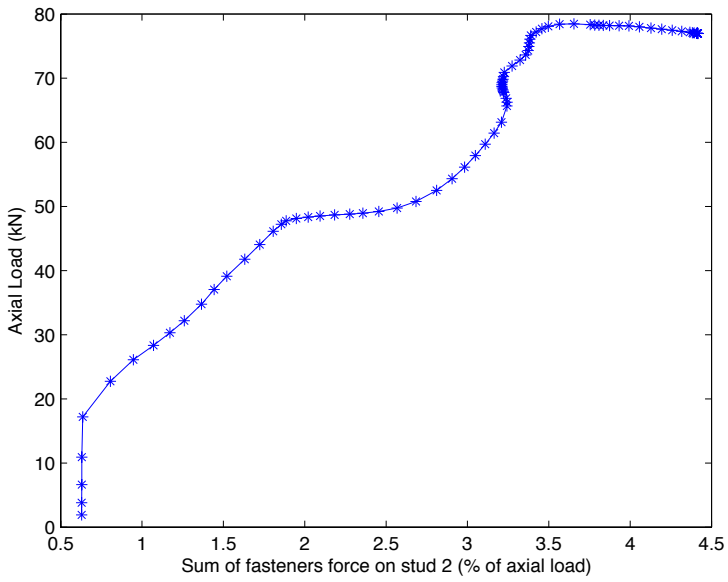

Figure 6.15 – Sum of fasteners force in the k_x spring on second stud (left to right) of sheathed wall-stud (Figure 6.11 (a)) versus axial load

6.3 COMPARISON BETWEEN FE MODELS AND ANALYTICAL SOLUTION

For global buckling, commented in Section 6.12.3, the fastener demands can be found based on the eigenvector solution for global buckling analysis. A geometric nonlinear FE model of a 362S162-68 stud, simply supported, with k_x, k_z, k_ϕ springs 12in. o.c. along the length, is used to verify the analytical solution. It is worth emphasizing that the analytical solution is for global buckling only, hence the fastener forces are only related to restricting global buckling. Purely for verification purposes, to eliminate local and distortional buckling, the stud thickness is changed from 1.67mm (0.0656in.) to 6.35mm (0.25in).

Initial imperfections play an important role in determining the fastener demand. If only twist is applied to the cross-section, FE and the analytical solution for fastener demand of the center fastener shows similar results, Figure 6.16(a). If camber or camber and twist are applied, FE and the analytical solution may lead to a different prediction of the fastener force, Figure 6.16 (b and c). A better approximation is given if the three buckling modes of the analytical solution are taken in account to amplify the lateral displacement, Eq. (6.9), Figure 6.16(d). It is common to consider only the first mode because in classical flexural buckling the other modes represent only a small contribution to the displaced shape, but in buckling of singly-symmetric studs flexural-torsional, and weak-axis buckling are often at similar elastic buckling values and magnification in both modes as load (P) goes to the buckling load (P_{cr}). For best accuracy in the fastener force prediction it is important to consider the extra buckling modes.

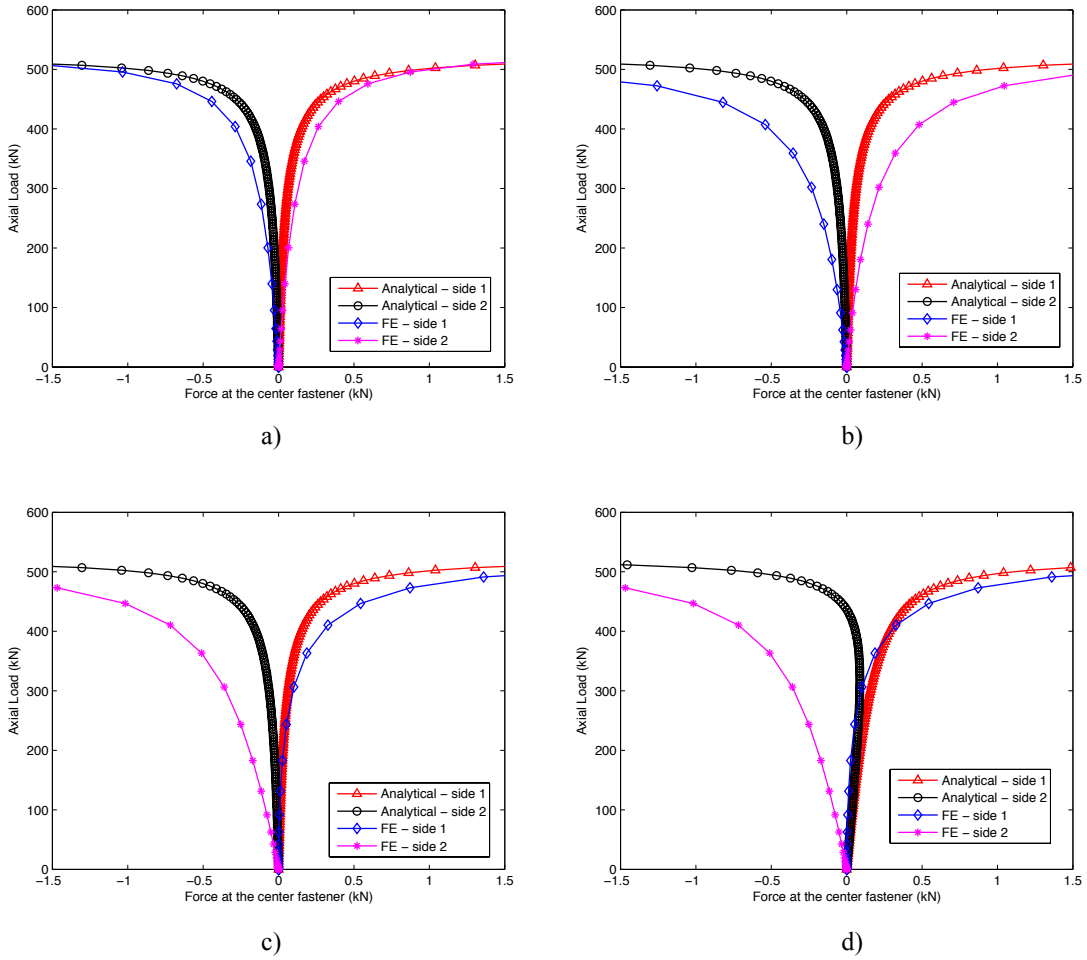

Figure 6.16 – Fastener demand in the x direction. Comparison between FE model and analytical solution of a simple-supported stud of geometry similar to 362S162-68, but thickness of 6.35mm (0.25in.) a) Stud with only twist initial imperfection (twist=1.23°), b) Stud with twist and camber initial imperfection (twist=1.23°, camber=L/2887), c) Stud with all global initial imperfections (twist=1.23°, camber=L/2887, bow=L/1659), d) Stud with all global initial imperfections (twist=1.23°, camber=L/2887, bow=L/1659), and analytical solution considers the displacement due to all three global buckling modes.

The analytical solution is also compared to the OSB-OSB single-column and the full-wall FE model as depicted in Figure 6.17. To take in account the clamped-clamped boundary conditions of the model, the analytical solution is found for a buckling length of half of the actual column height. Even though the FE models in this case consider not only global, but also local and distortional initial imperfection, the analytical solution –

all the global buckling modes are included. This results in a reasonable prediction of the fastener forces for single columns and wall studs. It is worth mentioning that the fasteners at mid-height are compared to the analytical solution, since these are the fasteners that are little influenced by local buckling deformations.

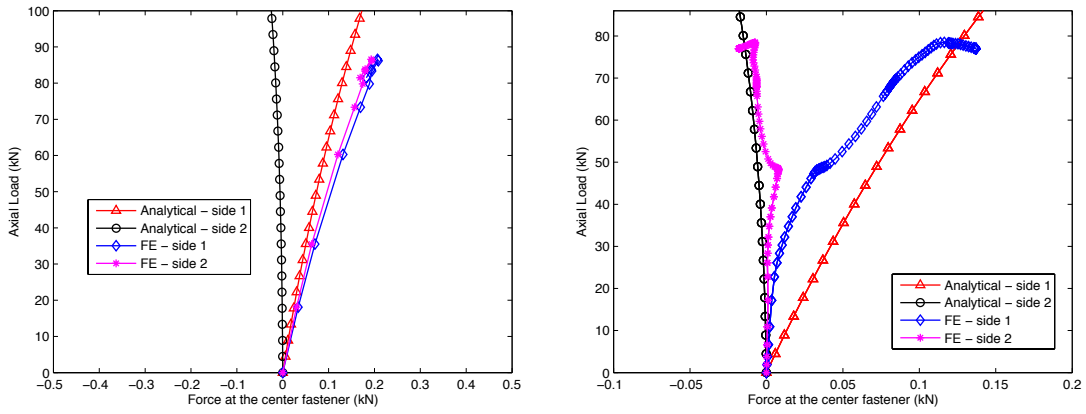

a) b)

Figure 6.17 – Comparison between FE model and analytical solution considering all the buckling modes. a) Single-column FE model as depicted in Figure 6.6, b) Wall stud as depicted in Figure 6.10.

6.4 STUD-TO-TRACK DEMAND

It was found in the FE models that the maximum shear force on the stud-to-track fasteners is around 5% of the axial load, but it is worth pointing out again that the FE models consider perfect contact between stud end and track web. More information on this regarding shall be find in [6.17].

REFERENCES CHAPTER 6

6.1. AISI-S100, *North American Specification for the Design of Cold-Formed Steel Structural Members.* American Iron and Steel Institute, 2007.

6.2. Li, Z. and B.W. Schafer. *Buckling analysis of cold-formed steel members with general boundary conditions using CUFSM: conventional and constrained finite strip methods*. in *Twentieth International Specialty Conference on Cold-Formed Steel Structures*. 2010. Saint Louis, Missouri, USA.

6.3. SSMA, *Product Technical Information, ICBO ER-4943P*, S.S.M. Association, Editor 2001.

6.4. AISI-S210, *North American Specification for the Design of Cold-Formed Steel Structural Members.* American Iron and Steel Institute, 2010.

6.5. Schafer, B.W., *Local, distortional, and Euler buckling of thin-walled columns.* Journal of Structural Engineering, 2002. **128**(3): p. 289-299.

6.6. Lau, S.C.W. and G.J. Hancock, *Distortional Buckling Formulas for Channel Columns.* Journal of structural engineering New York, N.Y., 1987. **113**(5): p. 1063-1078.

6.7. Timoshenko, S.P., Gere, James M., *Theory of Elastic Stability*1961, New York: McGraw-Hill.

6.8. Schafer, B.W. and S. Adany. *Buckling analysis of cold-formed steel members using CUFSM: Conventional and constrained finite strip methods*. in *Eighteenth International Specialty Conference on Cold-Formed Steel Structures: Recent Research and Developments in Cold-Formed Steel Design and Construction*. 2006. Orlando, FL.

6.9. Simaan, A. and T.B. Pekoz, *Diaphragm Braced Members and Design of Wall Studs.* ASCE J Struct Div, 1976. **102**(1): p. 77-92.

6.10. Miller, T.H. and T. Pekoz, *Behavior of cold-formed wall stud-assemblies.* Journal of structural engineering New York, N.Y., 1993. **119**(2): p. 641-651.

6.11. AISI-S211, *North American Specification for the Design of Cold-Formed Steel Structural Members.* American Iron and Steel Institute, 2007.

6.12. ABAQUS, *ABAQUS/Standard Version 6.7-1*, D. Systemes, Editor 2007.

6.13. Schafer, B.W. and T. Peköz, *Computational modeling of cold-formed steel: Characterizing geometric imperfections and residual stresses.* Journal of Constructional Steel Research, 1998. **47**(3): p. 193-210.

6.14. Schafer, B.W. and V.M. Zeinoddini. *Impact of global flexural imperfections on the cold-formed steel column curve*. in *19th International Specialty Conference on Recent Research and Developments in Cold-Formed Steel Design and Construction*. 2008.

6.15. Schafer, B.W., O. Iourio, and L.C.M. Vieira Jr, *Notes on AISI Design Methods for Sheathing Braced Design of Wall Studs in Compression*, in *A supplemental report for AISI-COFS Project on Sheathing Braced Design of Wall Studs*2008, The Johns Hopkins University: Baltimore.

6.16. Winter, G., *Lateral Bracing of Beams and Columns.* Journal of the Structural Division, 1960.

6.17. Laboube, R.A. and P.F. Findlay, *Wall stud-to-track gap: Experimental investigation.* Journal of Architectural Engineering, 2007. **13**(2): p. 105-110.

CHAPTER 7 - PROPOSED DESIGN METHOD

This chapter focuses on proposing the details of a new design method for sheathed walls in compression based on the Direct Strength Method (DSM) (AISI-S100-07 [7.1], Appendix 1). A procedure for the main body of the AISI Specification (AISI-S100-07 [7.1]) is also discussed. The design method is compared to the tests results presented in Chapters 4 and 5. Finally, the design of the connections between the stud and the sheathing is summarized based on available design standards. Supporting work and development of the expressions provided in this Chapter may be found within this thesis.

7.1 SPRING STIFFNESS

Table 7.1 summarizes and compares the proposed design method for member capacity. Using either DSM or the Main Specification (effective width) the spring stiffnesses representing the sheathing restraint to the studs (k_x, k_y and k_ϕ) shall first be determined. It is conservative to ignore any spring stiffness.

7.1.1 Translational Lateral Stiffness (k_x)

Translational lateral stiffness k_x is determined by combining the local translational stiffness ($k_{x\ell}$) and diaphragm translational stiffness (k_{xd}) via (as detailed in Chapter 3 Section 3.8):

$$k_x=(1/k_{x\ell} + 1/k_{xd})^{-1} \quad (7.1)$$

7.1.1.1 Local Translational Stiffness ($k_{x\ell}$)

Local translational stiffness $k_{x\ell}$ may be found by a translational test (as detailed in Chapter 3 Section 3.4), a new addition to the AISI Test Specifications (TS) is needed. Alternatively, $k_{x\ell}$ may also be found by a lowerbound formula (as detailed in Chapter 3 Section 3.5):

$$k_{x\ell} = \frac{3Ed^4t^3\pi}{4t_{board}^2(9d^4\pi + 16t_{board}t^3)} \tag{7.2}$$

where:

E = Young's modulus of the steel stud,

d = fastener diameter,

t = flange thickness,

t_{board} = board/sheathing thickness.

7.1.1.2 Diaphragm Translational Stiffness (k_{xd})

Diaphragm translational stiffness k_{xd} may be found by (as detailed in Chapter 3 Section 3.6):

$$k_{xd} = \frac{\pi^2 G t_{board} d_f w_{tf}}{L^2} \tag{7.3}$$

where:

G = shear modulus of sheathing, G may be found through testing by ASTM-D2719-89 [7.2], or G from NDS [7.3] may be used.

w_{tf} = fastener tributary width,

d_f = distance between fasteners,

L = sheathing height.

7.1.2 Out-of-plane Translational Stiffness (k_y)

Out-of-plane translational stiffness k_y may be found analytically using a lowerbound approximation as:

$$k_y = \frac{(EI)_w \pi^4 d_f}{L^4} \tag{7.4}$$

where:

$(EI)_w$ = sheathing rigidity per APA-D510C [7.4] for OSB and plywood sheathing, and GA-235-10 [7.5] for gypsum sheathing, APA-D510C [7.4] tables $(EI)_w$ based on the stress parallel or perpendicular to strength axis, if the sheathing is installed as depicted in Chapters 4 and 5 (stud parallel to long side of sheathing), $(EI)_w$ is given by the stress **parallel** to strength axis table.

d_f = distance between fasteners,

L = sheathing height.

Alternatively, $(EI)_w$ used for determining k_y may be found from an ASTM-E72 [7.6] test. This test provides bending stiffness of the system: stud plus sheathing ($(EI)_{system}$). For a two point load test $(EI)_{system}$ is given by Eq. (7.5), and for a uniform load $(EI)_{system}$ is given by Eq. (7.6).

$$(EI)_{system} = \frac{11Pl^3}{384\delta} \tag{7.5}$$

$$(EI)_{system} = \frac{5wl^4}{384\delta} \tag{7.6}$$

where:

P = concentrated load applied transversally to the wall,

l = spam,

δ = maximum measured displacement for respective loading case (P or w).

w = uniform load applied transversally to the wall,

Nonetheless, Eq. (7.4) only uses the bending stiffness of one sheathing ($(EI)_w$), hence the bending stiffness due to the stud ($(EI)_{stud}$) shall be subtract from $(EI)_{system}$, and the result shall be divided by 2, since there are two sheathings connected to the stud (one on each side):

$$(EI)_w = \frac{\left((EI)_{system} - (EI)_{stud}\right)}{2} \tag{7.7}$$

7.1.3 Rotational Stiffness (k_ϕ)

Rotational Stiffness k_ϕ may be found empirically by AISI-TS-1-02 [7.7]. AISI-S210 is adding in the 2011 version a method to find k_ϕ numerically, which is given by:

$k_{\phi c} = 0.00035Et^2 + 75$ (note: E in lbf/in^2, t in in.) (7.8)

$k_{\phi w} = (EI)_w / d_f$ (7.9)

$k_\phi = 1/(1/k_{\phi c} + 1/k_{\phi w})$ (7.10)

where:

E = Young's modulus of the steel stud,

t = flange thickness,

d_f = distance between fasteners,

$(EI)_w$ = sheathing rigidity per APA-D510C [7.4] for OSB and plywood sheathing, and GA-235-10 [7.5] for gypsum sheathing, APA-D510C [7.4] tables $(EI)_w$ based on the stress parallel or perpendicular to strength axis, if the sheathing is installed as depicted in Chapters 4 and 5 (stud parallel to long side of sheathing), $(EI)_w$ is given by the stress **perpendicular** to strength axis table.

7.2 ELASTIC BUCKLING

7.2.1 DSM Approach

7.2.1.1 Global Buckling

Global buckling load (P_{cre}) may be found by the finite element method (FEM), for example using the commercial program ABAQUS [7.8], or the finite strip method (FSM), e.g. CUFSM v4.03 [7.9] may also be used. Note that CUFSM v4.03 [7.9] is recommended if clamped-clamped boundary conditions are included for P_{cre}.

The Commentary of AISI-S100 (Appendix 1) [7.1] also explains how to determine the buckling load of a clamped-clamped stud based on the pin-pin solution (signature curve). The idea behind the commentary is that the buckling length (KL) can be adjusted based on the boundary condition. This approach has limitations for braced studs. The global buckling load may also be found analytically based on the eigenvalue problem provided in Section 6.1.2.3, but the solution is involved.

7.2.1.2 Local Buckling

The fastener-sheathing springs and the effect of clamped-clamped boundary condition can be ignored for determining the local buckling load ($P_{cr\ell}$) due to the short buckling

wave-length. For the finite strip method, any previous version of CUFSM is suitable to find $P_{cr\ell}$. The commentary of AISI-S100 (Appendix 1) [7.1] shows two possible ways of finding $P_{cr\ell}$ by formula: i) considering just individual elements, and ii) considering the interaction between any two elements. A summarized version of the formula is given by:

$$P_{cr\ell} = A_g f_{cr\ell} \tag{7.11}$$

where:

A_g = gross area of the member,

$f_{cr\ell}$ = local buckling stress of elements, or element combinations, per [7.1].

7.2.1.3 Distortional Buckling

Distortional buckling load (P_{crd}) can also be found using either FEM or FSM/CUFSM v4.03 (For distortional buckling predictions it is appropriate to use k_x and k_ϕ, but ignore k_y). The main specification AISI-S100 [7.1] already provides a procedure to find P_{crd} for pinned ends. Eq. (7.12) shows how to find P_{crd} based on the distortional buckling stress (f_{crd}). To account for fixed ends on P_{crd} the D_{boost} factor as determined by Moen [7.10] may be used. The approximation suggested by Moen [7.10] determines P_{crd} for a clamped-clamped member based on the signature curve (pin-pin) solution of P_{crd}.

$$P_{crd} = A_g f_{crd} \tag{7.12}$$

where:

A_g = gross area of the member,

f_{crd} = distortional buckling stress at the extreme compression fiber. Solutions and design aids for f_{crd} are available in [7.11, 12].

7.2.2 Main Specification Approach

7.2.2.1 Global Buckling

AISI-S100 [7.1] main specification allows the engineer to use a rational analysis to determine the global buckling load ($F_e=P_{cre}/A_g$), meaning that P_{cre} discussed above can also be used in the main body of the specification. The global buckling load may also be found analytically based on the eigenvalue problem provided in Section 6.1.2.3, but the solution is involved.

7.2.2.2 Local Buckling

Local buckling (F_{cr}) is determined in the main body of the specification by plate theory where the elements are considered separately but the plate-buckling coefficient (k) varies depending on the boundary condition and loading of the element:

$$F_{cr} = f_{cr\ell} = k\frac{\pi^2 E}{12(1-\mu^2)}\left(\frac{t}{w}\right)^2 \tag{7.13}$$

where:

E = Young's modulus of steel stud,

μ = Poisson's ratio,

t = element thickness,

w = element flat width,

k = element (plate) buckling coefficient. Chapter B of AISI-S100 [7.1] provides k values for all covered cases.

7.2.2.3 Distortional Buckling

AISI-S100 [7.1] main specification allows the engineer to use a rational analysis to determine distortional buckling load ($F_d=P_{crd}/A_g$), meaning that P_{crd} discussed above can be used also in the main body of the specification.

7.3 STRENGTH DETERMINATION

7.3.1 DSM Approach

DSM is presented in Appendix 1 of the AISI-S100 [7.1]. Based on the elastic buckling loads (local ($P_{cr\ell}$), distortional (P_{crd}), and global (P_{cre})) the DSM provides the nominal strength of a column.

7.3.1.1 Global Buckling

Based on the global slenderness (λ_c) the nominal global load (P_{ne}) is determined as:

$$\lambda_c = \sqrt{\frac{P_y}{P_{cre}}} \text{ , note (L) denotes that the quantity is a function of length} \quad (7.14)$$

$$\text{if } \lambda_c \le 1.5 \text{ , } P_{ne} = 0.658^{\lambda_c^2} P_y \quad (7.15)$$

$$\text{if } \lambda_c > 1.5 \text{ , } P_{ne} = \frac{0.877}{\lambda_c^2} P_y \quad (7.16)$$

where:

P_y = yielding load.

7.3.1.2 Local Buckling (Local-Global Interaction)

Based on the local slenderness (λ_ℓ) the nominal local load ($P_{n\ell}$) is determined as:

$$\lambda_l = \sqrt{\frac{P_{ne}}{P_{crl}}}\text{, note subscript } \textit{“l”} = \text{“}\ell\text{”} \tag{7.17}$$

$$\text{if } \lambda_l \le 0.776,\ P_{nl} = P_{ne} \tag{7.18}$$

$$\text{if } \lambda_l > 0.766,\ P_{nl} = \left[\left[1 - 0.15\left(\frac{P_{crl}}{P_{ne}}\right)^{0.4}\right]\left(\frac{P_{crl}}{P_{ne}}\right)^{0.4} P_{ne}\right] \tag{7.19}$$

7.3.1.3 Distortional Buckling

Based on the distortional slenderness (λ_d) the nominal distortional load (P_{nd}) is determined as:

$$\lambda_d = \sqrt{\frac{P_y}{P_{crd}}} \tag{7.20}$$

$$\text{if } \lambda_d \le 0.561,\ P_{nd} = P_y \tag{7.21}$$

$$\text{if } \lambda_d > 0.561,\ P_{nd} = \left[\left[1 - 0.25\left(\frac{P_{crd}}{P_y}\right)^{0.4}\right]\left(\frac{P_{crd}}{P_y}\right)^{0.4} P_y\right] \tag{7.22}$$

7.1.1.1 Nominal/Design Load

Finally, the lowest nominal load is the nominal/design load (P_n):

$$P_n = \min(P_{ne}, P_{nl}, P_{nd}) \tag{7.23}$$

7.3.2 Main Specification Approach

In section C4.1 of the AISI-S100 [7.1] the strength of a member (P_n) can be found based on the local and global interaction. The method in section C4.1 determines that the nominal stress (F_n) is a function of the global elastic buckling stress (F_e). While local buckling is taken in account by a reduction of the cross section area. The reduced cross section area is named: effective area (A_e), and it is a function of the critical buckling stress (F_{cr}). Finally, the nominal load (P_n), due to local and global interaction, is given by the product of the effective area (A_e) and the nominal stress (F_n).

The only change proposed here is that F_e, which is also equal to P_{cre}/A_g, is determined with the fastener-sheathing restraint included.

Distortional buckling is considered in section C4.2 of AISI-S100 [7.1], and the procedure also leads to a nominal load (P_n). Nonetheless, the "final" nominal load is given by the lowest nominal load found from section C4.1 and section C4.2. Note, if the impact of end boundary condition is to be included then the rational analysis clause of C4.2(b) must be invoked, then F_{crd} of C4.2 utilizes P_{crd}/A_g as discussed in Section 7.2.1.3.

Table 7.1 – Summary of proposed design method for member capacity.

<table>
<tr><td rowspan="4">Member Capacity</td><td> 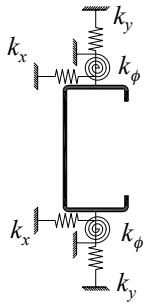
</td><td colspan="2">Determine springs to account for sheathing restraint
• k_x is determined from k_{xd} and $k_{x\ell}$
○ k_{xd} – Diaphragm stiffness
▪ Formula (new – S210/211 or S100)
▪ Material Test for G (e.g., ASTM D2719-89)
○ $k_{x\ell}$ – Local stiffness
▪ Test (new – TS)
▪ Lowerbound formula (new – S210/211 or S100)
• k_y
○ Test (ASTM – E72) + Conversion (ASTM-E72 + new – S210/211)
○ Lowerbound formula (new – S210/211)
• k_ϕ (AISI-S210-10)
○ Test (modify - AISI S901-08)
○ Formula (S210/S211)</td></tr>
<tr><td colspan="2">Elastic Buckling – DSM – AISI-S100 App. 1 (Note, Fixed-Fixed)
• Global (P_{cre})
○ Formula (new – S100 C4 formulas)
○ CUFSM 3 at KL (DSM Guide/App.1 Comm.)
○ CUFSM 4 (new – App.1 Commentary)
○ FEM/ABAQUS
• Distortional (P_{crd})
○ Formula (S100 C4.2)
○ CUFSM 3 × D_{boost} (new – App.1 Commentary)
○ CUFSM 4 (new – App.1 Commentary)
○ FEM/ABAQUS
• Local ($P_{cr\ell}$) (ignore springs)
○ Formula element only (DSM Guide/App.1 Comm.)
○ Formula with interaction (DSM Guide/App.1 Comm.)
○ CUFSM 3 or 4 (new – App.1 Commentary)</td><td>Elastic Buckling – Main Spec. – AISI-S100
• Global (F_e)
○ Formula (new S100 – C4 formulas)
○ Rational Analysis (see DSM $F_e=P_{cre}/A_g$)
• Distortional (F_d)
○ Formula (S100 C4.2)
○ Rational Analysis (see DSM $F_d=P_{crd}/A_g$)
• Local (F_{cr})
○ Formula element only (AISI-S100 k's in Ch. B)</td></tr>
<tr><td colspan="2">Strength – DSM – AISI-S100 App. 1
• Global (P_{ne})
○ Formula (S100 Eq.1.2.1.1)
• Distortional (P_{nd})
○ Formula (S100 Eq.1.2.1.3)
• Local-Global ($P_{n\ell}$)
○ Formula (S100 Eq.1.2.1.2)
• $P_n=\min(P_{ne}, P_{nd}, P_{n\ell})$</td><td>Strength – Main Spec. – AISI-S100
• Distortional (P_n)
○ Formula (S100 C4.2)
• Local-Global (P_n)
○ $P_n=A_eF_n$, $A_e=f(F_{cr})$, $F_n=f(F_e)$ (S100 C4.1)
• $P_n=\min(P_{n,C4.2}, P_{n,C4.1})$</td></tr>
</table>

7.4 COMPARISON WITH TESTS

As discussed previously, and demonstrated in Chapter 4, the bare column (no sheathing) behaves essentially as a member with fixed-fixed end conditions, rather than pin-pin. As a result, both the traditional pin-pin, and upper bound fixed-fixed boundary conditions are explored in the following.

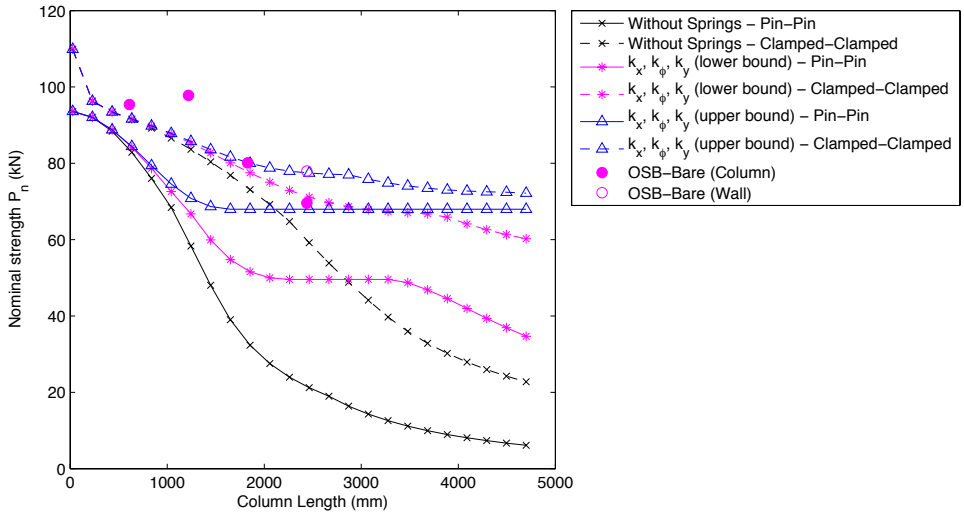

Figure 7.1 – Bare stud and stud restrained on one side compared to the possible design curves

Figure 7.1 provides a comparison of design assumptions for the OSB-Bare columns and walls. The tests all failed in a highly restrained version of flexural-torsional buckling. The test data most closely follows the assumption of fixed-fixed end conditions. In fact, up to 183cm (72 in.), the end conditions are more influential than the sheathing restraint. For longer columns the importance of the sheathing restraint grows significantly. For the fixed-fixed end conditions, the lower bound (noncomposite) approximation for the sheathing contribution to the major–axis bending of the stud (k_y) is sufficiently accurate.

For the columns and walls with sheathing restraint on both sides: Gyp-Gyp, OSB-Gyp and OSB-OSB Figure 7.2 provides a comparison with potential design assumptions (to provide some clarity the spring values employed in the design curves are those for OSB-OSB). All of the tested columns fail in local buckling, at approximately the same per stud strength. In stark contrast to the case with one-sided sheathing (OSB-Bare) having springs on both flanges dramatically decreases the impact of the end boundary conditions. Even when only considering the in-plane resistance (k_x and k_*) this restraint is enough to strongly restrict weak-axis bending and torsion, and up through 183cm (72 in.) length the end conditions have only a small influence on the result. However, for longer than 183cm (72 in.) the major-axis bending becomes increasingly important to restrain – either fixed-fixed end conditions or fully composite bending action with the sheathing (k_y upper bound) is required. The assumption of fixed-fixed end conditions and the noncomposite lower bound for k_y is again found to be a good predictor of the behavior. Pin-pin end conditions and only in-plane resistance (in essence the traditional model) is observed to be (a) a conservative predictor, and (b) one that reasonably follows the observed experimental trends.

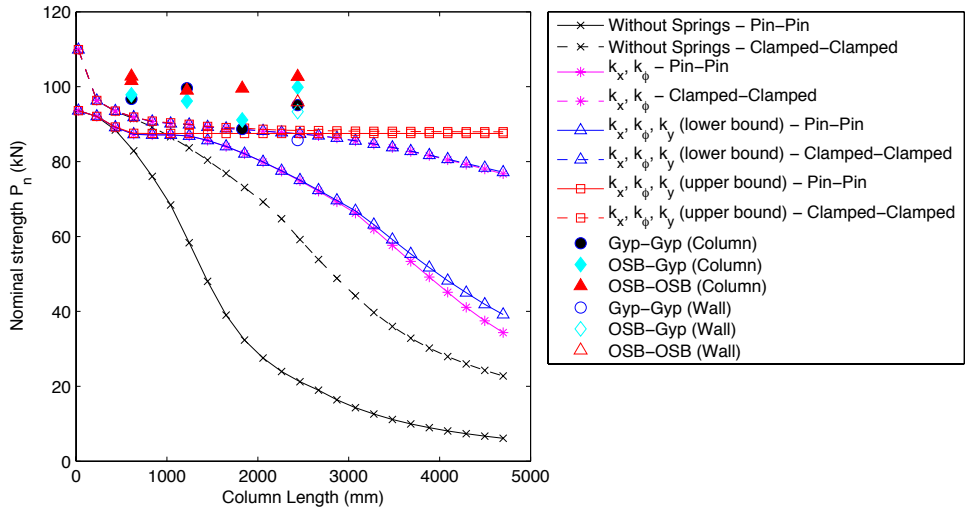

Figure 7.2 – Studs restrained on both sides compared to possible design curves

Finally, the proposed design method (using DSM and employing fixed-fixed end conditions, k_x and k_ϕ in-plane restraint and the non composite k_y lower bound resistance) is compared to the tests and other currently available design methods. In addition, the actual spring values for OSB and Gypsum board are utilized (per Table 6.1). The test data compares well with the proposed method and the small differences between OSB-OSB, OSB-Gyp, and Gyp-Gyp are even reflected in the predicted strength, along with the relatively pronounced decrease as a function of length for the one-sided sheathing case: OSB-Bare. The strength prediction is a significant improvement over AISI-S100-01 [7.13] (essentially the Simann and Peköz 1976 method [7.14]), Figure 7.3. The method is also an improvement over AISI-S210-07 both conceptually (AISI-S210-07 [7.1] simply assumes one fastener is defective and calculates the strength of a column with a length equal to twice the fastener spacing) and in terms of strength prediction.

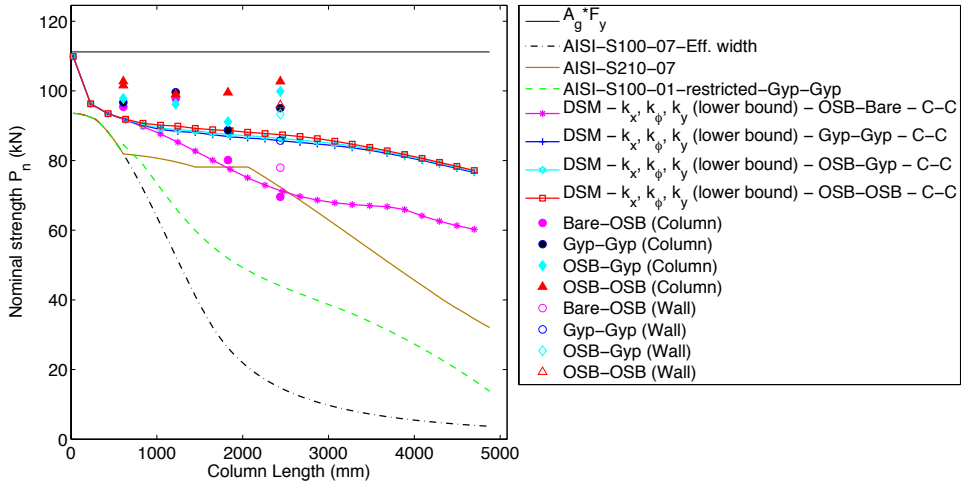

Figure 7.3 – Test results compared to former, current and proposed design methods

7.5 CONNECTIONS DESIGN

While the fastener demands aren't easily determined (Chapter 6), the capacity of the fastener, sheathing and assembly is addressed in several sources, which is summarized in Table 7.2.

AISI-S100 [7.1] provides shear and tension capacity for the fastener, which can be found by test or tables provided by the manufacturer. Nonetheless, the combination of shear and tension is not currently addressed in the AISI standard. The expressions provided for bolts under shear and tension are an option for rational analysis.

The capacity of the sheathing regarding shear is addressed for plywood and OSB by the APA (The engineering wood association) in the panel design specification [7.4]. The design of gypsum sheathing is addressed in GA 229-08 [7.15].

The bending capacity of OSB or plywood sheathing is given in the same design specification used for shear capacity [7.4], and gypsum can be designed in bending using GA 235-10 [7.5].

The connection of stud/track to the sheathing should be checked for tilting, bearing, edge tear-out, pull-out, and pull-through. For OSB and plywood the check can be completed by combining the design procedures given in AISI-S100 [7.1], NDS-2005 [7.3], and APA-E830D [7.16], but for gypsum sheathing explicit design checks do not currently exist. However, testing is also a viable option to determine the assembly capacity for any kind of sheathing, see Chapter 3.

Additional future work formalizing the connection design is needed.

Table 7.2 – Summary of proposed design method for connections.

Connections	Fastener	• Shear – AISI-S100-07 says per manufacturer table or test • Tension – AISI-S100-07 says per manufacturer table or test • Shear + Tension – No AISI provisions, expression for bolts could provide a rational answer
	Sheathing	• Shear o Wood – APA 2008 Panel Design Specification provides allowable stresses for plywood and OSB in shear o Gypsum – GA 229-08 • Bending o Wood – APA 2008 Panel Design Specification provides allowable stresses for plywood and OSB o Gypsum – GA 235-10 provides strength values for gypsum
	Assembly	• Stud/Track-Fastener-Sheathing o Tilting, Bearing, Edge tear out, Pull-out, Pull-through – AISI-S100-07 + NDS-2005 (Bearing eq. for wood alone) + APA E830D (limited set of values for plywood-to-steel) and Gypsum sheathing will need a technical note o Test

REFERENCES CHAPTER 7

7.1. AISI-S100, *North American Specification for the Design of Cold-Formed Steel Structural Members.* American Iron and Steel Institute, 2007.

7.2. ASTM, *Standard Test Method for Structural Panels in Shear Through-the-Thickness*, in *ASTM D2719-89*2002, American Society for Testing and Materials: West Conshohocken, PA.

7.3. NDS, *National Design Specification (NDS) for Wood Construction, ANSI/AF&PA NDS*, A.F.a.P. Association, Editor 2005: Washington, DC.

7.4. APA-D510C, *Panel Design Specification*, A.-T.e.W. Association, Editor 2008: Tacoma, Washington, USA.

7.5. GA-235-10, *Gypsum Board Typical Mechanical and Physical Properties*, 2010, Gypsum Association: Hyattsville, MD, USA.

7.6. ASTM, *Standard Test Methods of Conducting Strength Tests of Panels for Building Construction*, in *E 72-98*2002, American Society for Testing and Materials: West Conshohocken, PA.

7.7. AISI-TS-1-02, *Rotational-Lateral Stiffness Test Method for Beam-to-Panel Assemblies.* AISI Cold-Formed Steel Design Manual, 2002.

7.8. ABAQUS, *ABAQUS/Standard Version 6.7-1*, D. Systemes, Editor 2007.

7.9. Li, Z. and B.W. Schafer. *The constrained finite strip method for general end boundary conditions.* in *Structural Stability Research Council - 2010 Annual Stability Conference*. 2010. Orlando, FL, USA.

7.10. Moen, C.D. and B.W. Schafer, *Direct strength design of cold-formed steel members with perforations*. Vol. 69. 2009.

7.11. Schafer, B.W., *Local, distortional, and Euler buckling of thin-walled columns.* Journal of Structural Engineering, 2002. **128**(3): p. 289-299.

7.12. Lau, S.C.W. and G.J. Hancock, *Distortional Buckling Formulas for Channel Columns.* Journal of structural engineering New York, N.Y., 1987. **113**(5): p. 1063-1078.

7.13. AISI-S100, *North American Specification for the Design of Cold-Formed Steel Structural Members.* American Iron and Steel Institute, 2001.

7.14. Simaan, A. and T.B. Pekoz, *Diaphragm Braced Members and Design of Wall Studs.* ASCE J Struct Div, 1976. **102**(1): p. 77-92.

7.15. GA-229-08, *Shear Values for Screw Application of Gypsum Board on Walls*, 2008, Gypsum Association: Washignton, D.C.

7.16. APA-E830D, *Fastener Loads for Plywood - Screws*, A.-T.e.W. Association, Editor 2005: Tacoma, Washington, USA.

CHAPTER 8 - CONCLUSIONS AND PROPOSED FUTURE WORK

8.1. CONCLUSIONS

Sheathing has a significant impact on the stability and strength of cold-formed steel studs. The sheathing may be considered to "brace" the studs at fastener locations. This sheathing bracing derives from both local fastener deformations and global shear diaphragm behavior. Experiments measuring local fastener stiffness (and strength) indicate the relative difference between fasteners attached to studs through OSB and gypsum. The sensitivity, particularly of gypsum, to environmental and installation conditions is illustrated in the local stiffness testing. Analytical formulae are provided and verified for local translational stiffness and shear diaphragm stiffness. A full-scale wall test using strips of OSB sheathing instead of a full OSB board is carried out to demonstrate that the sheathing bracing derives from *both* local and diaphragm stiffness, not just local stiffness (or diaphragm stiffness) as has been classically assumed. A combined bracing model whereby local and diaphragm bracing are treated as two springs in series is proposed for modeling sheathing-braced studs.

A series of tests on cold-formed steel studs, sheathed with oriented strand and/or gypsum board, varying in length from 0.61 m (2 ft) to 2.44 m (8 ft) demonstrates that sheathing may restrict distortional and global buckling, thus causing local buckling to be the controlling limit state at all practical lengths. Sheathing must exist on both sides of the stud to restrict global buckling modes, and when gypsum sheathing is employed pull-through and other sheathing failures are common at deformations immediately past peak

load. Dissimilar sheathing (different on the two sides) has proved effective in observed tests, with the exception of OSB-Bare tests, which improves capacity from the unsheathed case, but with sheathing only on one side still allow flexural-torsional buckling to form. The behavior of the sheathed specimens is sensitive to testing details. The sheathing must be isolated from the loading platen, and thus avoid direct bearing, or artificially high composite action (as much as 20% increase in peak strength) is observed. Observed capacities are greatly in excess of current prediction methods, demonstrating the need for improvements in design.

Twelve full-scale tests of cold-formed steel stud walls with different sheathing configurations were performed in a new testing rig. The tests demonstrated the significant strength gains that may be achieved due to the presence of sheathing. Sheathing identical on both sides of the wall, either OSB or gypsum, are shown to beneficially change the limit state from global to local buckling and have stable post-buckling and post-peak response. However, the OSB sheathed walls do carry 12% higher load than the gypsum sheathed walls, indicating that even though direct bearing is not allowed in the tests partial composite action even in the axial direction does occur. Walls with dissimilar sheathing on the two sides may exhibit other, less desirable, behavior. At the extreme, dramatic flexural-torsional failure mode is observed with OSB sheathing on one side of the wall only, which has little post-peak reserve, and high imperfection sensitivity. The wall stud tests as well as the single column tests reinforce the necessity of a new design method.

Local and distortional buckling modes are modestly affected by the presence of the springs that simulate the sheathing, but global buckling is highly influenced by sheathing

restraint. Therefore, the spring stiffness must be carefully handled since it may drastically change the global buckling load. Although numerical solutions such as the Finite Strip Method (FSM), implemented in CUFSM v4.03 [1] are preferable, analytical solutions for the stability of sheathing braced studs are also possible. The Direct Strength Method (DSM) proved to be an effective design method for sheathed cold-formed steel wall-studs, but special attention must be given to the determination of the elastic buckling loads.

Finite element (FE) collapse models of sheathing braced studs agree reasonably well with tests, and may take into account the sheathing either explicitly or as a spring in series with local fastener springs. Fastener demands in sheathing braced studs may be predicted from FE collapse models. The highest demands are observed near local buckling deformations – although this is not a primary concern since local buckling strength predictions do not account for the fasteners. Redistribution of fastener demands within a wall is possible, and it has been observed. Demands on the rotational springs are small compared to their resistance. However, the translational springs, especially k_z, have demands near its maximum capacity in models of the wall-stud at collapse. The k_x springs, which are directly responsible for restricting global buckling, see high demands at the stud ends, where it is in fact undergoing local buckling.

The analytical solution for global buckling of sheathing braced studs can be reliably extended to predict fastener force demands due to global modes. Predicted fastener demands may be useful in connection design; however, all tested studs with sheathing on both sides failed in local, not global or distortional, buckling.

8.2. PROPOSED FUTURE WORK

Walls are subjected to other kinds of load, such as in-plane and out-of-plane bending, shear, and even twist. All the possible loads and interactions need to be explored. The FE models are a powerful tool to understand sheathed cold-formed steel walls, and they could be used to solve problems such as the role of bracing straps in stud bracing and the possible interaction of the walls with other structural components. The analytical model developed to find local-lateral stiffness ($k_{x\ell}$) does not take into account the contribution of the sheathing to $k_{x\ell}$; perhaps a strut-and-tie model as used in concrete structures would solve the problem. The reliability study carried out in this dissertation explores only the stiffness of the spring and the possibility of a defective fastener. Based on the new design method proposed in Chapter 7, it would be important to work on a reliability study that takes into account the most important variables and thus to propose a new resistance factor for the design of sheathed wall studs. The connection was explored under several adverse conditions, but it remains to be seen how the connection between stud and sheathing would behave under fire conditions. If there is a fire, the heat will affect the sheathing while the sprinklers may wet it, and such a situation may result in an ineffective bracing system. It is worth mentioning that in Chapter 3 we showed that gypsum sheathing behaves very poorly when saturated with water. The prediction of fastener demands is still an issue that needs more research. In Chapter 6, fastener demands are explored, but there is no simple solution to determine them. It seems possible that, given the eigenvector from CUFSM, the amplified initial imperfection can be used to obtain the displacement shape and so the fastener demand. A table with the

nominal load for different studs, boards and fasteners would be very useful for design engineers.

REFERENCE CHAPTER 8

1. Li, Z. and B.W. Schafer. *Buckling analysis of cold-formed steel members with general boundary conditions using CUFSM: conventional and constrained finite strip methods*. in *Twentieth International Specialty Conference on Cold-Formed Steel Structures*. 2010. Saint Louis, Missouri, USA.

Appendix A

In-plane Lateral Stiffness Test ($k_{x\ell}$)

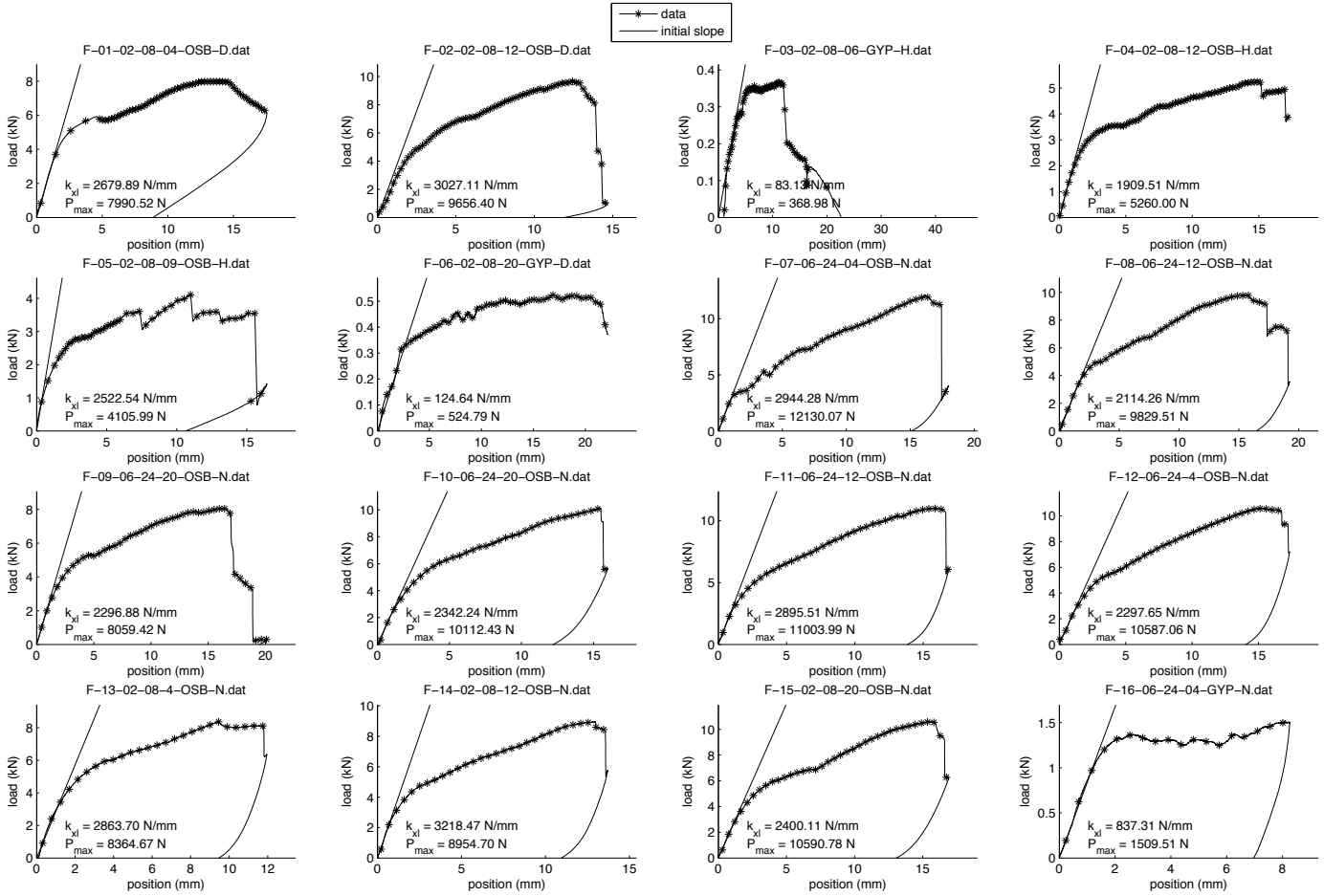

Figure A.1 – P-Δ curve of in-plane lateral stiffness tests of specimen 1 to 16

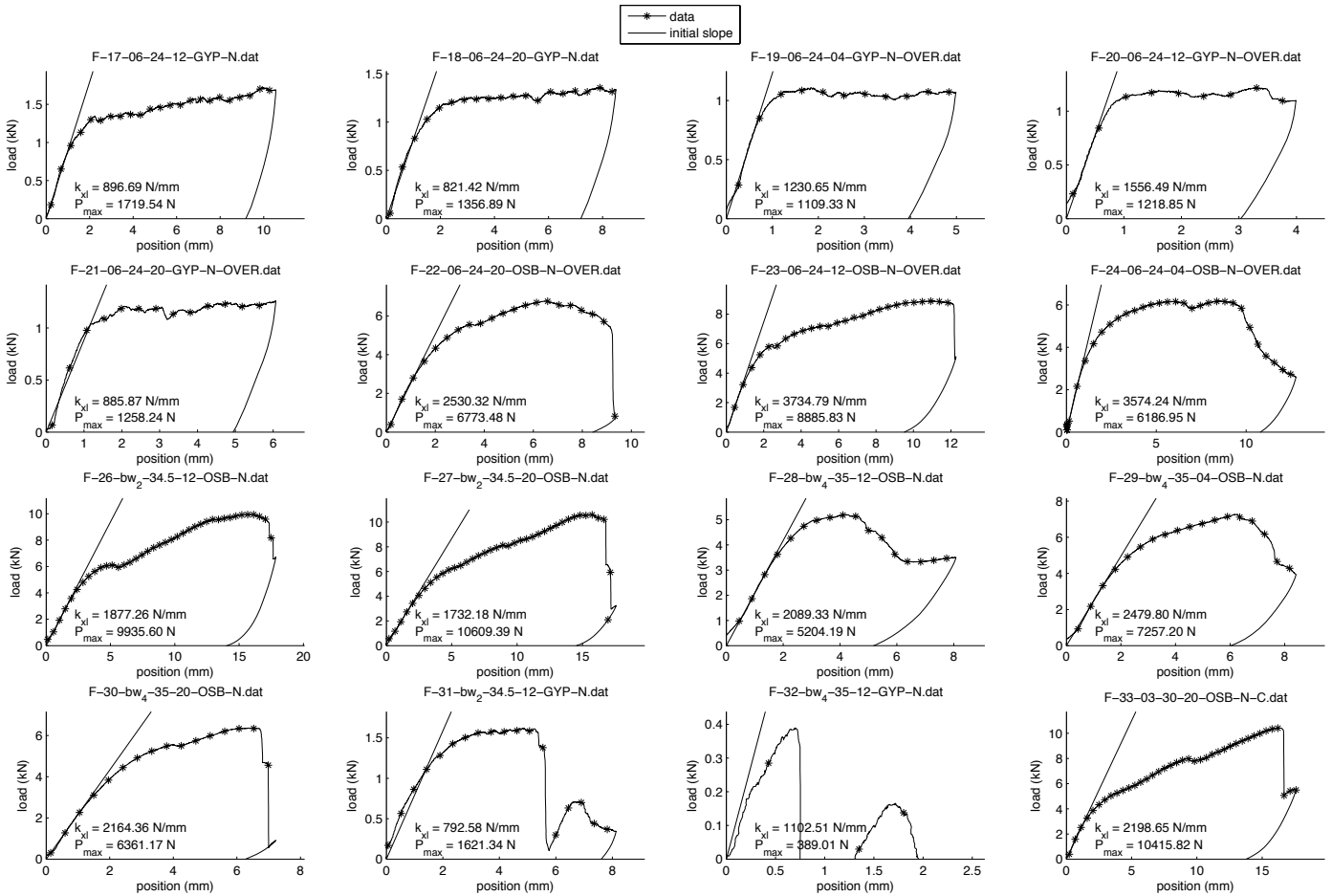

Figure A.2 – P-Δ curve of in-plane lateral stiffness tests of specimen 17 to 33, except 25

Table A.1 – Summary of all tests dimensions and results. (The results in the table are the test results, in order to find the per screw results, the load (P) has to be divided by 4, while the stiffness (k) has to be divided by 2, see item 3.4.2 for more details)

Filename	Test #	e (mm)	w (mm)	s (mm)	sheathing	Hum	over	$k_{x\ell}$ (N/mm)	k 40%P (N/mm)	δ @ P_{max} (mm)	P_{max} (N)	Failure mode
F-01-02-08-04-OSB-D.dat	1	50.8	203.2	101.6	OSB	D		2680	2173	13.14	7991	screw shear
F-02-02-08-12-OSB-D.dat	2	50.8	203.2	304.8	OSB	D		3027	1751	12.50	9656	screw shear
F-03-02-08-06-GYP-H.dat	3	50.8	203.2	152.4	GYP	H		83	95	10.55	369	tear out
F-04-02-08-12-OSB-H.dat	4	50.8	203.2	304.8	OSB	H		1910	1247	14.92	5260	screw shear
F-05-02-08-09-OSB-H.dat	5	50.8	203.2	228.6	OSB	H		2523	1078	10.99	4106	screw shear
F-06-02-08-20-GYP-D.dat	6	50.8	203.2	508.0	GYP	D		125	167	16.79	525	tear out
F-07-06-24-04-OSB-N.dat	7	152.4	609.6	101.6	OSB	N		2944	1495	16.14	12130	screw shear
F-08-06-24-12-OSB-N.dat	8	152.4	609.6	304.8	OSB	N		2114	1351	15.61	9830	screw shear
F-09-06-24-20-OSB-N.dat	9	152.4	609.6	508.0	OSB	N		2297	1368	16.16	8059	tilting
F-10-06-24-20-OSB-N.dat	10	152.4	609.6	508.0	OSB	N		2342	1350	15.50	10112	screw shear
F-11-06-24-12-OSB-N.dat	11	152.4	609.6	304.8	OSB	N		2896	1231	15.65	11004	screw shear
F-12-06-24-4-OSB-N.dat	12	152.4	609.6	101.6	OSB	N		2298	1290	15.26	10587	screw shear
F-13-02-08-4-OSB-N.dat	13	50.8	203.2	101.6	OSB	N		2864	1993	9.44	8365	screw shear
F-14-02-08-12-OSB-N.dat	14	50.8	203.2	304.8	OSB	N		3218	1488	12.94	8955	screw shear
F-15-02-08-20-OSB-N.dat	15	50.8	203.2	508.0	OSB	N		2400	1381	15.56	10591	screw shear
F-16-06-24-04-GYP-N.dat	16	152.4	609.6	101.6	GYP	N		837	917	8.12	1510	tear out
F-17-06-24-12-GYP-N.dat	17	152.4	609.6	304.8	GYP	N		897	857	9.96	1720	tear out
F-18-06-24-20-GYP-N.dat	18	152.4	609.6	508.0	GYP	N		821	817	7.94	1357	tear out
F-19-06-24-04-GYP-N-OVER.dat	19	152.4	609.6	101.6	GYP	N	OVER	1231	1462	1.84	1109	tear out
F-20-06-24-12-GYP-N-OVER.dat	20	152.4	609.6	304.8	GYP	N	OVER	1556	1561	3.31	1219	tear out
F-21-06-24-20-GYP-N-OVER.dat	21	152.4	609.6	508.0	GYP	N	OVER	886	1146	6.05	1258	tear out
F-22-06-24-20-OSB-N-OVER.dat	22	152.4	609.6	508.0	OSB	N	OVER	2530	2171	6.48	6773	screw shear
F-23-06-24-12-OSB-N-OVER.dat	23	152.4	609.6	304.8	OSB	N	OVER	3735	2694	11.09	8886	screw shear
F-24-06-24-04-OSB-N-OVER.dat	24	152.4	609.6	101.6	OSB	N	OVER	3574	2953	8.53	6187	screw shear
F-25-bw_2-34.5-04-OSB-N.dat	25	20.6	873.3	101.6	OSB	N		-	-	-	-	screw shear
F-26-bw_2-34.5-12-OSB-N.dat	26	20.6	873.3	304.8	OSB	N		1877	1451	15.83	9936	screw shear
F-27-bw_2-34.5-20-OSB-N.dat	27	20.6	873.3	508.0	OSB	N		1732	1291	15.60	10609	screw shear
F-28-bw_4-35-12-OSB-N.dat	28	10.4	893.8	304.8	OSB	N		2089	2190	4.22	5204	tear out
F-29-bw_4-35-04-OSB-N.dat	29	10.4	893.8	101.6	OSB	N		2480	2435	6.20	7257	tear out
F-30-bw_4-35-20-OSB-N.dat	30	10.4	893.8	508.0	OSB	N		2164	1914	6.44	6361	tear out
F-31-bw_2-34.5-12-GYP-N.dat	31	20.6	873.3	304.8	GYP	N		793	717	4.85	1621	tear out
F-32-bw_4-35-12-GYP-N.dat	32	10.4	893.8	304.8	GYP	N		1102	871	0.70	389	tear out
F-33-03-30-20-OSB-N-C.dat	33	76.2	762.0	508.0	OSB	N	C	2199	1002	16.29	10416	screw shear

Appendix B

In-plane Lateral Stiffness Test ($k_{x\ell}$) of American and Canadian Plywood Sheathing

B.1. INTRODUCTION

Fifteen tests were conducted comparing local stiffness ($k_{x\ell}$) of Canadian and American plywood, it is worth mentioning that the tests reported in the body of the dissertation only include OSB and gypsum sheathing.

The test setup is the same as used in Chapter 3 with dimensions equal to: fastener spacing (s=12in.), stud spacing (w=24in.) and edge distance (e=6in.). The plywood sheathings were kept in an environmental chamber for at least seven days before the test at a temperature of 20C and 65% humidity. The only variable is the type of plywood sheathing. Three kinds of sheathing were used, one original from USA and other two original from Canada.

The sheathing used to represent USA is the Structural 1 sheathing (4-ply) with DF-L outer plywood, thickness=15/32'', acquired by Simpson Strong-Tie in Southern California. The sheathings original from Canada were manufactured by Alberta Plywood Ltd., the Canadian sheathings were named as CSP and DFP. The Canadian Softwood Plywood (CSP) has thickness of ½'', it is from Mill AB244, and it uses Spruce for all its plies. The Douglas Fir Plywood (DFP), thickness of ½'', was acquired from Quebec City.

The steel studs used in tests are the 362S162-43 (SSMA Catalog) supplied by Dietrich Metal Framing.

The fasteners used were number 8 fasteners, supplied by Simpson Strong-Tie. The specifications provided by Simpson Strong-Tie are: #8 PPSD11516S, wood-to-steel fastener. The fastener has #2 drill point "to penetrate steel without the plywood 'riding-up' the threads", the maximum steel thickness can be of 54 mils, it consists of #3 Square drive - BIT3S, with yellow zinc dichromate coating, 0.315" head diameter, and 18 threads per inch, length = 1 15/16".

In other to identify any out-of-plane movement of the sheathing two position transducers were placed at the middle of the sheathing, Figure B.1.

a) Front view

b) Lateral view

Figure B.1 – Test Assembly

The tests were named following the rule: (i) first spot has the test number from one to fifteen, (ii) second spot shows the country where the sheathing was made, (iii) the number written on the sheathing at their arrival, 1 means CSP and 2 means DFP, and (iv)

if the sheathing is considered CSP or DFP, spot number (iv) is a mere repetition of number (iii) but it was helpful during the tests. Also, number (iii) and (iv) are information only necessary for the Canadian plywood.

B.2. RESULTS AND DISCUSSION

Table B.1 summarizes the test results and Figure B.3 shows all the load displacement curves. The CAN-DFP and the USA sheathings have similar values for the local stiffness ($k_{x\ell}$) and for the maximum load (P_{max}) of only 4 to 5% difference, the displacement at maximum load (δ @ P_{max}) presented a difference of 10%, meaning that the CAN-DFP sheathing is more flexible than the American sheathing. The CAN-CSP sheathing presented the lowest mean value of local stiffness and maximum load, but the highest mean value for the displacement at maximum load, which means that the sheathing is the weakest and the most flexible of all plywood sheathings tested.

Table B.1 – Summary of test results. Values per fastener (values of initial stiffness were divided by two and values of maximum load were divided by four as explained in Chapter 3).

Specimen	$k_{x\ell}$ test result (N/mm)	$k_{x\ell}$ mean (N/mm)	$k_{x\ell}$ CoV	P_{max} test result (N)	P_{max} mean (N)	P_{max} CoV	δ @ P_{max} test result (mm)	δ @ P_{max} mean (mm)	δ @ P_{max} CoV
1-CAN-2-DFP	1176			2497			17.5		
2-CAN-2-DFP	1044			2325			15.2		
3-CAN-2-DFP	1210	1053	0.14	2640	2516	0.06	15.7	15.6	0.08
4-CAN-2-DFP	830			2440			15.4		
5-CAN-2-DFP	1004			2678			14.1		
6-CAN-1-CSP	622			1820			16.4		
7-CAN-1-CSP	660			2087			15.9		
8-CAN-1-CSP	679	704	0.13	1944	1914	0.06	17.7	16.8	0.04
9-CAN-1-CSP	854			1906			17.3		
10-CAN-1-CSP	708			1811			16.6		
11-USA	1143			2240			14.1		
12-USA	1007			2430			14.1		
13-USA	994	1012	0.08	2525	2396	0.06	13.4	13.9	0.07
14-USA	1014			2516			15.3		
15-USA	904			2268			12.7		

a) Screws bending under load

b) Screw sheared

c) Screw bended

b) Screw sheared

c) Board torn by the screw

Figure B.2 – Typical failure mechanism

In every test the failure mechanism was shear of the fastener. Figure B.2 shows how the failure mechanism develops, first the fastener starts to bend and then it shears Figure B.2(c) shows a fastener bended, Figure B.2(d) shows a fastener that failed in shear. The damage in the plywood due to the force applied by the fastener is showed in Figure B.2(c).

Figure B.1 shows the location of the position transducers placed to measure the out-of-plane displacement of the board. The out-of-plane displacement shows the amount of moment that is being applied on the sheathing by the fastener. As showed in Figure 3.2 of Chapter 3 the fastener bends and tilts while the stud flange is pulled, this mechanism applies a moment on the connection. Our concern was that this moment would be of such intensity that the local stiffness (k_{x_ℓ}) would have a significant contribution of the rotation stiffness. Fortunately that is not true, k_{x_ℓ} is measured at the beginning of the load-displacement curve while the out-of-plane displacement are not representative.

It's worth to mention that the results in this Appendix should be carefully compared to the results in Chapter 3, the direct comparison may mislead the reader to conclude that the plywood tested is less stiff than the OSB tested, but the studs are also different. The studs used in the tests presented in this appendix are thinner (43 gauge) while the stud used in the tests reported in Chapter 3 are 68 gauge.

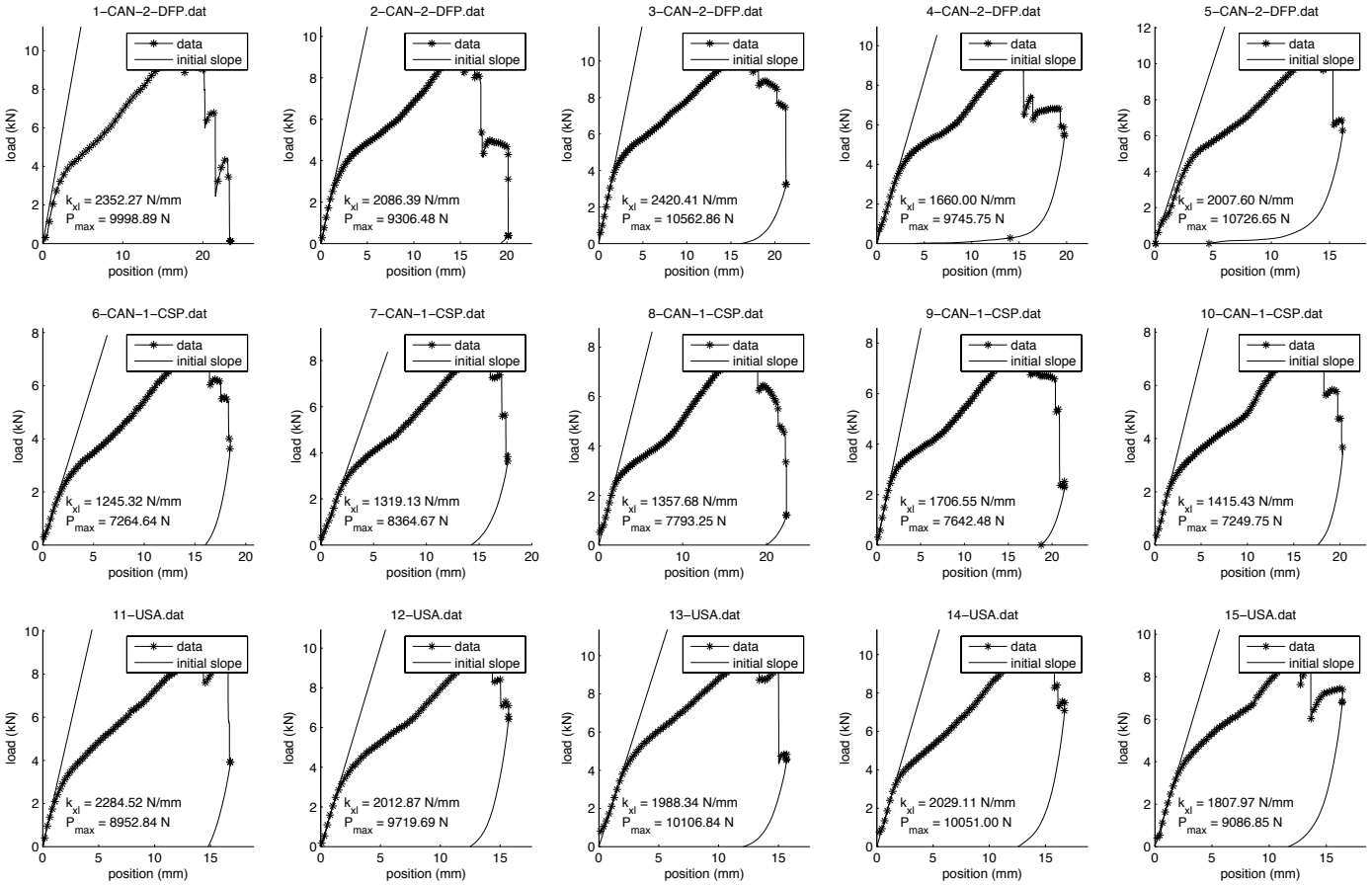

Figure B.3 – P-Δ curve and initial slope for all tests

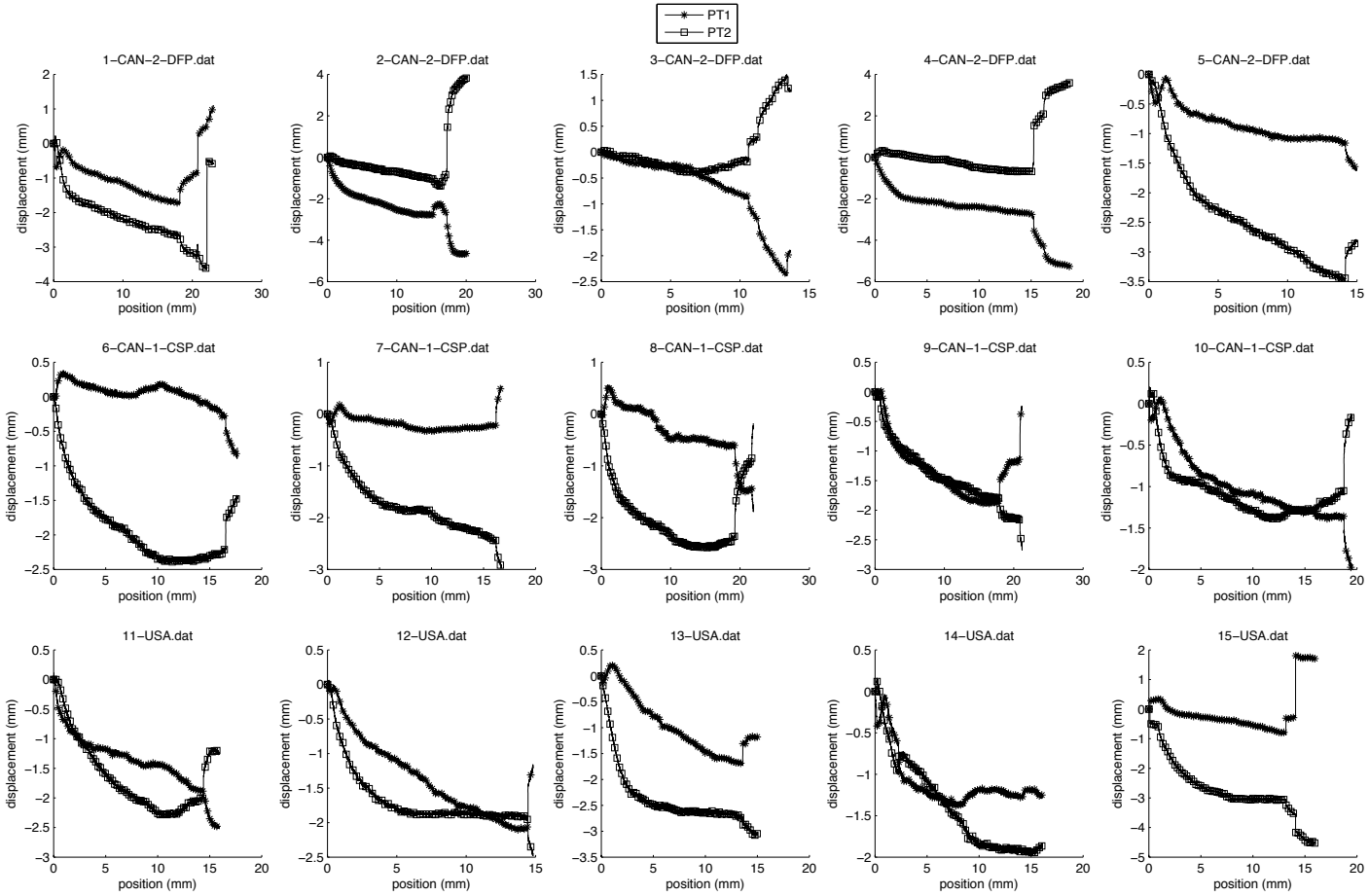

Figure B.4 – Lateral displacement, position transducers 1 and 2

Appendix C

Coupon Tests

Table C.1 – Coupon Tests: Measurements and Results

Member	Specimen	$t_{coated\text{-}average}$ (mm)	t_{bare} (mm)				b_{bare} (mm)				$f_{y\ (0.2\%\ offset)}$ (MPa)	$f_{y\ (autographic\ method)}$ (MPa)	f_u (MPa)	Δ_u (mm/mm)
			t_1	t_2	t_3	$t_{average}$	b_1	b_2	b_3	$b_{average}$				
Stud	1S4L	1.715	1.664	1.664	1.676	1.668	12.370	12.370	12.370	12.370	385.4	395.8	547.3	0.17
	2S4L	1.715	1.651	1.664	1.664	1.659	12.357	12.383	12.370	12.370	377.2	386.8	535.0	0.18
	3S4L	1.715	1.664	1.664	1.676	1.668	12.370	12.383	12.370	12.374	383.4	393.7	544.2	0.16
	1S6L	1.715	1.664	1.676	1.664	1.668	12.370	12.370	12.383	12.374	378.5	386.8	537.7	0.16
	2S6L	1.715	1.676	1.664	1.664	1.668	12.383	12.370	12.624	12.459	381.3	388.9	543.2	0.20
	6S6L*	1.715	1.664	1.664	1.664	1.664	12.370	12.370	12.357	12.366	381.3	386.1	546.2	0.24
	7S6L*	1.715	1.664	1.664	1.664	1.664	12.370	12.383	12.370	12.374	388.9	390.9	549.5	0.24
	61S8L	1.715	1.664	1.664	1.664	1.664	12.370	12.383	12.357	12.370	387.5	393.0	548.0	0.21
mean		1.715	1.664	1.665	1.667	1.665	12.370	12.376	12.400	12.382	382.9	390.3	543.9	0.19
CoV		-	0.000	0.016	0.015	0.003	0.003	0.985	0.586	0.004	0.011	0.009	0.009	0.163
Track	1T-1S8L*	2.032	1.981	1.981	1.956	1.973	12.370	12.383	12.395	12.383	487.5	472.3	535.3	0.24
	1T-2S8L*	2.032	1.969	1.981	1.981	1.977	12.370	12.370	12.395	12.378	487.5	480.6	540.5	0.24
mean		2.032	1.975	1.981	1.969	1.975	12.370	12.376	12.395	12.380	487.5	476.4	537.9	0.24
CoV		-	0.000	0.017	0.014	0.005	0.005	0.987	0.603	0.001	0.000	0.012	0.007	0.001

* Specimen that failed inside the gauge length (length covered by extensometer)

Δ_u (mm/mm) - the big value of CoV for Δ_u is due to the position of the extensometer compared to where it fails. If the crack is in the gauge length, Δ_u is bigger than if it is outside the gauge length.

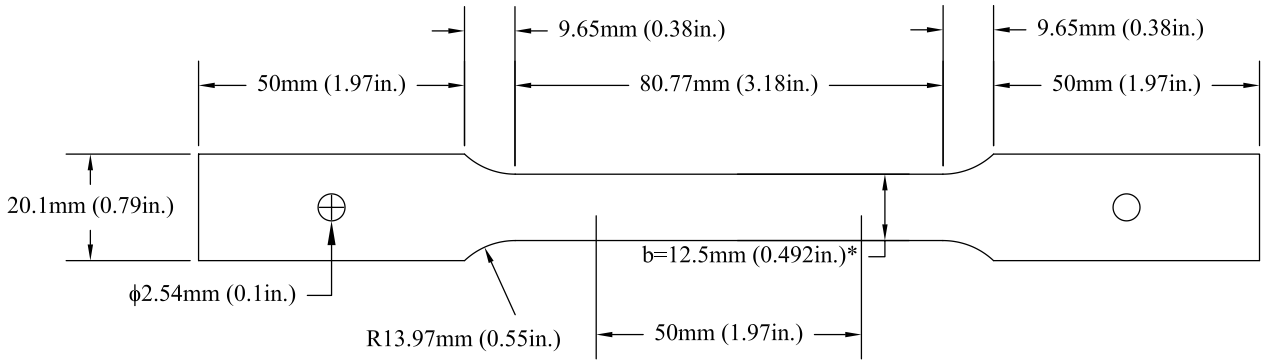

Figure C.1 – Tensile coupon dimensions. In order to machine the specimens the steel sheet is connected to a CNC machine; the holes in the specimen are due to the two bolts that connect the sheet to the machine. *b measurements are in Table C.1.

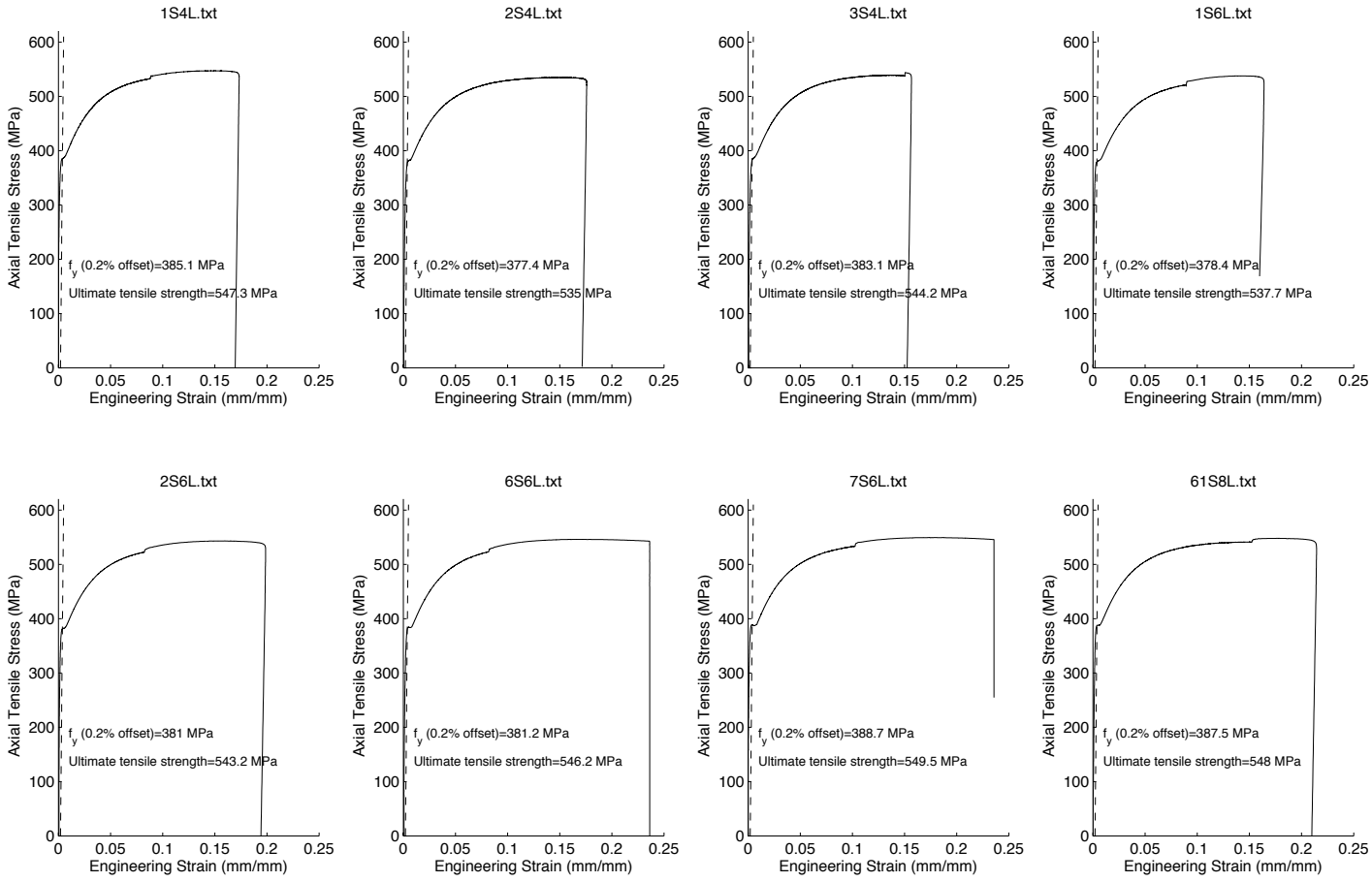

Figure C.2 – Stress-strain curves for studs (0.2% offset method)

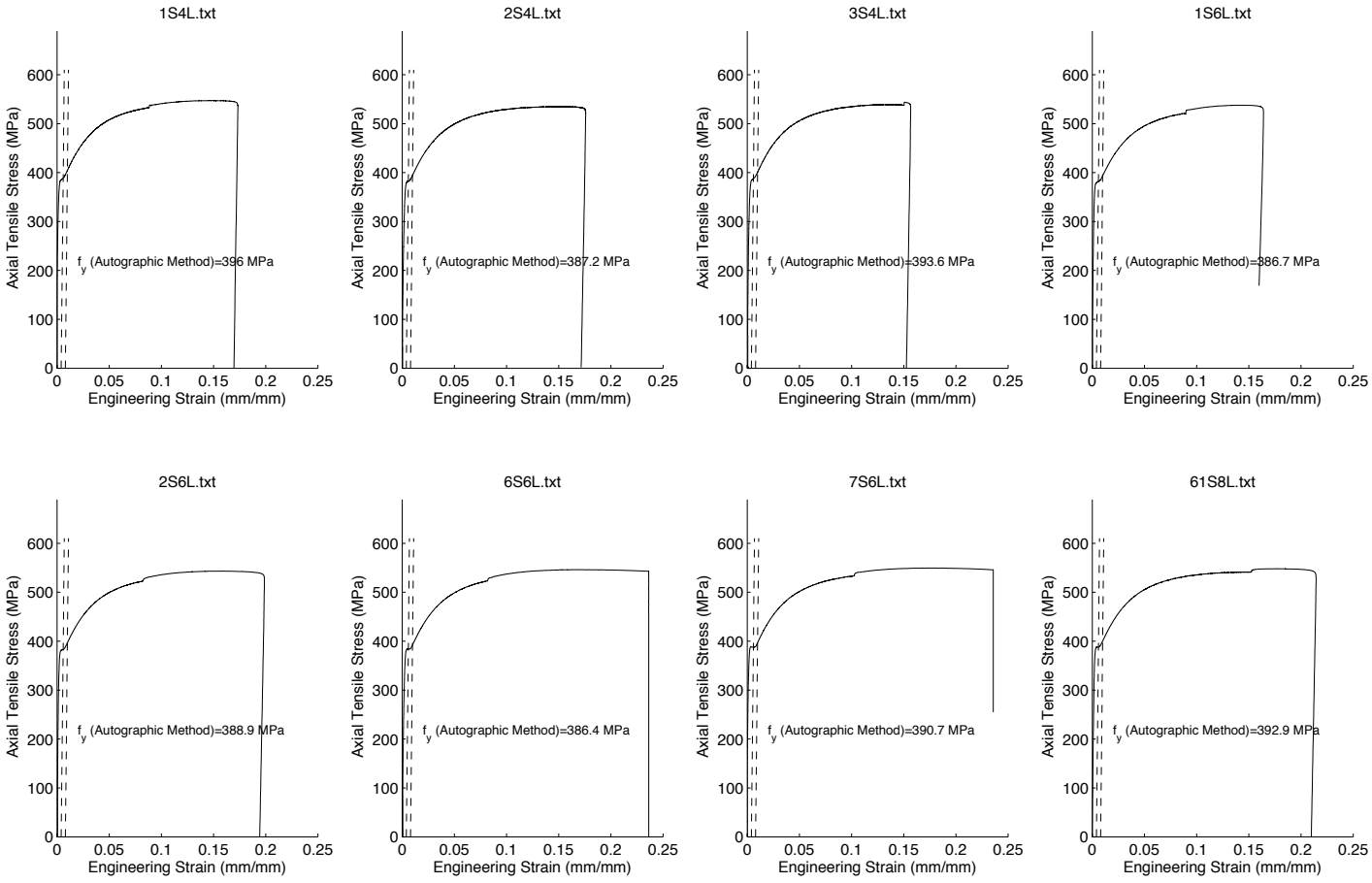

Figure C.3 – Stress-strain curves for studs (autographic method)

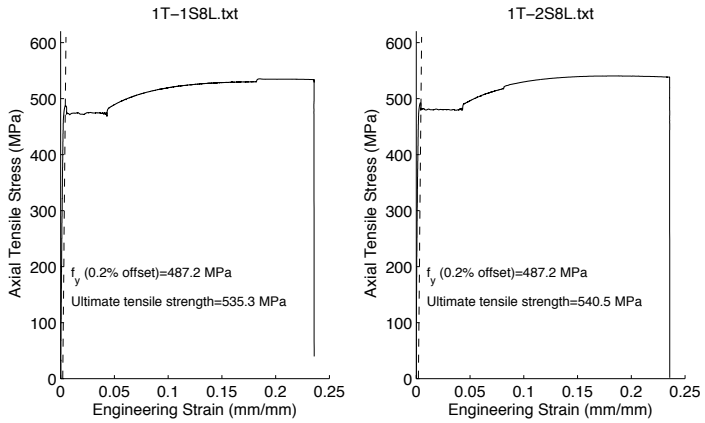

Figure C.4 – Stress-strain curves for tracks (0.2% offset method)

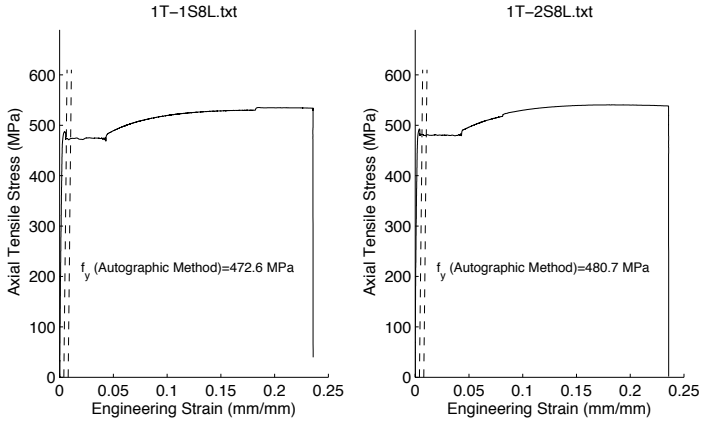

Figure C.5 – Stress-strain curves for tracks (autographic method)

Appendix D

Column Tests

Table D.1 – Extended version of Table 4.1 - Out-to-out cross-section measurement – Stud

Specimen	H (mm)	B_B (mm)	B_A (mm)	D_B (mm)	D_A (mm)	t[1] (mm)	r_{hbB} (mm)	r_{dbB} (mm)	r_{hbA} (mm)	r_{dbA} (mm)	θ_{hbB} (deg)	θ_{dbB} (deg)	θ_{hbA} (deg)	θ_{dbA} (deg)
1S2L	95.072	41.123	41.478	13.140	12.628	1.864	0.172	0.172	0.172	0.172	89.2	87.7	88.9	89.1
2S2L	93.053	41.830	41.842	12.865	12.848	1.852	0.172	0.172	0.172	0.172	89.3	88.4	88.8	89.6
3S2L	93.654	42.316	41.974	12.941	12.891	1.823	0.172	0.172	0.172	0.172	89.8	88.5	89.7	89.3
4S2L	93.552	42.401	42.249	13.056	13.060	1.832	0.172	0.172	0.172	0.172	89.3	89.2	89.8	89.2
5S2L	93.442	42.198	42.029	12.979	12.874	1.829	0.172	0.172	0.172	0.172	89.4	89.1	88.9	89.6
6S2L	93.315	42.316	42.071	12.967	12.941	1.856	0.172	0.172	0.172	0.172	89.6	89.6	89.1	89.2
1S4L	93.595	42.164	41.580	12.946	12.954	1.913	0.172	0.172	0.172	0.172	89.5	89.3	86.6	89.7
2S4L	93.061	41.436	41.254	12.806	12.950	1.840	0.172	0.172	0.172	0.172	88.3	89.6	89.0	88.0
3S4L	93.222	41.931	42.101	12.946	13.081	1.847	0.172	0.172	0.172	0.172	89.3	89.3	88.5	87.5
4S4L	93.663	42.350	42.122	13.001	12.912	1.828	0.172	0.172	0.172	0.172	89.8	86.5	89.2	88.5
5S4L	93.345	42.350	42.431	12.920	12.971	1.837	0.172	0.172	0.172	0.172	89.3	89.7	89.7	86.4
6S4L	93.370	42.380	42.219	13.018	12.878	1.836	0.172	0.172	0.172	0.172	89.7	89.4	89.0	89.4
1S6L	94.010	41.876	42.202	12.827	12.742	1.843	0.172	0.172	0.172	0.172	89.1	89.3	89.5	88.8
2S6L	94.094	42.126	42.189	12.912	12.861	1.819	0.172	0.172	0.172	0.172	89.8	89.6	89.9	89.6
3S6L	93.349	42.308	42.168	12.827	12.996	1.815	0.172	0.172	0.172	0.172	89.5	89.7	89.8	89.7
4S6L	93.379	41.923	41.791	12.912	12.967	1.811	0.172	0.172	0.172	0.172	89.0	89.6	89.1	88.8
5S6L	94.539	41.652	42.050	13.089	12.772	1.922	0.172	0.172	0.172	0.172	89.4	89.1	89.9	89.7
6S6L	93.561	42.164	41.474	12.755	12.789	1.961	0.172	0.172	0.172	0.172	88.7	88.5	89.6	89.5
7S6L	93.155	42.219	42.084	12.958	13.208	1.848	0.172	0.172	0.172	0.172	89.1	89.4	89.1	88.8
61S8L	93.510	42.287	41.978	13.005	12.893	1.876	0.172	0.172	0.172	0.172	88.3	88.9	89.8	89.9
62S8L	93.671	42.321	42.079	12.903	12.903	1.873	0.172	0.172	0.172	0.172	89.0	88.9	89.0	88.4
63S8L	93.438	42.003	42.172	13.428	12.996	1.900	0.172	0.172	0.172	0.172	88.6	89.0	89.0	88.6
64S8L	93.307	42.126	41.974	13.123	13.233	1.922	0.172	0.172	0.172	0.172	88.9	89.1	88.7	88.6
65S8L	93.489	42.228	42.109	13.233	13.115	1.902	0.172	0.172	0.172	0.172	88.5	88.9	87.8	87.9
Average[2]	93.577	42.084	41.984	12.982	12.936	1.860	0.172	0.172	0.172	0.172	89.2	89.0	89.1	88.9
CoV	0.008	0.009	0.007	0.014	0.014	0.033	-	-	-	-	0.007	0.009	0.010	0.011

(1) Thickness with coating

(2) Each stud was measured at three positions along the length (both ends and the middle) only the average of each variable to each stud is shown.

Table D.2 – Extended version of Table 4.2 - Average global, local and distortional imperfections

Specimen	L (m)	d_Φ (deg)	d_b (L/bow)	d_c (L/camber)	d_1/t	d_2/t
1S2L	0.61	0.4665	2527.4	1576.8	0.1535	0.9258
2S2L	0.61	0.5222	896.8	515.1	0.3384	0.1312
3S2L	0.61	0.5061	871.5	565.6	0.393	0.9794
4S2L	0.61	0.1046	1213.2	2892.4	0.3106	0.8929
5S2L	0.61	0.2902	1049.8	547.3	0.296	0.922
6S2L	0.61	0.3589	1168.3	542.9	0.4986	0.749
1S4L	1.22	0.5222	1793.7	1030.2	0.3384	0.1312
2S4L	1.22	0.6805	2531.4	917.5	0.1964	0.2254
3S4L	1.22	0.6307	2415.2	696.9	0.2188	0.3884
4S4L	1.22	0.2626	2323.8	1127.8	0.3498	0.1733
5S4L	1.22	0.6713	2581.9	657.3	0.2509	0.3575
6S4L	1.22	0.3878	1977.1	1105.6	0.4139	0.1392
1S6L	1.83	0.6189	4378.7	2646.6	0.1826	0.0563
2S6L	1.83	0.4806	2014.6	1236.4	0.3984	0.1158
3S6L	1.83	0.6889	2959.6	2714.6	0.2811	0.1673
4S6L	1.83	0.6421	3359.5	3690.6	0.216	0.2731
5S6L	1.83	0.6649	5353.1	1010	0.1856	0.2888
6S6L	1.83	0.5575	2944.2	1077.7	0.2359	0.1332
7S6L	1.83	0.4164	2996.4	2186.9	0.3508	0.1951
61S8L	2.44	0.6778	3392.3	1897	0.3474	0.2577
62S8L	2.44	0.7202	2266.7	1804.1	0.3643	0.328
63S8L	2.44	0.5157	3725.4	1676.7	0.3408	0.2865
64S8L	2.44	0.8219	2203.4	1184.5	0.341	0.1306
65S8L	2.44	0.7868	2607.5	1418.6	0.2817	0.1957
Total Average		0.547	2456.7	1426.5	0.306	0.354
CoV		0.323	0.439	0.589	0.282	0.846

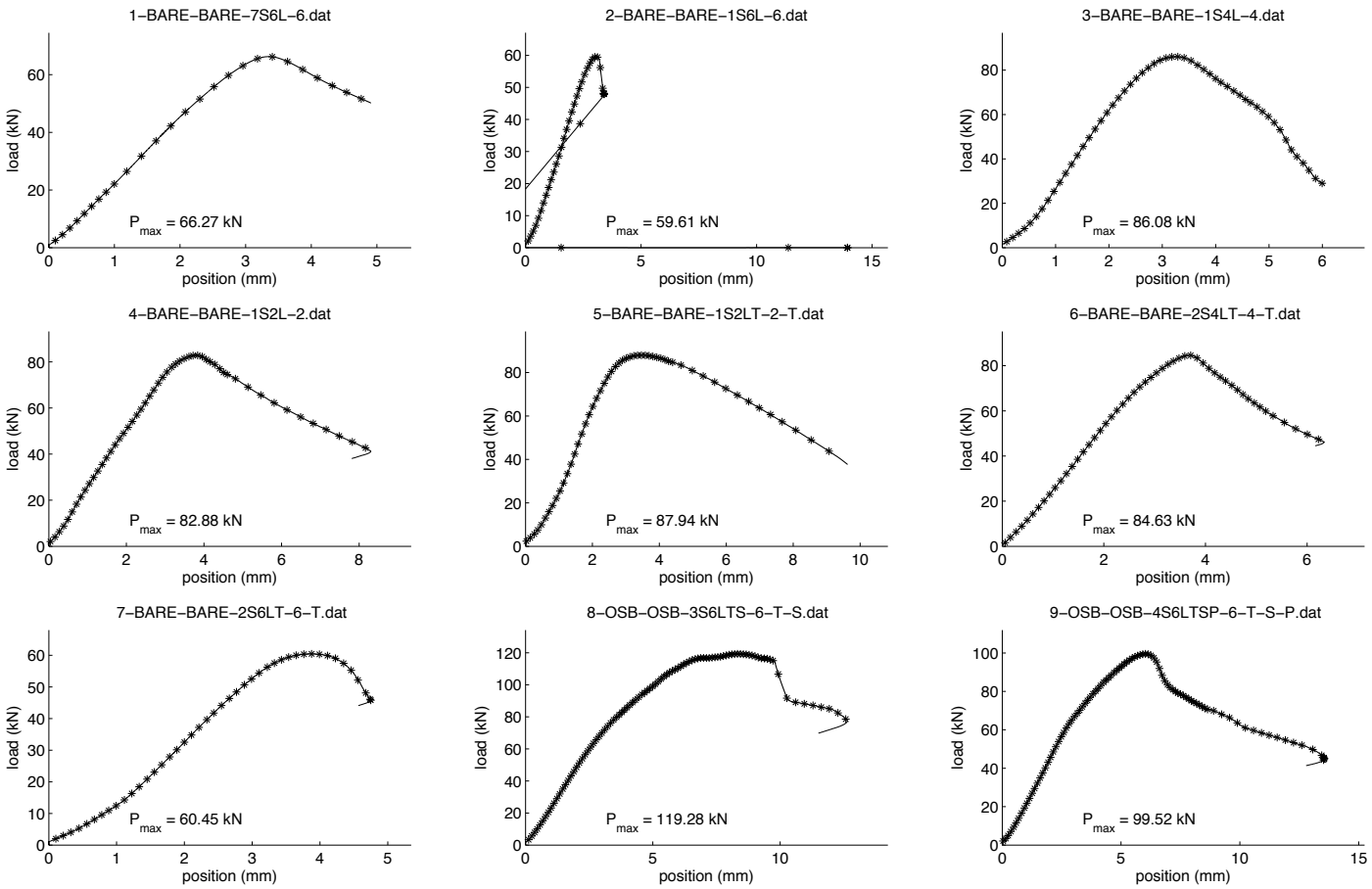

Figure D.1 – P-Δ curve for column tests. Tests 1 to 9

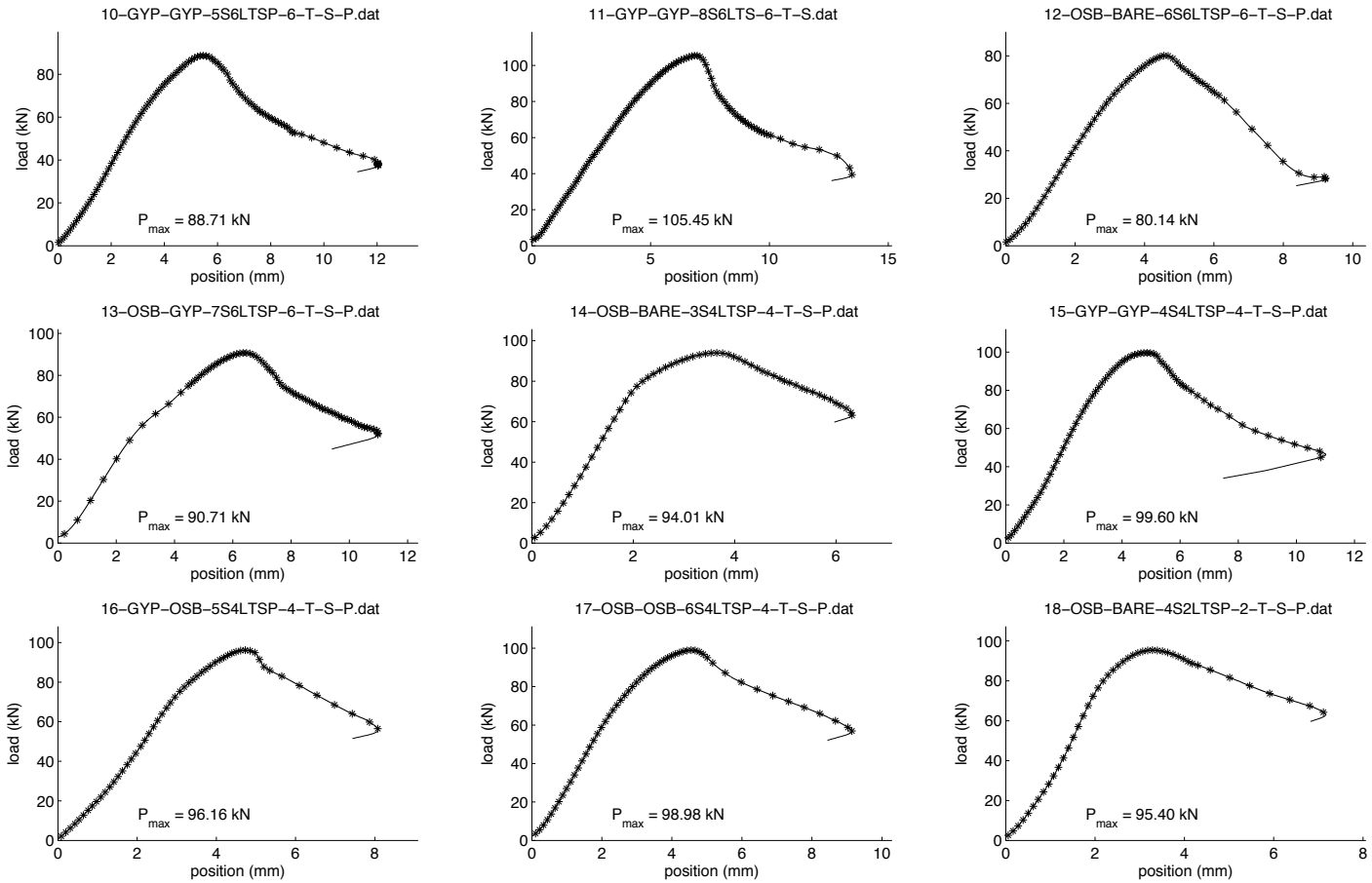

Figure D.2 – P-Δ curve for column tests. Tests 10 to 18

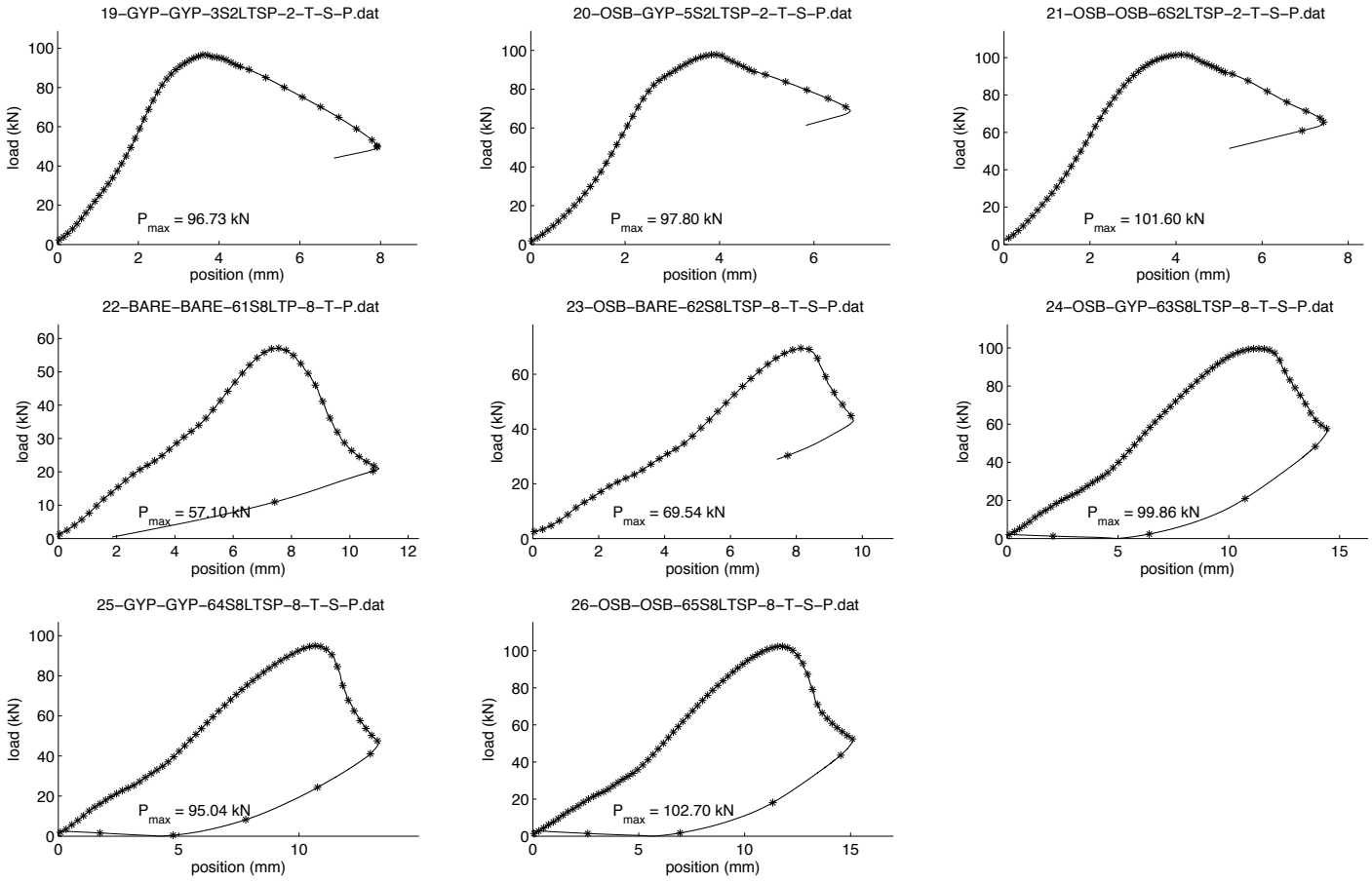

Figure D.3 – P-Δ curve for column tests. Tests 19 to 26

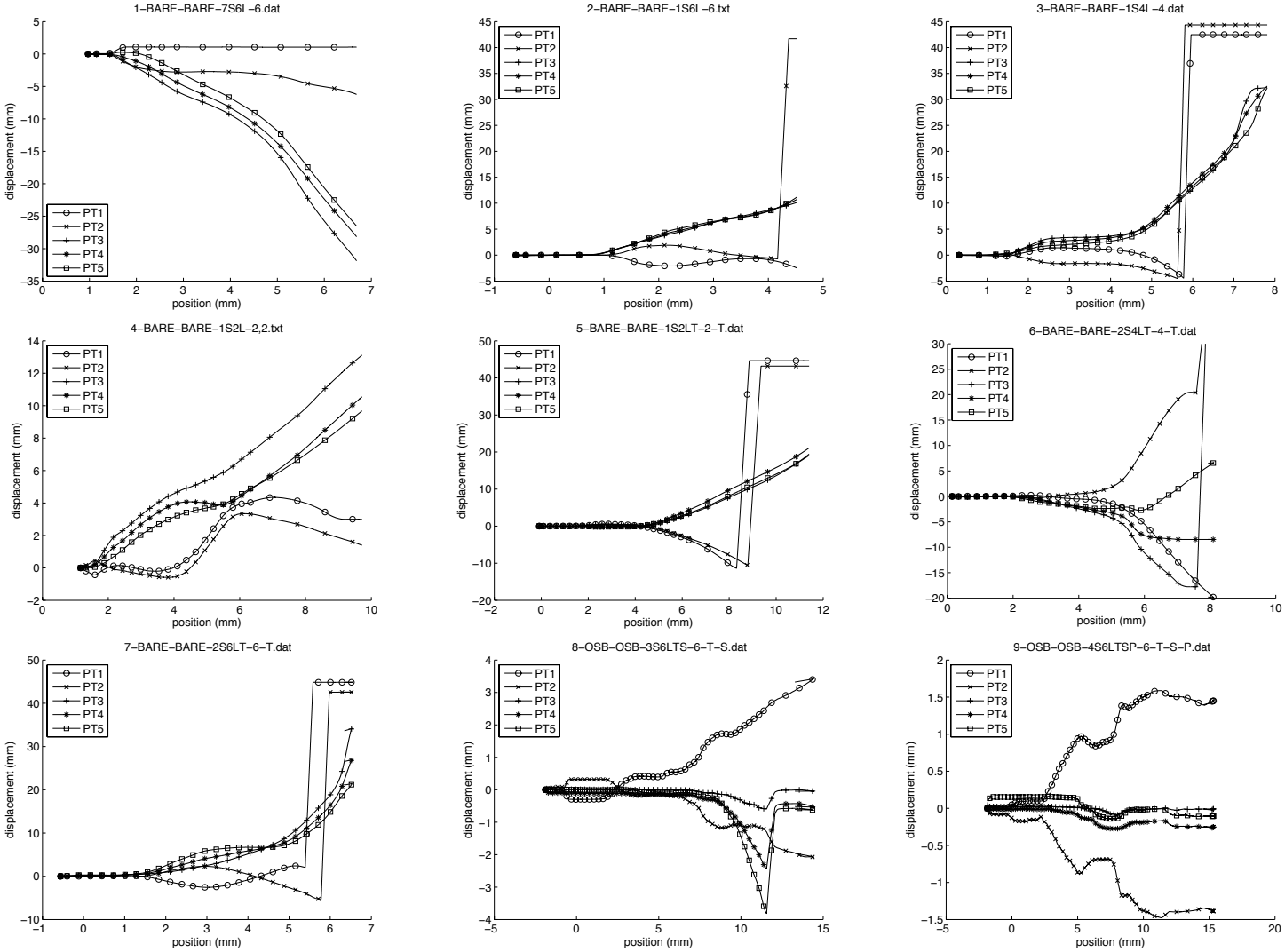

Figure D.4 – Position transducers plots. Tests 1 to 9

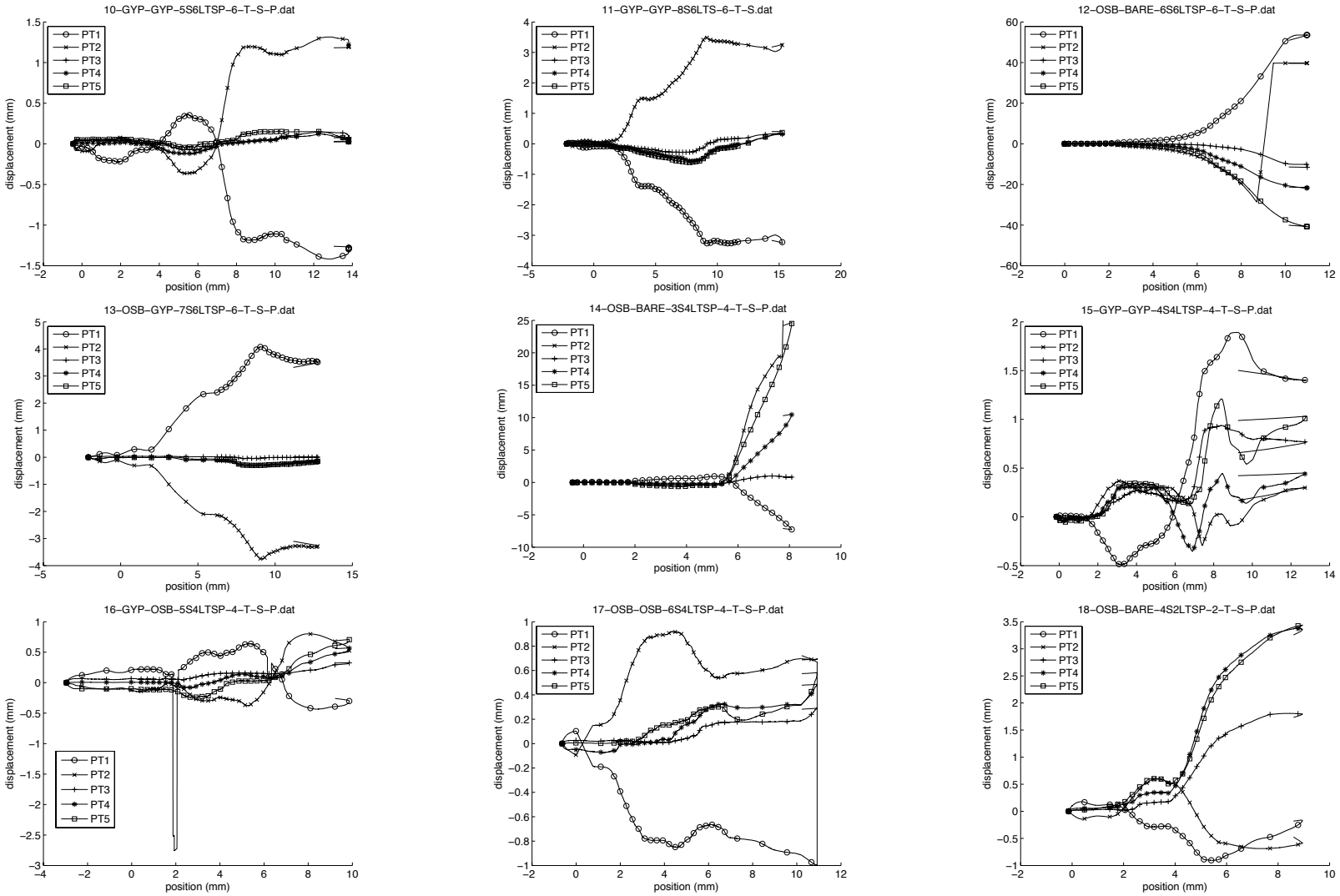

Figure D.5 – Position transducers plots. Tests 10 to 18

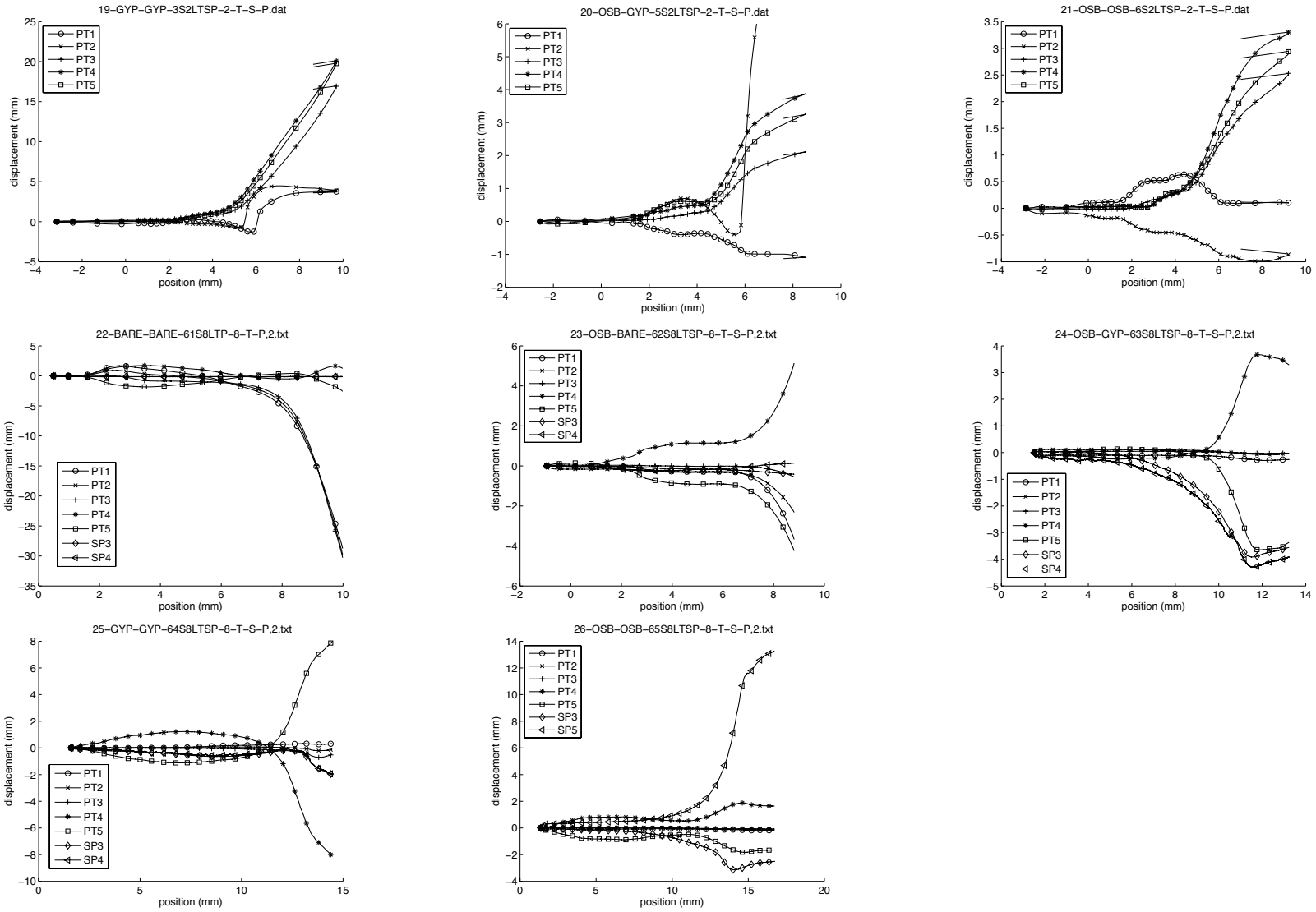

Figure D.6 – Position transducers plots. Tests 19 to 26

Appendix E

Wall Tests

Table E.1 – Out-to-out cross-section measurement

Specimen	H (mm)	B_B (mm)	B_A (mm)	D_B (mm)	D_A (mm)	t[1] (mm)	θ_{hbB} (deg)	θ_{dbB} (deg)	θ_{hbA} (deg)	θ_{dbA} (deg)
1S8L	93.582	42.007	42.088	12.819	13.013	1.969	89.1	89.3	89.7	89.8
2S8L	93.307	42.016	42.156	12.793	12.835	1.960	89.1	88.7	89.5	89.1
3S8L	93.650	41.821	42.164	12.734	12.869	1.919	89.5	89.3	89.1	88.9
4S8L	93.493	42.216	41.876	12.725	12.734	1.969	89.4	88.6	89.6	89.3
5S8L	93.565	42.274	42.037	12.802	12.598	2.019	89.8	89.8	89.3	89.1
6S8L	93.506	42.177	42.101	12.641	12.937	1.996	89.7	88.8	89.3	88.8
7S8L	93.519	42.333	42.160	12.531	12.886	1.914	89.5	88.9	89.1	88.8
8S8L	93.480	42.050	42.130	12.708	12.903	1.984	89.2	88.7	89.5	88.5
9S8L	93.929	42.202	42.664	12.615	12.844	1.949	89.5	88.3	89.7	89.2
10S8L	93.265	42.062	42.181	12.827	12.878	1.949	89.0	89.2	88.6	88.8
11S8L	93.400	42.426	40.729	12.598	12.946	1.953	89.1	88.7	89.5	89.1
12S8L	93.188	41.855	42.029	12.895	12.878	1.922	88.5	89.1	89.7	89.7
13S8L	93.070	42.215	42.050	13.115	12.827	1.966	89.1	89.3	89.7	89.8
14S8L	93.480	42.156	42.418	12.878	12.708	1.960	89.4	88.9	89.6	89.2
15S8L	94.876	41.876	42.041	12.734	12.852	1.891	89.4	88.9	89.6	89.2
16S8L	93.370	42.198	42.088	12.912	12.471	1.922	89.1	88.7	89.5	89.1
17S8L	93.917	42.122	42.164	12.615	12.751	1.891	88.9	89.3	89.7	89.8
18S8L	93.870	42.397	42.240	13.056	12.785	2.001	88.5	89.1	89.7	89.7
19S8L	93.624	42.156	42.211	12.751	12.717	1.914	89.1	88.7	89.5	89.1
20S8L	93.997	42.211	42.316	12.675	12.615	1.984	89.1	88.7	89.5	89.1
21S8L	93.726	42.422	42.359	12.632	13.013	1.984	89.4	88.9	89.6	89.2
22S8L	93.768	42.316	42.435	12.742	13.056	2.007	89.1	88.7	89.5	89.1
23S8L	93.379	42.299	42.211	13.005	13.030	1.819	89.7	89.0	89.6	89.2
24S8L	93.586	42.380	41.957	12.886	12.996	1.819	88.8	89.9	89.3	88.9
25S8L	93.544	42.452	41.952	12.590	12.776	1.929	89.3	89.0	89.2	89.1
26S8L	93.641	42.181	42.160	12.827	12.708	1.848	89.7	89.9	89.1	89.0
27S8L	93.561	41.978	42.105	12.734	12.480	1.892	89.1	89.8	89.3	89.1
28S8L	93.472	42.041	42.329	12.903	12.852	1.891	89.4	89.3	89.5	89.0
29S8L	93.476	42.151	42.261	12.751	12.632	1.891	89.2	89.5	89.3	89.1
30S8L	93.383	42.130	42.164	12.835	12.666	1.892	89.1	89.8	89.3	89.1
31S8L	93.248	42.020	42.270	13.030	12.996	1.896	88.5	89.0	89.2	89.0
32S8L	93.620	42.240	42.291	12.852	12.979	1.891	89.4	89.3	89.5	89.0
33S8L	94.213	42.223	42.126	13.183	13.064	1.844	88.8	89.5	89.5	89.0
34S8L	93.895	42.270	42.113	12.548	12.929	1.974	89.6	88.5	88.9	89.6
35S8L	93.523	42.359	42.541	12.861	13.030	1.868	88.9	88.5	89.9	89.6
36S8L	93.637	42.122	42.160	12.912	12.962	1.866	89.7	89.3	89.5	89.0
37S8L	93.468	42.024	42.117	12.903	12.971	1.883	89.6	89.0	88.4	89.0
38S8L	94.145	42.058	42.088	13.039	12.971	1.856	89.2	89.7	88.1	89.0
39S8L	93.646	42.105	41.957	12.819	12.954	1.898	89.9	89.4	89.1	89.7
40S8L	93.451	42.160	42.232	12.776	13.106	1.899	89.4	89.4	89.5	88.0
41S8L	93.607	42.003	42.113	13.191	12.937	1.878	89.1	88.9	89.1	89.4
42S8L	93.599	42.156	41.974	12.725	12.895	1.861	89.5	89.6	89.0	88.4
43S8L	93.447	42.113	42.122	13.157	12.852	1.851	89.0	88.9	88.9	88.9
44S8L	93.434	42.156	41.974	13.106	13.081	1.901	88.9	89.2	89.1	88.8
45S8L	93.315	42.189	41.969	12.446	13.064	1.899	89.0	88.9	88.9	88.9
46S8L	93.472	42.160	42.007	12.548	12.954	1.878	89.3	89.0	89.3	88.4
47S8L	93.527	42.278	41.999	12.810	12.971	1.839	89.6	89.3	89.2	88.7
48S8L	93.451	41.935	42.134	12.878	12.971	1.875	88.6	89.0	89.0	88.6
49S8L	94.154	42.084	42.084	12.700	12.946	1.867	89.4	89.5	88.3	89.2
50S8L	93.442	42.016	42.177	12.734	12.912	1.880	89.3	89.1	88.3	88.9
51S8L	93.607	41.999	42.139	12.531	12.844	2.001	89.4	88.9	89.6	89.2
52S8L	93.857	42.092	42.139	12.819	12.946	1.914	88.5	89.1	89.7	89.7
53S8L	93.531	42.016	42.067	13.437	13.140	1.900	89.4	89.5	88.3	89.2
54S8L	93.447	42.299	42.143	12.700	12.954	1.886	89.3	89.1	88.3	88.9
55S8L	94.285	42.164	42.105	12.996	12.861	1.828	88.5	89.4	89.5	88.9
56S8L	93.409	42.253	42.236	12.708	12.878	1.864	88.8	89.9	89.3	88.9
57S8L	93.328	41.961	42.143	12.268	12.895	1.865	88.8	89.2	89.5	88.0
58S8L	93.409	42.228	41.982	11.819	13.039	1.825	87.9	89.6	89.8	89.8
59S8L	93.663	42.139	41.944	11.870	12.658	1.880	88.9	88.4	89.4	88.9
60S8L	93.582	41.969	42.257	12.395	12.979	2.001	89.6	89.5	89.1	89.5
71S8L	93.654	42.397	42.414	13.013	13.640	1.867	89.7	89.8	89.3	89.3
72S8L	93.506	42.452	42.558	12.946	12.797	1.880	89.1	89.1	89.3	89.5
73S8L	93.510	42.308	42.156	13.005	12.852	1.857	89.5	89.8	89.1	89.4
74S8L	93.641	42.338	42.240	12.793	12.933	1.923	89.2	89.7	89.3	89.5
75S8L	93.514	42.075	42.147	12.971	12.954	1.869	89.3	89.3	89.7	89.8
Average[2]	93.598	42.161	42.137	12.782	12.895	1.907	89.190	89.161	89.277	89.124
CoV	0.003	0.004	0.006	0.021	0.013	0.027	0.004	0.005	0.005	0.004

(1) Thickness with coating

(2) Each stud was measured at three positions along the length (both ends and the middle) only the average of each variable to each stud is shown.

Table E.2 – Average global, local and distortional imperfections (Specimen 13S8L was disregarded due to error in the data measured)

Specimen	d_Φ (deg)	d_b (L/bow)	d_c (L/camber)	d_1/t	d_2/t
1S8L	1.1650	3235.1	1513.0	0.2743	0.1883
2S8L	0.0535	3866.4	1488.5	0.3241	0.1651
3S8L	0.6174	2547.3	1566.8	0.3272	0.1350
4S8L	0.9544	3513.9	1837.5	0.2767	0.1623
5S8L	1.0093	4777.7	1683.8	0.3158	0.1203
6S8L	1.2279	3690.6	1874.2	0.3902	0.3233
7S8L	1.0393	3825.7	1718.3	0.3423	0.1780
8S8L	0.7377	2408.6	1205.4	0.3596	0.1991
9S8L	0.9500	2756.2	1780.9	0.3702	0.1893
10S8L	0.7247	3466.4	1402.6	0.2950	0.0909
11S8L	0.6990	3991.1	1777.3	0.3546	0.1274
12S8L	0.5396	4730.5	2148.8	0.3398	0.8362
14S8L	0.5286	3047.7	2162.9	0.4833	0.1541
15S8L	0.7715	4455.3	1782.5	0.3587	0.2310
16S8L	0.6857	3590.6	2170.7	0.2813	0.1327
17S8L	0.6987	2596.4	1879.1	0.3146	0.0976
18S8L	1.1839	3350.5	1753.4	0.3254	0.1060
19S8L	0.8512	3510.4	1447.3	0.5995	0.1855
20S8L	0.8224	3071.4	2088.8	0.1067	0.1759
21S8L	1.3068	4204.9	2094.9	0.2911	0.1717
22S8L	1.1127	3547.8	2036.8	0.3069	0.1621
23S8L	1.0173	7285.7	1802.7	0.3540	0.2039
24S8L	0.8293	4703.0	1821.4	0.2339	0.1134
25S8L	1.0849	1683.5	1992.5	0.3519	0.1814
26S8L	1.1034	3113.8	1731.1	0.2852	0.2317
27S8L	0.5962	2742.6	1591.0	0.2725	0.1457
28S8L	0.7637	3270.0	1841.2	0.3949	0.1141
29S8L	0.5646	2710.5	1885.4	0.3527	0.1776
30S8L	0.6709	2808.5	1772.9	0.3090	0.1966
31S8L	0.6265	2920.2	2028.4	0.3445	0.1507
32S8L	0.5632	585.0	1486.8	0.3520	0.3408
33S8L	1.0928	4224.0	2239.0	0.3729	0.2194
34S8L	1.0718	1198.1	1659.4	0.2854	0.1630
35S8L	0.8034	3342.0	1989.0	0.3700	0.1082
36S8L	0.9850	5102.1	1943.2	0.2794	0.1568
37S8L	1.0595	2445.5	1699.2	0.2038	0.1714
38S8L	0.9220	2682.4	2072.3	0.3717	0.1382
39S8L	1.1814	3782.6	1954.3	0.3647	0.2897
40S8L	0.8056	3946.2	1770.9	0.3812	0.1304
41S8L	0.7391	2546.1	1440.9	0.2883	0.1304
42S8L	1.0326	3016.8	1598.4	0.2006	0.1070
43S8L	0.8585	2841.1	1533.2	0.4527	0.0991
44S8L	1.0364	3186.1	1440.8	0.2898	0.2115
45S8L	1.2409	3149.9	1983.0	0.3086	0.2514
46S8L	0.9994	2950.2	1741.0	0.3213	0.1412
47S8L	1.1254	3041.8	1878.7	0.2713	0.2322
48S8L	0.7329	3776.2	1862.5	0.4096	0.2778
49S8L	0.6270	3186.1	1957.9	0.3253	0.2430
50S8L	0.9135	3359.8	1884.1	0.3538	0.1043
51S8L	1.0283	3911.0	2003.9	0.2483	0.1596
52S8L	0.9755	3639.1	1912.1	0.3199	0.1481
53S8L	1.2740	2490.3	1904.5	0.3301	0.1940
54S8L	1.0052	3293.8	1714.0	0.3372	0.2546
55S8L	0.9708	3538.7	1645.9	0.2629	0.1650
56S8L	0.9373	3448.6	2212.1	0.4028	0.2354
57S8L	0.8706	3207.5	1959.9	0.3391	0.1256
58S8L	1.1358	1760.9	1708.4	0.2412	0.1368
59S8L	1.4423	2108.6	1270.3	0.4181	0.2792
60S8L	0.7791	1860.5	1755.6	0.3391	0.1824
71S8L	0.9001	2819.1	2234.3	0.4430	0.1132
72S8L	1.0598	2488.0	2813.9	0.4218	0.1802
73S8L	0.9734	2889.0	1972.9	0.2381	0.2475
74S8L	0.7593	2890.7	1853.0	0.2954	0.1853
75S8L	0.7137	3104.7	2423.5	0.5151	0.2244
Total Average	0.8992	3238.0	1834.4	0.3327	0.1874
CoV	0.262	0.298	0.150	0.227	0.532

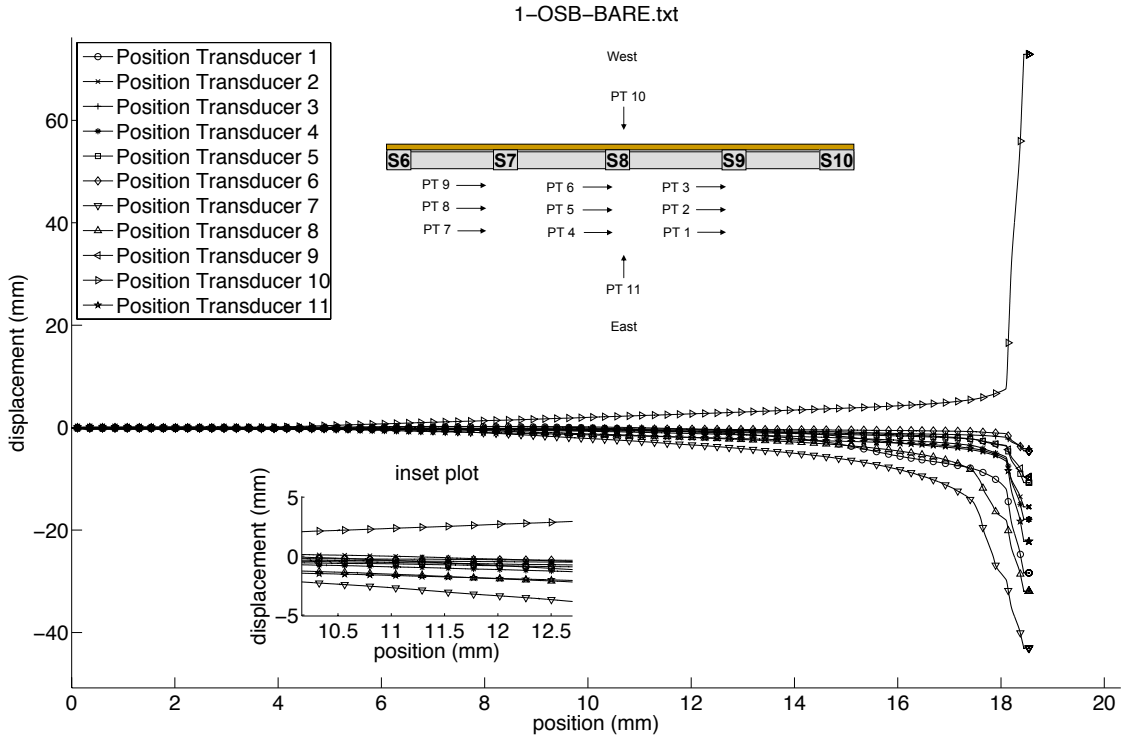

a) Position transducers plot

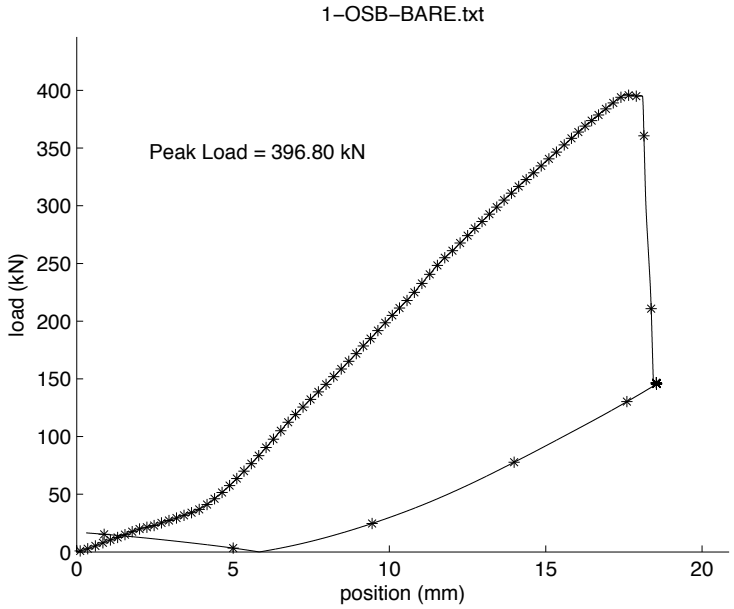

b) P-Δ curve

Figure E.1 – Specimen 1-OSB-BARE

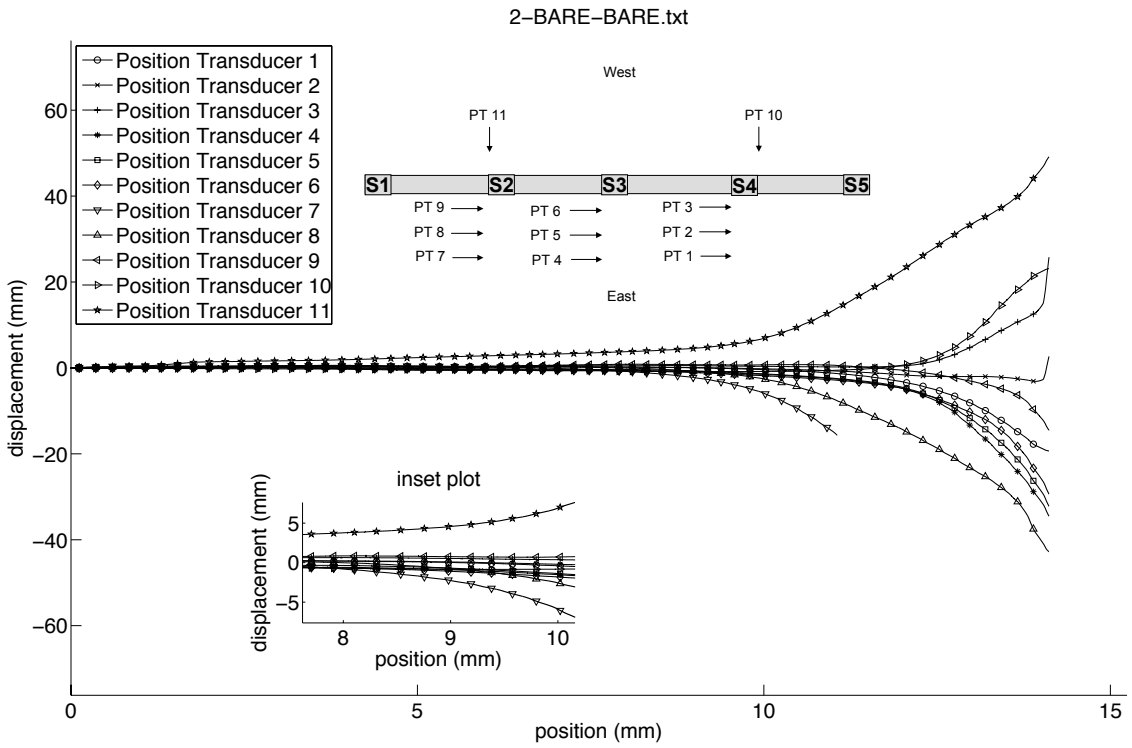

a) Position transducers plot

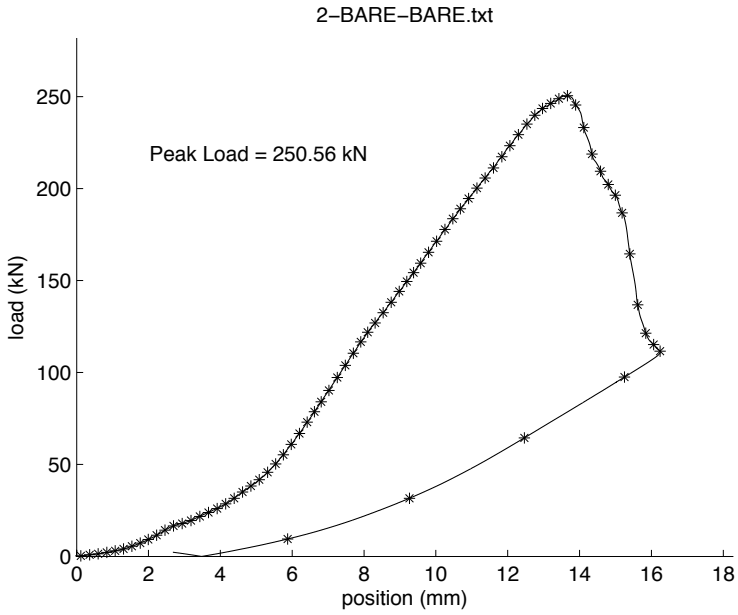

b) P-Δ curve

Figure E.2 – Specimen 2-BARE-BARE

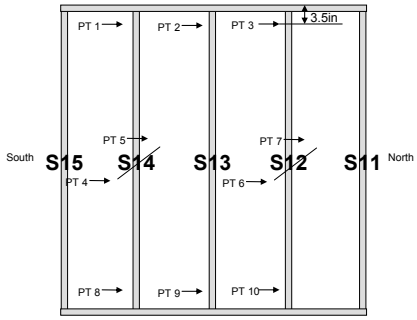

a) Location of position transducers, side view

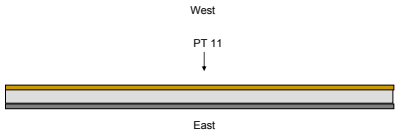

b) Location of position transducers, upper view

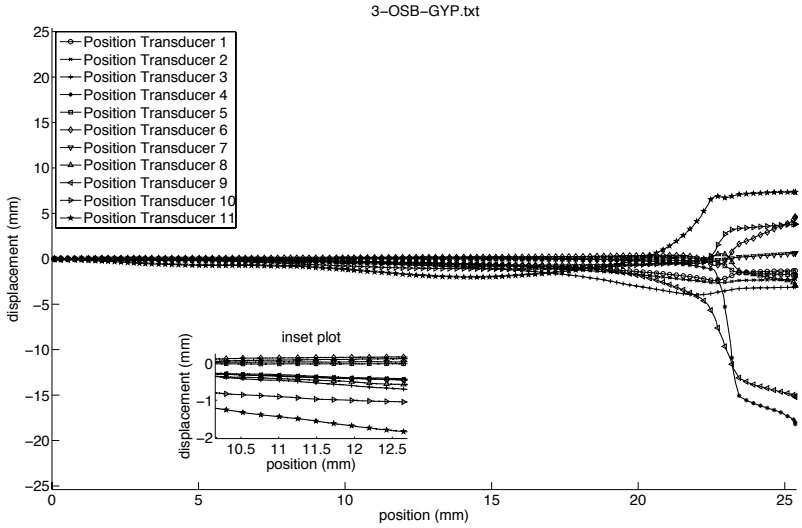

c) Position transducers plot

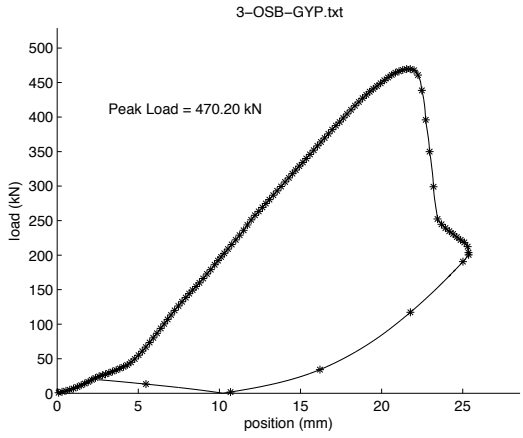

d) P-Δ curve

Figure E.3 – Specimen 3-OSB-Gyp

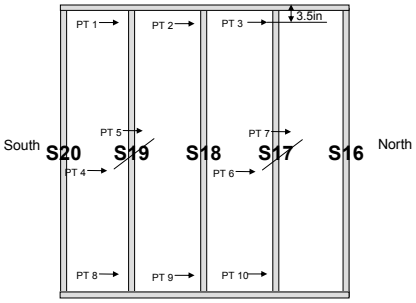

a) Location of position transducers, side view

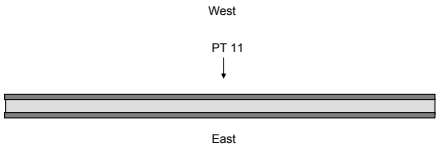

b) Location of position transducers, upper view

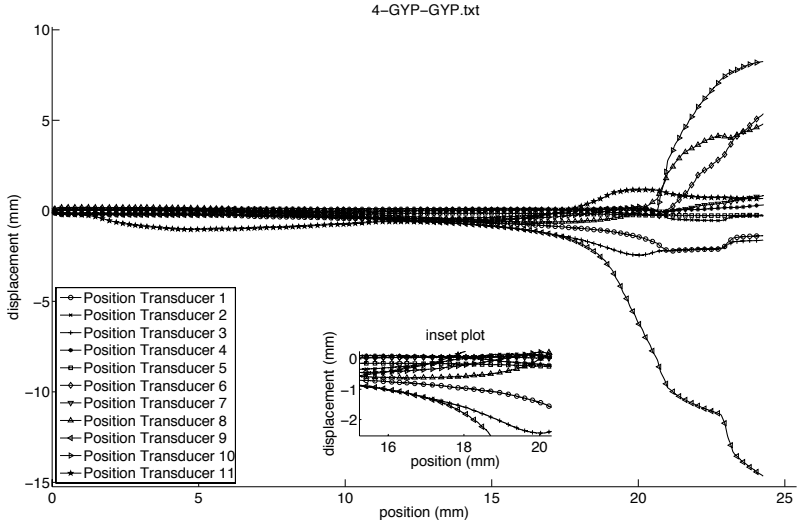

c) Position transducers plot

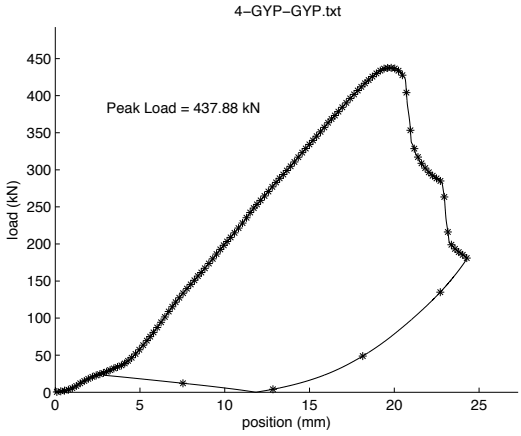

d) P-Δ curve

Figure E.4 – Specimen 4-OSB-Gyp

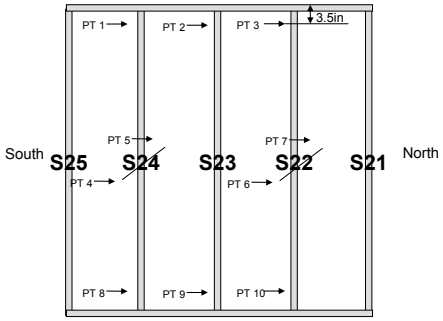

a) Location of position transducers, side view

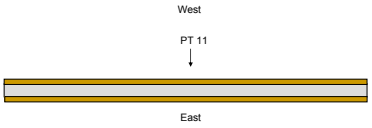

b) Location of position transducers, upper view

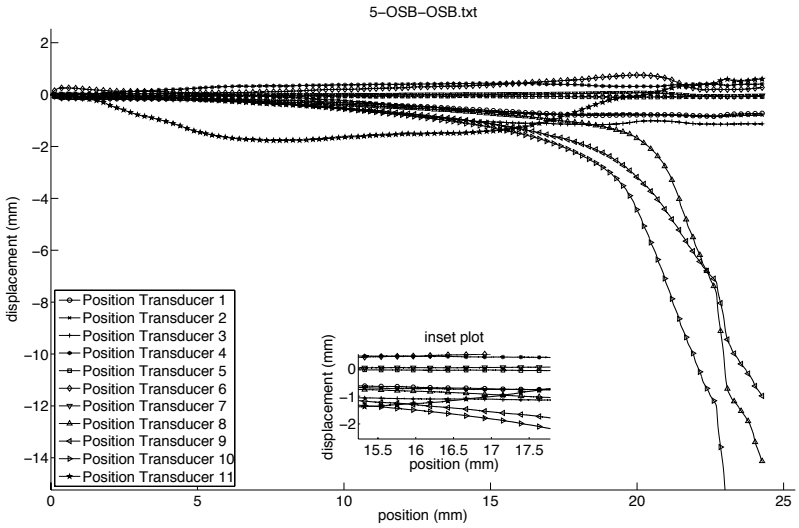

c) Position transducers plot

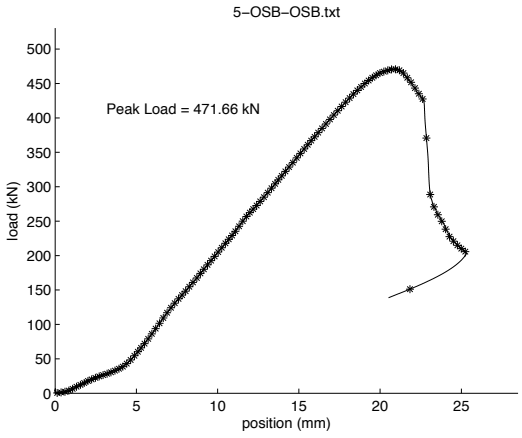

d) P-Δ curve

Figure E.5 – Specimen 5-OSB-OSB

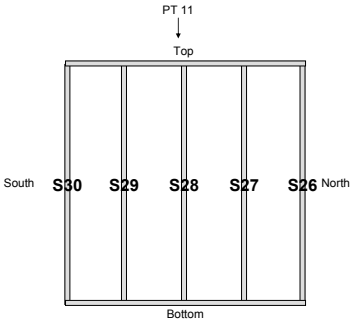

a) Location of position transducers, side view. PT depicted in side view are located at mid-high

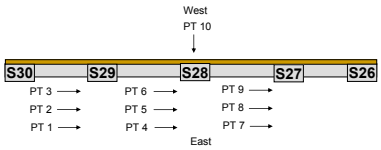

b) Location of position transducers, upper view

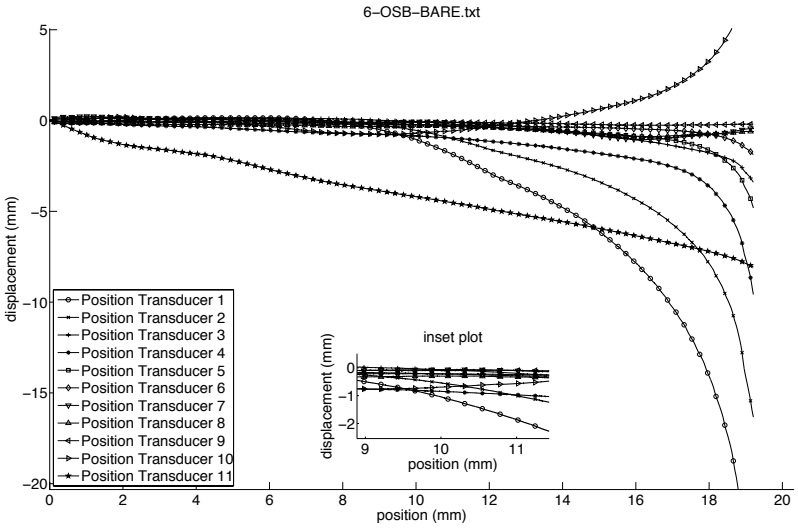

c) Position transducers plot

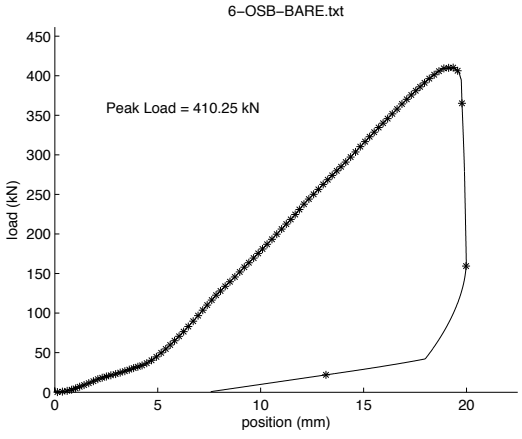

d) P-Δ curve

Figure E.6 – Specimen 6-OSB-BARE

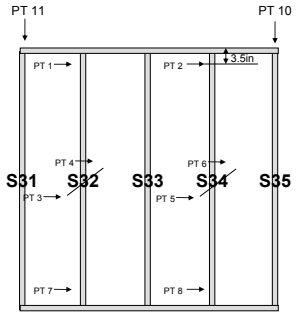

a) Location of position transducers, side view

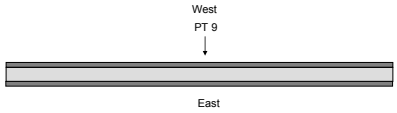

b) Location of position transducers, upper view

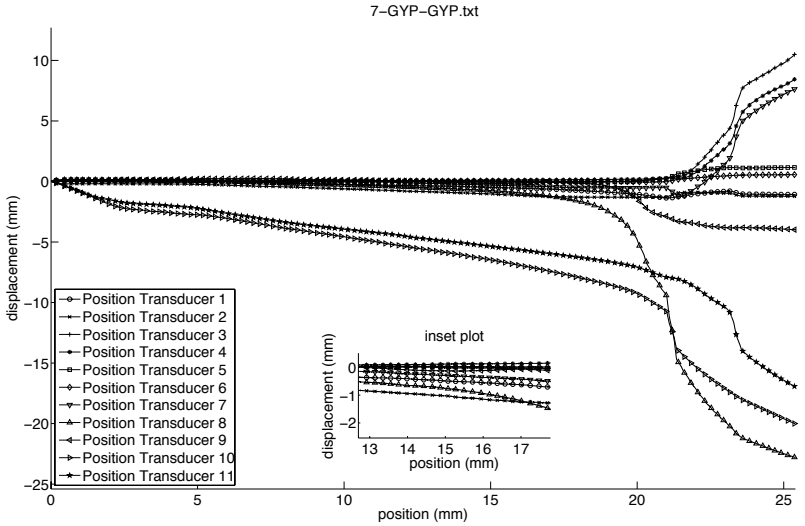

c) Position transducers plot

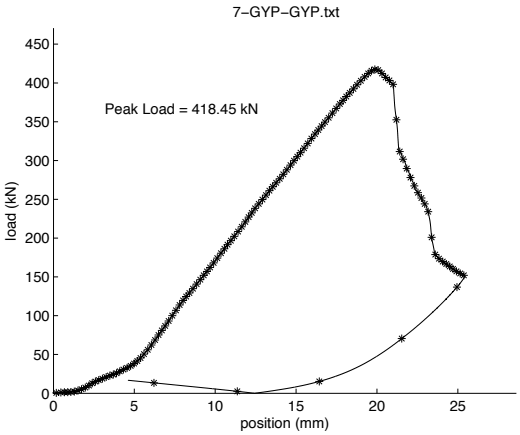

d) P-Δ curve

Figure E.7 – Specimen 7-Gyp-Gyp

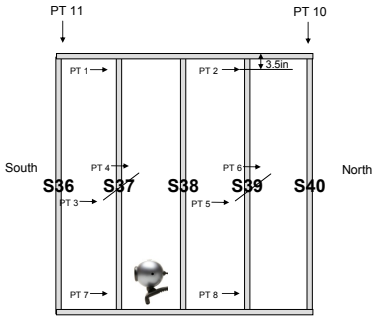

a) Location of position transducers, side view

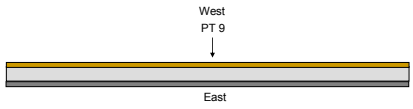

b) Location of position transducers, upper view

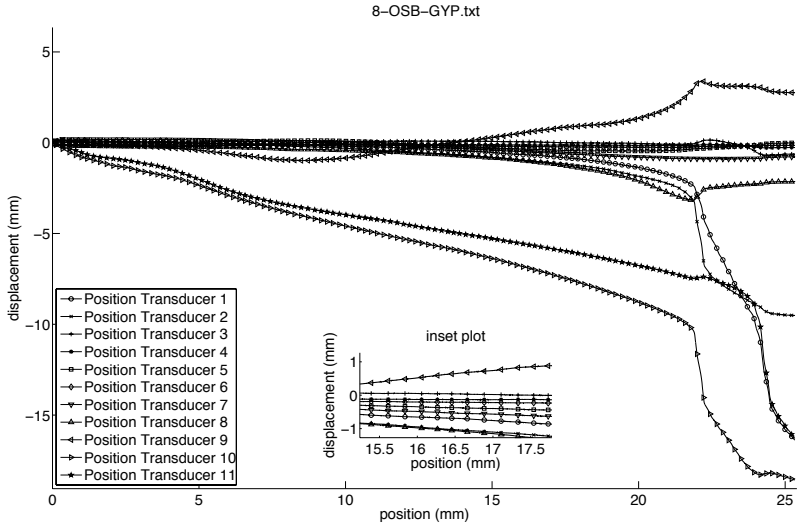

c) Position transducers plot

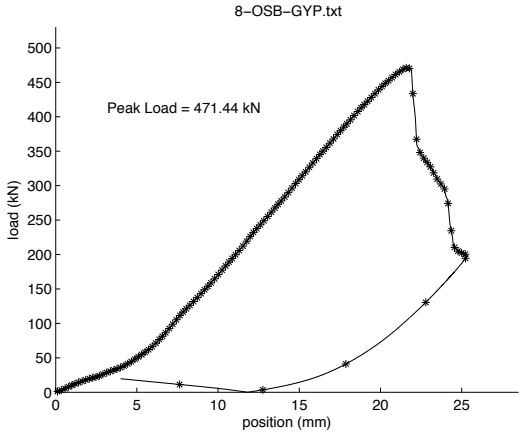

d) P-Δ curve

Figure E.8 – Specimen 8-OSB-Gyp

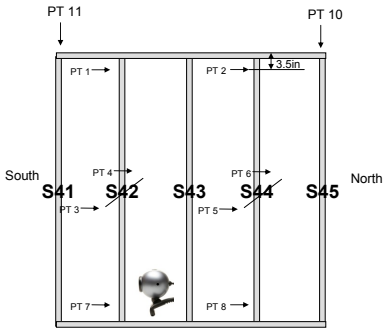

a) Location of position transducers, side view

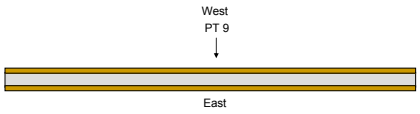

b) Location of position transducers, upper view

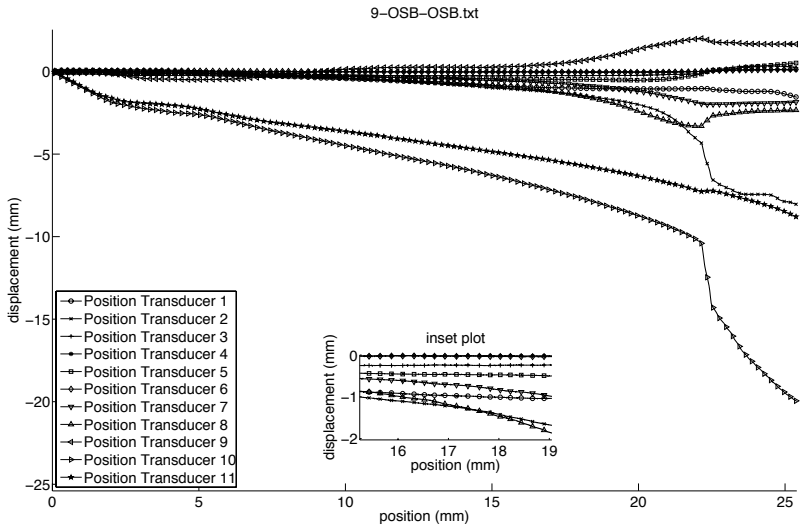

c) Position transducers plot

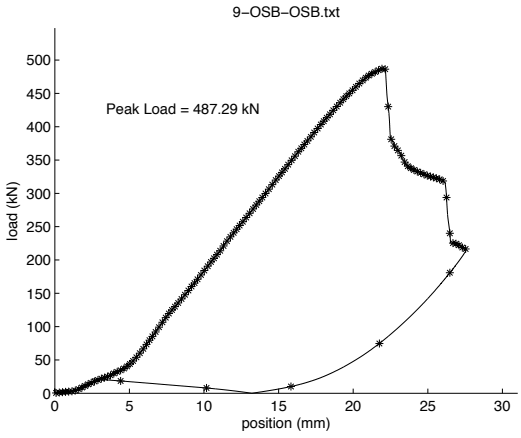

d) P-Δ curve

Figure E.9 – Specimen 9-OSB-OSB

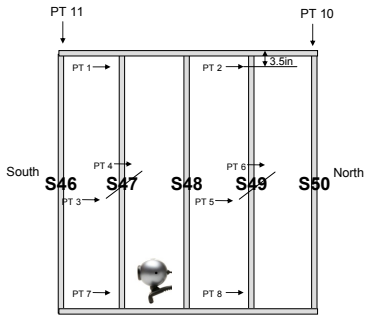

a) Location of position transducers, side view

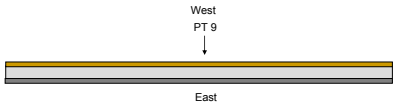

b) Location of position transducers, upper view

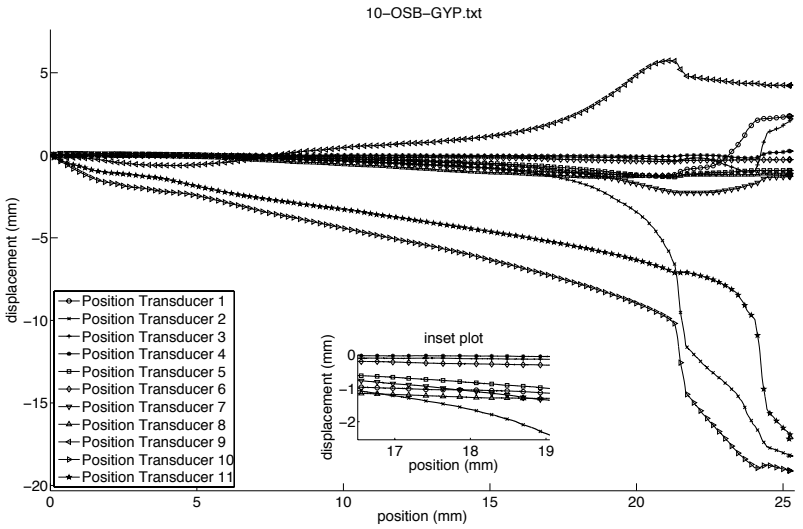

c) Position transducers plot

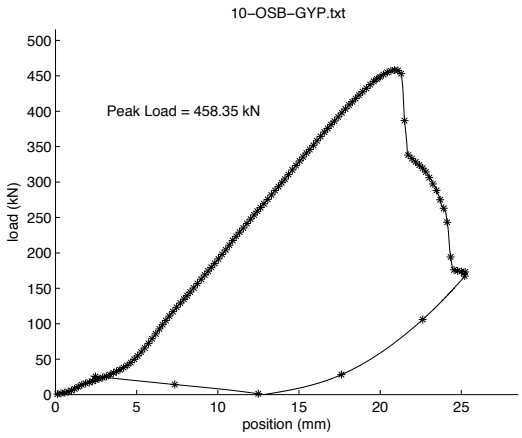

d) P-Δ curve

Figure E.10 – Specimen 10-OSB-Gyp

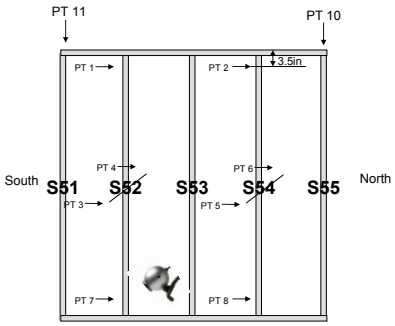

a) Location of position transducers, side view

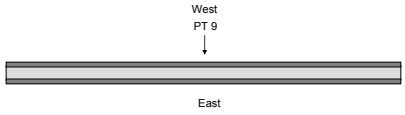

b) Location of position transducers, upper view

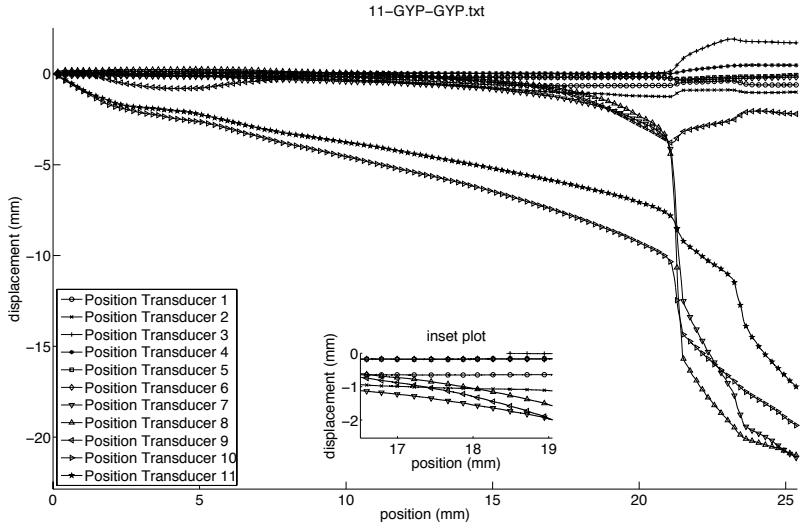

c) Position transducers plot

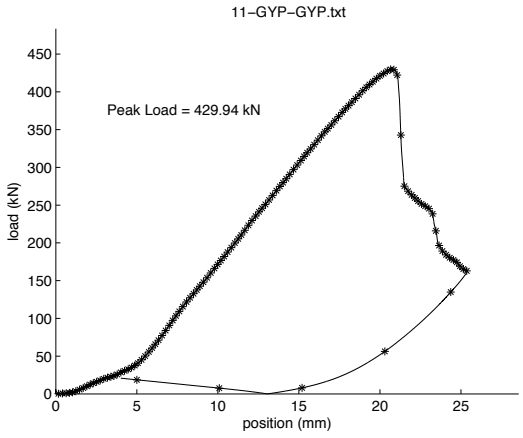

d) P-Δ curve

Figure E.11 – Specimen 11-Gyp-Gyp

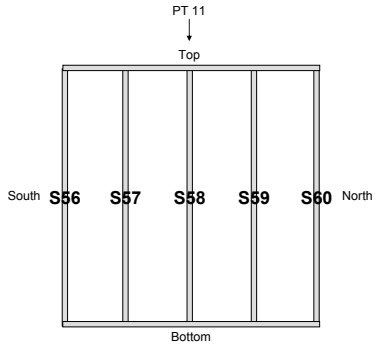

a) Location of position transducers, side view. PT depicted in side view are located at mid-high

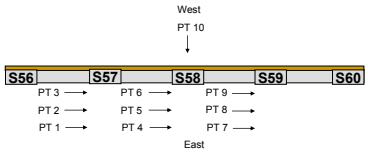

b) Location of position transducers, upper view

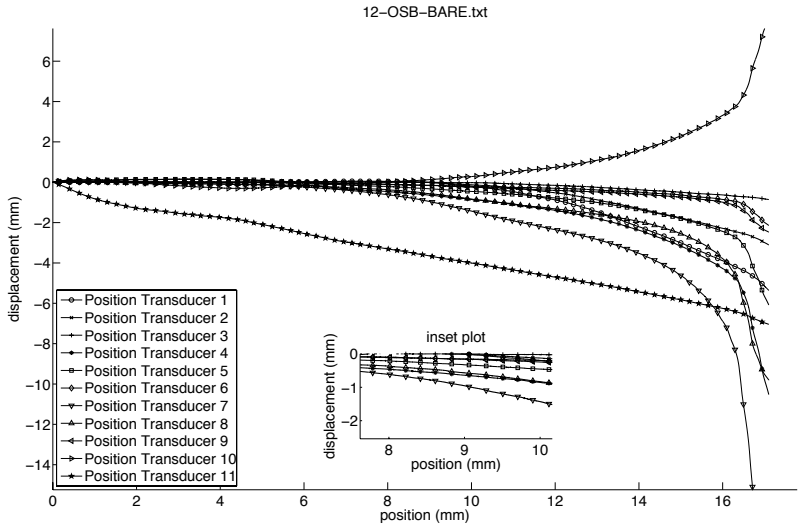

c) Position transducers plot

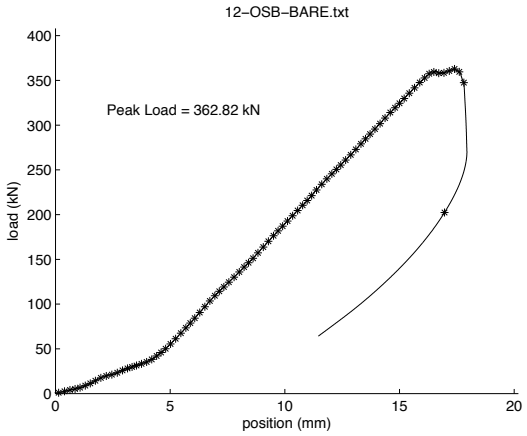

d) P-Δ curve

Figure E.12 – Specimen 12-OSB-BARE

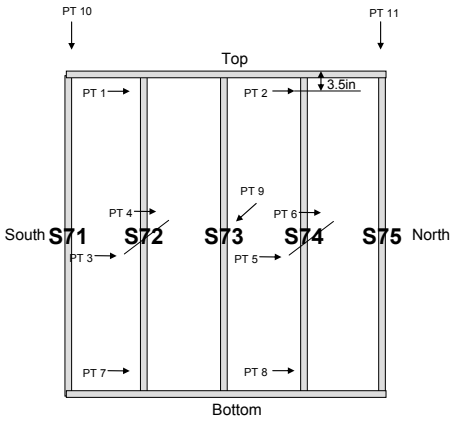

a) Location of position transducers

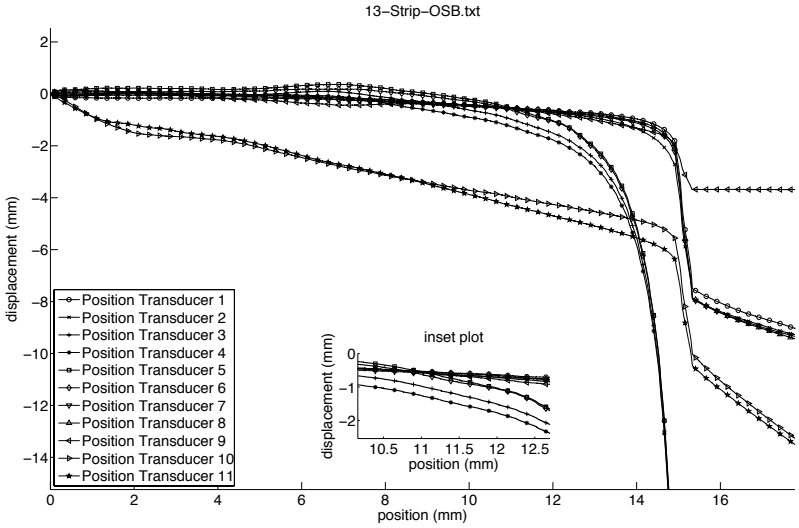

b) Position transducers plot

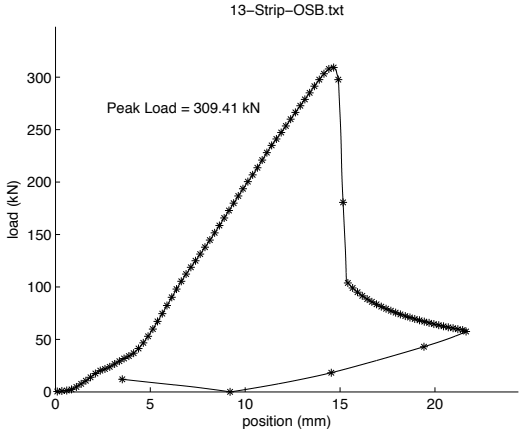

c) P-Δ curve

Figure E.13 – Specimen 13-Strip-OSB

Appendix F

Conversion Factors

Imperial Units to International System of Units (SI)

1ft = 0.305m

1in. = 25.4mm

$1in.^2 = 645.2mm^2$

$1in.^4 = 416231mm^4$

1lb = 4.448N

1kip = 4.448kN

1ksi = 6.895MPa

1kip·in. = 113N·m

1kip·in. = 112,979.2N·mm

1kip/in = 0.1752kN/mm

1kip/in/in = 6.895N/mm/mm

1kip·ft = 1356N·m

1psf = 0.0479kPa

Useful Force Relationships

1kN = 102kgf = 0.22kips = 224lbs or 1kip = 1000lbs = 454kgf = 4.448kN

Rule of Thumb for Force

1 Old VW Beetle*

= 2kips = 10kN

1000kgf

* Picture downloaded from: www.onemoregadget.com, accessed 07/13/2011.

Appendix G

Design Example Using CUFSM v4.03 to Determine the Elastic Buckling Loads and Direct Strength Method (DSM) to Find the Nominal Load*

* Imperial units are used in this example.

Problem description:

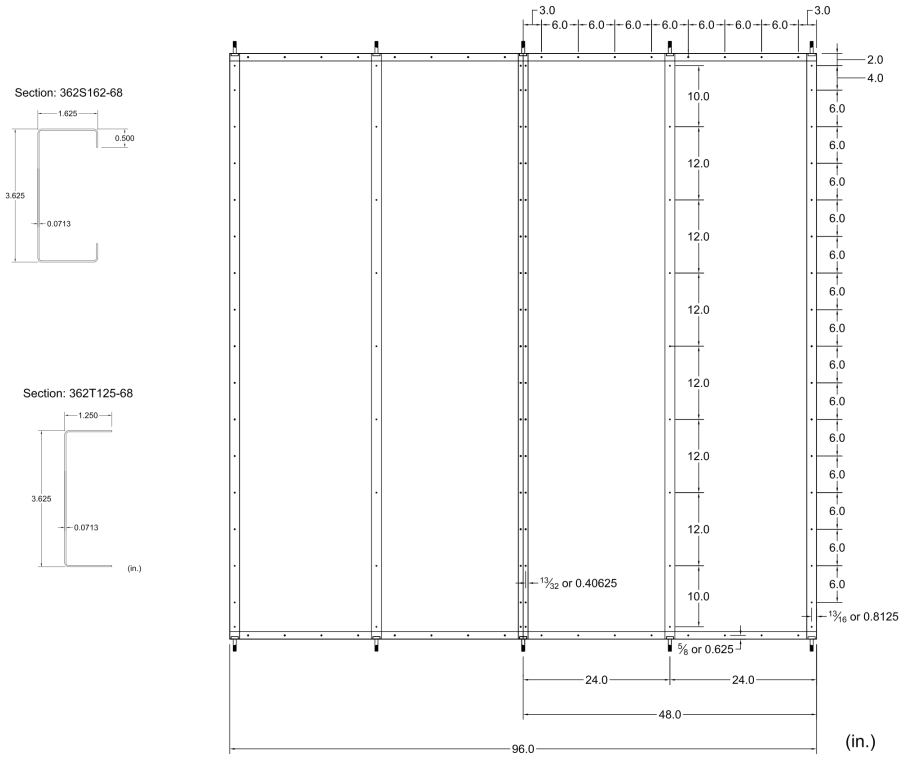

Figure G.1 – Cold-formed steel wall stud to be designed. Same specifications depicted in the tests commented in Chapter 5.

Cold-formed steel stud 362S162-68[†]:

Cross-section area[‡]: $A = 321.7mm^2\ (0.4987in^2)$

Young's modulus: $E = 203{,}395MPa\ (29{,}500ksi = 29{,}500{,}000lbf/in^2)$

Yielding stress: $f_y = 345MPa\ (50ksi)$

Measured flange thickness: $t = 1.67mm\ (0.0656in)$

Measured flange height divided by two: $y_{CG} = 4.6cm\ (1.81in)$

[†] SSMA nomenclature consists of: the first three numbers are the member depth in 1/100in. (ex.: 362➔362*1/100=3.62in.), the following letter designates the cross-section type (ex.: S, stands for Stud), the next three numbers are the flange width in 1/100in. (ex.: 162➔162*1/100≈1.625in.), and the last two numbers are the minimum base metal thickness in mils (ex.: 68➔68*1/1000=0.068in.).

[‡] Dimensions based on measured, not normal properties. As detailed in Chapter 4 Section 4.1.2.

OSB sheathing connected to both sides:

Shear stiffness of OSB: $G = 1310 MPa\ (190 ksi)$

OSB sheathing thickness: $t_{board} = 1.11 cm\ (7/16 in)$

Height of the sheathing: $L = 244 cm\ (96 in)$

Sheathing rigidity, stress parallel to strength axis:

$(EI)_{w-parallel} = 736 N \cdot m^2 / m\ (78{,}000 lbf \cdot in^2 / ft)$

Sheathing rigidity, stress perpendicular to strength axis:

$(EI)_{w-perpendicular} = 151 N \cdot m^2 / m\ (16{,}000 lbf \cdot in^2 / ft)$

Fasteners:

Distance between fasteners[§]: $d_f = 30.5 cm\ (12 in)$

Tributary width of fastener: $w_{tf} = 61 cm\ (24 in)$

Fastener's diameter (#8 fastener): $d = 3.35 mm\ (0.132 in)$

[§] The greatest distance between fasteners ($12 in$) is selected as d_f.

The spring stiffnesses can be determined by:

k_{xd} - The diaphragm stiffness (k_{xd}) can be calculated using the exact or simplified solution:

$$k_{xd} = \frac{2\pi G t_{board} w_{tf}}{L} \sin\left(\frac{\pi d_f}{2L}\right) = 25.473 kip/in \quad \rightarrow \quad \frac{k_{xd}}{d_f} = 2.123 kip/in/in \tag{3.21}$$

$$k_{xd} \approx \frac{\pi^2 G t_{board} d_f w_{tf}}{L^2} = 25.632 kip/in \quad \rightarrow \quad \frac{k_{xd}}{d_f} = 2.136 kip/in/in \tag{3.21}$$

$k_{x\ell}$ - The local stiffness ($k_{x\ell}$) may be found via test or it can be calculated analytically:

From tests conducted herein (see Table 3.2):

$k_{x\ell} = 7.08 kip/in \quad \rightarrow \quad k_{x\ell}/d_f = 0.59 kip/in/in$

Alternatively (and conservatively):

$$k_{x\ell} = \frac{3Ed^4 t^3 \pi}{4t_{board}^2 \left(9d^4\pi + 16 t_{board} t^3\right)} = 2.952 kip/in \quad \rightarrow \quad k_{x\ell}/d_f = 0.246 kip/in/in \tag{3.15}$$

k_x may be found by combining k_{xd} (exact or simplified) and $k_{x\ell}$ (test or analytical), in this example k_{xd} is determined from the exact solution and $k_{x\ell}$ from the laboratory test:

$$k_x = (1/k_{x\ell} + 1/k_{xd})^{-1} = 5.54 kip/in \quad \rightarrow \quad k_x/d_f = 0.462 kip/in/in \tag{3.22}$$

$\boldsymbol{k_y}$ – The out-of-plane stiffness may be calculated using a non-composite action approach (see Chapter 6 for discussion about composite or non-composite action):

Considering a sheathing tributary width of 2 feet, and stress parallel to strength axis:

$(EI)_{w-parallel} \times 2\,ft = 156 kips$

$$k_y = \frac{(EI)_{w-parallel}\,\pi^4}{L^4} d_f = 2.14E^{-3} kip/in \quad \rightarrow \quad \frac{k_y}{d_f} = 1.78 kip/in/in \tag{3.4}$$

$\boldsymbol{k_\phi}$ – The rotational stiffness (k_ϕ) can be found by test or it can be calculated using a semi-empirical method, following the latter:

Considering stress perpendicular to strength axis the sheathing rigidity must be transformed to lbf-in^2/in:

$(EI)_{w-perpendicular} = 16{,}000 lbf \cdot in^2/ft \quad \rightarrow \quad 1{,}333.33 lbf \cdot in^2/in$

$k_{\phi c} = 0.00035Et^2 + 75 = 119.4\ lbf\,in/in/rad$ (3.1)

$k_{\phi w} = (EI)_w/d_f = 111\ lbf\,in/in/rad$ (3.2)

$k_\phi = 1/(1/k_{\phi c} + 1/k_{\phi w}) = 57.52\ lbf\,in/in/rad = 0.0575\ kip\,in/in/rad$ (3.3)

Note, from laboratory test (see Chapter 3 Section 3.2):

$k_\phi = 0.0703\ kip\,in/in/rad$

Numerical buckling analysis using CUFSM v4.03

The following pictures depict step-by-step how to find the elastic buckling loads using CUFSM v4.03. Figure G.2 shows the required information to analyze a 362S162-

68 stud; special attention is brought to the spring stiffnesses that simulate the OSB sheathing.

A signature curve can be plotted by setting the boundary condition tab as depicted in Figure G.4. The Post tab shows the signature curve, where local and distortional minima can be found (Figure G.4 and Figure G.5). CUFSM v4.03 also allows the user to analyze clamped-clamped boundary condition. Figure G.6 depicts the boundary condition tab set to run an analysis of a member of 96in., clamped-clamped and considering 1 to 30 possible number of half-wave lengths.

Using the constrained finite strip method (cFSM) the buckling modes can be analyzed separately. Figure G.7 shows the necessary settings to analyze only local buckling, the results are given in Figure G.8. It is worth mentioning that the local-buckling load factor ($P_{cr\ell}$=0.99P_y) is very similar to the value found by the traditional signature curve ($P_{cr\ell}$ =1.0163P_y). Figure G.9 depicts the cFSM set to run a distortional buckling analysis, which results in Figure G.10. Distortional buckling by the signature curve result in a distortional-buckling load factor (P_{crd} =1.43P_y) slightly lower than the cFSM analysis (P_{crd} =1.6825P_y). The similarities of $P_{cr\ell}$ and P_{crd} show that a traditional buckling analysis would result in a good estimation of $P_{cr\ell}$ and P_{crd}.

Nonetheless, global buckling is highly influenced by the boundary condition and so it shall be checked by setting the boundary condition tab as depicted in Figure G.6 and the cFSM tab as depicted in Figure G.12. The global buckling analysis results is depicted in Figure G.12, note that global-buckling load factor (P_{cre}=3.7768P_y), when reflects the clamped end condition, is considerably higher than P_{cre} given by the signature curve (P_{cre}=1.267P_y).

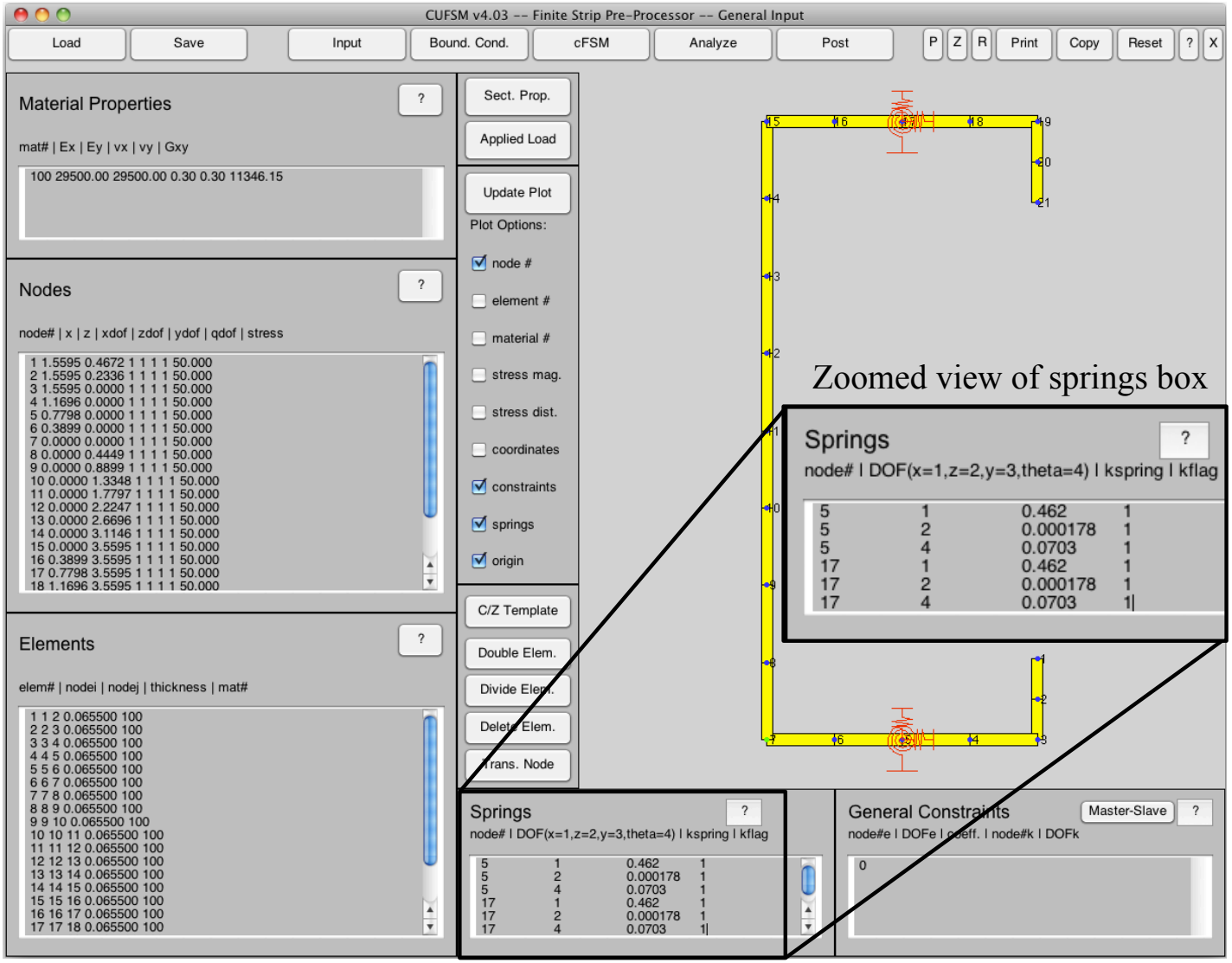

Figure G.2 – CUFSM v4.03, Input Window.

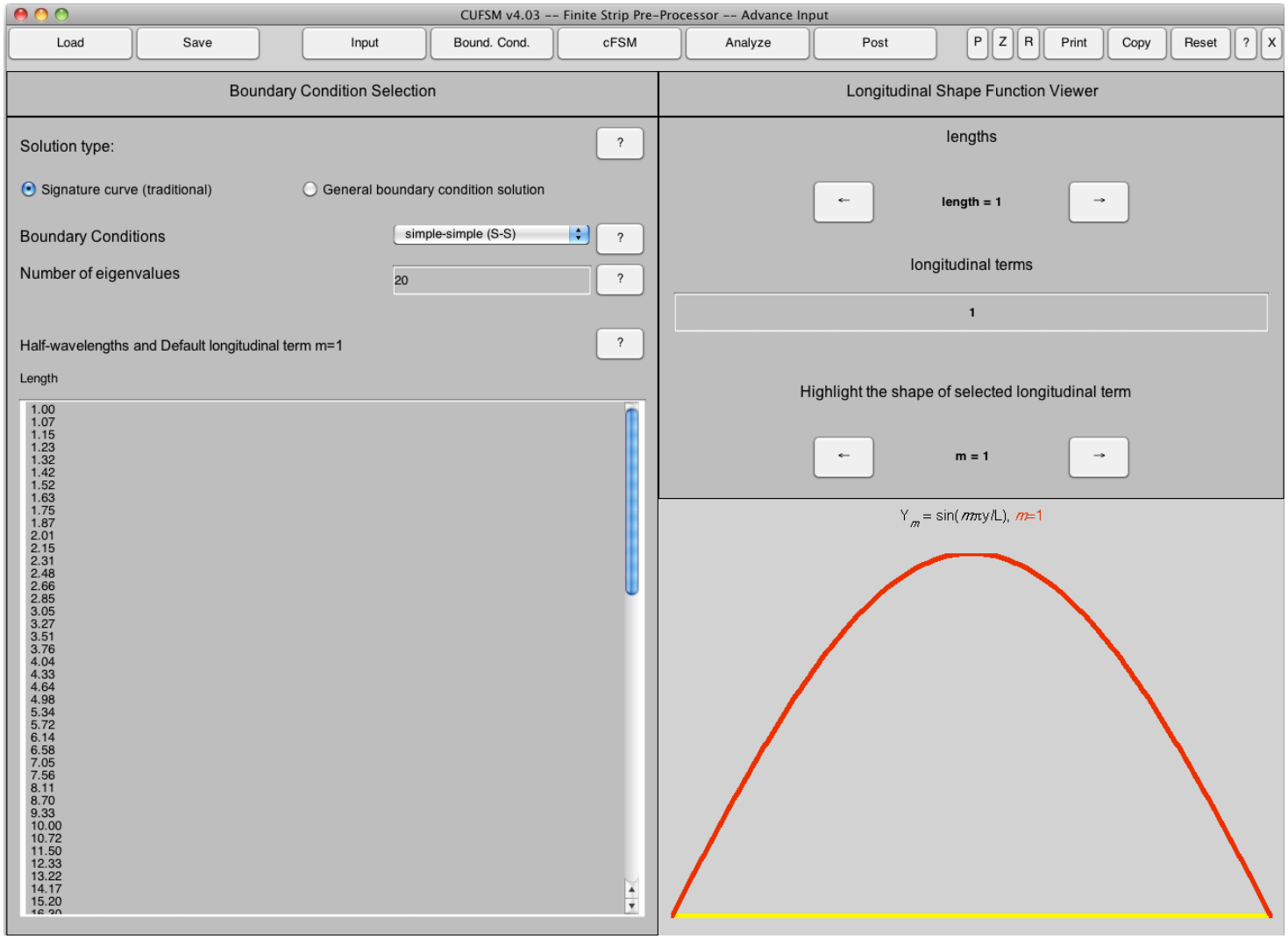

Figure G.3 – CUFSM v4.03, boundary condition tab for traditional CUFSM analysis.

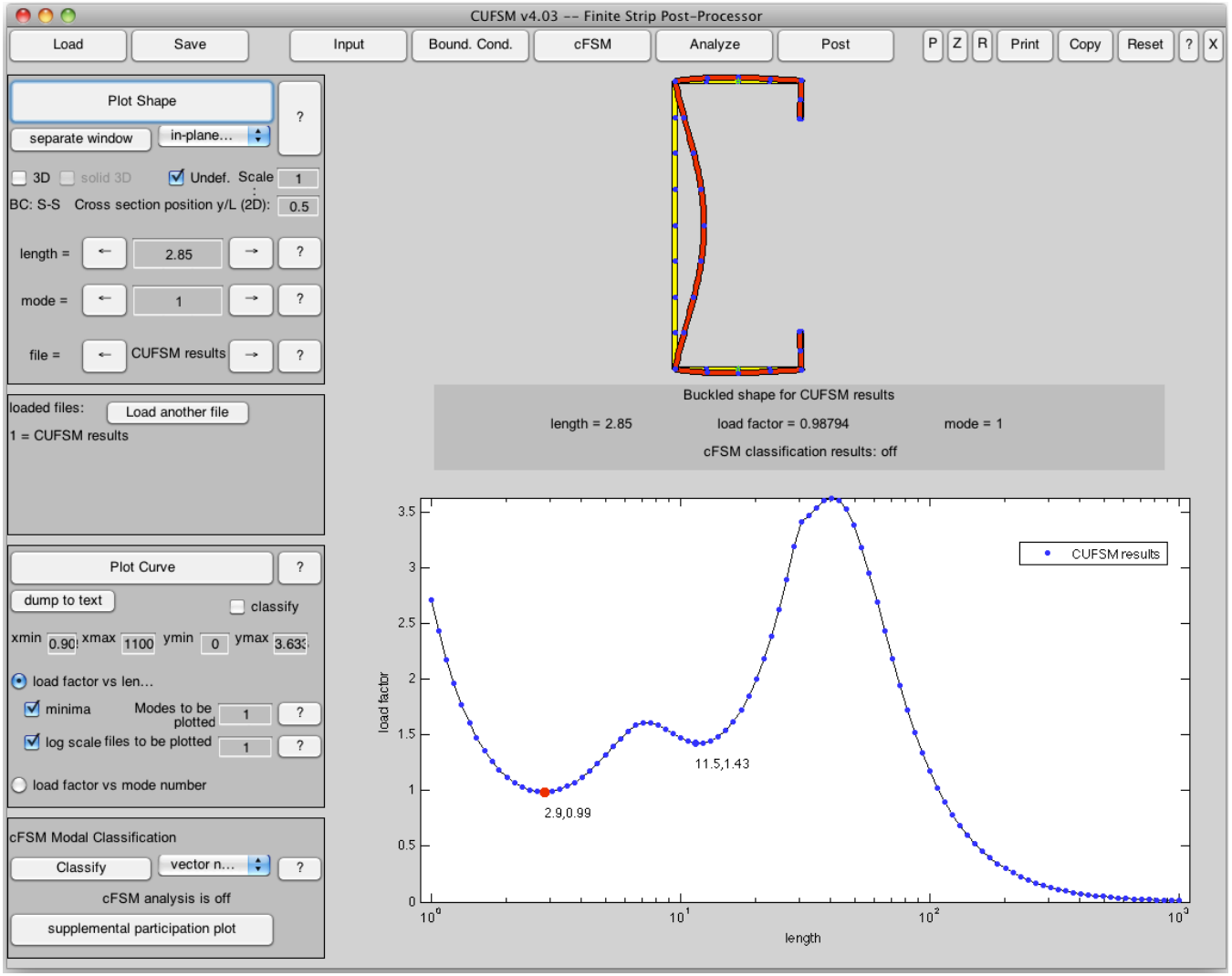

Figure G.4 – CUFSM v4.03, signature curve. Load factor for local buckling is 0.99 at a length of 2.9in.

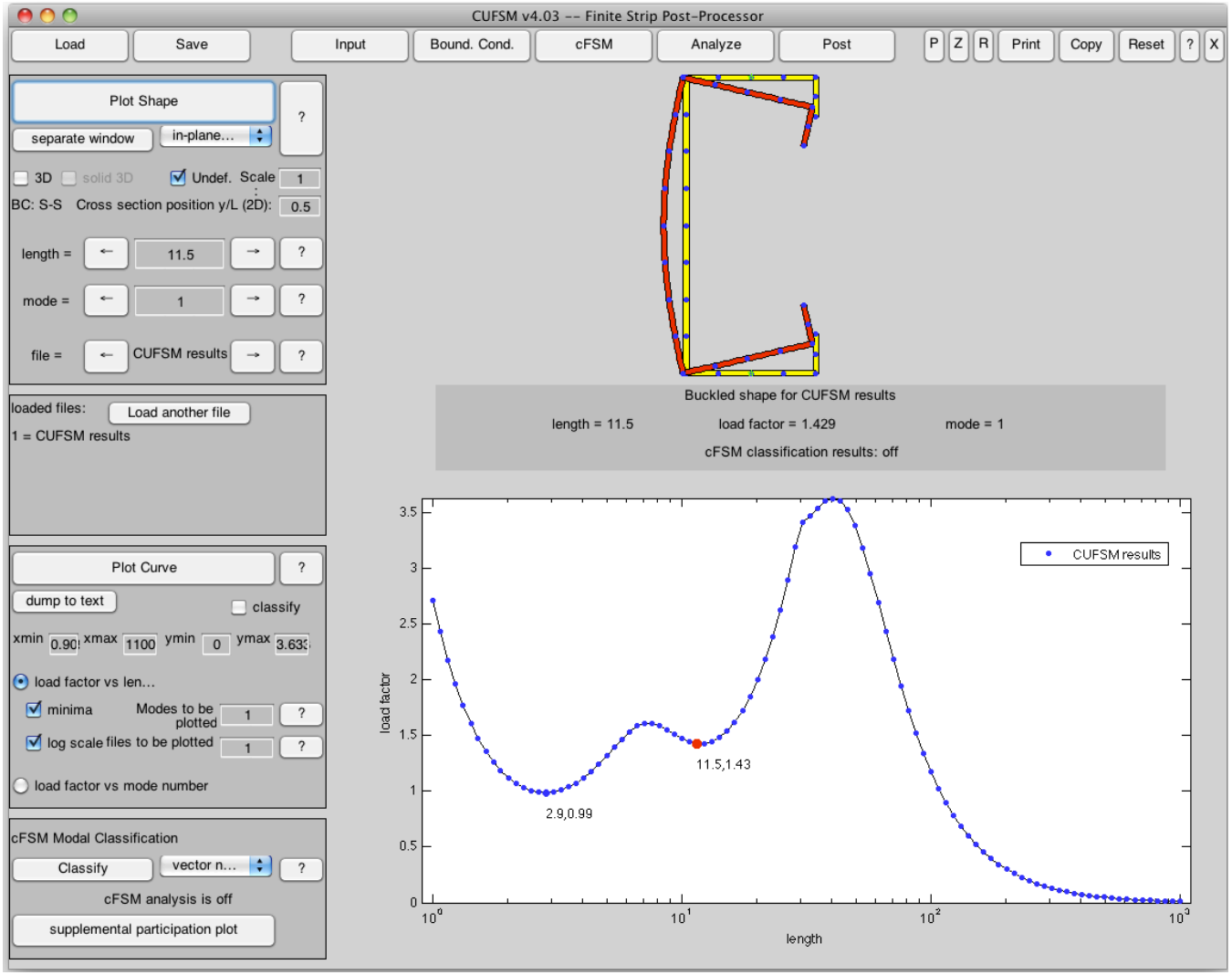

Figure G.5 – CUFSM v4.03, signature curve. Load factor for distortional buckling is 1.43 at a length of 11.5in. Since the stiffness of k_y spring is small, k_y was kept in the distortional analysis for convenience.

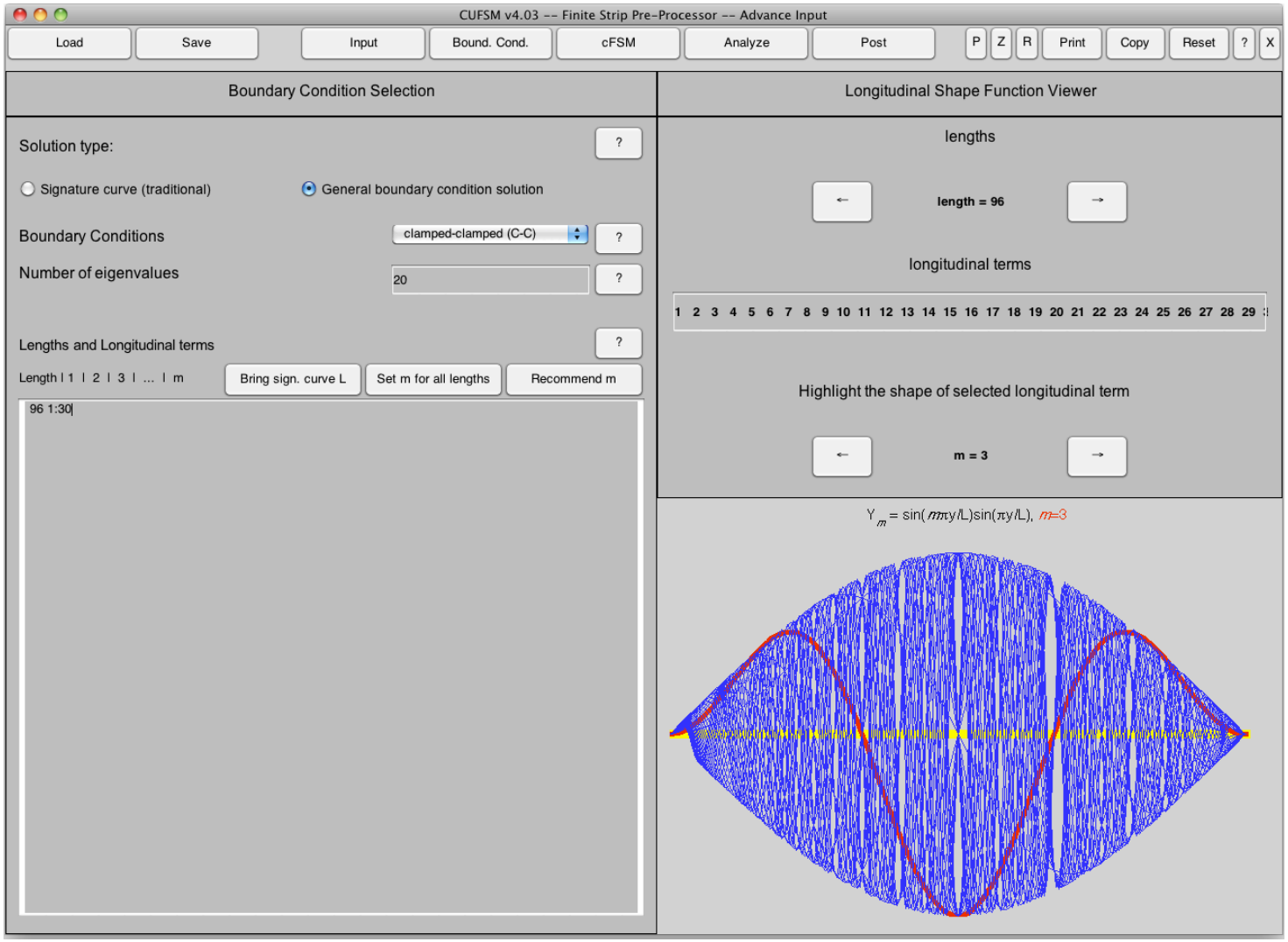

Figure G.6 – CUFSM v4.03, boundary condition tab for clamped-clamped analysis for a column of 96in and number of half-wave lengths (m) from 1 to 30.

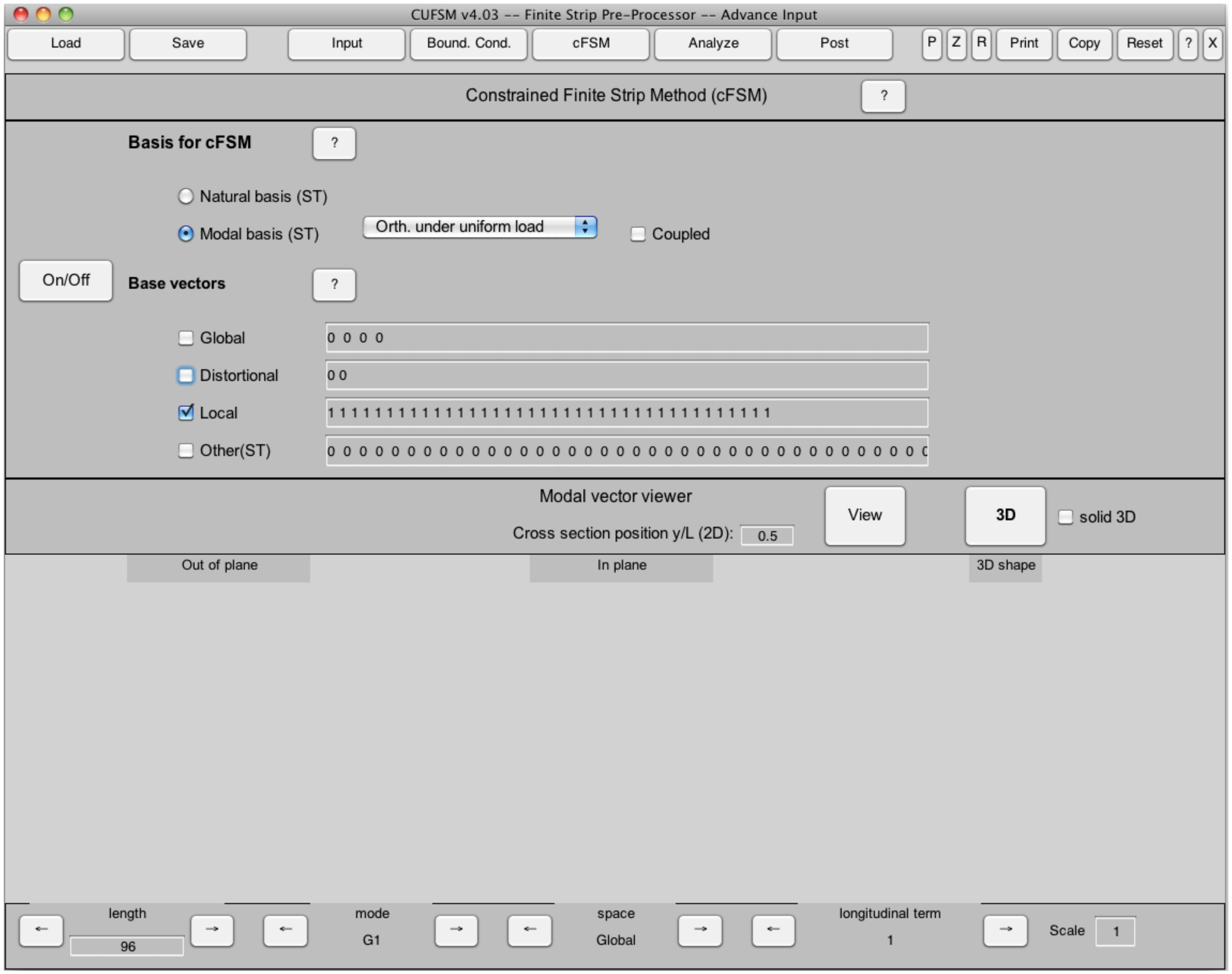

Figure G.7 – CUFSM v4.03, cFSM tab set for local buckling analysis.

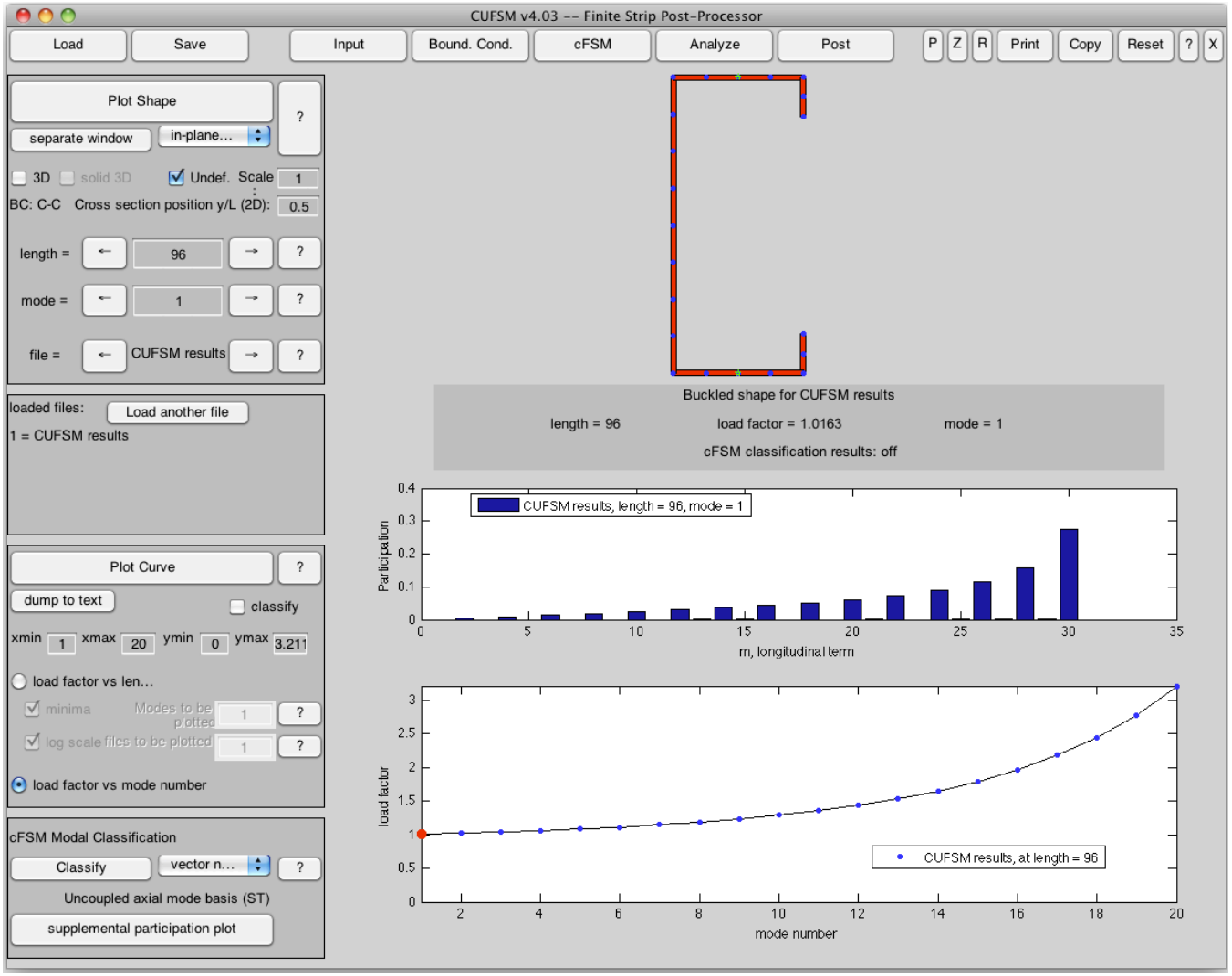

Figure G.8 – CUFSM v4.03, cFSM analysis result for local buckling. Load factor of 1.0163.

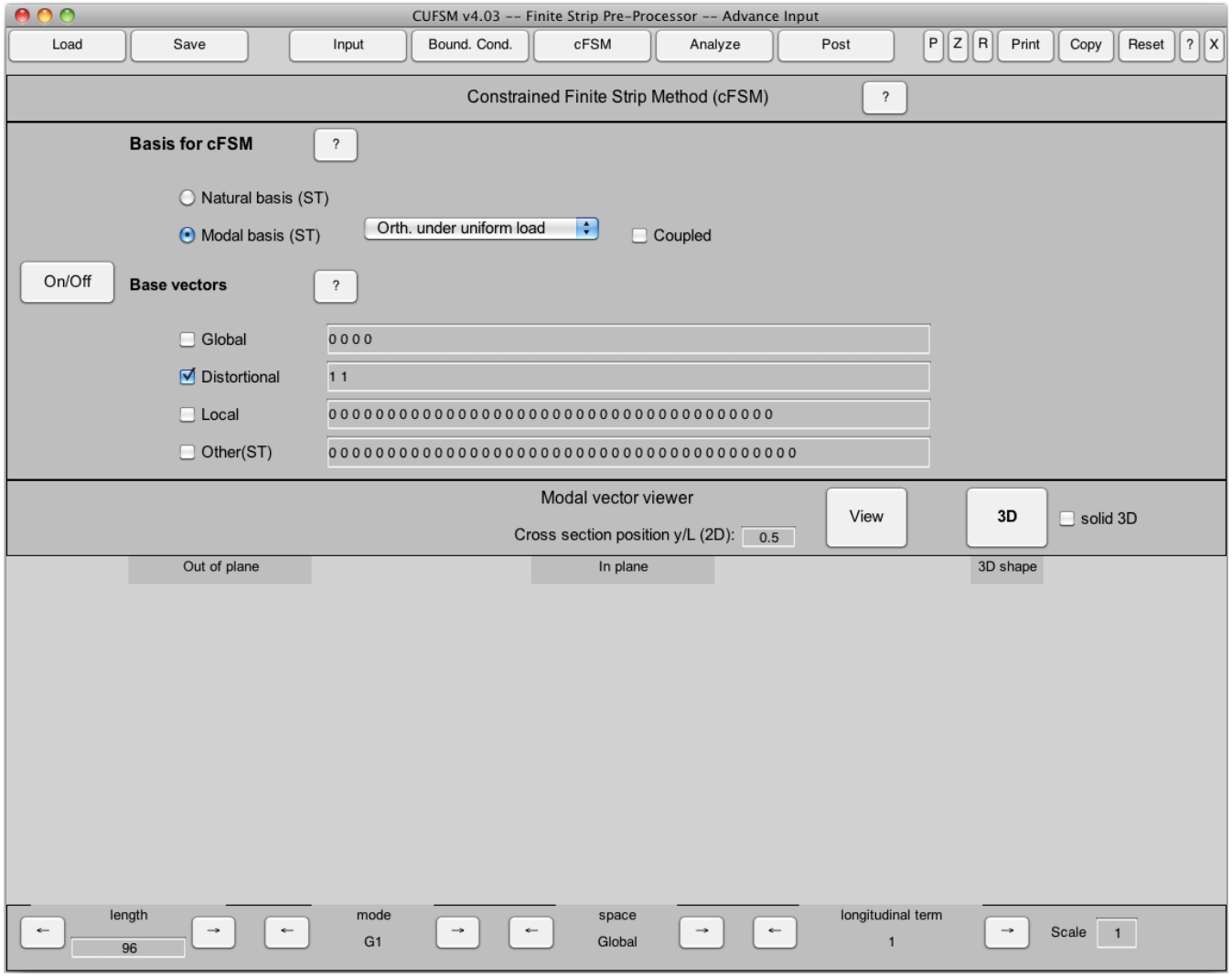

Figure G.9 – CUFSM v4.03, cFSM tab set for distortional buckling analysis.

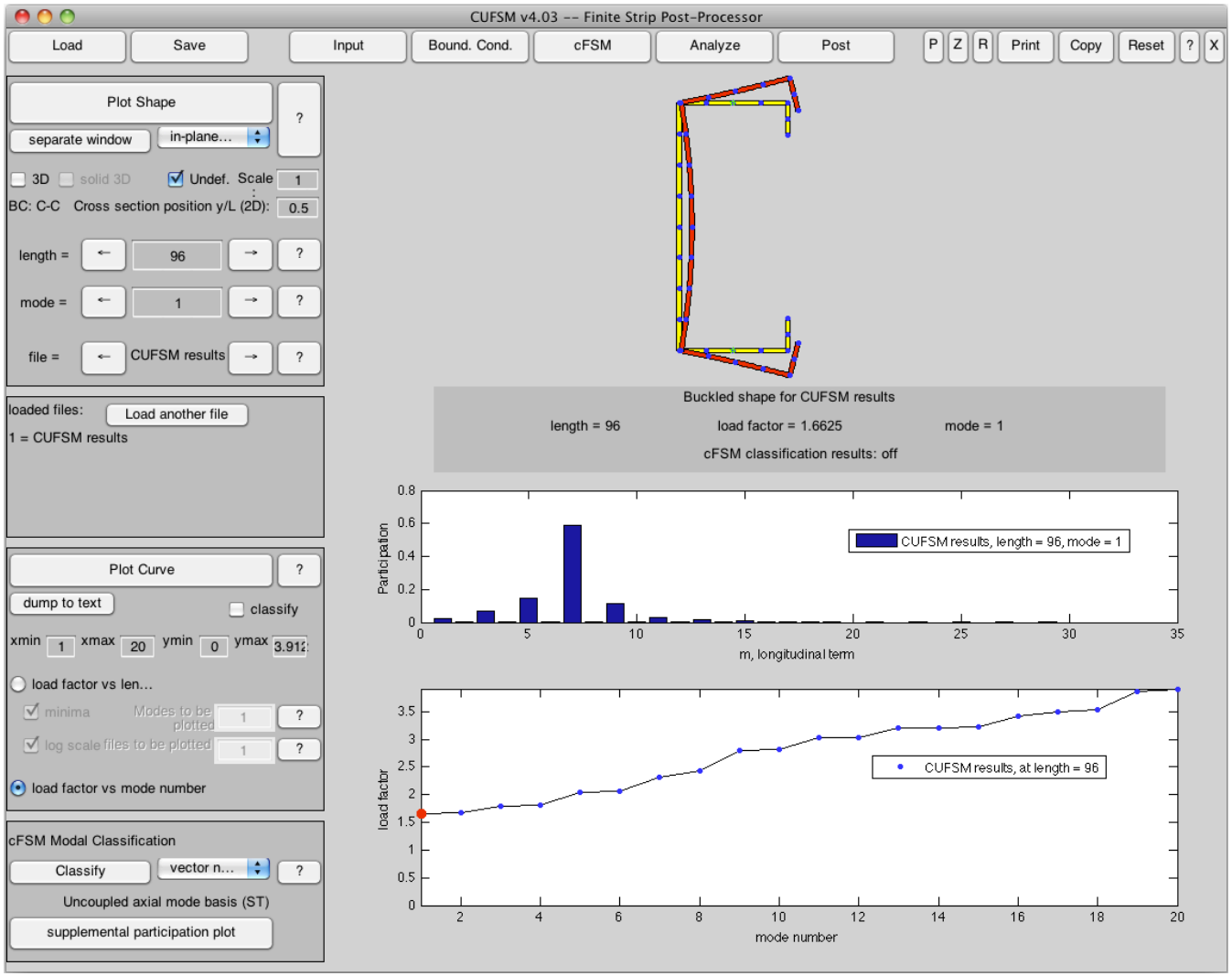

Figure G.10 – CUFSM v4.03, cFSM analysis result for distortional buckling. Load factor of 1.6625.

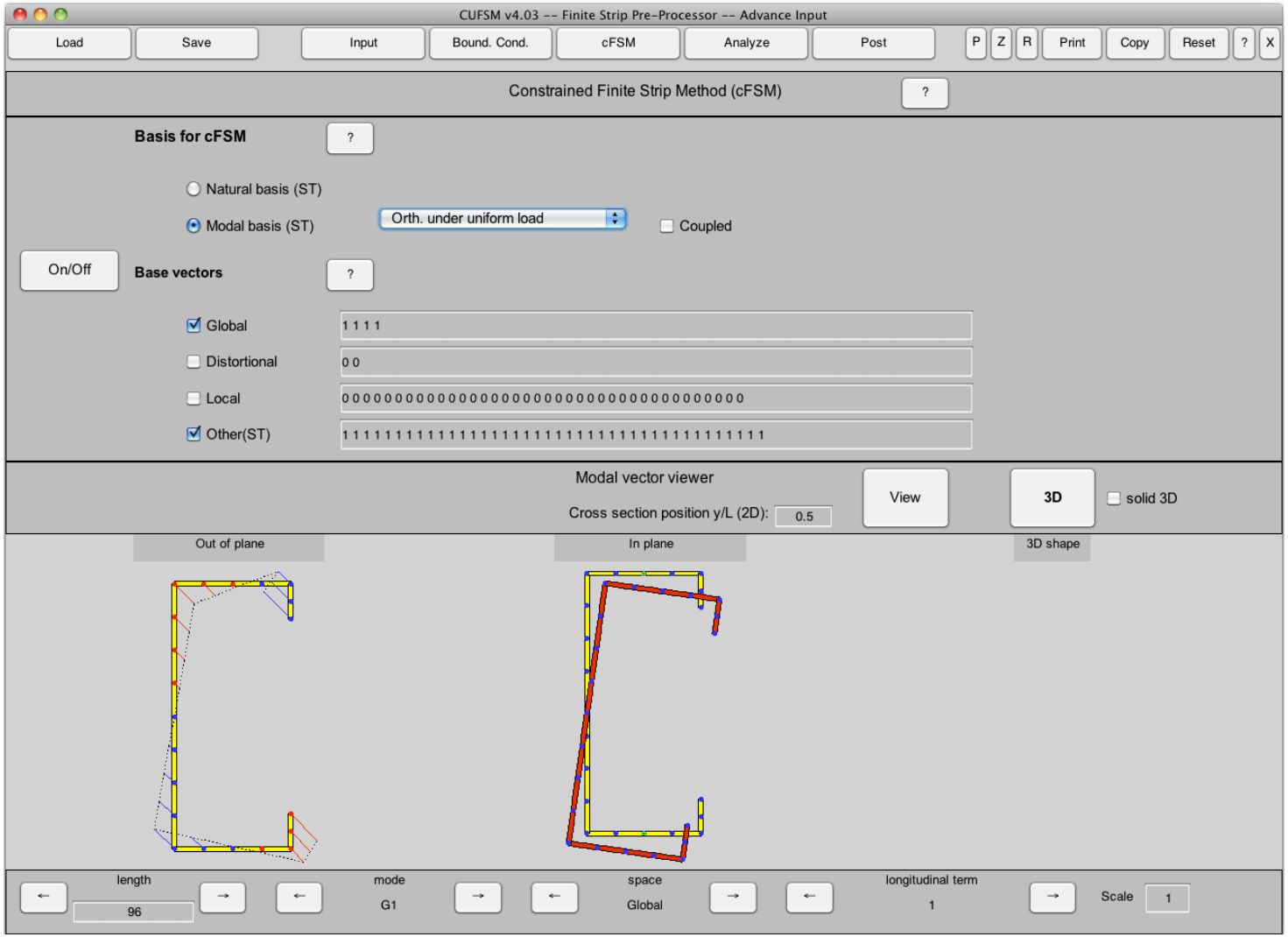

Figure G.11 – CUFSM v4.03, cFSM tab set for global/others buckling analysis.

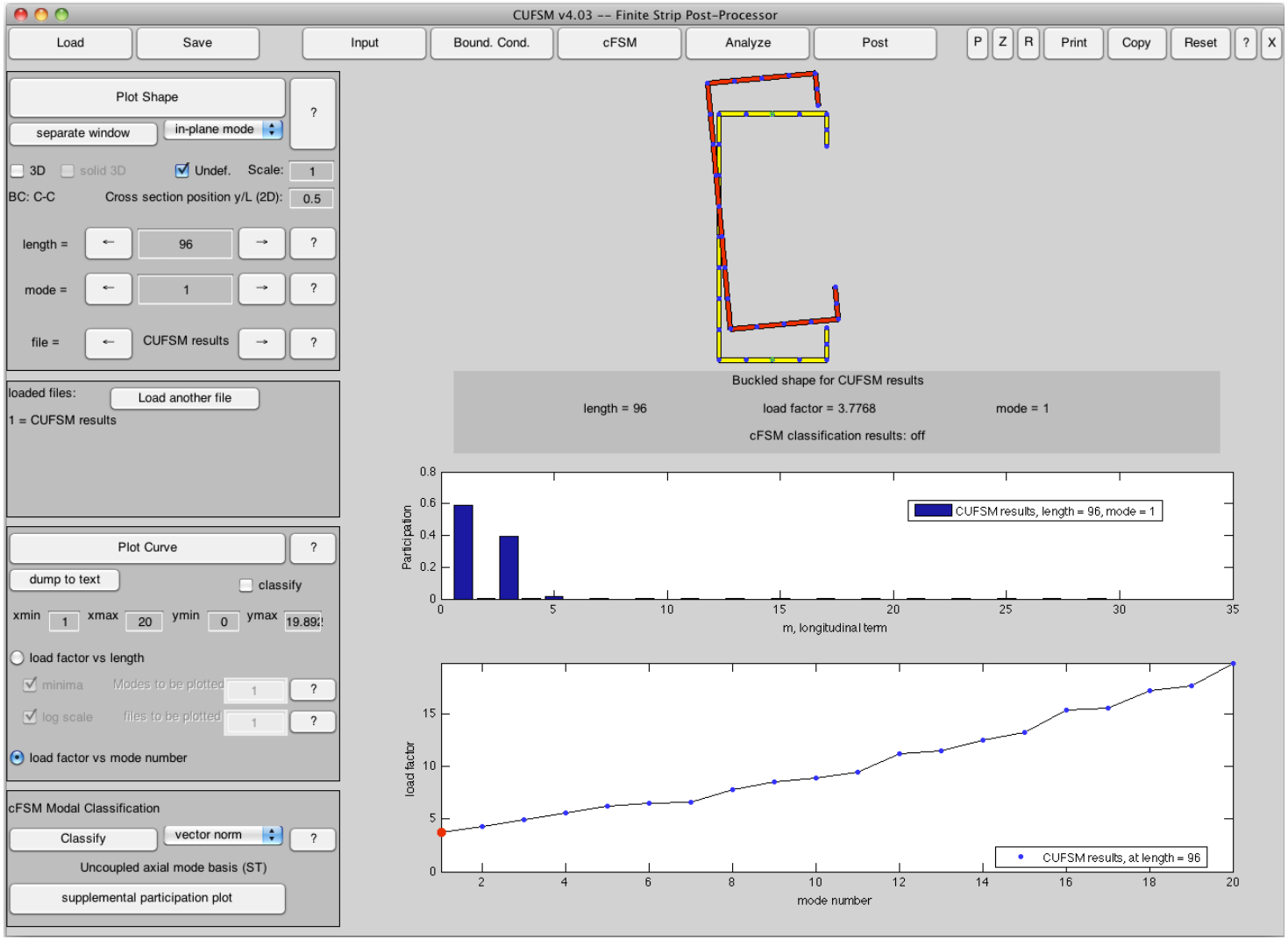

Figure G.12 – CUFSM v4.03, cFSM analysis result for global/others buckling. Load factor of 3.7768.

Given that:

$$P_y = A \cdot f_y = 0.4987 \cdot 50 = 24.9326 kips$$

The constrained finite strip analysis results in:

$P_{crl} = 1.0163 \cdot P_y = 25.339 kips$, note subscript *"l"* = "ℓ"

$P_{crd} = 1.6825 \cdot P_y = 41.949 kips$

$P_{cre} = 3.7768 \cdot P_y = 94.165 kips$

Global buckling check per DSM:

$$\lambda_c(L) = \sqrt{\frac{P_y}{P_{cre}(L)}} = 0.515 \tag{7.1}$$

Since: $\lambda_c(L) \le 1.5$, $P_{ne}(L) = 0.658^{\lambda_c(L)^2} P_y = 22.3 kips$ (7.2)

But if $\lambda_c(L) > 1.5$, the following equation shall be used: $P_{ne}(L) = \frac{0.877}{\lambda_c(L)^2} P_y$ (7.3)

Local buckling check per DSM:

$$\lambda_l(L) = \sqrt{\frac{P_{ne}(L)}{P_{crl}(L)}} = 0.938 \tag{7.4}$$

if $\lambda_l(L) \le 0.776$, the following equation shall be used: $P_{nl}(L) = P_{ne}(L)$ (7.5)

But in this case $\lambda_l(L) > 0.776$, thus:

$$P_{nl}(L) = \left[\left[1 - 0.15\left(\frac{P_{crl}(L)}{P_{ne}(L)}\right)^{0.4}\right]\left(\frac{P_{crl}(L)}{P_{ne}(L)}\right)^{0.4} P_{ne}(L)\right] = 19.8 kips \tag{7.6}$$

Distortional buckling check per DSM:

$$\lambda_d(L) = \sqrt{\frac{P_y}{P_{crd}(L)}} = 0.771 \tag{7.7}$$

if $\lambda_d(L) \le 0.561$, the following equation shall be used: $P_{nd}(L) = P_y$ (7.8)

But in this case $\lambda_l(L) > 0.561$, thus: (7.9)

$$P_{nd}(L) = \left[\left[1 - 0.25\left(\frac{P_{crd}(L)}{P_y}\right)^{0.4}\right]\left(\frac{P_{crd}(L)}{P_y}\right)^{0.4} P_y\right] = 22.4kips$$

And finally, the lowest nominal load is the nominal/design load (P_n):

$$P_n(L) = \min(P_{ne}(L), P_{nl}(L), P_{nd}(L)) = 19.8kips \quad (7.10)$$

The next figure depicts Figure 7.3 one more time. It also plotted in Figure G.13 the P_n just found, which coincides with the curve: DSM-k_x, k_ϕ, k_y (lower bound)-OSB-OSB-C-C.

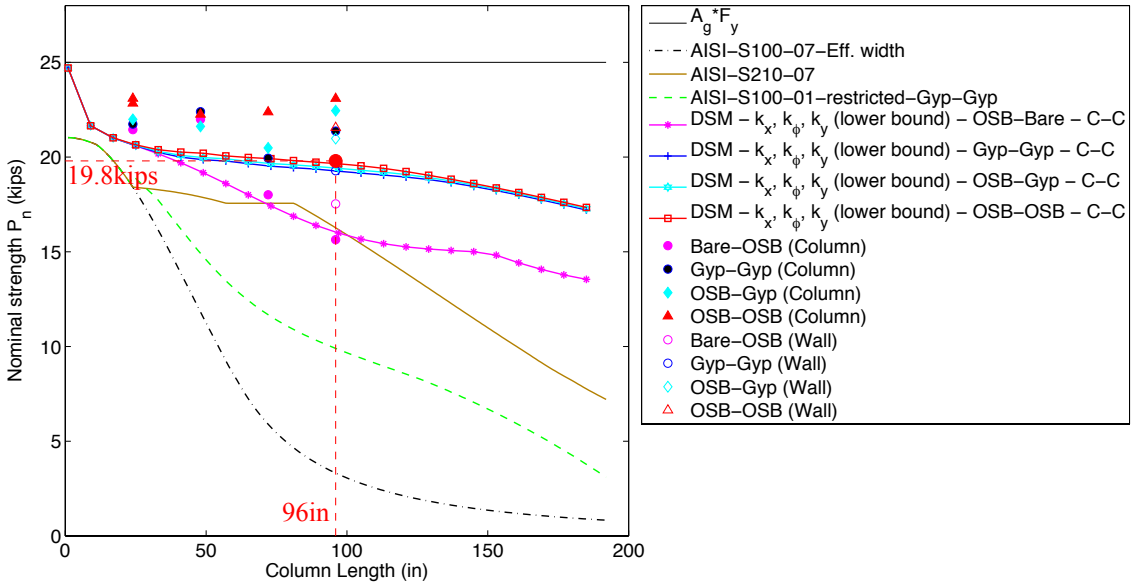

Figure G.13 – Test results compared to former, current and proposed design methods. (The point just found is highlighted)

Note, fastener and sheathing are assumed adequate in this example. See Chapter 6 and Chapter 7 Section 7.5 for further discussion on this point.

Curriculum Vitae

Luiz Carlos Marcos Vieira Junior was born in Londrina, Paraná, Brazil on October 30, 1982, the son of Luiz Carlos Marcos Vieira and Eunice Santos Santi Marcos Vieira. After completing his high school degree at Colégio Universitário, He attended Universidade Estadual de Londrina (UEL), in Brazil, where he received his Bachelor of Science in Civil Engineering and his Professional Engineering degrees. At UEL he started his research career, working with numerical methods and concrete structures. From 2003 to 2004 he worked for a consultancy and design company where he was involved in the design of concrete and steel bridges, tilt-up industrial buildings, and structural health monitoring of grain storage structures. In 2005, he enrolled in the Master of Science program at Universidade de São Paulo (USP-EESC), also in Brazil, where he did research on the Structural Behavior and Strength of Steel Purlins Restricted by Steel Sheathing. He received his Master degree from USP-EESC in 2007 and thereafter started his PhD at Johns Hopkins University (JHU) under the advising of Professor Benjamin Schafer. After four years of research on sheathed braced wall studs at JHU, he received the degree of Doctor of Philosophy in Civil Engineering in 2011. His dissertation presents and discusses several important findings on the behavior and strength of sheathed braced wall studs based on full-scale tests and numerical analyses. His research concludes with a new design method for sheathed braced wall studs, which he shows to be a significant improvement over former design methods both conceptually and in terms of strength prediction. He was hired as a faculty in the Tagliatela College of Engineering at the University of New Haven in July 2011.